

# **Monolithic separations and analysis of molecules of biological importance**

By

© Evan Langille, BScH

A Thesis submitted to the

School of Graduate Studies

in partial fulfillment of the requirements for the degree of

**Doctor of Philosophy**

**Department of Chemistry**

Faculty of Science  
Memorial University of Newfoundland  
St. John's, Newfoundland and Labrador, Canada

**January 2023**

## **Abstract**

Monolithic stationary phases are attractive tools for chromatographic separations and analyte extraction from complex matrices. Monoliths with porous surfaces can be cast as thin films or with flow channels for monolithic chromatographic columns. Monoliths describe a wide variety of materials, either organic or inorganic in nature, and in several physical forms. Methacrylate-co-ethylene glycol dimethacrylate polymers are especially of importance for separations of biomolecules. These polymers exhibit high biocompatibility and are highly tunable to isolate compounds ranging from small molecules to large molecular weight species, with a wide range of polarities. One way to achieve additional selectivity in these polymers is the introduction of molecular imprinting through the addition of a template molecule during casting. The template is removed after curing, leaving a cavity with high selectivity toward the analytes of interest. In this thesis, both molecularly imprinted and non-imprinted monoliths are employed for isolation and analysis of molecules of importance from complex biological matrices.

Mycophenolic acid (MPA) is an anti-rejection drug commonly administered after organ transplant. The interpatient variability of free MPA in blood is very high, due to complex pharmacokinetic and pharmacokinetic properties of the molecule and must be closely monitored during and after therapeutic drug administration. A monolithic thin film molecularly imprinted polymer (TF-MIP) was developed to selectively extract MPA from human plasma in a simple and rapid process.

Tyrosine kinase inhibitors (TKIs) are a class of compounds which are commonly used as chemotherapeutic agents for cancer patients. A TF-MIP was designed for the extraction of representative TKIs (imatinib, dasatinib, ponatinib, and nilotinib) in human plasma in a 96-well plate format. The developed extraction regime allowed for high-throughput sample processing with a minimum amount of sample handling using small volumes of plasma.

Gene transfer agents (GTAs) are virus-like particles that transport genetic material from one bacterium to another. Using a 2-step monolithic chromatographic approach, a new method for the preparative isolation of functional GTAs from *Rhodobacter capsulatus* was developed. The isolated particles were intact after isolation and could transfer genetic material. The newly developed process allows for purification and concentration of the particles for downstream use in biochemical, bacterial, and genetic assays, allowing for the advancement of knowledge about GTAs and the discovery of previously undiscovered GTAs. The method also has broad applicability to many small phages which are the focus of phage therapies that are used to fight antibiotic resistant bacterial infections in humans.

Coated-blade spray (CBS) mass spectrometry is a technique for direct sample introduction without traditional chromatographic separation. Innovative CBS workflows allow for rapid and simple analyses of a wide variety of compounds. Compared to traditional workflows, CBS methods are particularly attractive for biological matrices due to simplified sample processing. A custom coated-blade spray source was developed for the Xevo TQ-S where data is presented for measurement of mycophenolic acid, cocaine,

MDMA, methamphetamine, methadone and methadone-d<sub>3</sub> in human biological fluids. A custom source was designed and used to semi-quantitatively measure mycophenolic acid on the MX908 handheld MS. A fibreglass fabric-based MIP mesh was used with the thermal desorption accessory of the MX908 to measure the organophosphorus pesticides malathion and chlorpyrifos in water.

## General Summary

In this thesis, new methods for extracting drugs, pesticides, and virus-like particles are developed. Polymers were used to separate and extract the previously mentioned molecules. Custom polymers were developed that possess holes shaped like the molecules of interest, that act like a lock-and-key, allowing only the desired molecule to bind to the polymer. Samples of drugs, pesticides, and virus-like particles often contain many other molecules which make analyzing them difficult. When these polymers are put into samples containing the desired molecules, the molecules, acting as “keys”, can fit into the “lock”, and the rest of the sample can be washed away. This method is particularly useful for extracting molecules from samples such as blood, urine, wastewater, and cultures of bacteria.

An anti-rejection medication called mycophenolic acid (MPA) is frequently used after organ transplantation. MPA levels in blood vary greatly between patients and need to be constantly monitored. A polymer to extract MPA and a method to measure MPA in human plasma was created. Tyrosine kinase inhibitors (TKIs) are a class of drugs that are prescribed to cancer patients for chemotherapy. The representative TKIs imatinib, dasatinib, ponatinib, and nilotinib were extracted from human plasma using a polymer to extract TKIs and a method to measure TKIs in human plasma was created. Virus-like particles called gene transfer agents (GTAs) move genetic material from one organism to another. A new technique was created for the large-scale isolation of functional GTAs from *Rhodobacter capsulatus*. After isolation, the particles were intact, containing DNA, and capable of transferring genetic material to bacterial cells.

## **Acknowledgements**

I respectfully acknowledge the territory in which we gather as the ancestral homelands of the Beothuk, and the island of Newfoundland as the ancestral homelands of the Mi'kmaq and Beothuk. I would also like to recognize the Inuit of Nunatsiavut and NunatuKavut and the Innu of Nitassinan, and their ancestors, as the original people of Labrador. I strive for respectful relationships with all the peoples of this province as we search for collective healing and true reconciliation and honour this beautiful land together.

Many people have helped and supported my thesis research. First and foremost, I would like to acknowledge my best friend and wife, Roshni Kollipara. I could not have succeeded in this grand endeavour without her continued support. I thank Dr. Christina Bottaro for being my thesis supervisor. I thank Kristopher Hanrahan for being a friend and colleague during his honours work in the lab. I would also like to thank Dr. Andrew S. Lang for his continuous guidance, patience, and mentorship. He always gave me a new perspective to look at experiments and challenged me to think outside of my comfort zone. His interest and accessibility as well as his involvement and support made my research possible. I would like to thank all members, current and alumni, of the Lang lab for their help in times of crisis. The positive attitude of every lab member always made my time in the Lang lab more than enjoyable.

I would like to thank the people who took special effort in supporting my aspirations throughout my development, including June Brown, Christine Popowich, Jeanette Garrison, Sophia Smith, Grant MacQuarrie, Dr. Patrick Bergeron, Dr. Dale

Wood, Dr. Alexandre Drouin, Dr. Mihai Scarlete, Dr. Gregor Kos, Dr. Marc-André Simard, the late Phyllis Essex-Fraser, Dr. Lamont Sweet and, most influentially, Réjean Fortin. Réjean is a dear friend and mentor who has affected both my personal and professional development profoundly. During our multi-year collaboration, we worked on a large number of projects that largely widened my scientific scope and enhanced my analytical chemistry expertise. These few years were the best years of my entire schooling, and I am forever grateful for Réjean dedicating his time and energy to support me as an analytical scientist.

Finally, I thank my family who has supported me throughout my career. They made it possible for me to start university and continue my studies. Although it has not always been easy to be separated by the North Atlantic, their continued interest in my work and mental support have made me the person and researcher that I am today, and I am forever grateful to them.

My doctoral program and the research I have performed has been supported by a graduate student fellowship from the Memorial University School of Graduate Studies, Natural Sciences and Engineering Research Council (NSERC), and an ACOA Atlantic Innovation Fund award to Dr. Christina Bottaro. The research in Dr. Lang's laboratory was supported by grants from NSERC.

# Table of Contents

<b><u>ABSTRACT.....</u></b>	<b><u>II</u></b>
<b><u>GENERAL SUMMARY .....</u></b>	<b><u>V</u></b>
<b><u>ACKNOWLEDGEMENTS .....</u></b>	<b><u>VI</u></b>
<b><u>TABLE OF CONTENTS .....</u></b>	<b><u>VIII</u></b>
<b><u>LIST OF TABLES.....</u></b>	<b><u>XV</u></b>
<b><u>LIST OF FIGURES.....</u></b>	<b><u>XVII</u></b>
<b><u>LIST OF ABBREVIATIONS, SYMBOLS, AND NOMENCLATURE .....</u></b>	<b><u>XXII</u></b>
<b><u>LIST OF APPENDICES .....</u></b>	<b><u>XXVIII</u></b>
<b><u>CO-AUTHORSHIP STATEMENT .....</u></b>	<b><u>XXIX</u></b>
<b><u>1 INTRODUCTION AND OVERVIEW.....</u></b>	<b><u>1</u></b>
<b><u>1.1 MONOLITHS.....</u></b>	<b><u>1</u></b>
<b><u>1.2 MONOLITHIC THIN FILMS.....</u></b>	<b><u>2</u></b>
<b><u>1.3 MONOLITHIC MOLECULARLY IMPRINTED POLYMERS .....</u></b>	<b><u>2</u></b>
<b><u>1.4 CONVECTIVE INTERACTION MEDIA®.....</u></b>	<b><u>4</u></b>



<b>1.5</b>	<b>ANALYSIS OF THERAPEUTIC DRUGS IN BIOMATRICES .....</b>	<b>12</b>
1.5.1	THERAPEUTIC DRUG MONITORING .....	12
1.5.2	METABOLIC VARIABILITY AND BLOOD SAMPLE STABILITY .....	13
1.5.3	ENDOGENOUS INTERFERENTS.....	16
1.5.4	SAMPLE PREPARATION AND EXTRACTION OF THERAPEUTIC DRUGS IN BLOOD.....	17
1.5.5	MEASUREMENT OF THERAPEUTIC DRUGS USING MASS SPECTROMETRY.....	21
1.5.6	DIRECT COUPLING OF EXTRACTION DEVICES TO MS.....	22
<b>1.6</b>	<b>ISOLATION OF MACROMOLECULES.....</b>	<b>23</b>
<b>1.7</b>	<b>RESEARCH GOALS .....</b>	<b>27</b>
<b>2</b>	<b><u>DEVELOPMENT AND APPLICATION OF A THIN-FILM MOLECULARLY</u></b>	
	<b><u>IMPRINTED POLYMER FOR THE MEASUREMENT OF MYCOPHENOLIC ACID IN</u></b>	
	<b><u>HUMAN PLASMA.....</u></b>	<b><u>30</u></b>
<b>2.1</b>	<b>INTRODUCTION.....</b>	<b>30</b>
<b>2.2</b>	<b>METHODS.....</b>	<b>32</b>
2.2.1	REAGENTS AND MATERIALS .....	32
2.2.2	INSTRUMENTATION AND OPERATING CONDITIONS .....	33
2.2.3	PREPARATION OF EXTRACTION DEVICES.....	34
2.2.4	MOLECULARLY IMPRINTED POLYMER EXTRACTION OF PLASMA .....	34
2.2.5	PATIENT SAMPLES AND DEMOGRAPHICS .....	35
<b>2.3</b>	<b>RESULTS.....</b>	<b>37</b>
2.3.1	FORMULA DEVELOPMENT .....	37
2.3.2	OPTIMIZATION OF THE DESORPTION CONDITIONS.....	39
2.3.3	OPTIMIZATION OF EXTRACTION CONDITIONS.....	41

2.3.4	OPTIMIZATION OF EXTRACTION TIME AND EXTRACTION LINEARITY .....	43
2.3.5	ANALYTICAL PERFORMANCE THIN FILM MIPs FOR DETERMINATION OF MPA IN PLASMA 45	
2.3.6	ANALYTICAL FIGURES OF MERIT .....	46
2.3.7	ANALYSIS OF PATIENT SAMPLES .....	47
<b>2.4</b>	<b>DISCUSSION .....</b>	<b>50</b>
<b>3</b>	<b><u>A THIN-FILM MOLECULARLY IMPRINTED POLYMER FOR THE MEASUREMENT OF TYROSINE KINASE INHIBITORS IN HUMAN PLASMA .....</u></b>	<b>53</b>
<b>3.1</b>	<b>INTRODUCTION.....</b>	<b>53</b>
<b>3.2</b>	<b>EXPERIMENTAL.....</b>	<b>58</b>
3.2.1	REAGENTS AND MATERIALS .....	58
3.2.2	INSTRUMENTATION AND OPERATING CONDITIONS .....	59
3.2.3	INSTRUMENTATION AND OPERATING CONDITIONS: FORMULA DEVELOPMENT.....	61
3.2.4	PREPARATION OF EXTRACTION DEVICES.....	61
3.2.5	SELECTION OF MICROPLATES.....	61
3.2.6	MOLECULARLY IMPRINTED POLYMER EXTRACTION OF PLASMA .....	63
3.2.7	FORMULA DEVELOPMENT .....	64
<b>3.3</b>	<b>RESULTS AND DISCUSSION .....</b>	<b>65</b>
3.3.1	SCREENING METHOD DEVELOPMENT .....	65
3.3.2	FORMULA DEVELOPMENT .....	71
3.3.3	TEMPLATE STUDY .....	73
3.3.4	MONOMER STUDY .....	74
3.3.5	CROSSLINKER STUDY .....	76

3.3.6	POROGENIC SOLVENTS .....	79
3.3.7	PHOTOINITIATORS .....	82
3.3.8	FINAL FORMULA EVALUATION .....	84
3.3.9	BATCH-TO-BATCH REPEATABILITY .....	84
3.3.10	INTER-DEVICE VARIABILITY .....	85
3.3.11	EXTRACTION METHOD DEVELOPMENT.....	87
3.3.12	OPTIMIZATION OF THE DESORPTION SOLVENT .....	87
3.3.13	OPTIMIZATION OF THE WASH CONDITIONS .....	90
3.3.14	EXTRACTION TIME PROFILE .....	91
3.3.15	EXTRACTION CALIBRATION CURVES .....	95
3.3.16	BIOLOGICAL VALIDATION: ENDOGENOUS INTERFERENCES .....	97
3.3.17	METHOD VALIDATION.....	103
3.3.18	ANALYTICAL PERFORMANCE OF THIN FILM MIPs FOR DETERMINATION OF TKIS IN PLASMA 103	
3.3.19	FIGURES OF MERIT OF ANALYTICAL METHOD .....	104
<b>3.4</b>	<b>CONCLUSION .....</b>	<b>106</b>
<b>4</b>	<b><u>PURIFICATION OF FUNCTIONAL GENE TRANSFER AGENTS (GTAS) USING TWO-STEP PREPARATIVE MONOLITHIC CHROMATOGRAPHY .....</u></b>	<b><u>108</u></b>
<b>4.1</b>	<b>INTRODUCTION.....</b>	<b>108</b>
<b>4.2</b>	<b>MATERIALS AND METHODS .....</b>	<b>110</b>
4.2.1	STRAINS AND GROWTH CONDITIONS .....	110
4.2.2	CHROMATOGRAPHIC PURIFICATION OF GTAS.....	111
4.2.3	NANOPARTICLE TRACKING ANALYSIS.....	113

4.2.4	GENE TRANSFER BIOASSAYS .....	113
4.2.5	GTA DNA EXTRACTION .....	113
4.2.6	NEXT-GENERATION SEQUENCING.....	114
4.2.7	SDS-PAGE AND WESTERN BLOTTING .....	115
<b>4.3</b>	<b>RESULTS.....</b>	<b>115</b>
<b>4.4</b>	<b>DISCUSSION .....</b>	<b>126</b>
<b>4.5</b>	<b>ACKNOWLEDGEMENTS .....</b>	<b>127</b>
<b>5</b>	<b><u>DIRECT COUPLING OF EXTRACTION DEVICES TO MS.....</u></b>	<b>128</b>
<b>5.1</b>	<b>INTRODUCTION.....</b>	<b>128</b>
5.1.1	COATED BLADE SPRAY MASS SPECTROMETRY .....	128
5.1.2	HANDHELD MASS SPECTROMETRY .....	130
<b>5.2</b>	<b>MATERIALS AND METHODS .....</b>	<b>135</b>
5.2.1	GENERAL .....	135
<b>5.3</b>	<b>ANALYTICAL TARGETS AND DEVICE PREPARATION .....</b>	<b>135</b>
5.3.1	DRUGS OF ABUSE .....	135
5.3.2	MYCOPHENOLIC ACID.....	137
5.3.3	ORGANOPHOSPHORUS PESTICIDES .....	137
<b>5.4</b>	<b>INSTRUMENTATION AND OPERATING CONDITIONS .....</b>	<b>138</b>
5.4.1	BENCHTOP MS.....	138
5.4.2	HANDHELD MS.....	138
<b>5.5</b>	<b>RESULTS AND DISCUSSION .....</b>	<b>139</b>
5.5.1	XEVO TQ-S CUSTOM SOURCE INTERFACE.....	139

5.5.2	DRUGS OF ABUSE IN BIOLOGICAL MATRICES BY COATED BLADE SPRAY ON XEVO TQ-S	142
5.5.3	COUPLING MIP MESH TO MX908 .....	149
5.5.4	MX908 CUSTOM SOURCE INTERFACE .....	156
5.5.5	COATED BLADE TF-MIP MYCOPHENOLIC ACID ANALYSIS ON MX908 .....	159
5.6	CONCLUSIONS .....	168
5.7	ACKNOWLEDGEMENTS .....	170
<b>6</b>	<b><u>SUMMARY AND CONCLUSIONS.....</u></b>	<b>171</b>
<b>7</b>	<b><u>CHALLENGES, LIMITATIONS AND FUTURE WORK.....</u></b>	<b>180</b>
	<b><u>REFERENCES .....</u></b>	<b>185</b>
	<b><u>APPENDIX 1: OTHER SCIENTIFIC CONTRIBUTIONS.....</u></b>	<b>202</b>
	<b><u>APPENDIX 2: A NOVEL USE OF CATALYTIC ZINC-HYDROXYAPATITE COLUMNS FOR THE SELECTIVE DEPROTECTION OF N-TERT-BUTYLOXYCARBONYL (BOC) PROTECTING GROUP USING FLOW CHEMISTRY .....</u></b>	<b>206</b>
	<b>INTRODUCTION .....</b>	<b>206</b>
	<b>RESULTS AND DISCUSSION.....</b>	<b>209</b>
	<b>EXPERIMENTAL .....</b>	<b>219</b>
	GENERAL METHODS .....	219
	HYDROXYAPATITE SOLID SUPPORT PREPARATION.....	220
	ZINC-HYDROXYAPATITE .....	221

ZINC-HYDROXYAPATITE COLUMN .....	222
EXAMPLE DEPROTECTION PROTOCOL .....	222
CHIRAL SEPARATION BY MICELLAR ELECTROKINETIC CHROMATOGRAPHY (MEKC) .....	223
PREPARATION OF THE PRECURSORS .....	224

## List of Tables

Table 2.1: MRM transitions and mass spectrometer settings for mycophenolic acid.

Table 2.2: Patient information for mycophenolic acid.

Table 2.3: Analytical figures of merit for thin film MIP devices.

Table 2.4: Results of patient sample analysis for MPA.

Table 3.1: Structures, relevant physical constants, and generation number of studied TKIs.

Table 3.2: MRM transitions, mass spectrometer settings and retention compounds of TKIs.

Table 3.3: Structures and physiochemical properties of compounds used in the final formula.

Table 3.4: Composition of the optimal MIP thin film extraction device for the four TKIs.

Table 3.5: Analytical figures of merit for thin film MIP devices for the analysis of TKIs.

Table 4.1: List of *R. capsulatus* strains used in this study.

Table 4.2: Chromatographic parameters and instrument settings for GTA purification.

Table 4.3: Gene transfer bioassay using purified GTA.

Table 5.1: Selected portable trap-based MS instruments and their respective properties.

Table 5.2: Structures and physical properties of selected drugs of abuse.

Table 5.3: MRM transitions, cone voltage, and collision energy of selected drugs of abuse on Waters Xevo TQ-S.

Table 5.4: Figures of merit including linear range, LOD, LOQ for analysis of drugs of abuse using coated blade spray on Xevo TQ-S.

Table 5.5: Structure and relevant physical properties of selected OPPs.

Table A2.1: Deprotection of compound 1a in a flask.

Table A2.2: Deprotection of N-Boc protected amines using the Zn-HAP column.

Table A2.3: Chromatographic parameters for BOC compound separation.



## List of Figures

Figure 1.1: Overview of molecular imprinting technique and common reagents.

Figure 1.2: Glycidyl methacrylate monolith demonstrating post polymerization chemical conversion.

Figure 1.3: Comparison of hydrodynamics in particles, stacked membrane adsorbers, and monoliths.

Figure 1.4: Scanning electron micrograph of CIM monolith material.

Figure 1.5: The van Deemter equation for a given set of terms.

Figure 1.6: Metabolic transformations of the therapeutic drugs mycophenolic acid, isoniazid, and diazepam.

Figure 1.7: Blood sample workflow for analysis of plasma using TFME.

Figure 1.8: Comparison of porous particle media to monolithic stationary phases.

Figure 2.1: Relationship between porogen volume, relative recovery of MIP and NIP extractions of  $50 \text{ ng mL}^{-1}$  mycophenolic acid in plasma.

Figure 2.2: Comparison of desorption conditions on relative recovery of MIP extraction of mycophenolic acid.

Figure 2.3: Comparison of H adjustment on relative recovery of MIP extraction of mycophenolic acid.

Figure 2.4: Time profile of MIP and NIP extractions of  $50 \text{ ng mL}^{-1}$  mycophenolic acid from plasma.

Figure 2.5: Extraction calibration curve of mycophenolic acid in plasma.

Figure 2.6: External calibration curve of mycophenolic acid.

Figure 2.7: Transition ratio monitoring of MPA.

Figure 3.1: Comparison of plate type on recovery of mixed extraction of TKIs.

Figure 3.2: Comparison of relative recovery of F116 mixed extraction with different desorption solvents.

Figure 3.3: Comparison of desorption time of F116 mixed extraction.

Figure 3.4: Contact adsorption study.

Figure 3.5: Comparison of extraction pH of F116 extraction.

Figure 3.6: Overview of formula development.

Figure 3.7: Photographs of prepared films at various stages of formula development.

Figure 3.8: Comparison of adenine and 3-acetylpyridine molecularly imprinted polymers to their non-imprinted counterparts.

Figure 3.9: Effect of addition of MAA to N-MEMA on relative recovery of TKIs.

Figure 3.10: Comparison of crosslinker on relative recovery of TKIs.

Figure 3.11: Relationship between ratio of 2-*N*-morpholinoethyl methacrylate: EGDMA.

Figure 3.12: Relationship between porogen composition and relative recovery of TKIs.

Figure 3.13: Relationship between porogen volume based on F176 on recovery of TKIs.

Figure 3.14: Relative response for MIPs and NIPs produced using two different photoinitiators.

Figure 3.15: Control chart showing combined variability of 10 MIP formulas.

Figure 3.16: Inter-device variability of ten MIP devices.

Figure 3.17: Screening of desorption solvents.

Figure 3.18: Comparing chromatographic peak splitting of imatinib.

Figure 3.19: TKI Extraction time profiles.

Figure 3.20: Extraction calibration curves comparing MIP and NIP extractions with mixed TKIs.

Figure 3.21: Extraction calibration curves comparing mixed and individual extractions of TKIs.

Figure 3.22: Heatmap illustrating percent deviation of recovery of TKIs under effect of endogenous interferents.

Figure 3.23: Photographs comparing extraction of plasma containing endogenous interferents.

Figure 3.24: External calibration curves of TKIs.

Figure 4.1: Photoheterotrophic anaerobic cultures in RCV to compare GTA release.

Figure 4.2: CIMmultus OH purification of DE442 GTA.

Figure 4.3: Biochemical characterization of CIMmultus OH purification of DE442 GTA.

Figure 4.4: CIMmultus QA purification of DE442 GTA.

Figure 4.5: Biochemical characterization of CIMmultus QA purification of DE442 GTA.

Figure 4.6: Analysis of DNA extracted from purified DE442 GTAs.

Figure 5.1: Scheme for CBS-MS experiments using plasma.

Figure 5.2: MX908 software interface with built in drug detection algorithms showing the spectral matching, heatmap of signal and relative scan intensity in thermal desorption mode.

Figure 5.3: Direct coupling of coated blades to Xevo TQ-S.

Figure 5.4: Representative trace of mycophenolic acid captured from coated blade spray from MIP device.

Figure 5.5: Calibration curve constructed from coated blade spray of mycophenolic acid standards.

Figure 5.6: Calibration curves constructed by coated blade spray of mixed drugs of abuse standards using Xevo TQ-S.

Figure 5.7: Evaluation of matrix effects in blank and DOA spiked biological fluids by coated blade spray MS.

Figure 5.8: Evaluation of inter-device variability and percent recovery in mixed DOA-spiked plasma by coated blade spray MS.

Figure 5.9: MIP mesh coupled to MX908.

Figure 5.10: Solvent wash optimization.

Figure 5.11: Malathion analysis using MIP OPP mesh.

Figure 5.12: Chlorpyrifos analysis using MIP OPP mesh.

Figure 5.13: Attempted design of HV routing from corona discharge post in MX908.

Note the PTFE lined source for electrical insulation.

Figure 5.14: Custom nano electrospray interface for coated blade spray using the MX908 handheld MS.

Figure 5.15: MX908 Spectra of mycophenolic acid.

Figure 5.16: ESI (-) spectrum of mycophenolic acid at 5 ppm on Xevo TQ-S.

Figure 5.17: Collision energy experiments of MPA on Q-Exactive Orbitrap MS.

Figure 5.18: Calibration curve constructed from coated blade spray of mycophenolic acid standards.

Figure A2.1: Photograph of custom-built plug flow reactor (PFR) system.

Figure A2.2: Kinetic study of BOC protected compound in the PFR.

## List of abbreviations, symbols, and nomenclature

<b>Abbreviation</b>	<b>Meaning</b>
<b>%</b>	Per cent
<b>2-VP</b>	2-vinylpyridine
<b>4-VP</b>	4-vinylpyridine
<b>A</b>	Amp
<b>ACN</b>	Acetonitrile
<b>AM</b>	Acrylamide
<b>ANOVA</b>	Analysis of variance
<b>anti-VEGF</b>	Antibody against human vascular endothelial growth factor
<b>bp</b>	Basepair
<b>C18</b>	Octadecyl
<b>CBS</b>	Coated-blade spray
<b>CBS-MS</b>	Coated-blade spray mass spectrometry
<b>CE</b>	Collision energy
<b>CIM</b>	Convective Interaction Media®
<b>CMT</b>	Convective mass transport
<b>Conc.</b>	Concentration
<b>COVID-19</b>	Disease resulting from infection from SARS-CoV-2
<b>DART</b>	Direct analysis in real time
<b>Das</b>	Dasatinib

<b>DESI</b>	Direct electrospray ionization
<b>DMPA</b>	2,2-dimethoxy-2-phenylacetophenone
<b>DMPA</b>	2,2-Dimethoxy-2-phenylacetophenone
<b>DMSO</b>	Dimethyl sulfoxide
<b>DNA</b>	Deoxyribonucleic acid
<b>DOE</b>	Design of experiments
<b>DVB</b>	Divinylbenzene
<b>EGDMA</b>	Ethylene glycol dimethacrylate
<b>ELISA</b>	Enzyme-linked immunosorbent assays
<b>ESI</b>	Electrospray ionization
<b>EtOH</b>	Ethanol
<b>FA</b>	Formic acid
<b>GC</b>	Gas chromatography
<b>GMA</b>	Glycidyl methacrylate
<b>GTA</b>	Gene transfer agent
<b>Hac</b>	Acetic acid
<b>HEMA</b>	2-hydroxyethyl methacrylate
<b>HEMPA</b>	2-Hydroxy-4'-(2-hydroxyethoxy)-2-methylpropiophenone
<b>HGT</b>	Horizontal gene transfer
<b>His-tag</b>	Poly-histidine tag, commonly added to a protein
<b>HLB</b>	Hydrophilic-lipophilic balance
<b>HPLC</b>	High-performance liquid chromatography

<b>HV</b>	High voltage
<b>IF</b>	Imprinting factor
<b>Ima</b>	Imatinib
<b>IMAC</b>	Immobilized-metal affinity chromatography
<b>kb</b>	Kilobases
<b>kV</b>	Kilovolts
<b>LC</b>	Liquid chromatography
<b>LC-MS</b>	Liquid chromatography- mass spectrometry
<b>LC-MS/MS</b>	Liquid chromatography-tandem mass spectrometry
<b>LH2</b>	Light-harvesting complex II
<b>LLE</b>	Liquid-liquid extraction
<b>LOD</b>	Limit of detection
<b>LogP</b>	Logarithm of the partition coefficient
<b>LOQ</b>	Limit of quantitation
<b>LR</b>	Linear range
<b>m/z</b>	Mass to charge ratio
<b>mA</b>	Milliamp
<b>MAA</b>	Methacrylic acid
<b>MDMA</b>	3,4-Methylenedioxymethamphetamine
<b>MeOH</b>	Methanol
<b>MIPs</b>	Molecularly imprinted polymers
<b>MOPS</b>	3-(N-morpholino)propanesulfonic acid



<b>MPA</b>	Mycophenolic acid
<b>MRM</b>	Multiple reaction monitoring
<b>mRNA</b>	Messenger ribonucleic acid
<b>MS</b>	Mass spectrometry
<b>MS/MS</b>	Tandem mass spectrometry
<b>MW</b>	Molecular weight
<b>MWCO</b>	Molecular weight cut-off
<b>N-MEMA</b>	2- <i>N</i> -morpholinoethyl methacrylate
<b>nESI</b>	Nanoelectrospray ionization
<b>NGS</b>	Next-generation sequencing
<b>Ni-NTA</b>	Nickel-nitrilotriacetic acid
<b>Nil</b>	Nilotinib
<b>NIPs</b>	Non-imprinted polymers
<b>NL</b>	Measured concentration is higher than linear range
<b>nm</b>	Nanometers
<b>NP</b>	Normal Phase
<b>NQ</b>	Measured concentration is lower than LOQ
<b>nt</b>	Nucleotides
<b>OPPs</b>	Organophosphorous pesticides
<b>PAN</b>	Poly(acrylonitrile)
<b>PB</b>	Phosphate Buffer
<b>PBS</b>	Phosphate Buffered Saline

<b>PDMS</b>	poly(dimethyl)siloxane
<b>PEG</b>	Polyethylene glycol
<b>PES</b>	Polyethersulfone
<b>PETA</b>	Pentaerythritol tetraacrylate
<b>Pon</b>	Ponatinib
<b>PS</b>	Paper spray
<b>PS-DVB</b>	Polystyrene-divinylbenzene
<b>PTFE</b>	Polytetrafluoroethylene
<b>QA</b>	Quaternary-ammonium
<b>QqQ</b>	Triple quadrupole mass spectrometer
<b>Qual</b>	Qualitative
<b>Quant</b>	Quantitative
<b><i>R</i><sup>2</sup></b>	The coefficient of determination for linear regression
<b>RcGTA</b>	Rhodobacter capsulatus gene transfer agent
<b>RCV</b>	Rhodobacter Capsulatus Defined Medium
<b>RNA</b>	Ribonucleic acid
<b>RP</b>	Reversed phase
<b>Rpm</b>	Revolutions per minute
<b>Rpm</b>	Rotation per minute
<b>RSD</b>	Relative standard deviation
<b>s</b>	Seconds
<b>SAX</b>	Strong anion exchange

<b>SD</b>	Standard deviation
<b>SDS</b>	Sodium dodecyl sulfate
<b>SDS-PAGE</b>	Sodium dodecyl sulfate-polyacrylamide gel electrophoresis
<b>SEM</b>	Scanning electron microscopy
<b>SNR</b>	Signal-to-noise ratio
<b>SPE</b>	Solid phase extraction
<b>SPME</b>	Solid phase microextraction
<b>SST</b>	Serum separator tube

## List of Appendices

Appendix 1: Other Scientific Contributions

Appendix 2: **Langille, E.**, Bottaro, C.S., Drouin, A.: A novel use of catalytic zinc-hydroxyapatite columns for the selective deprotection of N-tert-butyloxycarbonyl (BOC) protecting group using flow chemistry. *J Flow Chem.* 10, 377–387 (2020).

<https://doi.org/10.1007/s41981-019-00052-x>

## Co-Authorship Statement

The principal author has conducted the research and literature review presented in Chapters 1-7 of this thesis for the degree of Doctor of Philosophy under the supervision of Prof. Christina S. Bottaro.

Chapter 2 is a version of a manuscript that is currently under review (revision submitted) with the Journal of Clinical Laboratory Analysis “**Development and application of a thin-film molecularly imprinted polymer for the measurement of mycophenolic acid in human plasma**”. C.S. Bottaro and I designed the research, I carried out the experiments, as well as the data analysis. The manuscript was drafted by me, with subsequent editorial input from C.S. Bottaro.

Chapter 3 is an extended version of a manuscript that is currently being prepared for submission to a special issue in Talanta Open entitled “**A thin-film molecularly imprinted polymer for the measurement of tyrosine kinase inhibitors in human plasma**”. Research in this chapter was proposed and designed by me. Kristopher Hanrahan (BSc Honours student) and I carried out the formula development experiments. K. Hanrahan worked under my direction and supervision in the laboratory. K. Hanrahan’s honours thesis focused on preliminary performance data of imatinib using the same TF-MIP that I developed for this chapter. The final imatinib data presented in this chapter is based on improved methodologies and is not the same data presented in K. Hanrahan’s

thesis. I performed all the data analysis in this chapter. The manuscript was drafted by me, with subsequent editorial input from C.S. Bottaro.

Chapter 4 is an accepted version of a manuscript that is published in *PHAGE: Therapy, Applications, and Research* entitled “**Purification of functional gene transfer agents (GTAs) using two-step preparative monolithic chromatography**” (doi: 10.1089/phage.2022.0035). Experiments in this chapter were proposed and designed by me and A.S. Lang. I carried out all the experiments, as well as all data analysis. The manuscript was drafted and prepared by me, with subsequent editorial input from C.S. Bottaro and A.S. Lang.

Chapter 5 is a preliminary data chapter on direct coupling of extraction devices to both benchtop and handheld MS instruments. Experiments in this chapter were proposed and designed by me. The Xevo TQ-S custom CBS source was designed by Hamed Piri-Moghadam (a former Postdoctoral Fellow in the group). I carried out all the experiments, as well as all data analysis. The chapter was drafted and prepared by me, with subsequent editorial input from C.S. Bottaro

# 1 Introduction and Overview

## 1.1 Monoliths

Chromatographic monoliths, referred to as “monoliths” in this thesis, are stationary phases that are cast as a single continuous polymers [1]. Monoliths can be cast with porous surfaces in the case of thin film monoliths, or with continuous open pores for monolithic chromatographic columns. Monoliths describe a wide group of polymeric phases being either organic or inorganic, resins, or gels. The first report of monolith preparations for chromatography was in 1966, where a swelled polymer gel was described [2], shortly followed by a porous polyurethane [3] reported in 1970. However, these early monoliths failed to attain interest for use in further work, mainly due to negative chromatographic behaviours and physical performance issues, such as swelling or shrinking of the phases when exposed to varying solvent compositions [4].

The area of monoliths once again gained traction due to advances in the field when ultrafiltration membranes began to be manufactured and used in the biotechnology industry [4]. In fact, these ultrafiltration membranes are still a staple of macromolecular purification workflows today, with Amicon® Ultrafiltration membranes (developed in the 1980s) commonly employed in most biology and biochemistry labs. One of the first reports of a modern-resembling methacrylate based monolithic disc column was developed in 1989 by a team of Czech and Russian researchers [5,6], and used for protein purification at pressures 3-5 times less than that of similar packed columns at the time [4]. Commonly prepared and used monoliths are polyacrylamide gels [7], cryogels [8], silica monoliths [9–12], and methacrylate-based chemistries [4,5]. Industrial research and

development efforts have majorly led the development of monoliths, particularly in the biotechnology market where the powerful technology has made many biological therapies possible.

## 1.2 Monolithic Thin Films

Thin film microextraction (TFME) is a technique analogous to solid phase extraction (SPE) that consists of a thin film of sorbent, usually a thin layer of monolithic polymer, coated on a substrate [13]. Depending on the application, thin films can be prepared on numerous substrates from glass, stainless steel, fibreglass, and carbon mesh, or even microfibres as in solid phase microextraction (SPME). TFME usually has a larger geometric surface area than SPME and the increase in surface area leads to an increased capacity. The thin films can be made robust and are resistant to fouling in biological matrices like whole blood and plasma. The polarity of the films can be tuned by adjusting the constituents and ratios of the polymer components making them more hydrophilic or lipophilic.

## 1.3 Monolithic Molecularly Imprinted Polymers

Molecular imprinting is the creation of template-shaped cavities in a polymer matrix. By introducing molecular imprinting into monolithic polymers used in TFME, we can introduce another mode of selectivity [14,15]. Thin film molecularly imprinted polymers (TF-MIPs) are analogous to enzyme-substrate binding in biochemistry (Figure 1.1). A template molecule that is designed to interact with the functional monomer is



added to the solution of polymer components (Figure 1.1 C I and II). After polymerization in the presence of a crosslinking agent (Figure 1.1 B and C III), the template can be removed via washing since the interactions are generally weak and can be broken under gentle conditions, allowing for a cavity with a shape and chemical affinity for the analyte (Figure 1.1 C IV). For example, an analyte with basic functionality would be extracted using a film prepared with an acidic functional monomer and vice-versa (Figure 1.1 A). In this way, hydrogen bonding is the main force allowing interaction of the analytes with the TF-MIP (Figure 1.1 C III).

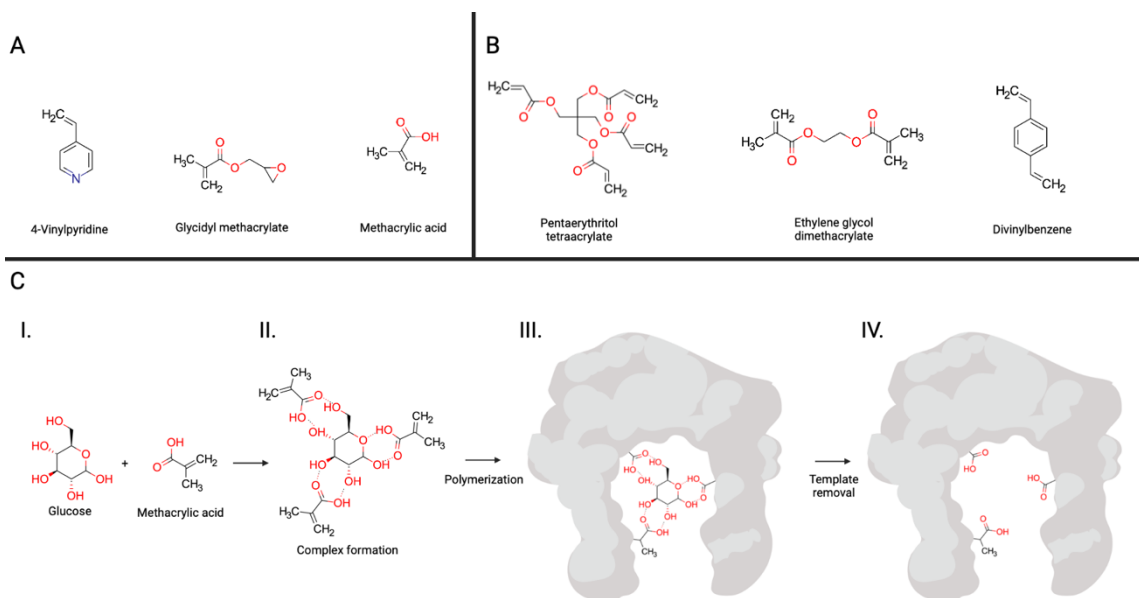


Figure 1.1. An overview of molecular imprinting technique and common reagents. A) Common functional monomers used in MIP monolith synthesis. B) Common biocompatible crosslinking agents used in MIP monolith synthesis. C) A stylized scheme of molecular imprinting glucose with methacrylic acid. Created with Biorender.com.

Molecular imprinting allows for enrichment of analytes through extraction into high affinity binding sites, but the films also have a large number of lower affinity, non-selective sites for adsorption of non-targeted analytes [16]. Depending on the chemistry of the polymer (namely the monomer, crosslinker, and porogenic solvent(s) used in preparation of the TF-MIPs), compounds within a specific polarity range will be enriched [15,17]. The enrichment of the targeted analyte or class allows for an analytical method less hindered by co-extracted matrix interferences as compared to a sample without a cleanup step. By employing TF-MIPs in complex biological samples, the need for complicated analytical methods and instruments may be diminished based on the performance of a particular TF-MIP for a specific set of analytes and the matrix of the sample [15]. This allows for more challenging or complex analyses to be carried out on cheaper, simpler, and more commonly available equipment, reducing the requirement for specialist staff to carry out tests in some cases.

#### 1.4 Convective Interaction Media®

Convective interaction media (CIM) are bulk polymerized short methacrylate monoliths developed through the joint project between the Czechoslovak Academy of Sciences in the Institute of Macromolecular Chemistry and the Institute of High Molecular Compounds in the Academy of Sciences of the USSR [4] and was commercialized by BIA Separations (Slovenia) in the early 2000s (BIA Separations has since been acquired by Sartorius). The methacrylate-based monoliths are cast using glycidyl methacrylate as the functional monomer. The glycidyl functional group allows

the monoliths to be further functionalized into an array of chemistries for different applications for reversed phase, ion exchange, bio-affinity and hydrophobic interaction chromatography (Figure 1.2) [4].

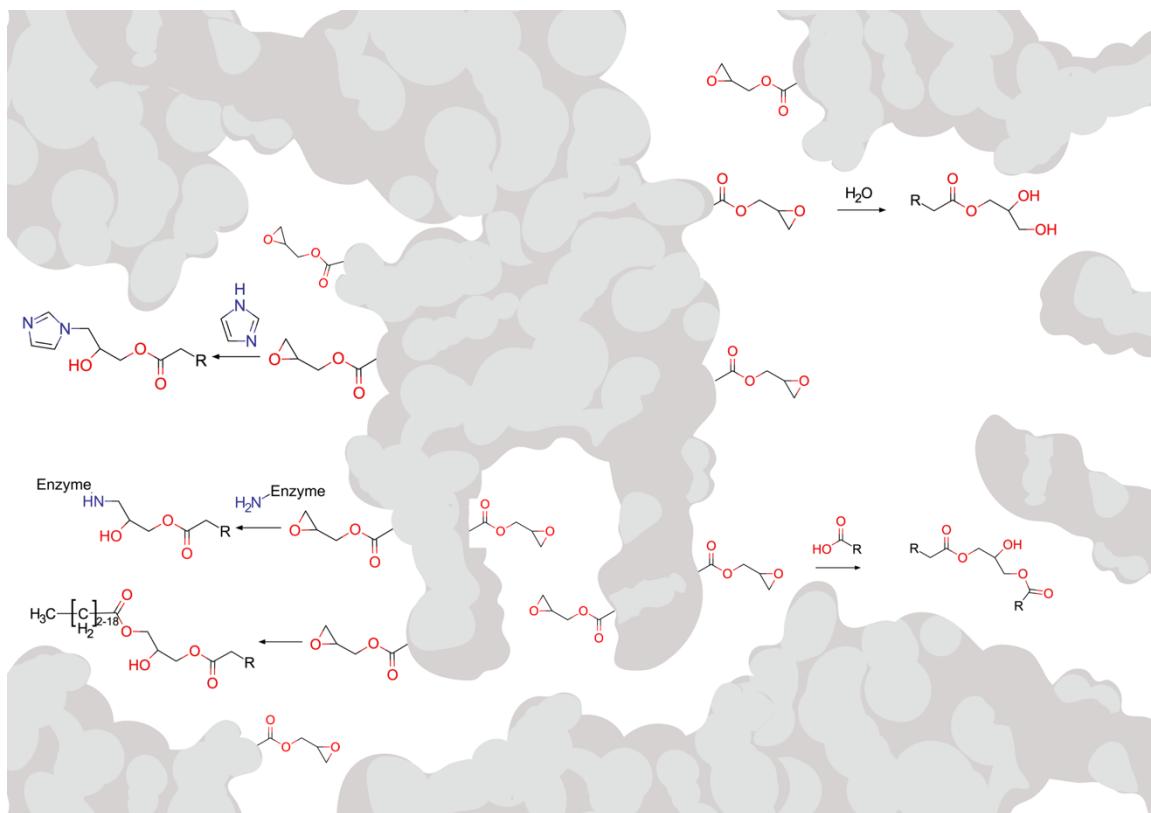


Figure 1.2: Stylized glycidyl methacrylate monolith demonstrating the post polymerization conversions of the epoxide group to useful column chemistries. The left side of the graphic shows imidazole functionalization (immobilized metal affinity chromatography for tagged proteins), enzyme linkage through a free amino group, and reversed phase linkers (for reverse phase chromatography) in descending order. The right side of the graphic shows the addition of water (for hydrophobic interaction chromatography), addition of amine (for strong anion exchange chromatography), and carboxylic acid coupling in descending order. Created with Biorender.com.

CIM columns have several practical advantages over traditional particle-based or membrane adsorption columns. Firstly, the columns utilize convective mass transport (CMT), which relies on the relatively large open pores in the monolith to rapidly move the mobile phase and analytes through the column, which is a useful attribute as diffusive mass transport into terminal pores is mass-dependent and with compounds of high molecular weight, this occurs very slowly [5,18,19]. Additionally, due to the open nature of monoliths, there are minimal shear or turbulent forces acting on the molecules as in the void volume between particle-based media (Figure 1.3A), or the layers of membrane in a stacked-membrane adsorber (Figure 1.3B). The discontinuous flow pathway of stacked-membrane adsorbers causes turbulent forces in the layers between sheets due to irregularity of pores. The highly porous surfaces of the monolith allow for a high binding capacity through convective mass transport (Figure 1.3C), while minimizing the effects observed in both particle-based and stacked-membrane approaches.

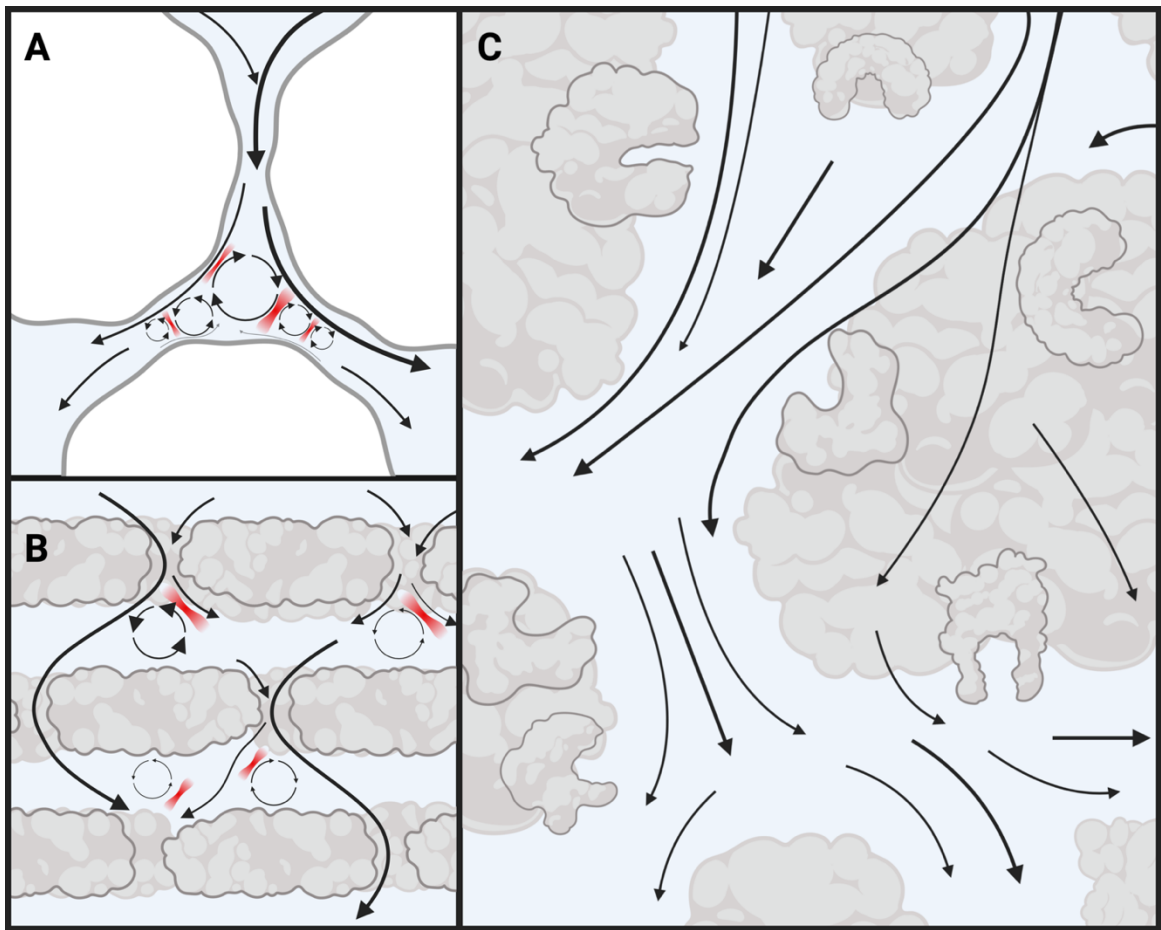


Figure 1.3: A) Traditional particle-based sorbent possessing dead volume between spherical particles. Points of shear stress as expected by counter-flow are indicated in red. B) Stacked membrane adsorber possessing dead volume between layers of membrane. Points of shear stress as expected by counter-flow are indicated in red. C) Methacrylate based monolith possessing large open pores allowing unrestricted and low-pressure flow of sample and mobile phase throughout the sorbent. Created with Biorender.com.

Most binding occurs on the surfaces of the monoliths which are highly porous in nature, with large open pores in the structure for unhindered flow of the sample (Figure 1.4) [18]. The combination of convective flow, in addition to both pore diffusion and film diffusion on the surface of the monoliths, are responsible for the binding of analytes. The binding capacity of these monoliths is quite high as compared to other similar chromatographic media, and the low backpressure due to the open pores allows these columns to be run at preparative and industrial scale with no loss of chromatographic performance. Specifically, it has been demonstrated that these monoliths possess chromatographic resolution and binding capacity that are unaffected by flow rates [1,20].

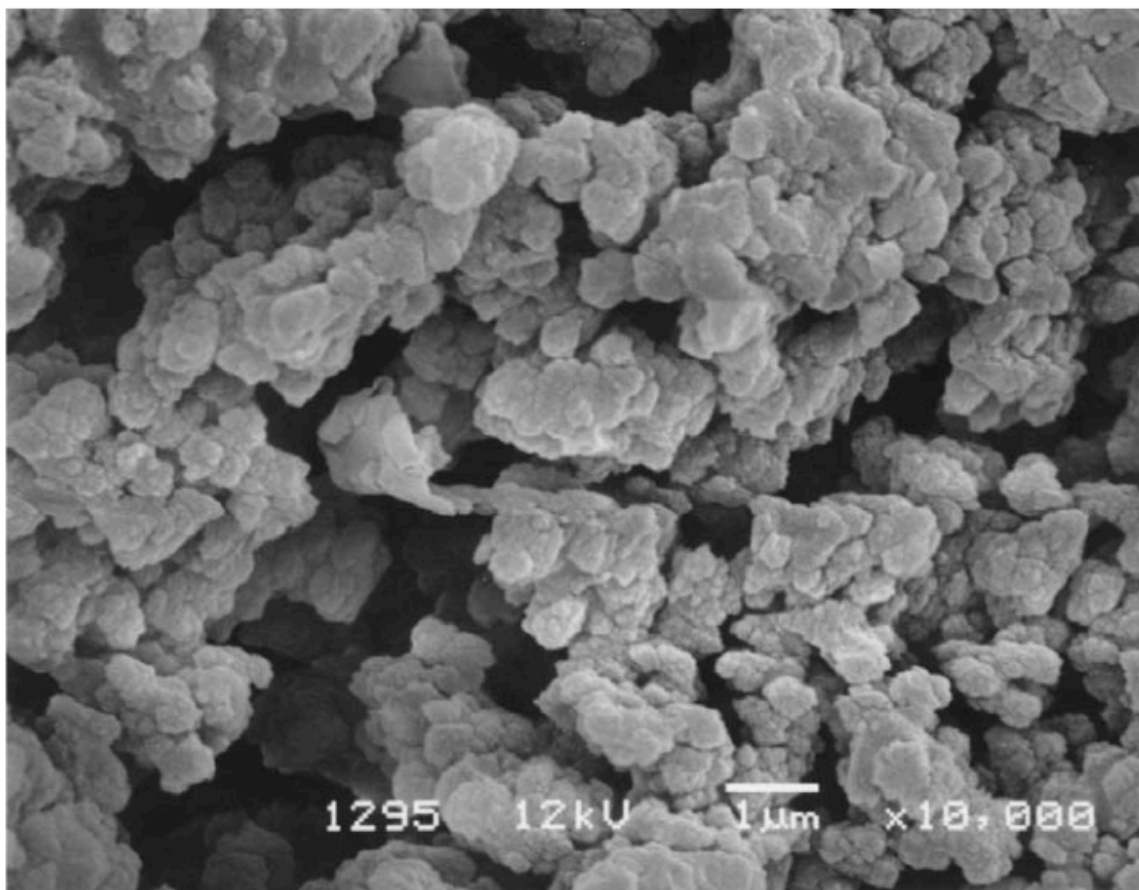


Figure 1.4: Scanning electron micrograph at X10,000 magnification of CIM monolith material. A highly porous material with a high surface is observed along with large, interconnected channels allowing for rapid and low-pressure flow of samples through the column. Image reproduced without modification, with permission from Sartorius (Ajdovscina, Slovenia), original image captured by Aleš Podgornik and Aleš Štrancar [19].

The van Deemter equation,  $HETP = A + \frac{B}{u} + C \times u$ , is a key component of traditional chromatographic theory and describes the relationship between flow rate and the “plate height” of a column with given dimensions (Figure 1.5) [21]. The equation contains a constant “multiple paths” ( $A$ ) term which accounts for the channeling obtained from non-ideal packing of the column, a “longitudinal diffusion” ( $\frac{B}{u}$ ) term which is flow rate dependent and exponentially decreases with increasing flow rate, and a “mass transfer” ( $C \times u$ ) term that considers resistance to mass transfer by the analyte between the mobile and stationary phases, and linearly increases with increasing flow rate. Traditional packed chromatographic beds will behave as the plotted example provided in Figure 1.5, where a clear minimum in the plate height is obtained at an optimal flow ( $u_{opt}$ ). At flow rates (linear velocity of the mobile phase) less than that of  $u_{opt}$  results in a rapid increase in plate height due to longitudinal diffusion becoming large at low flow rates. In contrast, at flow rates in excess of  $u_{opt}$  a gradual increase in plate height is observed, due to the increasing mass transfer resistance term as increasing flow rates make partitioning equilibrium harder to achieve. CMT is the most common process in monolithic columns, which allows for a nearly flat van Deemter curve eliminating upper limits of flow rate in the columns [22,23].



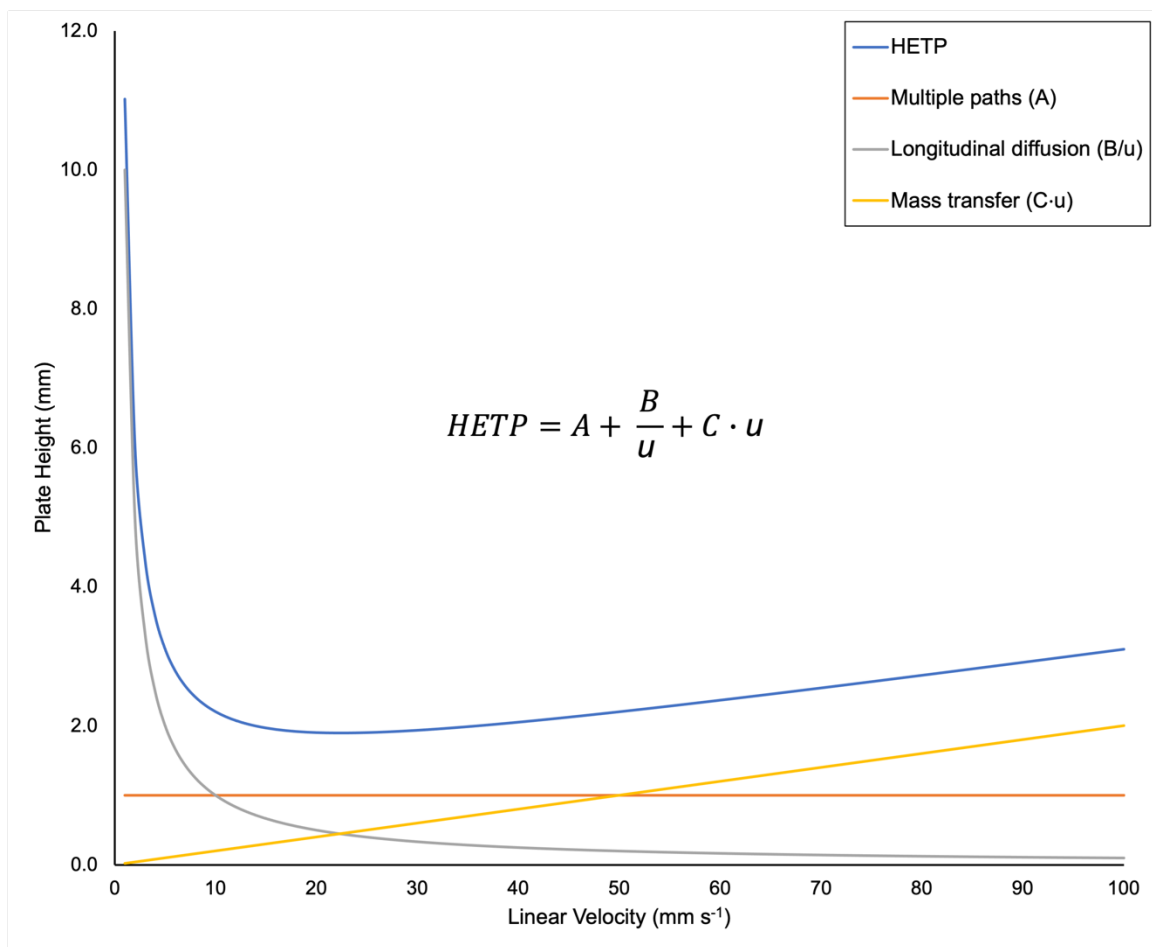


Figure 1.5. The van Deemter equation, and the relationship between each term for the following hypothetical conditions:  $A = 1.0$  mm;  $B = 10.0$  mm;  $C = 0.02$  mm s<sup>-1</sup> for  $u$  from 0-100 mm s<sup>-1</sup>

The porosity of the monoliths can be easily tailored by adjusting the ratio of monomer to porogenic solvent [19]. As porogens do not incorporate into the polymer, the volume of porogen is a direct way to estimate the void volume of the resulting pores [24,25]. The pore size distribution is an important factor in making reproducible devices [19]. The pore size is affected by the onset and kinetics of the phase separation process,

where monomers and crosslinkers begin to form chains in solution until they reach a length that precipitates from the porogenic solvent, forming the solid polymer [26]. The pore size is also affected by temperature which directly acts on reaction kinetics, solubility of the polymer and the viscosity and diffusion properties of the monomers to the growing polymer [27].

The properties that make monoliths attractive materials are their generally simple preparation [28], high porosity [29] and thus, surface area, which leads to a high capacity for binding various samples and compounds [30], as well as CMT [5]. CMT is more efficient for high molecular weight species, and convection-based flow through open pores have low shear stress and minimal turbulent flow experienced by the analytes. This is especially important for delicate biomolecules like proteins, enzymes, and antibodies where conformation imparted through non-covalent intramolecular interactions must be maintained to conserve activity of the molecule after purification. Due to the beneficial properties of monoliths, chromatographic monoliths continue to be an important type of chromatographic phase with applications ranging from small molecule separations to the largest supramolecular complexes and bioparticles like viruses and phages.

## 1.5 Analysis of Therapeutic Drugs in Biomatrices

### 1.5.1 Therapeutic Drug Monitoring

Advances in mass spectrometry (MS) have allowed for the growth of its use in routine clinical diagnostic testing over the past 20 years [31]. Mass spectrometers bring increased sensitivity and selectivity toward analytes of interest as compared to previously

dominant technologies such as spectrophotometry and enzyme-linked immunosorbent assays (ELISAs) [32,33]. Mass spectrometers are a staple in many clinical laboratories due to the increasing complexity of treatments and drugs and the associated responses from individual patients becoming more differentiated. Some cases can become very complex and therefore a single regimen for medicating all patients is no longer acceptable. In the era when mass spectrometers are in most clinical diagnostic facilities, we can employ them to carefully monitor therapeutic targets in each patient. This is the definition of personalized medicine, where we can employ individualized drug monitoring at very close timepoints to dose the patient at the appropriate level [34]. As many diseases are not standalone, meaning that a single disease may cause or lead to several co-morbidities, each patients' samples are very diverse and complex.

Human plasma is comprised of hundreds of compounds that can interfere in traditional analysis methods. The benefit of mass spectrometry related protocols is that analytes can be isolated from many of these interfering substances, either chromatographically before MS separation or in the MS itself.

#### 1.5.2 Metabolic variability and blood sample stability

The most prominent and important consideration when developing a method is sample stability [35]. There are several stability tests that can be performed to determine how long collected samples are stable under a certain set of conditions. The biggest risk to biological sample stability is the presence of reactive molecules and enzymes. Several enzymes are still active, even after collection and storage of blood samples, that can continue to convert or metabolize targets of interest into a number of metabolites. This

would lead to a change in the analytical result that would not accurately represent therapeutic levels in patients. Examples of these transformations are glucuronidation, acetylation, and methylation (Figure 1.6) [36]. Glucuronic acid can react with therapeutics converting it to a glucuronide, of which adducts can be very easily disturbed and therefore the amount of free drug can be changed. Glucuronides are sensitive to sample preparation and these metabolites can be converted back to the free drug. Alternatively, depending on the nature of the drug, we may decide to force all the bound compound to be freed from the protein by base hydrolysis, for example [37]. In this type of preparation, we can measure the total amount of a drug in the biological system. In addition, for a drug with liberal interconversion between free drug and metabolites, we may decide to measure both the free drug and the metabolite to obtain a better picture of the complete system. Some approaches have been to ensure the MS ionization parameters are harsh enough to quantitatively convert drug derivatives back into their parent compounds [38].

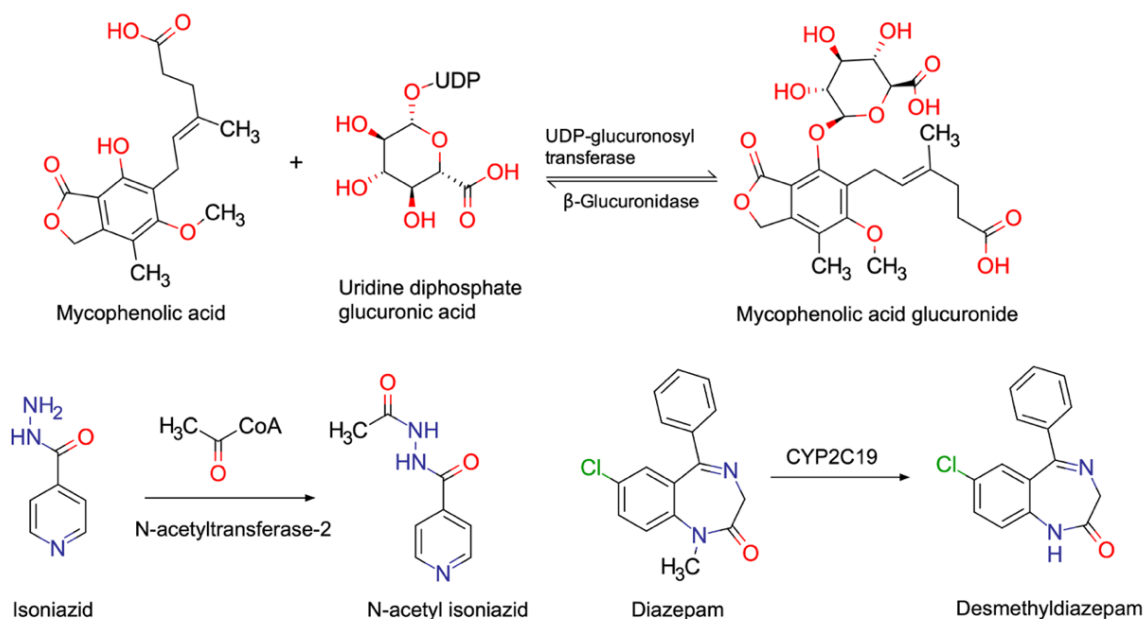


Figure 1.6: Metabolic transformations of the therapeutic drugs mycophenolic acid, isoniazid, and diazepam, demonstrating glucuronidation, acetylation, and methyl group cleavage (respectively) to pharmacologically important metabolites.

The most common way to store blood plasma is at  $-80\text{ }^\circ\text{C}$  and normally with the addition of an anticoagulant or preservative. At this temperature, enzyme activity is minimal, and the extreme temperature will slow any transformation processes that may occur. It is important to minimize freeze-thaw cycles as these temperature changes will negatively affect the quality of the plasma and the result. Each time the samples are thawed, the enzymatic activity increases, converting between forms of the therapeutics [33]. The anticoagulant choice could also influence the sample and drug stability. There are several different collection chemistries that can be employed, the most problematic of which are serum separator tubes (SST). These tubes contain a thixotropic polymeric gel,

normally including benzyldene sorbitol that acts as barrier allowing for centrifugal separation of serum from whole blood [39]. These gels have been reported to trap analytes such as tricyclic antidepressants and less polar antibiotics due to their hydrophobic nature therefore they are not suitable for all analyses [39–41].

### 1.5.3 Endogenous interferents

Matrix interferences are the impact of the sample matrix on a particular analysis. Matrix interferences can cause a number of issues related to analytical workflows including extraction, separation (normally chromatographic) and detection and normally result in an erroneous test result for a given analyte and can either over or under quantify the analyte in a given matrix. Endogenous components such as proteins can cause matrix interference through a variety of actions [33]. The main actions are binding of drugs to protein and proteins acting as a sorbent for the drugs. Due to the nature of the protein, a hydrophobic drug may become adsorbed onto the surface of the protein rather than staying in the aqueous saline buffer of blood. Proteins have a high surface area, with many sites for nonspecific interactions of drugs, as well as specific cavities that can bind drugs. Proteins may also precipitate on stationary phases during both sample preparation and analytical separations, which can reduce the efficiency of the preparation and analysis. Proteins can irreversibly bind to stationary phases, requiring their replacement at more frequent time intervals.

Lipids, due to their hydrophobic nature will interact with hydrophobic drug moieties. Lipids may form micelles in the solution that analytes can partition into. Surfactants act in a similar way as lipids toward the drugs and may cause reduction in

recoveries during sample preparation. There have been many strategies proposed for the removal of lipids including chromatographic separation [35], SPE cleanup, and liquid-liquid extraction [42].

Sugars and sugar derivatives can react with some drugs to form more polar adducts such as glucuronide derivatives previously discussed. Usually in MS analysis, the flow from the chromatographic front end is heated while being sprayed to cause a desolvation. Generally, to continue this process the orifice and the ion source block of the mass spectrometer are heated above 100 °C. At this temperature, sugars will burn on the cone and on the first lenses of the mass spectrometer which will quickly diminish the sensitivity of the instrument and can cause moderate to major damage to the instrument. Sugars and carbohydrates also have the tendency to act as ionization suppressors, therefore sufficient chromatographic separation of analytes from these highly polar compounds is required [35].

#### 1.5.4 Sample Preparation and Extraction of Therapeutic Drugs in Blood

The most common form of sample preparation in a clinical setting is a simple “dilute-and-shoot” methodology. This is where a volume of plasma is simply diluted with an organic solvent (normally acetonitrile). The resulting mixture is spun down in a centrifuge to pellet precipitated protein and other insoluble matrix components. The supernatant is then filtered and analyzed [33,43]. This method is quick, cheap, and easy; however, it suffers from a lack of preconcentration and in fact, dilutes the sample. The benefit of this method is that sample preparation is simple, and in most cases, does not usually affect the ratio of free to bound drugs. Several methods have been developed

based on this method, frequently using buffer, acid, base or incubation to optimize the performance [44].

SPE is a preferred method of sample treatment. In this method, a solid sorbent packed in a column is used to extract analytes of interest from a sample. This technique benefits from good preconcentration factors but the phases are expensive and are normally single use due to frequent fouling. SPE methods require several optimization steps including: breakthrough, loading and desorption volumes [33,44,45]. Developed SPE methods are specific to a chosen analyte and cannot be easily transferred to other classes of compounds. Several types of sorbents are available including normal phase (NP), such as bare silica, or reversed phase (RP), such as C<sub>18</sub>. Less popular types include cation and anion exchange resins and hydrophilic-lipophilic balance (HLB) resins.

Solid phase microextraction (SPME) has gained attention for its applications in biological samples [46–48]. SPME is a microfibre coated with a sorbent, normally a mixture of polystyrene/ divinylbenzene (PS-DVB), polyacrylonitrile (PAN), or poly(dimethyl)siloxane (PDMS). Due to the small size of the fibre, it is useful for sampling in very small volumes such as blood samples. SPME has an equilibrium-based quantification as compared to the exhaustive extraction in SPE. SPME is more influenced by matrix effects due to this sampling regime. The disadvantages of SPME are the high cost of each fibre and the requirement to reuse the fibres. SPME is also easily fouled in the biological matrix upon a single exposure which impairs reuse and subsequent performance. SPME has many drawbacks as compared to other emerging technologies that is likely to restrict widespread clinical adoption.



Analogous to SPME, TFME is a microextraction technique that employs a thin film of polymer (typically monolithic) cast onto a solid support. TFME devices generally have higher surface area of sorbent as compared to SPME and are more flexible in terms of polymer chemistry. TFME has proven to be a useful sample preparation technique for drugs in plasma when used in conjunction with mass spectrometry [49,50].

TFME can be used with an MS in two main ways: the first is solvent desorption where the analyte adsorbed on the film is desorbed into a suitable solvent for the analytical system (Figure 1.7). For acidic or basic molecules, a pH modifier may be added to aid in desorption. This is most commonly employed for liquid chromatography (LC) based applications but can also be used for gas chromatography (GC) with a less polar desorption solvent. The second approach is by directly coupling the thin films to a mass spectrometer, discussed in section 1.5.6.

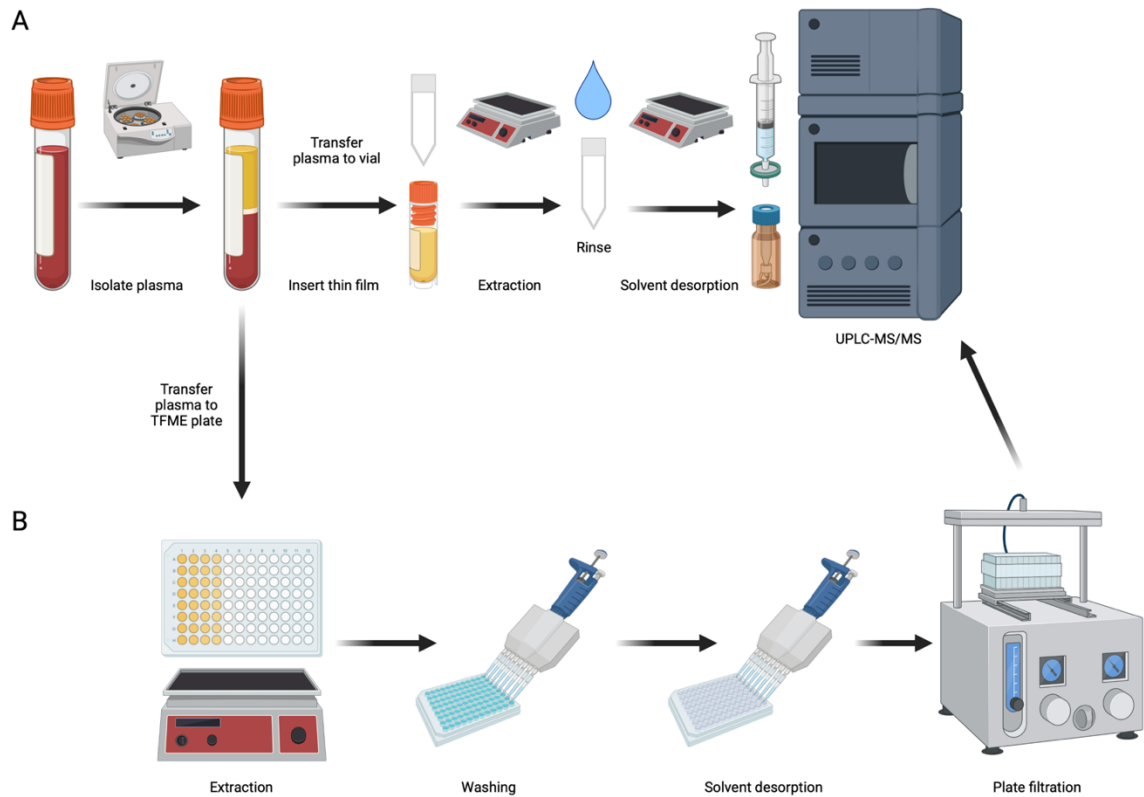


Figure 1.7: Blood sample workflow for analysis of plasma using thin films, followed by solvent desorption. A) TFME in coated-blade format used for individual sample processing of plasma in vial format. B) TFME in 96-well microplate format for high-throughput processing of many patient samples. Automation such as multichannel pipetting and 96-well filter plates allow for many samples to be processed simultaneously with minimal handling. The filtrate can be directly loaded into a plate and analyzed. Created with Biorender.com.

### 1.5.5 Measurement of Therapeutic Drugs Using Mass Spectrometry

The most common mass spectrometer in the clinical laboratory is the triple quadrupole (QqQ, or more generally MS/MS). Triple quads can isolate specific precursor ions from complex mixtures and matrices. Once the selected precursor ions are isolated, a collision energy (CE), generated through application of radio frequency (RF) potential is applied to the ions in a reaction cell containing collision gas, normally argon, which causes further fragmentation. Some of these fragments, or product ions, will break from the precursor ion in a very repeatable way, and in an abundance that can be used for quantitation at a desired concentration range. Other fragments are not as stable or abundant, and thus are typically used as qualifier ions. The main analytical approach to monitoring drugs in patient samples is by chromatographic separation before quantitation. Triple quadrupole mass spectrometers can be coupled to liquid chromatography systems (LC-MS/MS) and are the main workhorses of therapeutic drug monitoring labs [33,38,45,51–54]. As compared to their single quadrupole counterparts, triple quadrupoles are useful for separating and identifying ions of interest from complex samples and noisy backgrounds.

The main drawback of chromatographic separation is that it can be time consuming, requiring additional equipment and higher volumes of solvent as compared to MS methods alone. There has been recent interest on developing direct-coupling methods to the mass spectrometer [55–58]. In these techniques, an analyte would be desorbed via one of several methods directly into the mass spectrometer. The benefit is increased sample throughput and less complex equipment. This technique also can introduce the

entire extracted mass into the instrument, thereby offering detection limits far below the required clinical limits [59–61]. The design of the sorbent is very important for direct coupling as any co-extracted matrix interferences will also be desorbed and introduced into the MS.

#### 1.5.6 Direct Coupling of Extraction Devices to MS

There are a number of ways for direct sample introduction to MS, including direct analysis in real-time (DART) [62], desorption electrospray ionization (DESI) [63], coated blade, and paper spray. Coated blade spray (CBS) is a subcategory of TFME where solid substrate thin films made of a conductive material such as stainless steel can be directly coupled to MS. The dried blade, after extraction, is positioned in front of the cone of the mass spectrometer [55]. A high voltage is applied followed by a  $\mu\text{L}$ -scale addition of a suitable desorption solvent. Under the influence of an electric potential, the solvent will migrate toward the tip of the blade where a stream of droplets of the desorbed analyte solution is sprayed into the MS. The benefit of this type of coupling is that the analysis time is very short (15-30 s), and the entire extracted mass can be introduced into the MS. This allows for very low limits of detection (LODs) to be achieved with limited sample preparation.

Paper spray (PS) is a technique where a piece of filter paper acts as the electrospray ionization (ESI) emitter. Paper spray can directly couple dried blood spots to a mass spectrometer. Paper spray has several drawbacks such as being susceptible to matrix effects that can lead to rapid fouling of MS inlets [64]. In the past few years, commercial paper spray devices have allowed for preanalytical rinsing of the paper to elute some of

the interfering substances without introducing them into the orifice of the MS [65,66]. There have been several demonstrations of clinical application for PS-MS including generating pharmacokinetic curves, however reliable quantitative analysis is still a challenge using this technique [58,59].

## 1.6 Isolation of Macromolecules

Macromolecules are large molecules containing more than  $10^3$  atoms; the term was first coined in 1922 by Staudinger and Fritsch [67]. The IUPAC definition of macromolecules is “A molecule of high relative molecular mass, the structure of which essentially comprises the multiple repetition of units derived, actually or conceptually, from molecules of low relative molecular mass” [68]. The most common examples of biological macromolecules are the building blocks of life: nucleic acids (DNA and RNA), proteins and saccharides. In addition to these macromolecules, there is also a class of supramolecular assemblies in which several macromolecular subunits make up a larger superstructure through intermolecular interactions [69]. Examples of supramolecular assemblies important to life are structural element of viruses, cell membranes and walls, as well as multimeric proteins, enzymes, and antibodies. As both macromolecules and supramolecular assemblies are very large, traditional chromatographic theory and approaches rarely work effectively for their isolation. In recent years, much attention has been given to these molecules as a new era of therapies and treatments for several diseases. Examples of treatments that benefit from preparative monolithic purification are: mRNA for the COVID-19 vaccine [70], production of anti-VEGF for treatment of

macular degeneration [71], and production of interferon [72], which is used as a treatment for multiple sclerosis.

The first approaches to chromatographic sorbents for macromolecules were both cross-linked dextran [73] and modified cellulose columns [74], in the late 1950s, both of which are polysaccharide-based and targeted at the size-separation of proteins through sieving and buffer exchange/desalting. These phases are highly polar and exhibit significant swelling and shrinkage of the phase in addition to being susceptible to compression and deformation. These drawbacks led to the development of more rigid phases such as modified silica [75] and vinyl polymer gels [76]. These superior phases were more rigid and thus more resistant to the pitfalls of the carbohydrate columns preceding them. Due to the rigidity of the particles, particle size could be reduced, thus increasing the surface area and efficiency of the columns. This allowed for macromolecular separations that would have regularly taken several hours to be achieved in less than an hour [19].

Although the more rigid stationary phases were much improved over the first generation of macromolecular purification columns, there was still a major barrier to increasing efficiency of the separations- the mass transfer. In these phases, mass transfer occurs in pores of the particles where the velocity of the mobile phase is close to zero. The relationship between mass transfer and molecular weight is inversely proportional, thus for macromolecules, mass transfer is very low [19].

A unique solution to the issue of low mass transfer is to utilize convective mass transport (CMT) [77]. Mass transfer occurs in terminal pores, which are single, narrow

openings that do not allow a continuous flow and the mobile phase flow in these pores is nearly stagnant. In contrast, CMT occurs in open pores, which are tubular openings with a 3D structure that have defined ends and usually consist of a highly interconnected network of pores. In open pores, mobile phase flow has a much higher relative velocity than in terminal pores [77]. The first application of a hybrid particle with both properties of conventional chromatographic particles in addition to introduction of CMT through open channels created by pores in the particle was perfusion particles, in 1990 [78]. Perfusion particles possess open pores where mobile phase and analytes flow through in addition to terminal pores which allow for an increase in total surface area (Figure 1.8) [19]. The benefit of open pores and terminal pores in the same particle is an overall reduction in backpressure and an increase in flow rate of sample through the particles. Due to the high number of open pores, even particles with a smaller diameter of 2-3  $\mu\text{m}$  do not suffer from a high backpressure as compared to a similar sized non-porous particle, which is a benefit to increase overall surface area without affecting backpressure, in addition to minimal loss in capacity even at much higher flow rates [79]. The main drawback of any packed-particle stationary phase is that there is a turbulent void between particles and even with reduced particle diameter, the void volume is still significant. These effects also cause more mobile phase to flow around the particles, rather than through the pores, resulting in less convective mass transfer [80].

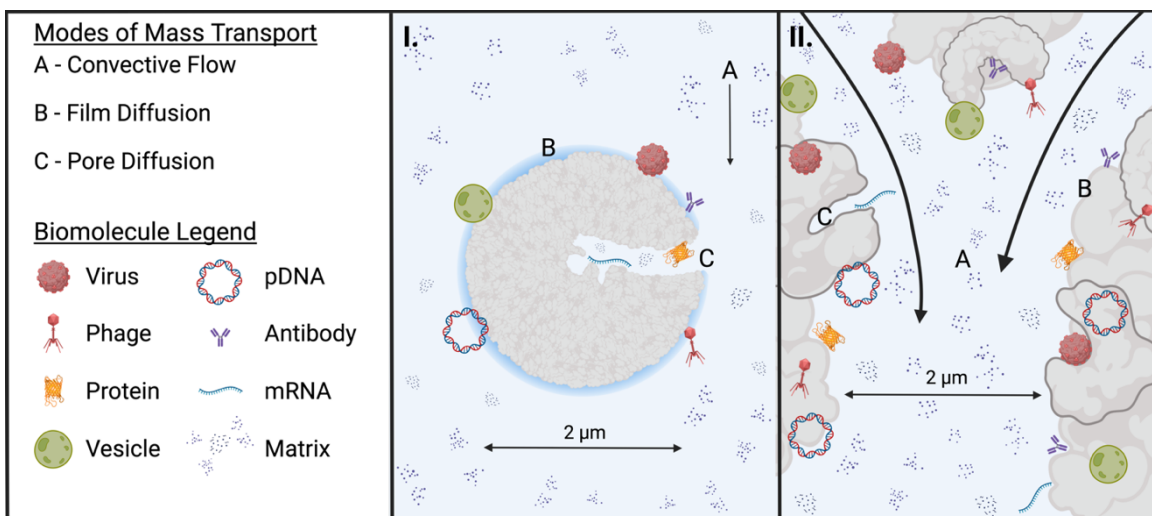


Figure 1.8: Comparison of modes of mass transport in porous particle media and monolithic stationary phases: convective flow (A) around the particle and through the channels, film diffusion (B) in a microlayer around the sorbent surface, and pore diffusion (C) in the terminal pores. I) Porous particle highlighting the three modes of sorption onto particle surfaces. II) CIM monolith possessing a 2  $\mu\text{m}$  open channel in which large analytes will bind to the surface through convective mass transfer. Image reproduced with modification, with permission from Sartorius (Ajdovscina, Slovenia), original image produced by Pete Gagnon. Created with Biorender.com.

Membranes - defined by IUPAC as “a continuous layer, usually consisting of a semi-permeable material, with controlled permeability, covering a structure” [68], were the next solution to overcome the issue of the void volume between porous particles in perfusion chromatography. Membranes exhibit exemplary hydrodynamic properties as mobile phases can be passed both over (tangential flow) and through them with negligible back pressure and other beneficial hydrodynamic properties in addition to negative



chromatographic effects such as significant peak broadening [81]. The main drawback of membranes is the low capacity for analytes due to a very low surface area; sometimes stacking of several membranes is used to increase capacity, though still with a much lower capacity than packed bed columns of similar dimensions [82].

Although these techniques were powerful, and sometimes still used in niche applications, the multitude of drawbacks and the negative chromatographic effects, especially when scaling these technologies up to preparative scale have hindered their widespread use in industry. The most revolutionary technology in the field of macromolecule purification in the past 30 years are monolithic columns. Monoliths have been coined “the fourth generation of chromatographic sorbents” for biopolymers [1]. Monoliths have rapidly become the leading technology for macromolecule purification and have an ideal array of positive chromatographic behaviours, high capacity, reusability, and easy scalability. These applications underline how important both macromolecular chromatography and specifically, monoliths, have and will be in this era of medicine and biotechnology.

## 1.7 Research goals

In this thesis work, the use of methacrylate-co-ethylene glycol dimethacrylate monoliths for the extraction and chromatographic separation of molecules in biological matrices is explored. In Chapters 2 and 3, molecularly imprinted monolithic thin films for analysis of therapeutic drugs in human plasma were developed. The compatibility of

these devices in several blood pathologies was studied yielding an extraction method that is reliable, efficient, and easy to employ for therapeutic drug monitoring.

In Chapter 2, I designed a TF-MIP for the extraction of MPA from human plasma, using a monolith coated stainless steel blade. These coated blades could be used as extraction devices in 700- $\mu$ L of plasma, and with subsequent washing and solvent desorption, could effectively extract MPA from plasma with an imprinting factor greater than one.

In Chapter 3, I sought to develop a TF-MIP for the extraction of a representative group of tyrosine kinase inhibitors (TKIs). I selected TKIs with varying polarities and pKa across the spectrum of therapeutics in this class to demonstrate the broad applicability of my developed MIP for TDM of TKIs in plasma. I developed the devices in 96-well plates allowing for high-throughput analysis of these drugs in plasma. The 96-well format allowed for easy and rapid sample processing with minimal input required from a technician.

In Chapter 4, I used commercially available preparative monolithic columns to isolate gene transfer agent (GTA) particles from *Rhodobacter capsulatus* cultures. I employed a 2-step chromatographic approach with a first separation employing hydrophobic interaction chromatography (-OH functionalized monolith) to capture the particles, followed by separation using a strong anion exchange column (-quaternary amine functionalized monolith) which allowed for polishing of the crude particle extract, as well as on-column buffer exchange required to elute the particles in a buffer that would support activity of the functional GTA particles. I optimized the process starting from

culture conditions and media selection, through chromatographic gradient design and validated the method using both nanoparticle tracking analysis (NS-300), SDS-polyacrylamide gel electrophoresis and bioassays to measure gene transfer activity the isolated particles.

In Chapter 5, I present preliminary data on directly coupling monolithic extraction devices to MS. Custom source interfaces were developed and presented for CBS-MS on both the benchtop Xevo TQ-S and the handheld MX908. Various data are presented employing both CBS-MS and thermal desorption from MIP mesh for measurement of drugs of abuse, mycophenolic acid, and organophosphorus pesticides in various matrices. A discussion on limitations and future of the presented devices and systems is provided.

Overall, various techniques using methacrylate-based monoliths were used to isolate both small and large molecules from biological matrices. As these materials are becoming an important part of modern biotechnology and pharmaceutical processes, developing new applications and methods is important. I have obtained a wide array of experience in both preparing monolithic thin films, with and without molecular imprinting, in addition to employing commercial columns for preparative monolithic chromatography and coupling of extraction devices directly to MS.

## **2 Development and application of a thin-film molecularly imprinted polymer for the measurement of mycophenolic acid in human plasma**

### 2.1 Introduction

Mycophenolic acid (MPA) is a small-molecule pharmaceutical used as an immunosuppressant during stem cell [83] and organ transplantation [84], most commonly administered after kidney transplantation as an anti-rejection agent. MPA acts by inhibiting inosine monophosphate dehydrogenase which prevents synthesis of guanosine which in turn quells production of DNA and proliferation of T- and B-lymphocytes [85]. Since 1995, MPA has been widely adopted as the anti-rejection drug of choice for organ transplants [84]. Pharmacokinetic and pharmacodynamic variabilities for an individual patient, and between patients, continue to present challenges for optimal dosing [86]. The observed variability can be attributed to a number of factors, including drug interactions, kidney and liver function, and disease status [87].

The pharmacokinetics are complex; enterohepatic recirculation leads to serum concentration increases for 8-12 h after administration, followed by a rapid decrease in concentration as the drug is metabolized [88]. Over the course of recovery from renal transplant, the bioavailability of MPA steadily increases as renal function is re-established [89]. The plasma concentration in the early stages of recovery can vary in an individual by as much as a factor of four, leading to dosing challenges [31,90]. Side effects from high doses of MPA, which can be mitigated by reducing the dosage to the minimum

effective concentration, are abdominal pain, diarrhea and nausea, among others [90,91]. Additionally, longer term overdosage of MPA can lead to several physiological and hematologic conditions, including the possibility of opportunistic pathogen and viral infections as well as significant damage to both the renal system and heart [92,93]. Therapeutic drug monitoring (TDM) of MPA has previously been employed when graft deterioration and compliance issues are a concern, however logistical and method limitations are barriers to widespread TDM [94]. Nevertheless, TDM for MPA has been previously reported using LC-MS [95–99] using common sample preparation methods, including protein precipitation [96–98], solid phase extraction [96,100], on-line microdialysis [99] or ultrafiltration [97,98]. These approaches are largely manual, time consuming, and often require large volumes of plasma. Alternative micro-extraction methods are promising for TDM [101]. One previous study reported a carbowax/templates resin SPME method with HPLC-UV detection for the measurement of MPA in human serum [102].

Of the micro-extraction methods, TFME has been employed most often for environmental samples [103,104], with additional sensitivity and specificity imparted through incorporation of molecular imprinting [105–107]. Recently, this approach has been extended to biological samples [108]. By introducing molecular imprinting into polymers used in TFME (MIP-TFME) we can add another mode of selectivity to polymeric sorbents [14,15]. MIPs are prepared by polymerization in the presence of a template molecule with functionality and shape similar to the analyte to form selective

cavities in the polymer that are conserved once the template is removed. This selectivity allows for development of highly efficient extraction materials suitable for use in TDM.

Herein, a new method based on a TF-MIP device is presented for the extraction and analysis of mycophenolic acid in human plasma. The process is time and resource efficient and capable of accurately quantifying MPA small volumes of plasma (e.g. 35  $\mu\text{L}$ ).

## 2.2 Methods

### 2.2.1 Reagents and Materials

All chemicals and reagents were purchased from Sigma-Aldrich (Oakville, ON, Canada), were of reagent grade or higher, and were used without further purification unless otherwise noted. LC-MS solvents were purchased from Fisher Scientific (Whitby, ON, Canada). Ultrapure water was made in-house using a Millipore Milli-Q water system (resistivity  $\geq 18.2 \text{ M}\Omega \text{ cm}^{-1}$ ). Both ethylene glycol dimethacrylate (EGDMA) and 4-vinylpyridine (4-VP) were passed through gravity columns of basic aluminum oxide (Brockmann-type I, 50-200  $\mu\text{m}$ , 60  $\text{\AA}$ ), to remove polymerization inhibitors; purified products were used within 3 h of purification. A pH 3.0 phosphate buffer was prepared according to the European Pharmacopeia 5.0. In short, 12.0 g of anhydrous sodium dihydrogen phosphate was dissolved in 700 mL ultrapure water. The pH was adjusted by dropwise addition, with stirring, of 10% v/v phosphoric acid in water to a final pH of 3.0. The solution was finally diluted to a final volume of 1.0 L and the pH was checked again to confirm the final pH of 3.0 was maintained.

## 2.2.2 Instrumentation and Operating Conditions

The separation and quantification of mycophenolic acid was performed using an Acquity ultra performance liquid chromatograph (UPLC) and a Xevo TQ-S triple quadrupole mass spectrometer (Waters Corporation, Milford, Massachusetts, USA ) operated in positive ionization mode equipped with an electrospray ionization (ESI) source. Chromatographic separations were carried out using an Acquity BEH-C<sub>18</sub> column (2.1 × 50 mm, 1.7 μm) maintained at 30.0 °C. Isocratic elution consisted of 40% water and 60% acetonitrile both with 0.1% formic acid at a flow rate of 0.5 mL min<sup>-1</sup>. The runtime of the method was 1.8 min and the retention time of MPA was 1.13 ± 0.02 min. The mass spectrometer was operated in multiple reaction monitoring (MRM) mode monitoring two transitions (Table 2.1) that were identified by infusion of a 50 ng mL<sup>-1</sup> solution of MPA into the mass spectrometer using the IntelliStart software (Waters Corp.) and confirmed as previously reported [109]. Extracted samples were stored in polypropylene vials (700 μL) at 4 °C in the autosampler (SM-FTN, Waters Corp.) prior to analysis.

Table 2.1. MRM transitions and mass spectrometer settings.

Precursor Ion (m/z)	Product Ion (m/z)	Dwell Time (s)	Cone Voltage (V)	Collision energy (eV)
321.1	159.0	0.100	14	30
321.1	207.0	0.100	14	22

### 2.2.3 Preparation of Extraction Devices

Extraction devices were prepared by drop-casting an aliquot of an optimized mixture of polymer components made with 5 mmol (905  $\mu\text{L}$ ) EGDMA (cross linker), 1 mmol (106  $\mu\text{L}$ ) 4-VP (functional monomer), 0.25 mmol (108 mg) mycophenolate mofetil (template), 0.06 mmol (16 mg) 2,2-dimethoxy-2-phenylacetophenone (initiator), 2.5 mmol (130  $\mu\text{L}$ ) acetonitrile (porogen), and 8.3 mmol (1300  $\mu\text{L}$ ) 1-octanol (porogen). The solution was sonicated to dissolve the components and to degas the mixture. The solution was prepared fresh each time films were to be made. A 3.0  $\mu\text{L}$  aliquot of the solution was drop-casted between a stainless-steel blade ( $0.5 \times 2$  cm) and a microscope cover slide, and then exposed to UV light (254 nm) for 20 min to induce polymerization as previously reported [108,110]. The cover slides were gently removed from the resulting films, which were subsequently washed with methanol until no template could be detected in a blank extraction using a subset of devices from each batch. Methanol, a protic solvent, disrupts hydrogen bonding between the template molecule and the polymer, allowing for template removal.

### 2.2.4 Molecularly Imprinted Polymer Extraction of Plasma

Plasma pH was adjusted by adding 0.1 M phosphate buffer pH 3.0 to a final volume of 30% v/v. Conical vials (700  $\mu\text{L}$ , polypropylene) were used for extraction of MPA from plasma. Seven hundred  $\mu\text{L}$  of pH adjusted plasma (blank, patient samples, or spiked for method development) was added to the conical vial, followed by the MIP-TFME device. Agitation to assist extraction was applied using a multi-tube vortex at 1000 rev  $\text{min}^{-1}$ . After a 30 min extraction, the MIP thin film was washed with 5.0 mL of



ultrapure water to remove residual sample matrix components. The MPA was desorbed from the MIP devices using 700  $\mu\text{L}$  of 90% acetonitrile, 9.9% water and 0.1% formic acid in a conical vial vortex mixed at 1000  $\text{rev min}^{-1}$  for 2 min. Following desorption, MIP thin films were removed from the vial and the solution was syringe filtered (0.20  $\mu\text{m}$ , 4 mm, polyethersulfone) before analysis by LC-MS/MS.

### 2.2.5 Patient Samples and Demographics

Plasma from three patients who were prescribed MPA was purchased from BioIVT (Hicksville, NY, USA). All samples were provided as 3.5 mL isolated plasma which was shipped at  $-78\text{ }^{\circ}\text{C}$  on dry ice, stored at  $-20\text{ }^{\circ}\text{C}$  until use and thawed at  $4\text{ }^{\circ}\text{C}$  for 1 h prior to use. Patient 1 was a 68-year-old Caucasian male diagnosed with myelofibrosis, type 2 diabetes, and hypothyroidism. Patient 1 was prescribed 500 mg mycophenolate mofetil *qd*. Patient 2 was a 52-year-old Hispanic male diagnosed with end-stage renal disease. Patient 2 was prescribed 180 mg mycophenolate sodium *qd*. Patient 3 was a 48-year-old female of undisclosed race diagnosed with end stage renal disease, hyperparathyroidism, vitamin D deficiency, hypertension, and glomerulonephritis. Patient 3 was prescribed 360 mg mycophenolate sodium *qd*. Patient demographics and prescribed drugs can be found in Table 2.2.

Table 2.2. Patient information

<b>Patient</b>	<b>1</b>	<b>2</b>	<b>3</b>
<b>Anticoagulant</b>	Sodium heparin	Dipotassium EDTA	Dipotassium EDTA
<b>Gender</b>	Male	Male	Female
<b>Age</b>	68	52	48
<b>Ethnicity</b>	Caucasian	Hispanic	Other
<b>Diagnosis</b>	Myelofibrosis  Type 2 diabetes  Hypothyroidism	End stage renal  disease	End stage renal disease  Hyperparathyroidism  Vitamin D deficiency  Hypertension  Glomerulonephritis
<b>Medications</b>	Actos 30 mg  Aricept 5 mg  Aspirin 81 mg  <b>Cellcept 500 mg</b> <b>(mycophenolate</b> <b>mofetil)</b>  Lyrica 50 mg  Metformin 500 mg  Namenda 5 mg  Plavix 75 mg  Prednisone 10 mg  Ramipril 5 mg  Synthroid 125 µg	Amlodipine 10 mg  Atorvastatin 40 mg  Epogen 300 units  Humalog 8 units  Lantus 50 units  <b>Myfortic 180 mg</b> <b>(mycophenolate</b> <b>sodium)</b>  Prograf 1 mg	Lisinopril 5 mg  Lovastatin 40 mg  Furosemide 40 mg  <b>Myfortic 360 mg</b> <b>(mycophenolate</b> <b>sodium)</b>  Tacrolimus 10 mg  Norvasc 10 mg  Omeprazole 20 mg  Prednisone 5 mg  Prograf 1 mg  Rocaltrol 0.25 µg

## 2.3 Results

### 2.3.1 Formula Development

Mycophenolate mofetil, a morpholinyl ethyl ester and pro-drug of MPA [111], was selected as the template due to its similarity to MPA and commercial availability. A functional monomer that can act as a proton acceptor, 4-VP, was selected given the acidic nature of MPA and crosslinked with EGDMA for its appreciable biocompatibility when polymerized [112]. The porogen (porogenic solvent) was optimized by screening several solvents that are commonly used in preparing MIPs in biological applications including: 1-octanol, octanoic acid, diethylene glycol, diethylene glycol diethyl ether, ethylene glycol, methanol, acetonitrile, 1-butanol, 1-pentanol, 1,4-pentanediol (data not shown). Porogens were only considered if the template molecule, mycophenolate mofetil was soluble, then from the porogens that allowed dissolution of mycophenolate mofetil, experiments were carried out to identify the most mechanically stable film. The optimal solvent in terms of film stability was 1-octanol. This produced a film with excellent mechanical stability sufficient to limit polymer erosion during rapid agitation and physical manipulation of the MIP-TFME devices in the extraction process. The porogen solvent system was modified with 10% v/v acetonitrile required to solubilize mycophenolate mofetil. Due to the crucial role in formation of a porous sorbent, porogen loading is one of the most important factors to optimize when developing thin film MIPs.

Experiments to determine the optimal volume of porogen in the polymer components solution (Figure 2.1) demonstrate how subtle changes in porogen loading can lead to significant changes in adsorption behavior. Similar phenomena for similar MIPs

have been previously reported [110]. The highest total MPA recovery was obtained with the formula with 1430  $\mu\text{L}$ , which corresponds to the lowest concentration of polymer components in the series but resulted in a film with superior mechanical stability as compared to lower porogen volume candidates. Increasing the amount of porogen relative to the polymer components led to a dramatic decrease in recovery for the non-imprinted polymer (NIP) and a general increase in variability between devices. This is likely due to the increased fraction of porogen, as compared to the MIP that likely influences when phase separation occurs. The variability improves with increased volume of porogenic solvent for the MIP. Ultimately, this led us to select the 1430  $\mu\text{L}$  formula, which also revealed the greatest imprinting factor (IF 6.04) and MPA recovery. The total volume of porogen in the final formula is 1300  $\mu\text{L}$  1-octanol and 130  $\mu\text{L}$  acetonitrile.

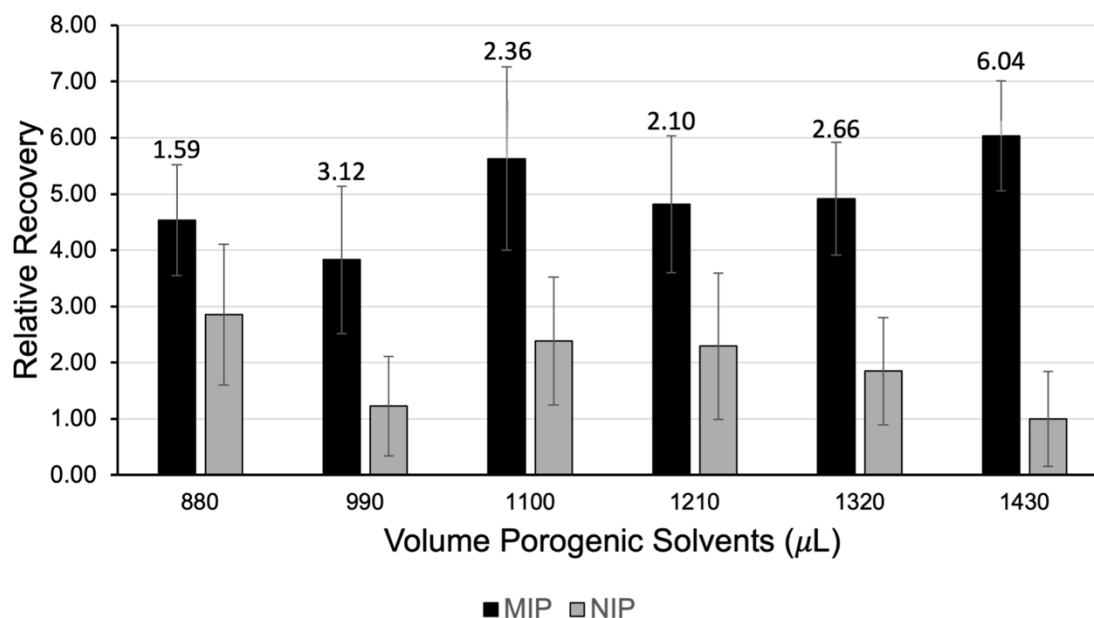


Figure 2.1. Relationship between porogen volume, relative recovery of MIP and NIP extractions of  $50 \text{ ng mL}^{-1}$  mycophenolic acid in plasma, and imprinting factor of imprinted polymers as compared to non-imprinted polymers. Imprinting factors are shown as data labels above the MIP bars for the respective MIP/NIP pair. Data is normalized to the lowest-performing NIP ( $1430 \mu\text{L}$ ). Error bars  $\pm\text{SD}$  ( $n=3$ ).

### 2.3.2 Optimization of the Desorption Conditions

Quantitative desorption from the sorbent is required for a reliable analytical method. Various solvent systems and desorption times were studied to determine the optimum desorption conditions. Acetonitrile (ACN), methanol (MeOH), water, and formic acid (FA) in various mixtures were chosen as potential candidates for the desorption solvent, due to their compatibility with the chromatographic separation (Figure 2.2A). From this data, it can be observed that the highest desorbed recovery was

achieved using a solvent system consisting of 90% ACN, 9.9% water and 0.1% FA.

Another factor in selecting ACN, as opposed to MeOH, as the organic component to the desorption solvent as it was more compatible with the LC solvent system, yielding narrower, more symmetrical peaks.

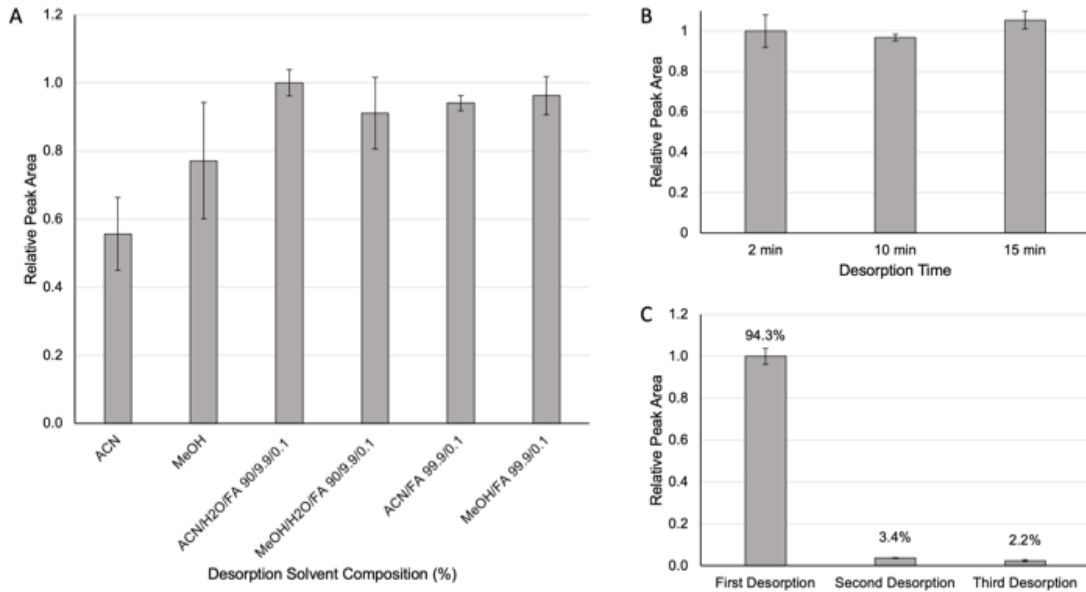


Figure 2.2 A. Comparison of relative recovery of MIP extraction of 50 ng mL<sup>-1</sup> mycophenolic acid in plasma with different desorption solvents. The relative peak area is relative to the final selected conditions (ACN/H<sub>2</sub>O/FA 90/9.9/0.1). B. Comparison of desorption time of MIP extraction of 50 ng mL<sup>-1</sup> mycophenolic acid in plasma with 90% acetonitrile, 9.9% water, 0.1% formic acid. Relative peak area is relative to the final selected desorption time (2 minute). C. Sequential two-min desorptions of MPA extracted by MIP-TFME from 50 ng mL<sup>-1</sup> mycophenolic acid in plasma. Desorption solvent: 90:10 acetonitrile: 0.1% aqueous formic acid. Error bars  $\pm$ SD (n=3).

The desorption time was studied to determine the minimal time required to extract the majority of the MPA from the film. Desorption times of 2-, 10- and 15 min were tested (Figure 2.2B). These times were selected based on initial screening that showed that the desorption process with selected solvent was quite fast. No significant difference between the desorption times tested were observed, where both 10- and 15 min desorptions were yielding the same recovery compared that a two-min desorption. The high observed variability in standard deviation (SD) is expected because three individual devices were used for each condition, thus contributing to the presented error due to inter-device variability. In conclusion, a single, two-min desorption with 90% acetonitrile, 9.9% water and 0.1% formic acid is used to quantitatively desorb the extracted MPA from the thin films.

It was then investigated if a single 2 min desorption could recover the majority of the extracted mass (Figure 2.2C). Nearly 95% of the extracted mass is recovered in the first desorption while 3.4% and 2.2% are recovered during second and third desorptions, respectively.

### 2.3.3 Optimization of Extraction Conditions

The pH of the sample during extraction can have a significant impact on the extraction efficiency mainly due to the ionization of labile protons ( $pK_a$ ). As MPA is neutral in its protonated form ( $pH < pK_a$ ), reducing the plasma pH will convert more MPA to its neutral form, which is favored for adsorption to the thin film. We compared unadjusted plasma, plasma supplemented with 0.1× PBS pH 7.4 (10% v/v), and plasma with varying amounts (10-40% v/v) of a 0.1 M pH 3.0 phosphate buffer (Figure 2.3).

When increasing amounts of pH 3.0 phosphate buffer are added to the plasma, a marked increase in total MPA recovery was observed, whereas recovery was slightly reduced with addition of PBS (pH 7.4). The increased recovery due to sample acidification was as high as 10× relative to unadjusted samples, which demonstrates the need for pH adjustment in the plasma samples as a pre-treatment before extraction. Although addition of 40 mM concentration led to the highest apparent recovery, the increased inter-sample variability is a demerit and meant that the recovery was not statistically different than adjustment with 30 mM PB pH 3.0. A final concentration of 30 mM PB pH 3.0 was selected with 19.4% recovery relative to 2.2% for the unadjusted samples. Adjusting the PB concentration above 40 mM is impractical due to excessive dilution of the sample and concentrations greater than 0.1 M PB required to dilute the plasma may cause precipitation of blood plasma components, resulting in reduction of analyte recovery. The dilution of plasma samples is considered mathematically when calculating the plasma concentration. As this is an equilibrium-based extraction regime, we do not expect 100% recovery, and thus the obtained percent recoveries presented as data labels in Figure 2.3 are sufficient to obtain the required clinical lower limits of quantification for the method.



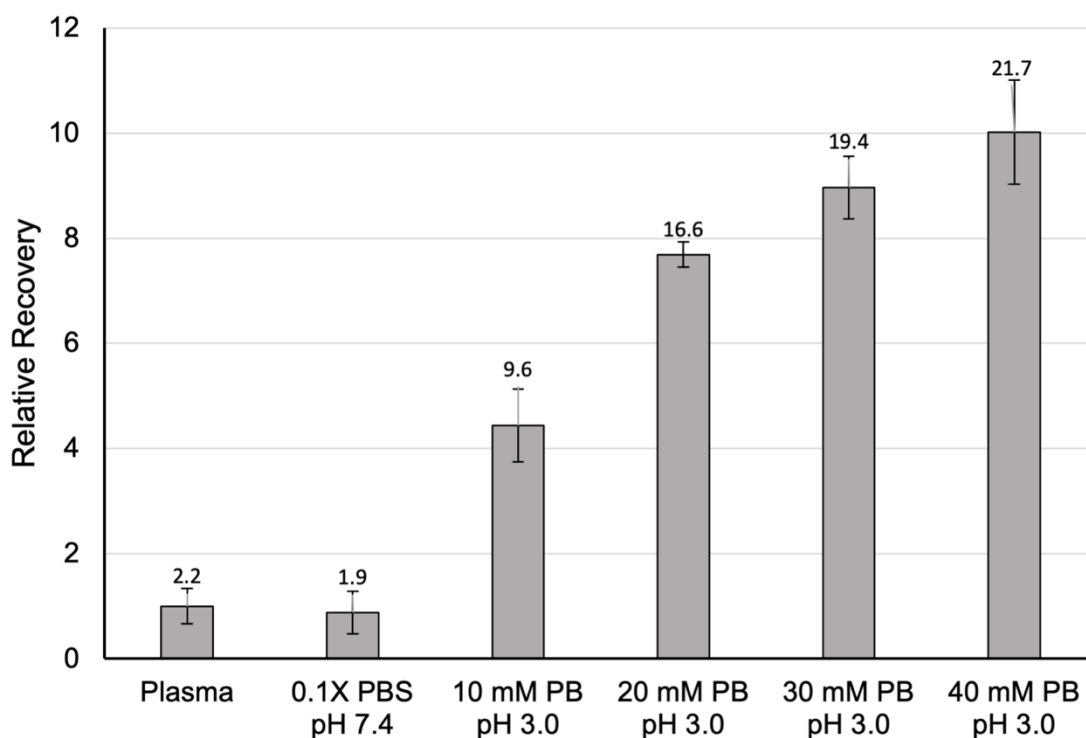


Figure 2.3. Comparison of relative recovery of MIP extraction of  $50 \text{ ng mL}^{-1}$  mycophenolic acid in plasma, and with addition of phosphate buffer solution (PBS).  $0.1 \times$  PBS pH 7.4 contains the following: 13.7 mM NaCl, 0.27 mM KCl, 1.0 mM  $\text{Na}_2\text{HPO}_4$ , and 0.18 mM  $\text{KH}_2\text{PO}_4$ . Relative recovery to unadjusted plasma. Data labels are % recovery, error bars  $\pm$ SD (n=3).

#### 2.3.4 Optimization of Extraction Time and Extraction Linearity

To determine optimal extraction time, an extraction time profile was generated that compared the MIP extractions, NIP extractions, and imprinting factor at varying time points (Figure 2.4). We observe a significant imprinting effect from the MIP at early time points, with the NIP lagging in initial extraction rate. From the observed trends, 30 min

extractions were selected as they had relatively high recovery but were still rapid enough not to be logistically limiting in the laboratory when processing many samples in parallel. This timepoint also appears to be nearly equilibrium for the MIP, but not the NIP, and gives an imprinting factor of 2 at this time.

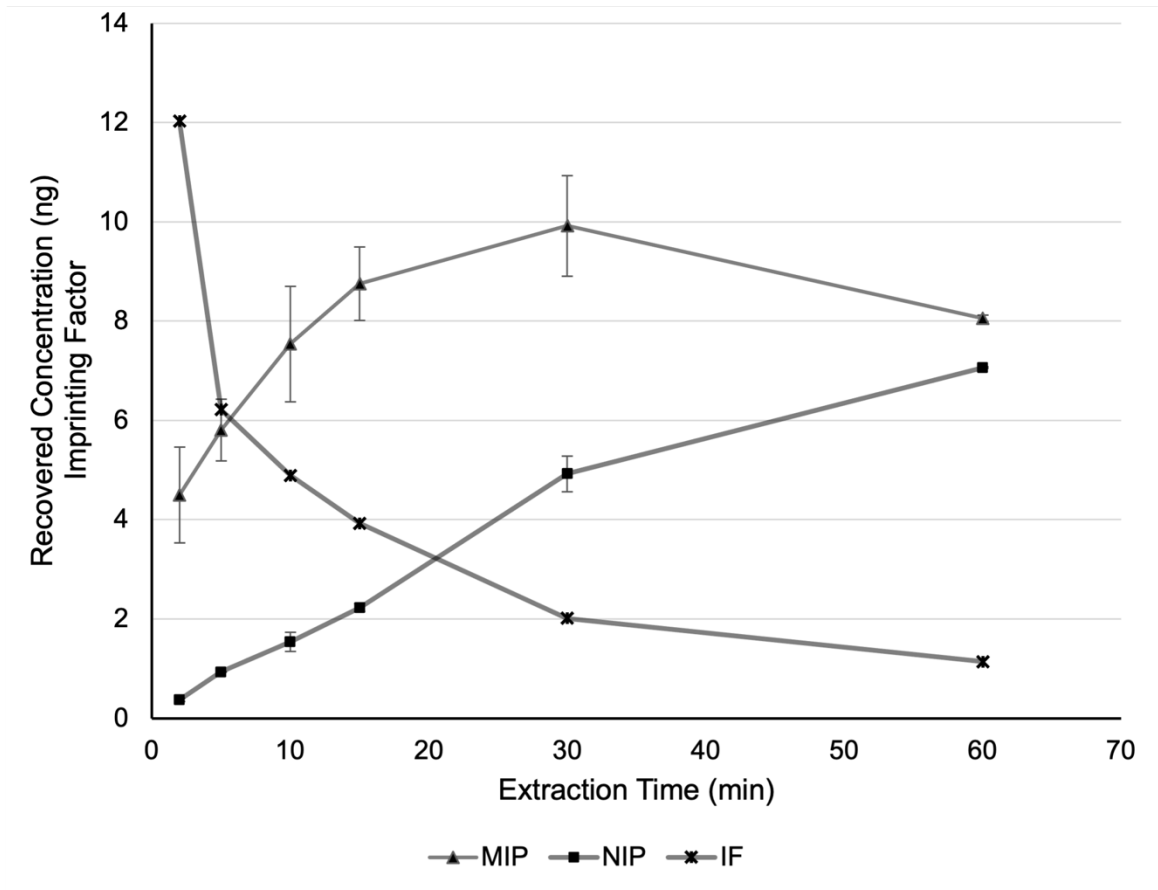


Figure 2.4. Time profile of MIP and NIP extractions of 50 ng mL<sup>-1</sup> mycophenolic acid from plasma, and the corresponding imprinting factor at each time point. IF represents the imprinting factor of the molecularly imprinted polymer as compared to the non-imprinted polymer at each timepoint. Error bars  $\pm$ SD (n=3).

Using the 30 min extraction time, an extraction calibration curve was generated from spiked, pooled plasma (Figure 2.5). The extraction of MPA from plasma using this device is linear from 5-250 ng mL<sup>-1</sup>. The obtained linear range is relevant to clinical samples as the target concentration of free MPA in the plasma is expected to be approximately 50 ng mL<sup>-1</sup> [113].

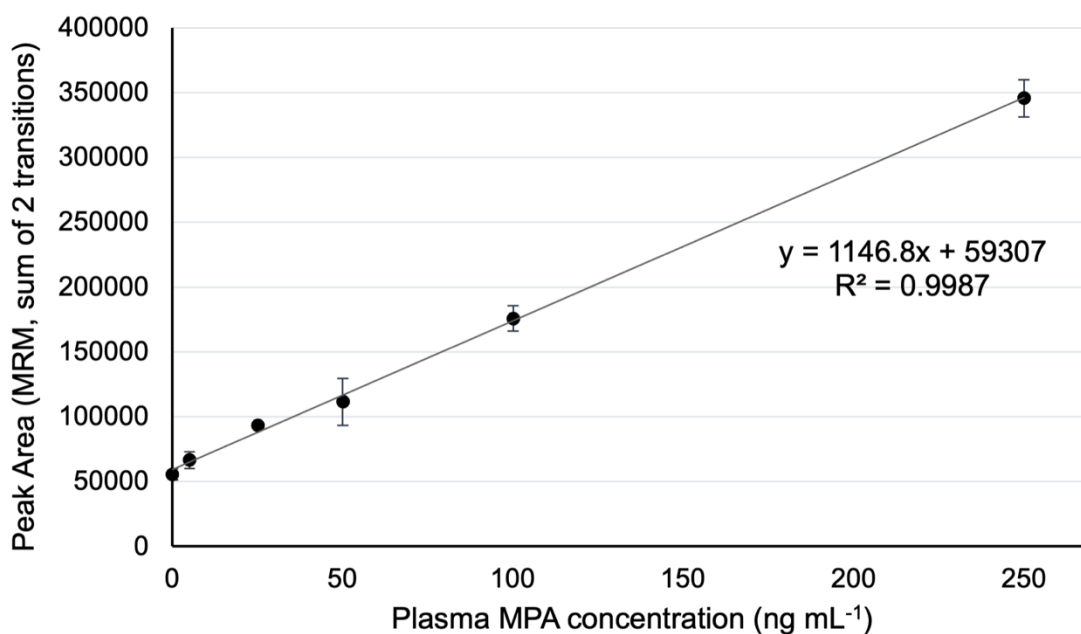


Figure 2.5. Extraction calibration curve of mycophenolic acid in plasma. Error bars  $\pm$ SD (n=3).

### 2.3.5 Analytical Performance Thin Film MIPs for Determination of MPA in Plasma

The sum of the peak areas for two MRM transitions (321.1 $\rightarrow$ 159.0 and 321.1  $\rightarrow$  207.0) for MPA were used for all quantitation. An external calibration curve was prepared to determine the instrumental linear range (Figure 2.6). We determine the

instrumental response to be linear from 1-500 ng mL<sup>-1</sup>. This range is suitable for the extraction calibration range that has been determined for our device (Figure 2.5).

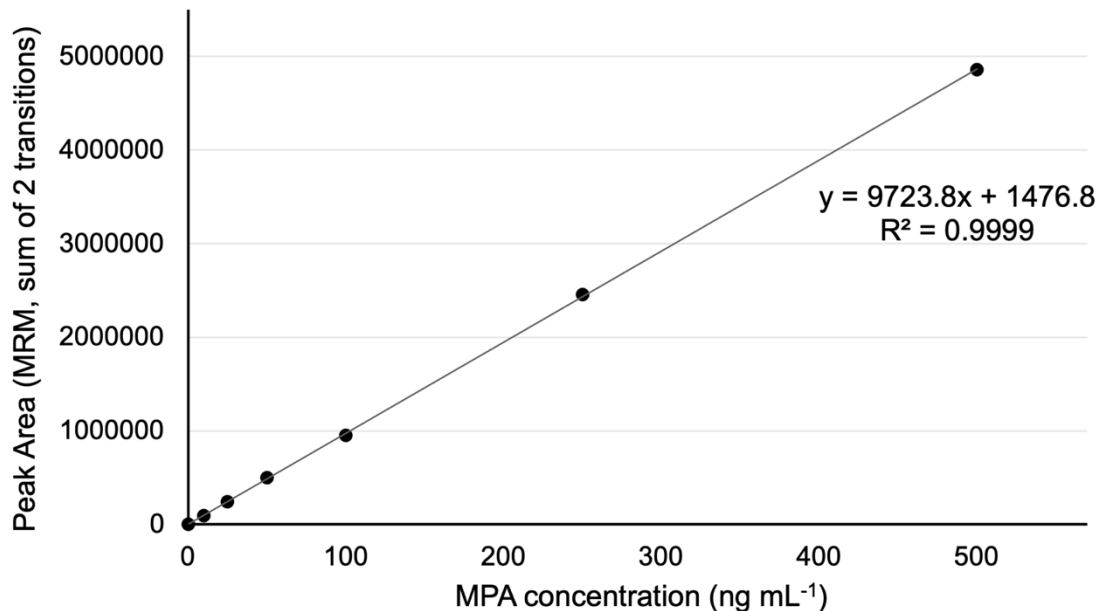


Figure 2.6. External calibration curve of mycophenolic acid from 1-500 ng mL<sup>-1</sup>. Error bars  $\pm$ SD and are too small to be observed on this scale. The %RSD ranged from 0.4% to 1.69% with an average RSD per point of 0.77% (n=3).

### 2.3.6 Analytical Figures of Merit

The figures of merit for the method are found in Table 2.3. The inter-device variability was slightly less than 10% (n=10). This indicates that the devices could be used as a disposable device with high repeatability associated with manufacturing of the coatings. The method working range is from 5-250 ng mL<sup>-1</sup> and was linear across all concentrations studied. The dose of free MPA observed in patients is expected to fall within both the method and instrumental (1-500 ng mL<sup>-1</sup>) linear ranges. The expected

concentration of free MPA in the plasma ranges from 5-270 ng mL<sup>-1</sup> [87,109], while the total MPA in plasma ranges from 1000- 3500 ng mL<sup>-1</sup> [83]. As we did not incorporate a hydrolysis step into the method, we expect to be measuring free MPA.

Table 2.3: Analytical figures of merit for thin film MIP devices for the analysis of mycophenolic acid from human plasma.

Instrumental linear range	1-500 ng mL <sup>-1</sup>
Method linear range	5-250 ng mL <sup>-1</sup>
Instrumental limit of detection (LOD)	0.3 ng mL <sup>-1</sup>
Instrumental lower limit of quantification (LLOQ)	1 ng mL <sup>-1</sup>
Intra-day variability	15 ng mL <sup>-1</sup> = 13.8% (n=3) 85 ng mL <sup>-1</sup> = 4.3% (n=3)
Inter-day variability	15 ng mL <sup>-1</sup> = 13.5% (n=3) 85 ng mL <sup>-1</sup> = 11.5% (n=3)
Inter-device variability	9.6% (n=10)

### 2.3.7 Analysis of Patient Samples

As organ transplantation is not conducted in the province of Newfoundland and Labrador, we did not have access to fresh patient specimens undergoing treatment with an MPA based regimen. Alternatively, we sourced donated plasma from patients from the United States of America who were undergoing MPA treatment. The plasma was thawed

to be aliquoted for shipment to us, in addition to several freeze-thaw cycles from unplanned power outages on campus and the COVID-19 pandemic lockdowns. Upon return to the laboratory, we attempted to acquire new samples, however the pandemic situation in the US resulted in no sample availability due to closure of collection sites. We suspected the samples may have elevated free MPA concentrations as repeated freeze-thaw cycles and elevated temperatures will cause bound MPA to degrade back into the unbound form.

As anticipated, patient samples showed very high concentrations of MPA in the plasma outside of the calibration range of the method. To accurately quantify MPA in the treated patient samples, a 1:20 dilution in twice charcoal stripped pooled plasma was used as a diluent for extraction before pH adjustment as previously described. By using charcoal stripped plasma for dilution of the samples, a consistent amount of matrix was present in the samples allowing for variable dilutions based on patient dosage, while maintaining the complexity of the sample with respect to potential interference by endogenous compounds and maintaining consistency in the physicochemical properties of the sample. The method could also be modified to incorporate dilution with standard buffer systems, which will not diminish device performance. In the case of our plasma samples, only 35  $\mu\text{L}$  was used for each extraction representing a 20 $\times$  dilution. This allows for a broader range of concentrations to be measured using this method, by adjusting the volume of patient sample used, should it be necessary. However, the greatest advantage to the method is the small sample size required which allows for a reduction in the required blood draw from the patient, enabling more tests to be conducted on less blood, and thus

less harm to the patient. As can be observed in Table 2.4, the measured plasma concentrations correlate well with the daily prescribed doses bearing in mind that pharmacodynamics vary dramatically between patients.

Table 2.4. Results of patient sample analysis for MPA. Plasma concentrations correlate with daily prescribed dosage. Samples were quantified using the extraction calibration curve (Figure 2.5) generated by spiked pooled plasma.

Patient	Measured Concentration (avg ng mL <sup>-1</sup> , n=3)	Dilution factor	SD	RSD (%)	Plasma concentration (ng mL <sup>-1</sup> )	Daily prescribed dose (mg, as MPA)
1	196.2	1:20	19.6	10	3924±392	369
2	49.2	1:20	1.5	3	984±30	168
3	189.6	1:20	19.0	10	3791±379	337

The transition ratios for MPA were tabulated for all types of experiments as a simple assessment of matrix effects. Ratio variability is within acceptable ranges as defined by the Clinical Laboratory Standards Institute (CLSI) C50-A guidance documentation [114]. The maximum allowable tolerance for a second transition is  $\leq 25\%$  for a transition that is 20-50% of the base peak response. For 126 measurements, the average transition ratio was stable at  $0.489 \pm 0.018$  (Figure 2.7). This small variability between calibration standards, matrix, and patient samples indicates that spectral matrix effects are minimal. Blank matrix extraction of plasma gives signal far below the LOD of

the method, indicating that the MIP extraction was successful in removing potential chromatographic interferents, as compared to plasma that is directly injected in which large, interfering peaks can be observed. The overall variability of 3.7% for a transition at ~ 49% of the base peak, with the authentic samples giving less than 8%, is well within prescribed limits.

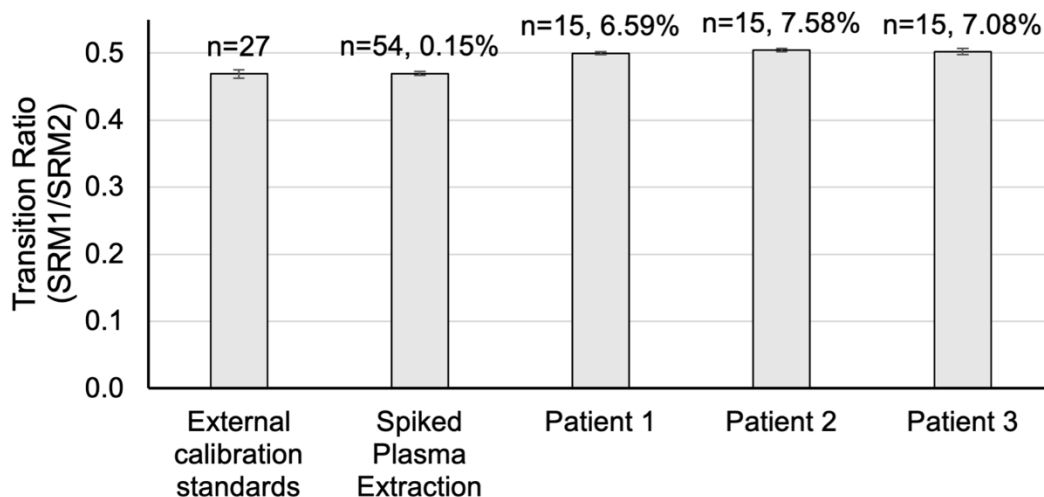


Figure 2.7. Transition ratio monitoring of two channels in calibration standards, spiked pooled plasma and patient samples. For each column, n = the number of injections for each sample is presented with %difference between the response for the samples relative to calibration standards. Error bars are  $\pm$ SD for n measurements.

## 2.4 Discussion

A MIP thin film device was developed to rapidly extract MPA from human plasma. The MIP yielded a higher recovery of the drug compared to the analogous non-imprinted polymer (NIP). The method was optimized using pooled blank human plasma.



Analysis of an extraction time profile showed 30 min provides sufficient recovery to meet detection limits required for the MPA therapeutic clinical range. The desorption solvent system, 90% acetonitrile, 9.9% water and 0.1% formic acid, has been optimized to allow for near-complete desorption of the MPA from the film in 2 min. The full method, including sample preparation and UPLC-MS analysis, can be completed in 45 min. Use of equipment for multiplexed sample processing (e.g., a multi-position vortex mixer), allow a single technician to process more than 96 samples per h.

The LOD and LOQ are 0.3 and 1.0 ng mL<sup>-1</sup> respectively with a linear range from 5-250 ng mL<sup>-1</sup>. The intra- and inter-day variability was determined to be 13.8% and 4.3% (15 ng mL<sup>-1</sup>) and 13.5% and 11.0% (85 ng mL<sup>-1</sup>), respectively (n=3). The inter-device variability was 9.6% (n=10). The low inter-device variability makes these devices suitable for single use in a clinical setting. Due to complexities with the acquisition of patient plasma, the samples tested were above the linear range of the method. The volume of patient plasma was reduced to 35 µL using the method for the samples to place concentrations within the linear range of the method. We expect that with fresh patient plasma, we would be able to effectively measure free MPA in the linear range of the method. Dilution of the patient samples (20×) was completed with charcoal stripped pooled plasma which allowed for less volume requirement from patients and standardization of the amount of matrix independent of treated plasma input. This demonstrates that the method can be adapted for limited plasma volumes with minimal effect on performance, demonstrating the highly flexible nature of MIP thin film extraction devices for both clinical applications and TDM. Plasma was obtained and

analyzed from patients prescribed MPA. The amount of MPA in the samples ranged from 984-3924 ng mL<sup>-1</sup> with an average RSD of 7.7% (n=3). As demonstrated by the required dilution of the degraded plasma, this method could be easily modified to include a hydrolysis step to measure total MPA, if desired. The main modifications to the protocol would be hydrolysis followed by dilution of the sample, approximately 20×.

In conclusion, the developed devices extract MPA in a single step and time from sampling to result is 45-minutes. The films demonstrate a high level of reproducibility and sensitivity toward the analyte, being assisted by molecular imprinting. This novel method and device could be used for TDM of MPA in a clinical setting where throughput and time-to-result are critical. This approach can easily meet sensitivity requirements while using small volumes of plasma as demonstrated by 35 and 700 μL volumes used in this study. Since the cost-effective single-use devices can be made quickly and efficiently, they can be used to increase throughput in clinical labs and are adaptable for use in microplate preparation systems.

### **3 A thin-film molecularly imprinted polymer for the measurement of tyrosine kinase inhibitors in human plasma**

#### 3.1 Introduction

Tyrosine kinase inhibitors (TKIs) are common anti-tumor agents. As the name suggests, they inhibit tyrosine kinases and were first identified as tyrosine phosphorylation inhibitors in 1988 [115]. Through computational and combinatorial approaches, many TKIs were developed during the past 30 years. A benefit of this class of drugs is the specificity of enzyme targets, with the ability to accurately distinguish one kinase from another, thus being very specific for a single type of cancer, for example. This has led to widespread usage of these drugs to treat various types of cancers and tumors ranging from blood cancers to solid tumors. One drawback in the use of TKIs in clinical practice is the high concentrations of drug required for treatment. Dosage is also close to the toxic limit for the patient, and thus warranting the use of therapeutic drug monitoring (TDM). In the current study, we developed a molecularly imprinted polymer (MIP) based extraction system in a 96-well format for the rapid extraction and quantification of 4 TKIs from human plasma using LC-MS/MS.

The four TKIs used in this study are imatinib (Ima), nilotinib (Nil), dasatinib (Das), and ponatinib (Pon). A table containing their structures and relevant physical constants can be found in Table 3.1. These four drugs were selected as they are currently the commonly prescribed TKIs in North America and are exemplary of the wide range of concentrations often employed in TKI dosage. For example, imatinib and nilotinib are

high-range TKIs with a target plasma concentration of at least 800 ng mL<sup>-1</sup>. Ponatinib is a low dosage TKI with target plasma concentration of at least 22 ng mL<sup>-1</sup> and dasatinib is an extremely low range TKI with a target plasma concentration of 1.5-50 ng mL<sup>-1</sup> [116].

Table 3.1. Structures, relevant physical constants, and generation number of studied TKIs.

Compound	Chemical Structure	Mol. Wt.	logP	pKa	TKI Generation
Imatinib (Ima)		493.6	3.5	11.96	1
Nilotinib (Nil)		529.5	5.36	11.89	2
Dasatinib (Das)		488.0	1.8	8.56	2
Ponatinib (Pon)		532.6	4.97	11.96	3

Imatinib was the first TKI to be developed and commercialized. Unlike previously developed drugs, imatinib was one of the first to bind to ABL [117,118], a tyrosine protein kinase thus blocking the nearby ATP binding site, while previous drugs targeted the enzyme substrate binding site explicitly [119]. Limiting the accessibility to the ATP binding site provides for high specificity toward leukemic cells versus healthy cells [118]. Unknown at the time of commercialization, imatinib would become one of the most influential TKIs used in clinical practice [120,121], especially for the treatment of chronic myelogenous leukemia (CML). Although imatinib has increased the life expectancy of patients with CML to near-general population levels [122], the long duration of treatment has led to proliferation of drug-resistant cancers in some patients through random mutation of ABL with a lower binding affinity [123].

Nilotinib, a second-generation TKI, is 10-30 times more potent than imatinib [124] used in severe cases of CML or with patients who do not respond to imatinib treatment. Although nilotinib is more effective than imatinib, higher risk of serious side effects limits its use [125]. Ponatinib is a third-generation inhibitor of ABL kinase specifically developed to overcome several mutations that lead to resistance of both imatinib and nilotinib [126], including the most common T315I mutant [127]. Of the second-generation TKIs, dasatinib is unique as it shows broader inhibition of both tyrosine kinases and Src kinases, with the latter commonly associated with breast cancers [128]. Like nilotinib, dasatinib is a more potent TKI developed to overcome resistance to imatinib and analogues and is a much stronger inhibitor of activated BCR-ABL kinase than either imatinib or nilotinib [129].

In contrast to many anticancer drugs administered by intravenous infusion, TKIs are normally administered orally. Oral administration of drugs leads to an increased variability in plasma concentration due to several factors including rate of gastrointestinal absorption, genetics, drug-interactions, diet, and other patient habits [130]. Complicating matters, some TKIs also interact with their own transporters and enzymes responsible for their metabolism, thus making estimation of plasma concentration very unpredictable [131]. This variability, in addition to risks of numerous adverse events associated with high dosage of TKIs, warrant the institution of therapeutic drug monitoring (TDM) in clinical practice. As a clinical tool, TDM is useful in optimizing drug dosing to maximize clinical effectiveness while avoiding toxicity and other adverse events [132]. For example, interpatient trough levels of Ima have been shown to be as high as 16-fold with a typical 400 mg dosage once per day [133]; similar variation is reported for other TKIs [134–136].

Analytical approaches to the quantitation of TKIs are numerous and varied including capillary electrophoresis [137], enzyme-linked immunosorbent assay [138], high-performance liquid chromatography with UV detection (HPLC-UV), with mass spectrometry (LC-MS), and coupled to tandem mass spectrometers (LC-MS/MS) [116,139–141]. A large number of methods focus on Ima as it was the first and most prominent TKI. Of all approaches, LC-MS/MS is the most commonly reported in the literature for a number of reasons, primarily related to the specificity and sensitivity of a triple quadrupole mass spectrometer [142]. Sample preparation approaches for measurement of TKIs in plasma are extensively LLE and SPE based methods [139].

These techniques can be time consuming and often involve multiple extractions using hazardous solvents. Thin-film molecularly imprinted polymers (TF-MIPs) have been used for environmental samples [105–107,110] and most recently, for biological samples [108]. TF-MIPs have many advantages over LLE and SPE based approaches due to the ease-of-use, tunability, simple manufacture, and low cost to produce [49]. By introducing molecular imprinting, we can add another factor of selectivity to polymeric sorbents for thin-film microextraction [14,15]. MIPs are prepared by polymerization in the presence of a template molecule with functionality and shape similar to the analyte to form complementary selective cavities in the polymer once the template is removed. The added selectivity of molecular imprinting in TFME devices allows for development of highly efficient extraction materials suitable for use in therapeutic drug monitoring.

Herein we present a TF-MIP in a 96-well plate format for the extraction and analysis of Ima, Nil, Das, and Pon in human plasma. The process is time and resource efficient and capable of accurately and concurrently extracting and quantifying TKIs from 200  $\mu$ L plasma with little sample preparation.

## 3.2 Experimental

### 3.2.1 Reagents and Materials

All chemicals and reagents were purchased from Sigma-Aldrich (ON, Canada) and were of reagent grade or higher and were used without further purification unless otherwise noted. Imatinib (98.0+%, I09061G) was purchased from TCI America (OR, USA); dastinib (99%, D3307500MG) from LC Laboratories (MA, USA); and ponatinib



(99.5+%, AP24534) and nilotinib (99.5+%, AMN-107) from Selleckchem (TX, USA). LC-MS grade solvents were purchased from Fisher Scientific (ON, Canada). Ultrapure water was made in-house using a Millipore Milli-Q water system (Resistivity  $\geq$  18.2 M $\Omega$  cm<sup>-1</sup>). Both ethylene glycol dimethacrylate (EGDMA) and 2-*N*-morpholinoethyl methacrylate (N-MEMA) were passed through gravity columns of basic aluminum oxide (Brockmann-type I, 50-200  $\mu$ m, 60 Å), to remove polymerization inhibitors prior to use. The ASSURANCE™ Interference Test Kit for routine interferents (INT-01) was purchased from Sun Diagnostics (ME, USA). Pooled human plasma (2 $\times$  charcoal stripped) was used for all experiments and was purchased from BioIVT (NY, USA). Plasma was stored at -20 °C until use and thawed at 4 °C for 1 h prior to use.

### 3.2.2 Instrumentation and Operating Conditions

The separation and quantification of TKIs was performed using an Acquity ultra performance liquid chromatograph (UPLC) and a Xevo TQ-S tandem mass spectrometer (Waters Corporation) operated in positive ionization mode equipped with an electrospray ionization (ESI) source. Chromatographic separation was carried out using an Acquity BEH-C<sub>18</sub> column (2.1  $\times$  50 mm, 1.7  $\mu$ m) maintained at 30.0 °C. Gradient elution with solvents A (water and 0.1% FA) and B (ACN and 0.1% FA) at a flow rate of 0.5 mL min<sup>-1</sup> initially at 12% B, and increased from 12 to 15% B from 0 min to 0.25 min, then increase to 40% B from 0.25 min to 1.5 min, then to 60% B from 1.5 min to 2.4 min and to 90% B from 1.5min to 3.0 min. The system then returned to initial conditions at 3.10 mins with a total runtime of 3.90 min. The mass spectrometer was operated in multiple reaction monitoring (MRM) mode using two transitions for each drug

(Table 3.2). MIP extracted samples were filtered using MultiScreen Solvinert hydrophilic PTFE 0.45  $\mu\text{m}$  filter plates (Millipore) into flat-bottomed polystyrene 96 well plates (Corning 9017) and sealed with a polypropylene adhesive sealing film (BrandTech 781930) at 18  $^{\circ}\text{C}$  in the autosampler (SM-FTN, Waters Corp.) prior to analysis.

Table 3.2. MRM transitions, mass spectrometer settings and retention compounds of monitored analytes.

<b>Compound</b>	<b>RT (min)</b>	<b>Transition type</b>	<b>Precursor Ion (m/z)</b>	<b>Product Ion (m/z)</b>	<b>Dwell Time (s)</b>	<b>Cone Voltage (V)</b>	<b>Collision energy (eV)</b>
<b>Das</b>	2.20	Qual	488.2	232.1	0.066	55	30
		Quant		401.1			
<b>Ima</b>	1.75	Qual	496.4	104.1	0.049	50	30
		Quant		184.1			
<b>Nil</b>	2.60	Qual	530.1	259.1	0.066	70	55
		Quant		289.1			30
<b>Pon</b>	2.90	Qual	533.00	101.0	0.049	42	22
		Quant		260.2			30

### 3.2.3 Instrumentation and Operating Conditions: Formula Development

The separation and quantification of TKIs for formula development was performed as above except isocratic chromatographic separations were carried out using 55% water and 45% acetonitrile both with 0.1% formic acid at a flow rate of 0.5 mL min<sup>-1</sup> on an Acquity BEH-C<sub>18</sub> column (2.1 × 150 mm, 1.7 μm) with a method runtime of 1.8 min. The MS conditions were the same as above.

### 3.2.4 Preparation of Extraction Devices

Extraction devices were prepared by drop casting 30.0 μL of a freshly prepared and degassed (by sonication) solution of polymer components {2 mmol (378 μL) EGDMA (crosslinker), 1 mmol (191 μL) N-MEMA (functional monomer), 1 mmol (172 mg) adenine hydrochloride (template), 16 mg 2,2-dimethoxy-2-phenylacetophenone (initiator) in 1100 μL of dimethyl sulfoxide (DMSO)} into wells of flat-bottomed polystyrene 96 well plates (Corning 9017). The polymer solutions in microplates were exposed to UV light (254 nm) for 30 min in a UV Crosslinker (UVP, CL-1000) to form a porous opaque film in the bottom of the well. The films were washed with acetonitrile for 10 min (several exchanges of solvent) followed by several volumes of distilled water over 10 min. The prepared devices were then able to be used directly. A non-imprinted polymer (NIP) was prepared in the same way as a control, except that adenine hydrochloride (template) was omitted from the formulation.

### 3.2.5 Selection of Microplates

Plastic microplates are produced from a range of materials that can affect the stability of the film coatings and the specificity of the adsorption. During initial

experimentation of drop casting MIPs in microplates, we tested both polypropylene and polystyrene microplates. Casting polymers with vast differences in porogen and monomer, we were unable to easily prepare stably bonded MIPs in polypropylene plates, likely due to the inert nature of PP and the smooth finished surface. Polystyrene plates were determined to be better candidates for making MIPs as they yielded stable films under the varied conditions tested (data not shown). One factor that may enhance the physical bonding of the cast polymers in this experimental setup is that DMSO may partially dissolve the well surface of the plate and allow for a rougher surface for the polymer to bind to. We selected three polystyrene plates with different coating options, as candidates to use for these MIP devices. The first plate, an untreated polystyrene microplate manufactured by Corning (P/N 9107), is considered “medium binding” with a primarily hydrophobic surface. The second and third plates tested were considered “treated”; though the exact treatment is a proprietary process typical treatments involve surface modification by a plasma to add hydroxyl functionality to make the hydrophobic surface into a more hydrophilic one by directly functionalizing the surface with polar moieties [143,144]. In this study, we compared the plates from both Celltreat (“tissue culture treated” P/N 229015) and Thermo Scientific (“Nunclon-Delta treated” P/N 168055). Twelve different formulas, representing two different photoinitiators and a non-imprinted polymer as well as several adenine imprinted polymers were cast and tested in triplicate in each plate type (Figure 3.1). The relative sum of peak areas for the four drugs was compared to the untreated (Corning 9017) plates. It was determined that the untreated plate provided the highest recovery as compared to the treated plates.

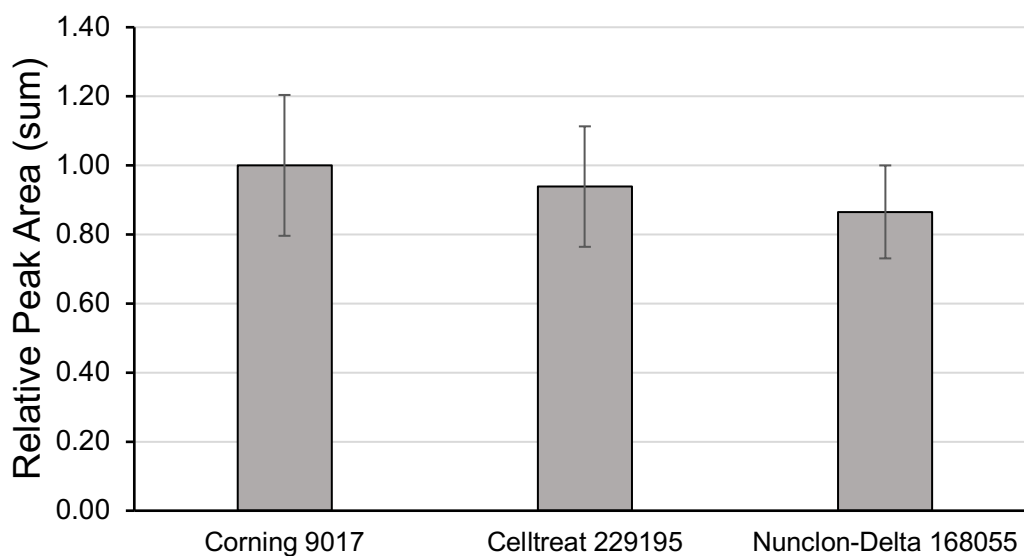


Figure 3.1. Comparison of plate type on recovery of mixed extraction of imatinib and nilotinib ( $5000 \text{ ng mL}^{-1}$  each), dasatinib ( $100 \text{ ng mL}^{-1}$ ) and ponatinib ( $200 \text{ ng mL}^{-1}$ ) in plasma. Data represents 12 formulas in triplicate for each plate (6 MIPs and 6 NIPs). Relative peak areas are the sum of the recovery of 12 formulas as compared to the non-treated plates. Error bars are average SD of the 12 formulas ( $n=12$ ).

### 3.2.6 Molecularly Imprinted Polymer Extraction of Plasma

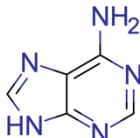
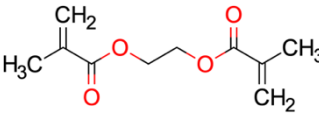
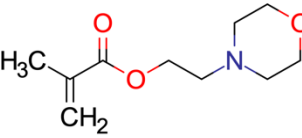
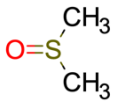
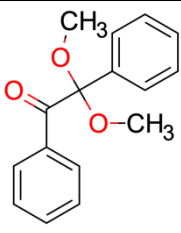
Plasma, untreated or spiked with individual drugs or mixtures in ACN such that sample contained no more than 5% ACN v/v (i.e.,  $50 \mu\text{L}/1 \text{ mL}$  plasma), was deposited in  $200 \mu\text{L}$  aliquots to selected wells of the 96 well plate. The plate was sealed with an adhesive polyester-based sealing film (PCR-SP, Axygen) and agitated for 30 min using a digital advanced vortex mixer (VWR, 89399-884) with a microplate attachment at  $1000 \text{ rev min}^{-1}$  to enhance extraction. After extraction, the plasma samples were removed, and the wells of the plate were washed with  $300 \mu\text{L}$  of ultrapure water. The plate was

inverted on paper tissue momentarily to remove excess water. The analytes were then desorbed from the film using 200  $\mu\text{L}$  ACN in each well with agitation at 1000  $\text{rev min}^{-1}$  for 15 min. Following the desorption, the solution was removed from the plate using a multichannel pipette and passed through a MultiScreen Solvinert hydrophilic PTFE 0.45  $\mu\text{m}$  filter plates (Millipore) into a clean 96 well plate for analysis.

### 3.2.7 Formula Development

The final formula was obtained through screening of selected candidate templates, functional monomers, crosslinkers and porogens for both their chemistry and amount. Templates tested include, 2-(2-methyl-5-nitrophenylamino)-4-(3-pyridyl) pyrimidine, 3-amino-4-methoxybenzanilide, 4-aminobenzanilide, adenine hydrochloride, and 4-acetylpyridine. Functional monomers included methacrylic acid, 2-aminoethyl methacrylate, 2-*N*-morpholinoethyl methacrylate, tetrahydrofurfuryl methacrylate, and glycidyl methacrylate. Crosslinkers included ethylene glycol dimethacrylate, pentaerythritol tetraacrylate and 1,4-divinylbenzene. Porogenic solvents tested were DMF, DMSO, 1-octanol, and ACN. Structures and physiochemical properties of components of the final formula can be found in Table 3.3.

Table 3.3. Structures and physiochemical properties of compounds used in the final formula.

Compound	Chemical Structure	Mol. Wt.	logP	pKa	Density (g/mL)
Adenine		135.13	-0.1	9.80	-
Ethylene glycol dimethacrylate		198.218	1.9	-6.5	1.051
2-N-morpholinoethyl methacrylate		199.25	1.11	4.9	1.045
Dimethyl sulfoxide		78.13	-1.35	35	1.100
2,2-Dimethoxy-2-phenylacetophenone		256.30	3	36	-

### 3.3 Results and Discussion

#### 3.3.1 Screening Method Development

To begin optimization of polymer film formulas, an initial screening method was developed working from the end of the extraction process (desorption solvent selection)

to the beginning, analyzing plasma spiked with a mixture of the 4 TKIs for relative recovery. Since near-quantitative desorption is required for a reliable development protocol, various desorption solvent systems based on ACN and desorption times were evaluated for efficiency of analyte recovery (Figure 3.2) using NIP Formulation 116 (F116), which is comprised of DMPA (16 mg), EGDMA (944  $\mu$ L), MEMA (191  $\mu$ L) and DMSO (1000  $\mu$ L). No advantage was found for the use of acid, base, or water, so neat ACN was used for further work. Upon comparison of desorption time (Figure 3.3), 15 min provided consistent desorption recovery with low variability between samples; less than 15 min led to higher error and 30 min provided no improvement in analyte recovery (Figure 3.3).



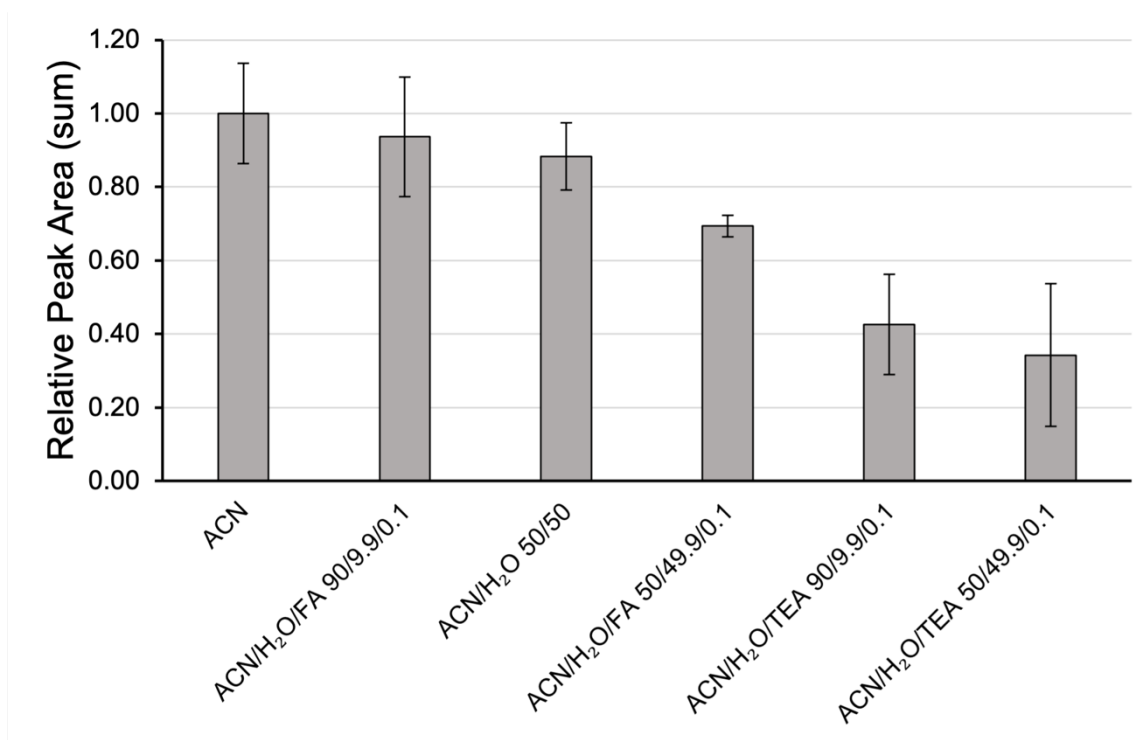


Figure 3.2. Comparison of relative recovery of F116 mixed extraction of imatinib and nilotinib (5000 ng mL<sup>-1</sup> each), dasatinib (100 ng mL<sup>-1</sup>) and ponatinib (200 ng mL<sup>-1</sup>) in plasma with different desorption solvents. Error bars are the sum of the standard deviations (n=3). FA: formic acid; TEA: triethylamine.

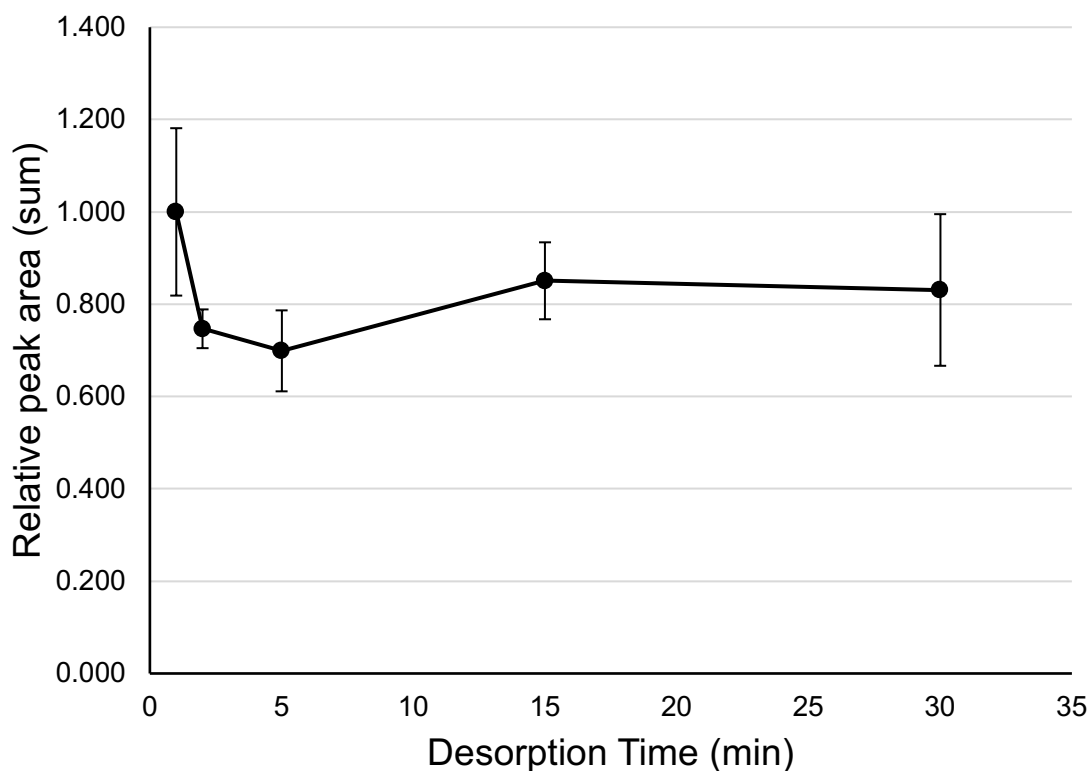


Figure 3.3. Comparison of desorption time of F116 mixed extraction of imatinib and nilotinib ( $5000 \text{ ng mL}^{-1}$  each), dasatinib ( $100 \text{ ng mL}^{-1}$ ) and ponatinib ( $200 \text{ ng mL}^{-1}$ ) in plasma using acetonitrile as the desorption solvent. Data is relative to the 2-min desorption time. Error bars are sum of SDs for all drugs ( $n=3$ ).

One consideration in deciding on a plate is determining the non-specific binding of both interferents and the desired analytes onto the walls of the plate as previously described [145]. To investigate this, we conducted a contact study using the Corning 9017 plates and spiked mixed TKIs in plasma. We found no significant nonspecific adsorption to both pipette tips and the wells of the plate (Figure 3.4). The effect of nonspecific adsorption was minimal, with less than 5% deviation from the starting concentration with

no detectable adsorptive loss. The slight increase in measured concentration is likely due to evaporation during the experiment, considering the high number of liquid handling steps in the experiment (moving spiked plasma into 10 subsequent wells, using 10 fresh pipette tips), which represented an extreme amount of contact to new plastic than what is required in this work.

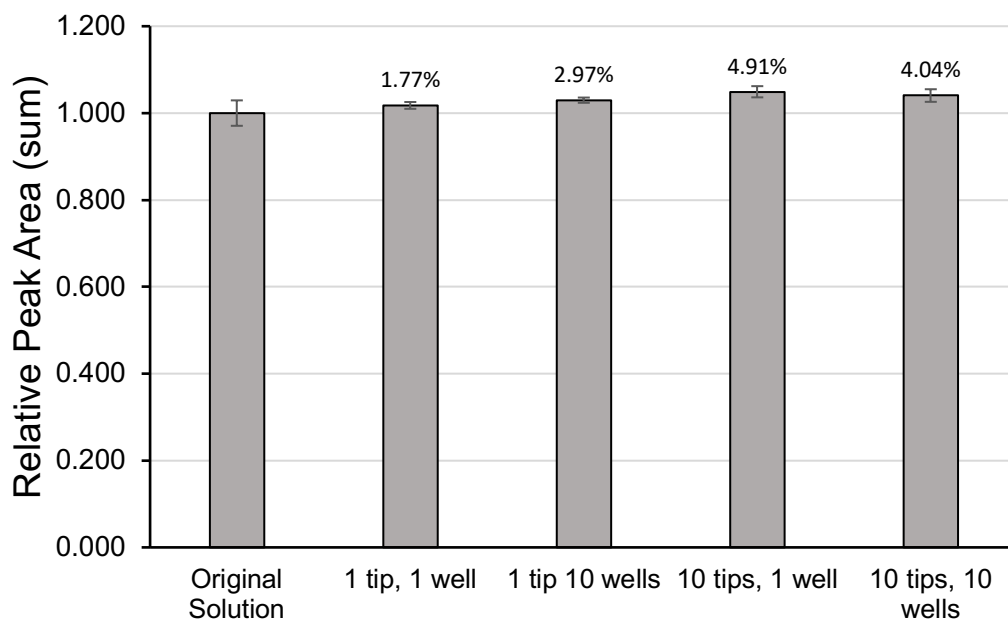


Figure 3.4. Contact adsorption study of mixed extraction of imatinib and nilotinib (5000 ng mL<sup>-1</sup> each), dasatinib (100 ng mL<sup>-1</sup>) and ponatinib (200 ng mL<sup>-1</sup>) in plasma, tested using Corning 9017 plates. Comparing adsorption to wells of plate and pipette tips used in study. Error bars are sum SD for all four analytes (n=3). Data labels are percent deviation from assay of original solution.

Considering all TKIs studied in this work are basic (positively charged at low pH), we expect that a high pH would be favourable for extraction of the neutral form of the analytes onto our surface. We tested an acidic, neutral, and basic pH for extraction yield of the four TKIs using NIP F116 (Figure 3.5). As expected, the non-imprinted formula yielded a marked increase in recovery with adjustment of plasma pH with an alkaline buffer as compared to a neutral pH 7.0 buffer. All further adsorption/desorption experiments were carried out using samples adjusted to pH 10.9, with desorption by ACN.

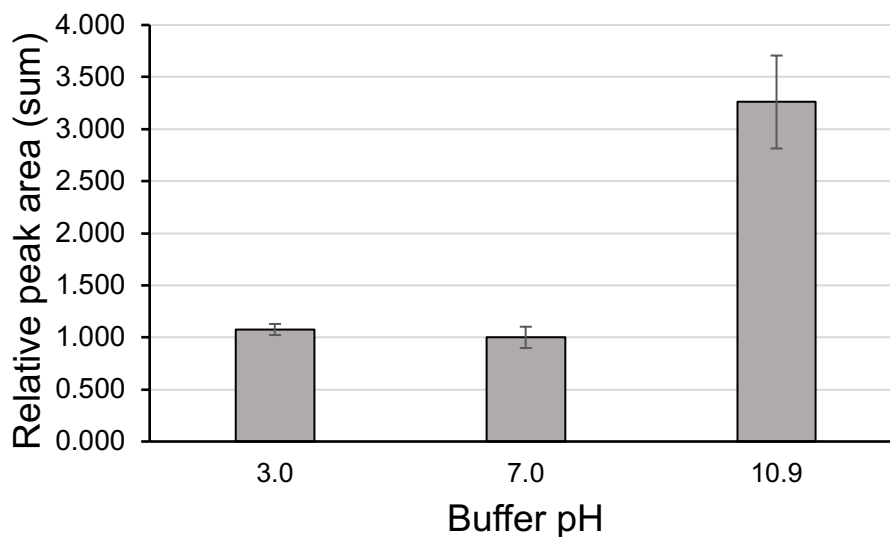


Figure 3.5. Comparison of extraction pH of F116 extraction mixed extraction of imatinib and nilotinib ( $5000 \text{ ng mL}^{-1}$  each), dasatinib ( $100 \text{ ng mL}^{-1}$ ) and ponatinib ( $200 \text{ ng mL}^{-1}$ ) in plasma with acetonitrile. Desorption was completed in 15 min with ACN. Error bars are sum of SDs for all drugs ( $n=3$ ).

### 3.3.2 Formula Development

A total of 335 formulas were designed (Figure 3.6) based on a broad range of chemistries and physical properties of the reagents and resulting polymers. Through initial screening, we were able to narrow down the candidates for each component based on analyte recovery, general solubility, and physical stability (i.e., films remained in the 96-well plate or degraded in storage). Photographs of films at various stages of formula development can be found in Figure 3.7.

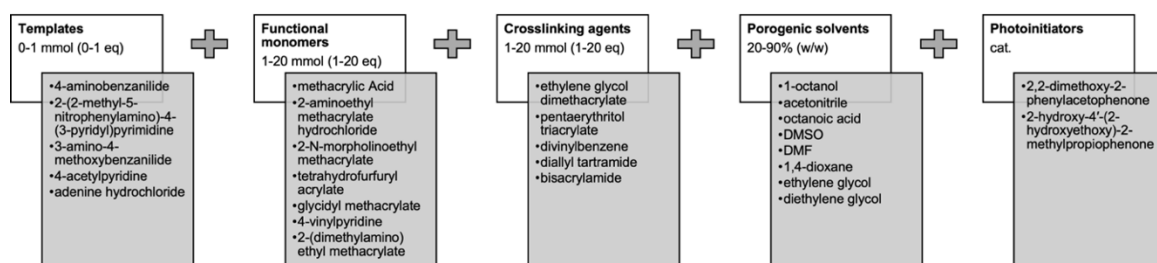


Figure 3.6. Overview of formula development.

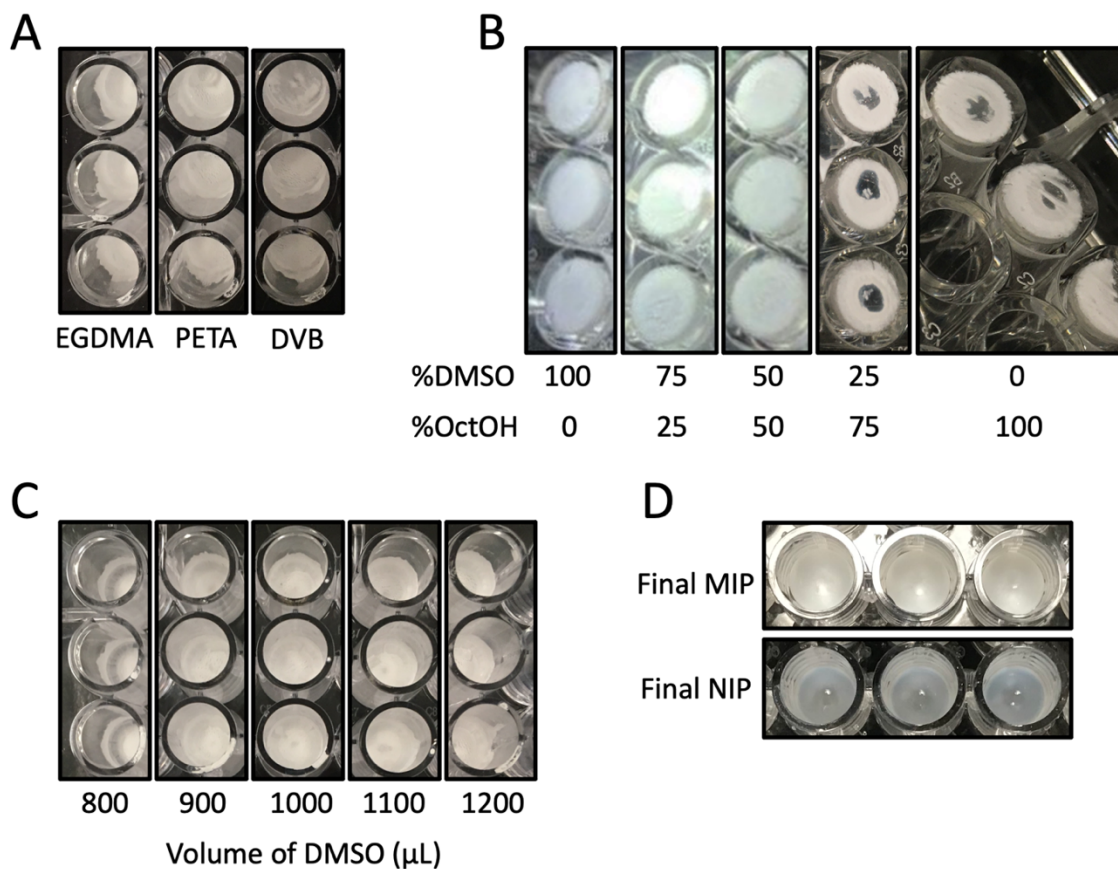


Figure 3.7. Photographs of prepared films at various stages of formula development.

A) Comparison of crosslinking agent corresponding to data presented in Figure 3.10.

B) Comparison of DMSO/OctOH ratio on film stability corresponding to data presented in Figure 3.12. C) Comparison of DMSO volume on film stability corresponding to data presented in Figure 3.13.

D) Final MIP and NIP films used throughout the work; the final formula can be found in Table 3.4. All films in this figure are presented in triplicate.

### 3.3.3 Template Study

Five templates were selected as candidates in this study. We considered structure and positioning of the chemical moieties shared by the TKIs and found molecules that closely resembled those structures. As we know that the TKIs involved in our study act through a mechanism of binding and blocking ATP from docking on the kinases, we included adenine as a template as there is potential that an imprinted cavity complementary for adenine would be a good fit for the drugs of interest. Through preliminary screening, we reduced the candidates down to two: adenine and 3-acetylpyridine. All other tested templates produced MIPs that performed poorly compared to NIP and particularly poor solubility of 2-(2-methyl-5-nitrophenylamino)-4-(3-pyridyl) pyrimidine in ACN, DMF, DMSO and 1-octanol prohibited testing as a candidate for the template. We compared extraction using both 3-acetylpyridine and adenine templated MIPs along with their NIPs (Figure 3.8): F190 is a NIP comprised of DMPA (16 mg, 0.06 mmol), EGDMA (378  $\mu$ L, 397 mg, 2 mmol), N-MEMA (191  $\mu$ L, 199.25 mg, 1 mmol) and DMSO (1000  $\mu$ L); F212 is the adenine MIP where 11 mg adenine hydrochloride is added to F190; F271 is a NIP comprised of DMPA (16 mg, 0.06 mmol), EGDMA (359  $\mu$ L, 376 mg, 1.90 mmol), N-MEMA (106  $\mu$ L, 111 mg, 0.55 mmol) and DMSO (400  $\mu$ L); F270 is the 3-acetylpyridine MIP based on F271, with the addition of 135  $\mu$ L (149 mg) 3-acetylpyridine.

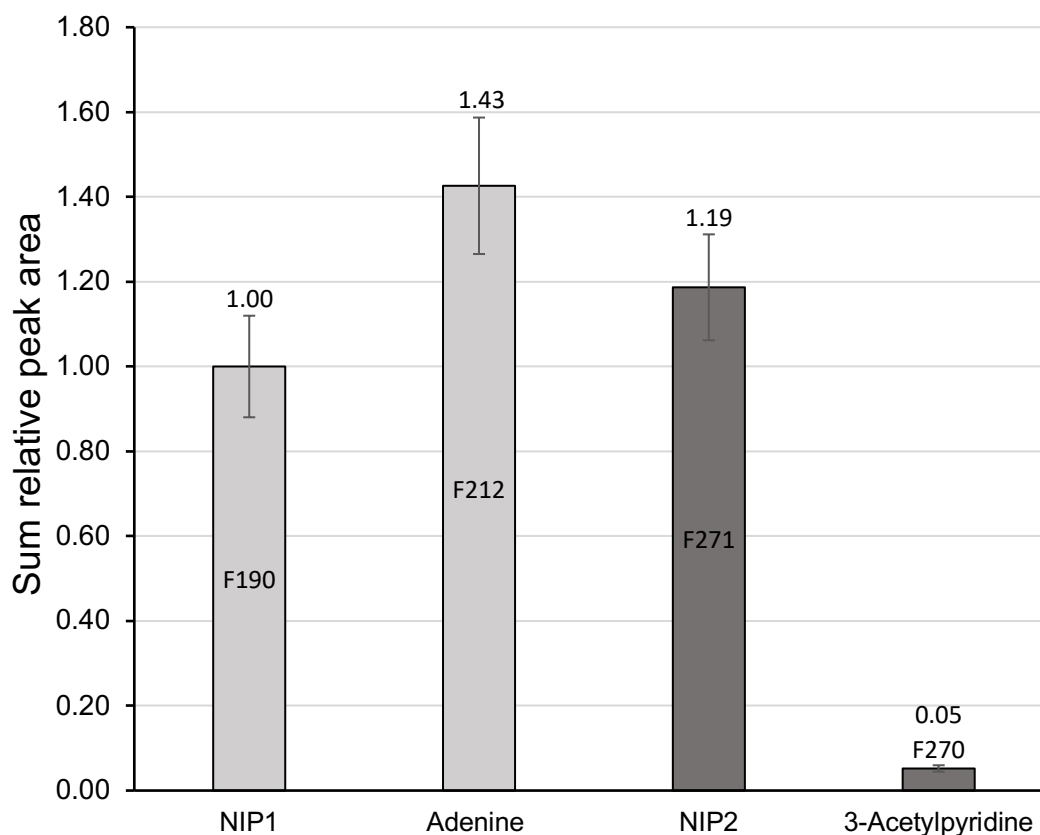


Figure 3.8. Comparison of adenine and 3-acetylpyridine molecularly imprinted polymers to their non-imprinted counterparts (shown in corresponding colors). A 30 min mixed extraction of imatinib and nilotinib ( $5000 \text{ ng mL}^{-1}$  each), dasatinib ( $100 \text{ ng mL}^{-1}$ ) and ponatinib ( $200 \text{ ng mL}^{-1}$ ) in plasma with a 15 min desorption in acetonitrile. Results are the sum of peak areas for all four TKIs. Data labels are imprinting factor as compared to F190. Error bars are SD ( $n=3$ ).

### 3.3.4 Monomer Study

Seven different functional monomers with varying chemistries were evaluated for efficiency of extraction. Although, it is possible to predict a likely candidate based on



potential for interactions with the template and target analytes, performance in these polymer systems is a complex interplay of monomer-template interactions that are influenced by the porogen and crosslinkers, and as such requires testing. Initial screening under standard conditions provided two candidate functional monomers: MAA and N-MEMA. As a secondary screen, we would compare formulas containing mixtures of the two monomers from 0-100% of each, in 9 increments (Figure 3.9).

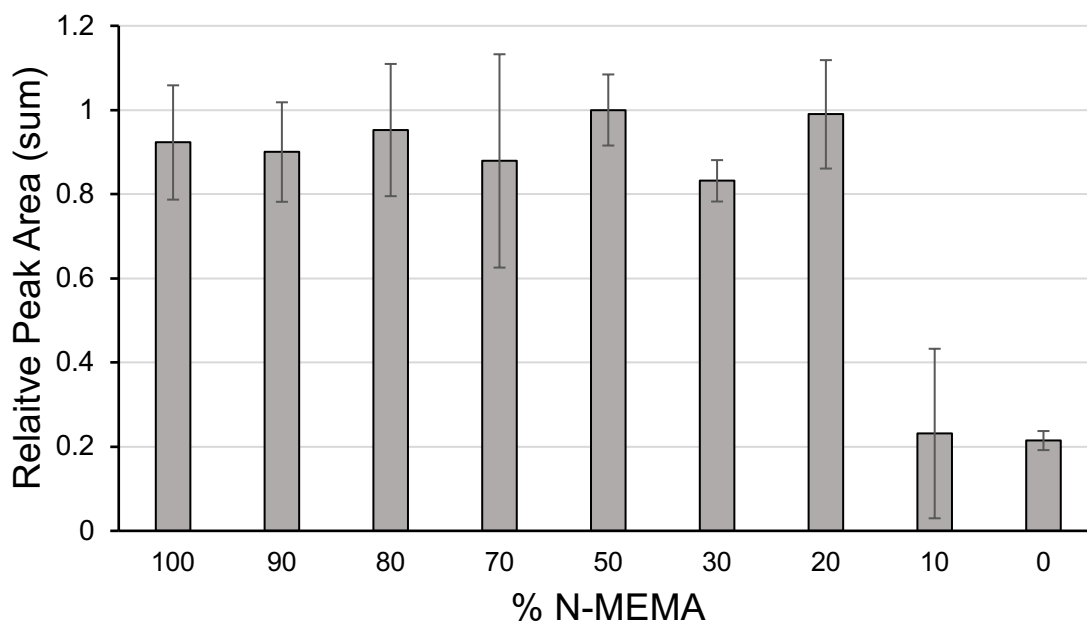


Figure 3.9. Effect of addition of MAA to N-MEMA on relative recovery of extraction of imatinib and nilotinib ( $5000 \text{ ng mL}^{-1}$  each), dasatinib ( $100 \text{ ng mL}^{-1}$ ) and ponatinib ( $200 \text{ ng mL}^{-1}$ ) from plasma: 30 min mixed extract with a 15 min desorption in acetonitrile. Results are the sum of peak areas for all four TKIs. Data is normalized to 50% N-MEMA. Films were cast with  $1000 \mu\text{L}$  DMSO as porogen. Error bars are SD ( $n=3$ ).

We determined that no significant beneficial effect was coming from adding MAA to the mixture, and thus decided to continue with N-MEMA as the sole functional monomer. It should be noted that the increase in recovery of compounds seen with increasing N-MEMA percentage of monomer was quite dramatic, with 20% N-MEMA yielding a much higher recovery than 0-10% N-MEMA (Figure 3.9), and it was by-far the best functional monomer in terms of recovery of compounds. As can be observed from Figure 3.9. The formula prepared using only MAA as monomer was only about 20% the signal of N-MEMA, with recovery from all other monomers tested much below this. The porogen was 1000  $\mu$ L DMSO in all ratios.

### 3.3.5 Crosslinker Study

Three candidate crosslinking agents were tested: EGDMA, PETA, and divinylbenzene (DVB). Using the same base formula of DMPA (16 mg), DMSO (1000  $\mu$ L), N-MEMA (96  $\mu$ L, 0.5 mmol) and MAA (42  $\mu$ L, 0.5 mmol), we prepared three unique formulas: F176-EGDMA (944  $\mu$ L, 5 mmol), F184-PETA (1286  $\mu$ L, 5 mmol) and F185-DVB (712  $\mu$ L, 5 mmol). As can be interpreted from the data, EGDMA was the best crosslinking agent for these devices (Figure 3.10), possessing the highest relative recovery and lowest relative variation of the three crosslinking agents tested. The reduced recovery of PETA and the large error between devices is indicative of a poor device with mechanical instability with polymers flaking and peeling off the substrates after template removal (Figure 3.7A). Wettability is an important consideration in designing an effective extraction device for biological matrices. Wettability relates the ability for a liquid to interact with a solid surface, normally measured through contact angle [146]. The low

recoveries for devices prepared with DVB could be attributed to both the nonpolar characteristics of this cross-linker, which yields a film with low wettability which is unfavourable for mass transport of analytes from aqueous matrices and the differences in polymerization kinetics, where self-polymerization of the DVB is much more favorable than inclusion of the functional monomer. The impact of a nonpolar crosslinker was observed in the formation of highly rounded droplets with a relatively high surface contact angle with the film, as opposed to EGDMA crosslinked films, which was readily saturated with plasma.

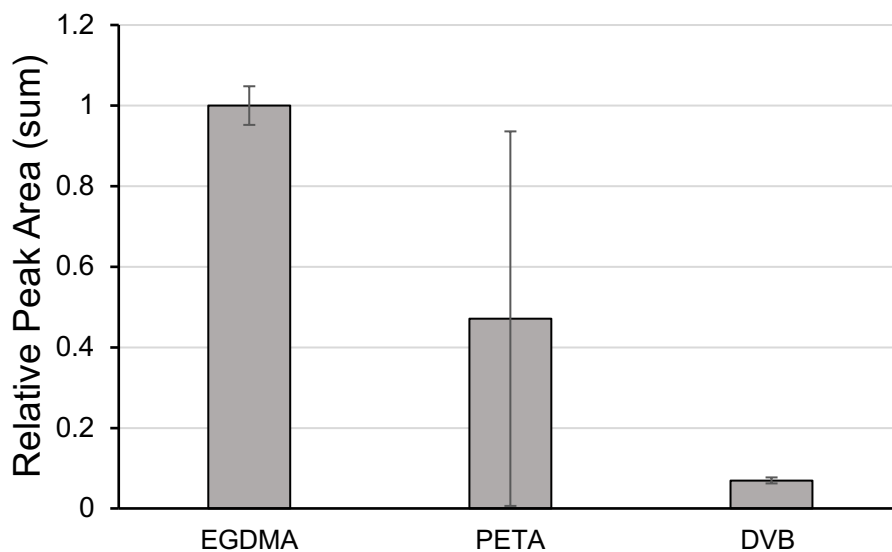


Figure 3.10. Comparison of relative recovery of a 30 min mixed extraction of imatinib and nilotinib ( $5000 \text{ ng mL}^{-1}$  each), dasatinib ( $100 \text{ ng mL}^{-1}$ ) and ponatinib ( $200 \text{ ng mL}^{-1}$ ) in plasma with a 15 min desorption in acetonitrile. Results are the sum of peak areas for all four TKIs. Error bars are the sum of SD of 4 TKIs ( $n=3$ ).

In addition to the nature of the crosslinker, the relative loading is also important as it determines the stability of the polymer as well as influencing chemical and physical properties of the material including wettability (polarity) and porosity. A monomer:crosslinker ratio of 1:1 yields high relative recovery with the lowest variability between devices (Figure 3.11), however the 1:2 ratio yielded films that were more mechanically stable and thus 1:2 was used in subsequent devices. The instability observed from the 1:1 ratio is likely due to the high component:porogen ratio that affects the phase separation process, particularly as the solvent qualities of the porogen differ for MAA and N-MEMA as functional monomers. A ratio of 1:8 also yielded similar recoveries, however the films contracted and flaked from the substrate. Upon further optimization, it was possible to lower the variability in the final formula selection (Table 3.3).

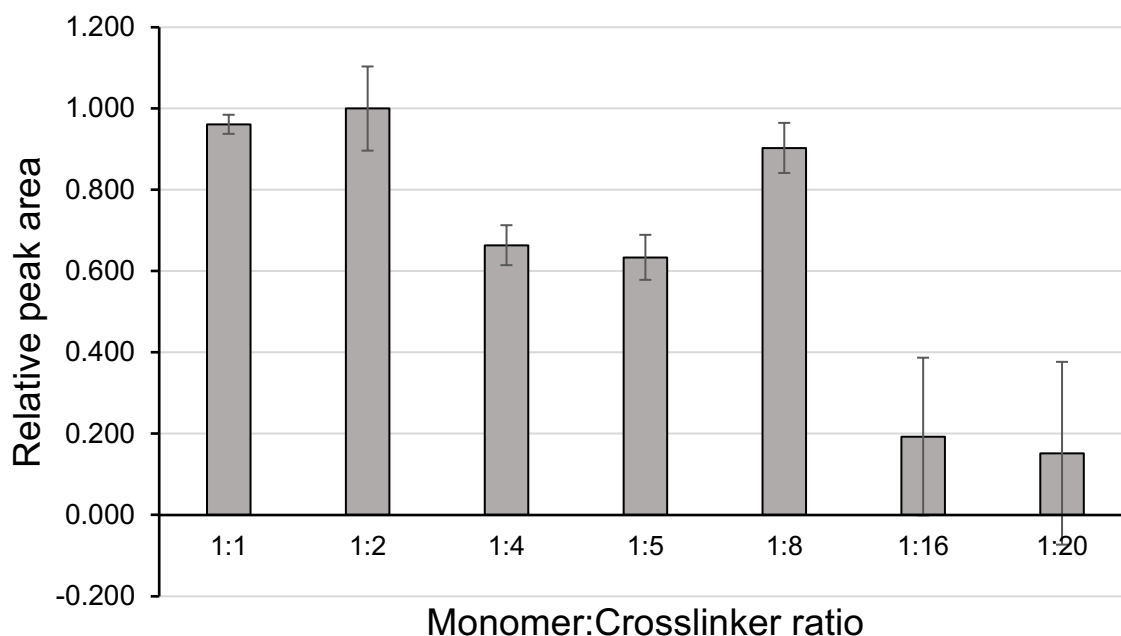


Figure 3.11. Relationship between ratio of 2-*N*-morpholinoethyl methacrylate: EGDMA non-imprinted polymers, relative peak area of a 30 min mixed extraction of imatinib and nilotinib (5000 ng mL<sup>-1</sup> each), dasatinib (100 ng mL<sup>-1</sup>) and ponatinib (200 ng mL<sup>-1</sup>) in plasma with a 15 min desorption in acetonitrile. Results are the sum of peak areas for all four TKIs Error bars are SD (n=3).

### 3.3.6 Porogenic Solvents

Upon initial screening of eight solvent systems (neat solvents and binary mixtures), DMSO yielded films with the highest recoveries of TKIs. This was unexpected as our previous work with porogens showed that 1-octanol is uniquely well suited for use as a porogen producing films with high porosity and good wettability [103,104,106,110]. To determine if 1-octanol may provide some improvements in film performance, binary

mixtures of DMSO and 1-octanol were evaluated for adsorption efficiency for mixtures of TKIs (Figure 3.12).

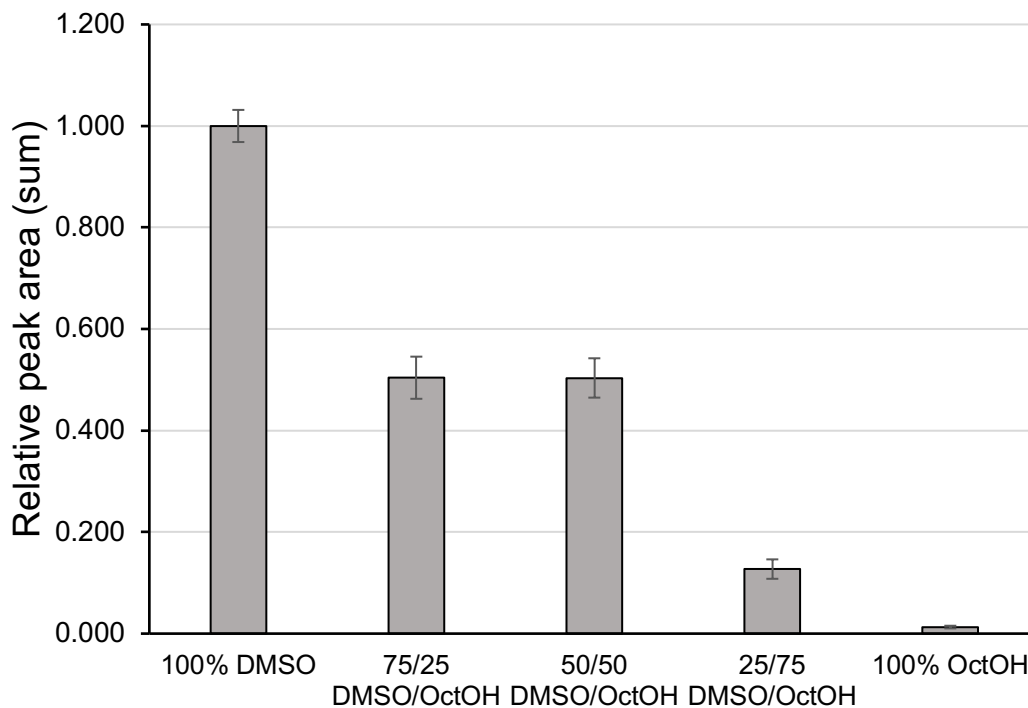


Figure 3.12. Relationship between porogen composition and relative recovery of a 30 min mixed extraction of imatinib and nilotinib ( $5000 \text{ ng mL}^{-1}$  each), dasatinib ( $100 \text{ ng mL}^{-1}$ ) and ponatinib ( $200 \text{ ng mL}^{-1}$ ) in plasma with a 15 min desorption in acetonitrile. Error bars are sum of SD ( $n=3$ ).

It was observed that an increasing ratio of 1-octanol lead to a decreasing analyte recovery from the MIPs, decreasing physical stability, and poor polymerization properties (Figure 3.7B). The phase separation process is crucial to the preparation of stable and porous films [147,148]. We hypothesize that the template-monomer complex formation encourages incorporation of a higher proportion of functional monomer in the growth of

the polymer, in contrast to the respective NIP thin film. The MIP possesses a porous, wettable, opaque white phase whereas the NIP thin films are glassy and semi-translucent, generally indicative of low porosity, possibly due to a higher degree of crosslinking due to incorporation of less functional monomer into the final polymer (Figure 3.7D). This notion is further supported by the instability of the films made with 1:1 monomer: crosslinker ratio, which may cause phase separation behaviour to change due to saturation of the porogenic solvent, causing very short polymers to precipitate thereby inhibiting a high degree of crosslinking. A combination of factors, such as a highly polar template, the polar, aprotic nature of DMSO (in contrast to 1-octanol which is protic), and a polymer components solution near saturation, promote and stabilize interactions between the template and monomer through hydrogen bonding. Pure DMSO was selected as the porogenic solvent in this work.

Previous work has shown that the v/v ratio of porogenic solvent to polymerizable components has a significant effect on porosity of organic polymer films [110]. The influence of porogen volume for DMSO relative to the polymerization components was evaluated based on a fixed loading of polymer components {1 mmol scale (F176) with varied volumes of DMSO} (Figure 3.13). The best result obtained was for the 1200  $\mu\text{L}$  film, however this film lacked mechanical stability and cracked upon drying. In contrast, at 800 and 900  $\mu\text{L}$  DMSO components of the polymer component solution exceeded solubility and precipitated upon standing. Thus, we selected the ratio corresponding to 1100  $\mu\text{L}$  for its favourable variability relative to 1000  $\mu\text{L}$  and higher mechanical stability than the 1200  $\mu\text{L}$  film.

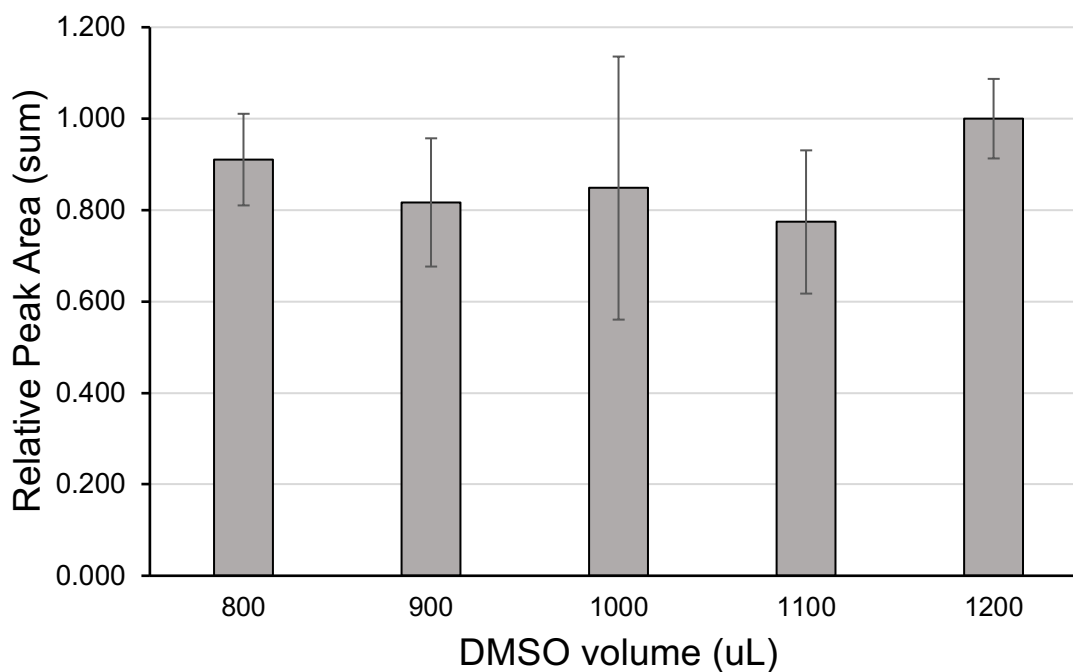


Figure 3.13. Relationship between porogen volume based on F176 on a 30 min mixed extraction of imatinib and nilotinib ( $5000 \text{ ng mL}^{-1}$  each), dasatinib ( $100 \text{ ng mL}^{-1}$ ) and ponatinib ( $200 \text{ ng mL}^{-1}$ ) in plasma with a 15 min desorption in ACN. Results are the sum of peak areas for all four TKIs. Error bars are sum of SD ( $n=3$ ).

### 3.3.7 Photoinitiators

DMPA and 2-hydroxy-4'-(2-hydroxyethoxy)-2-methylpropiophenone (HEMPA) are both radical photoinitiators similar in structure, however DMPA has been most used for less polar films with solvents such as 1-octanol. As HEMPA is a more polar photoinitiator as compared to DMPA, photoinitiator solubility in more polar solvents such as DMSO is possible. Two sets of MIPs and their corresponding NIPs were prepared with each photoinitiator, using UV lamps of their respective maximal absorption



wavelengths (254 nm for DMPA and 365 nm for HEMPA). Figure 3.14 shows that DMPA provided much better analytical performance in recovery and inter-device variability than HEMPA (RSD = 30% HEMPA, 10% DMPA) and physical characteristics. In addition, a positive imprinting effect was detected when DMPA was used, whereas the adsorption was not statistically different from the respective NIP using HEMPA.

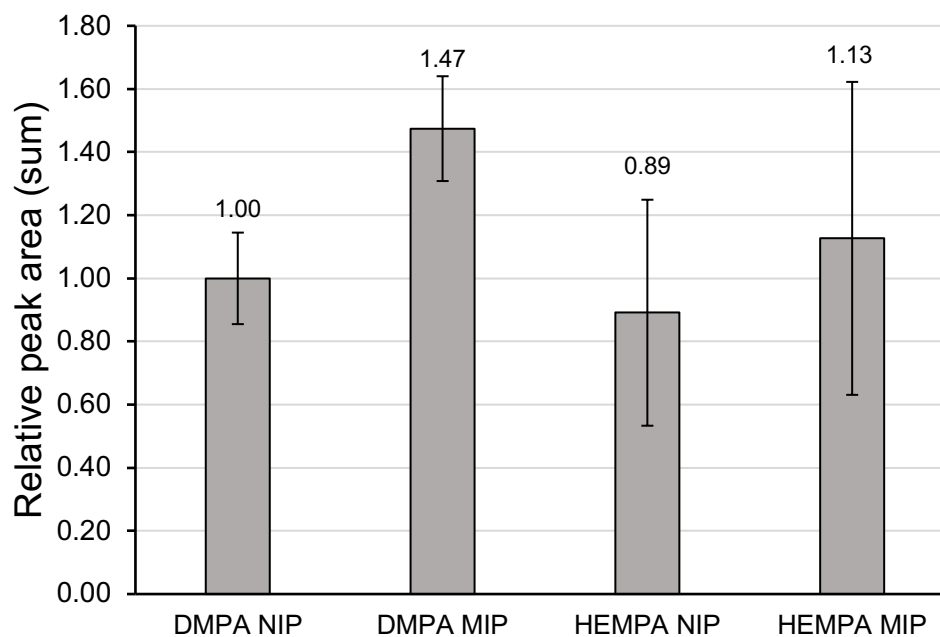


Figure 3.14. Relative response for MIPs and NIPs produced using two different photoinitiators. 30 min mixed extraction of imatinib and nilotinib (5000 ng mL<sup>-1</sup> each), dasatinib (100 ng mL<sup>-1</sup>) and ponatinib (200 ng mL<sup>-1</sup>) in plasma with a 15 min desorption in acetonitrile. Results are the sum of peak areas for all four TKIs. Formula is based on F190, with 16 mg of either DMPA or HEMPA, MIPs are supplemented with 1 mmol (11 mg) adenine hydrochloride. Data labels are imprinting factor as compared to the DMPA NIP. Error bars are the sum of SD of 4 TKIs (n=3).

### 3.3.8 Final Formula Evaluation

Rigorous and iterative testing of the 335 formulas yielded an optimal formula for casting molecularly imprinted polymers in a 96 well format. The final formula is presented in Table 3.4. This formula has been shown to be optimal in terms of all performance and stability parameters important in this work.

Table 3.4. Composition of the optimal MIP thin film extraction device for the four TKIs: Ima, Pon, Nil, and Das.

<b>Component</b>	<b>Compound</b>	<b>Amount</b>
Porogen	DMSO	1100 $\mu$ L
Photoinitiator	DMPA	16 mg
Functional monomer	N-MEMA	191 $\mu$ L (1 mmol)
Cross-linker	EGDMA	378 $\mu$ L (2 mmol)
Template	Adenine	172 mg (1 mmol)

### 3.3.9 Batch-to-Batch Repeatability

To demonstrate repeatability of the film fabrication using this formula ten batches of formula were prepared and used to cast films (n=10, for each batch of formula) and used for extraction from a mixture of TKIs. In Figure 3.15, the average of the summed peak areas from each batch of ten devices is presented with the batch variability (data label). Added to this chart are the upper and lower control limits corresponding to  $\pm 3s$  (n=10, for the averaged batch responses). The between separate batches is within the

control limit and less than 5% RSD for all but one batch (#9), which demonstrates that the films production is very reproducible and films from different batches can be used without depreciating the results.

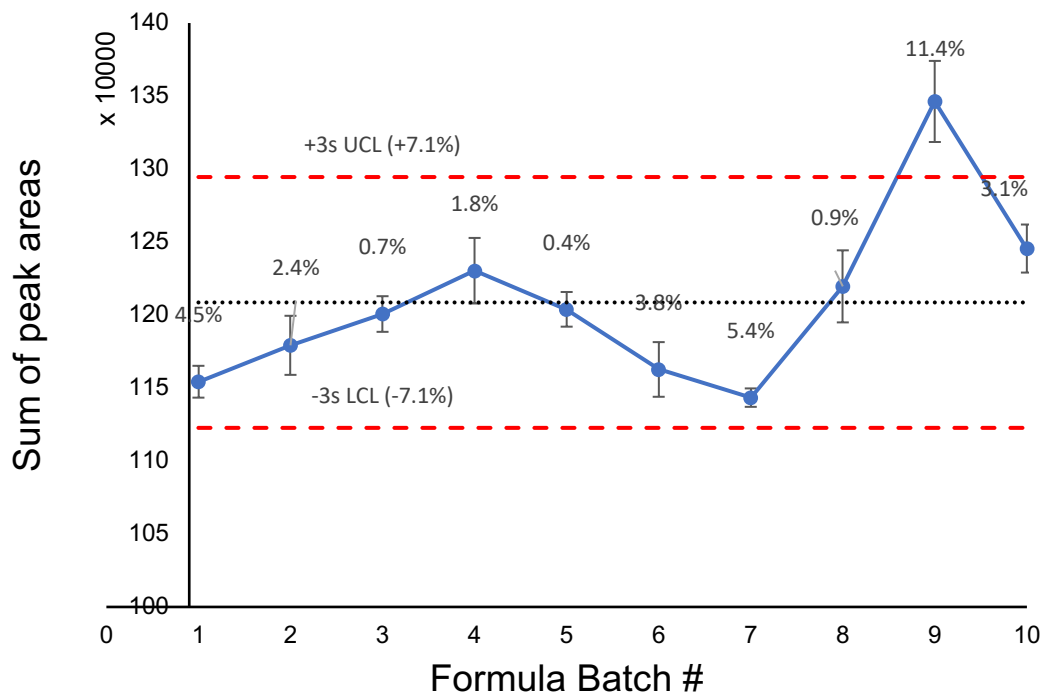


Figure 3.15. Control chart showing combined variability of 10 MIP formulas with four TKIs. Error bars are SD of triplicate extractions (n=10). Data labels are percent deviation from the mean (black dotted line). Red dashed lines represent  $\pm 3\sigma$  for the upper control limit (UCL) and lower control limit (LCL).

### 3.3.10 Inter-Device Variability

Ten devices from a single batch were tested at three concentration levels, which were appropriate for the expected clinical ranges of the drugs (Figure 3.16). We found that variability was below 15% for all concentrations and drugs tested, in addition many

of the tests yielded variability around or below 5% which is well within global regulatory guidelines for bioanalytical method validation [145,149–152]. This, in combination with the batch-to-batch variability shows the production of these films is a very consistent process with low variability, thus allowing for assays to be carried out across batches without eroding data quality.

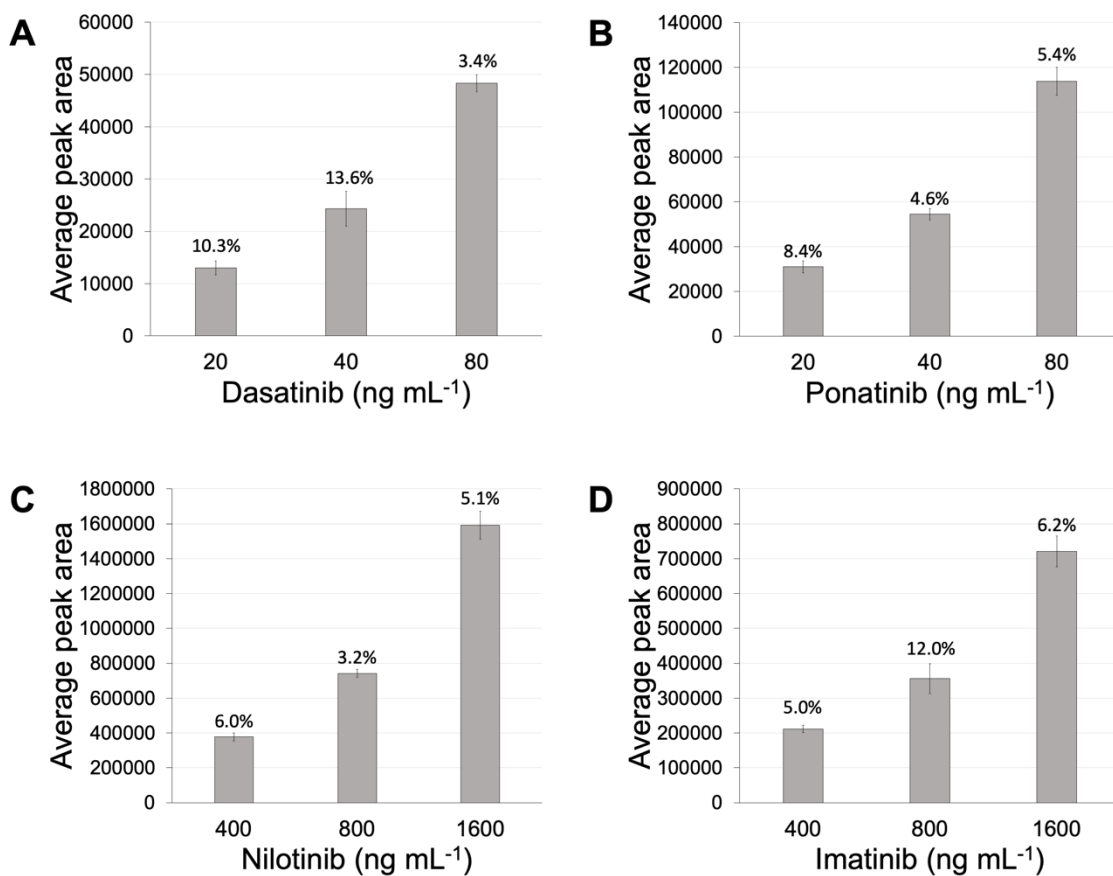


Figure 3.16. Inter-device variability of ten MIP devices, tested against four TKIs at their respective QC concentrations. Error bars are SD and data labels are RSD (n=10).

### 3.3.11 Extraction Method Development

Although the initial extraction conditions for screening were useful for the formula optimization, extraction parameters such as extraction pH adjustment and desorption conditions were refined to ensure the best performance using the optimized formula.

### 3.3.12 Optimization of the Desorption Solvent

Although ACN was used as the desorption solvent in preliminary studies, a range of solvent systems were studied and compared to pure ACN, using the final TF-MIP formula (Figure 3.17A). As can be observed from the data, the highest desorption was achieved using 49% acetonitrile, 50% water, 1%  $\text{NH}_4\text{OH}$ , however this desorption solvent system was incompatible with the analysis method as the mobile phase is supplemented with 0.1% formic acid. The addition of base interfered with chromatographic separation causing peak splitting that affected the quantified amount of Ima (Figure 3.18). By using a pure solvent without modification as the desorption solvent we allow the most flexibility and least interference for downstream analytical processes and that does not affect chromatographic separation of TKIs.

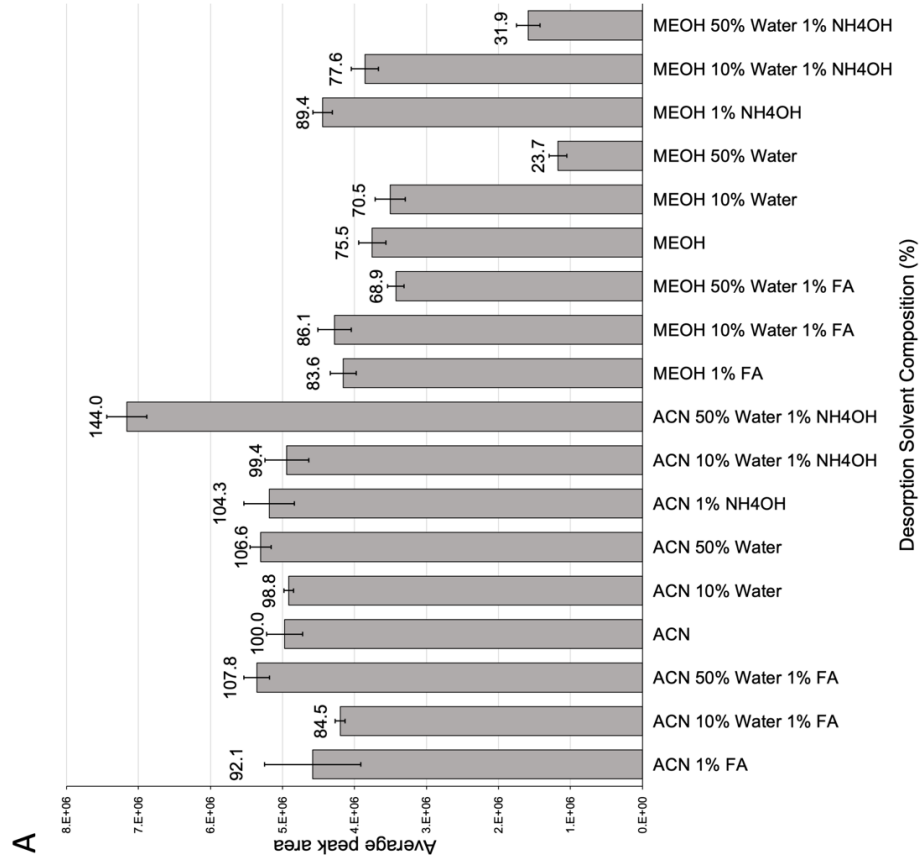
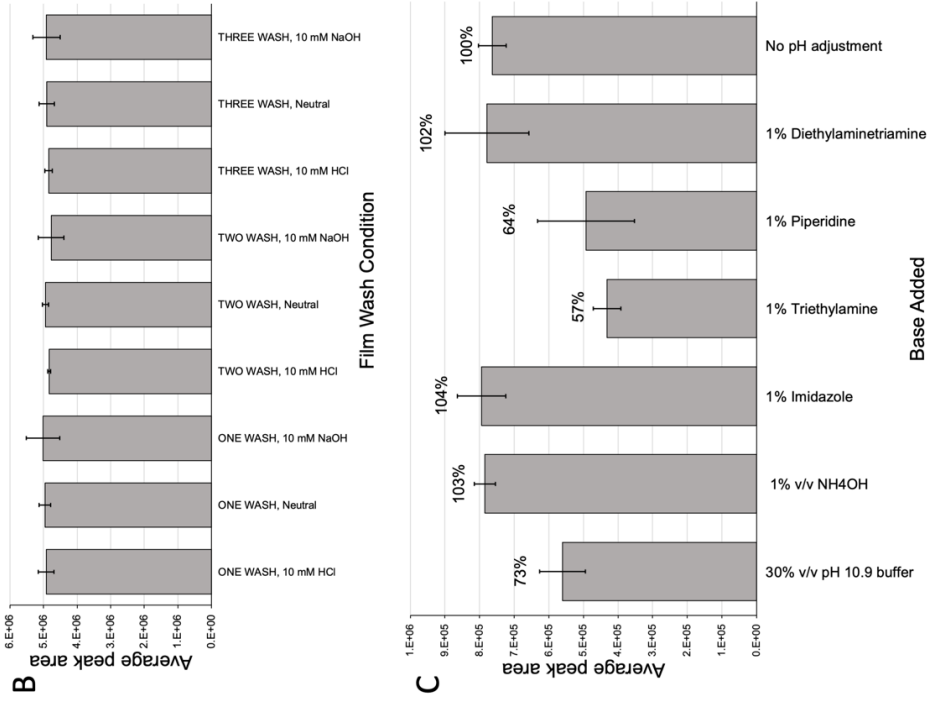


Figure 3.17. A) Screening of desorption solvents. Assessing either acid, base or neutral solvents (ACN or MeOH, and mixtures of these with water, with or without pH adjustment) would be optimal. Error bars are standard deviation (n=3) and data labels are relative peak areas as compared to pure ACN. B) Recovery of analytes after MIPs were washed with various wash solutions and number of washes. Error bars are standard deviation (n=3). C) Comparison of relative recovery of MIP extraction of TKIs in plasma, and with addition of various bases and buffers. 1× pH 10.9 buffer contains 6.75 g ammonium chloride in 100 mL ammonium hydroxide (28% in water). Percent recovery as compared to pH-unadjusted plasma is shown as data labels above the bars. Error bars are SD (n=3).

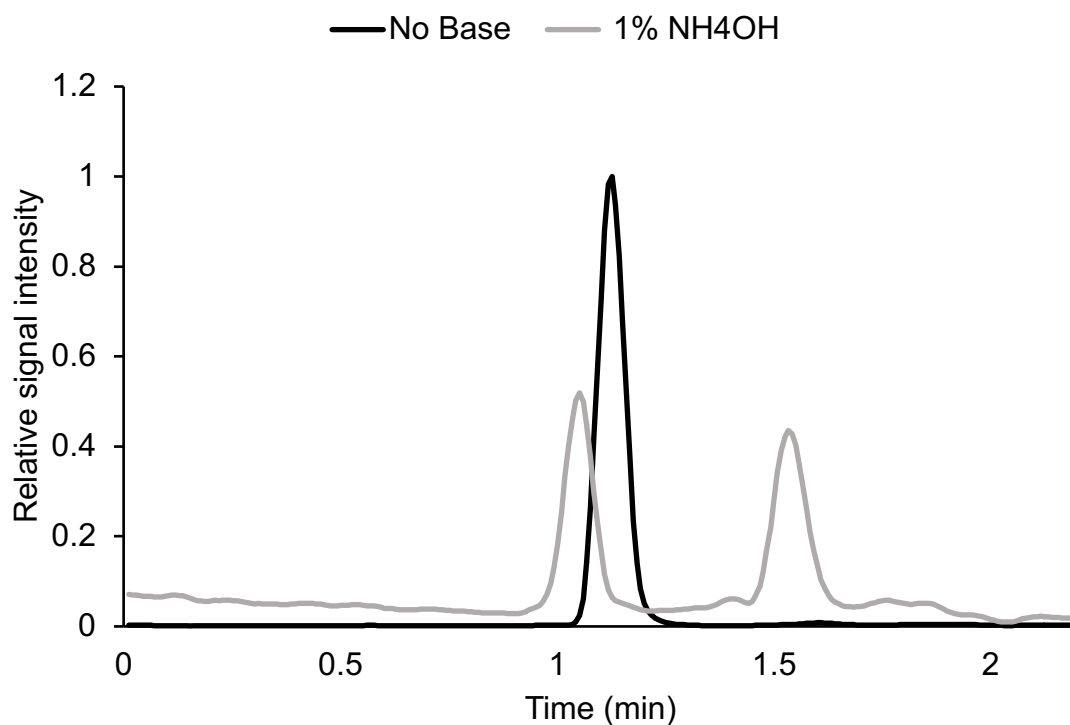


Figure 3.18. Comparing chromatographic peak splitting of imatinib when ammonium hydroxide is used in the desorption solution as compared to the single peak obtained when base is not used.

### 3.3.13 Optimization of the Wash Conditions

Washing of the thin films is required to reduce the background noise and remove weakly bound compounds. A number of washes were tested, adjusting the pH of the wash solutions, to determine what conditions were optimal for our analytes to reduce premature elution and thus a reduction in sensitivity (Figure 3.17B).

We determined two washes with neutral water to be optimal. Amending the pH of the water had little effect, though acidic conditions showed slightly better results. Washes



in basic conditions such as 10 mM NaOH elevated the RSD of analyte recovery, likely from bleeding of the compounds from the film. This would be explained by the expected pH of 10 mM NaOH being 12.0, and at this pH, as analyte pKa values are less than 12, a proportion of the analytes will become charged and thus will likely partition into the aqueous phase. To keep the process simple, we opted for two washes using pH-unadjusted ultrapure water for maximum recovery while minimizing RSD.

The pH of the sample during extraction can have a significant impact on the amount extracted. This is mainly due to the physical properties of the analyte, namely the pKa. As TKIs are naturally basic, we can predict that increasing the plasma pH will afford increased recovery since the TKIs would largely exist in their neutral form, therefore more analyte will be extracted by the thin film. We compared unadjusted plasma to plasma supplemented with various bases (Figure 3.17C). We observed a reduction in recovery when the pH 10.9 ammonia-based buffer, piperidine, or triethylamine are used to alter the pH. We also observed slight increases of recovery when using ammonium hydroxide, imidazole, or diethylene triamine is added to the sample. In addition, these incremental increases in recovery were associated with relatively higher RSD for each condition, and thus we opted to conduct extractions using pH-unadjusted plasma.

#### 3.3.14 Extraction Time Profile

Extraction time profiles (Figure 3.19) were prepared to determine the optimum extraction time using MIP and contrasted with data for the NIPs to demonstrate the effect of extraction time on the imprinting factors for extraction from both mixed and individual

TKIs solutions at varying concentrations (consistent with appropriate clinical ranges). The MIPs demonstrated significant imprinting ponatinib compared to the NIPs (Figure 3.19), IF values near 2 at 20 min at all three concentration intervals, with a slight reduction of imprinting from 30 to 90 min. The rapid rise in imprinting factor in the early timepoints would suggest that the molecularly imprinted polymer has a higher binding affinity for Pon than the non-imprinted polymer. The percent recovery lies around 20% for all concentrations tested, comparable to and higher than some previously reported SPE and LLE methods [139]; as this is an equilibrium based extraction, 100% recovery is unlikely. The IF for Nil demonstrates less desirable results, with imprinting factors slightly below 1 to the NIP (Figure 3.19). Nil possesses the highest logP (5.36) of the TKIs in this study and the consequence of a high logP is low bioavailability in humans (between 17-44%) [153]. The concept of bioavailability in a biological system can provide insight into behaviours of analytes during extraction. In this case, it is likely that Nil is highly protein and lipid bound in the plasma and thus a limited amount of analyte is in a free form in the plasma that is capable of binding to the extraction devices. In contrast to Pon, Nil is used at relatively high clinical doses and thus a slight reduction in recovery does not affect the clinical range of this method significantly. It is also important to note that the recovery of Nil at the end of the time profile is over 35% and thus this recovery, along with the high dose, means a very high peak area, that is well above the detection limits of the method. Ima demonstrates similar trends to Pon with an initial rise in IF to ~1.3 as compared to the non-imprinted polymer (Figure 3.19). However, by the end of the time course the IF reduces to about 1.2 by the end of the time course, which

corresponds to a continued increase in the NIP recovery. This suggests that the MIP equilibrates sooner than the NIP, which is desirable despite the lack of substantial imprinting. Das shows a slight reduction in recovery in the final MIP (IF 0.86 at 30 min) and displays a percent recovery around 22% at the same timepoint (Figure 3.19). The extracted concentration is within the linear range of the analytical method presented and correlates with the therapeutic range in human plasma, meaning results obtained with this recovery are suitable for clinical decision-making and patient monitoring [139].

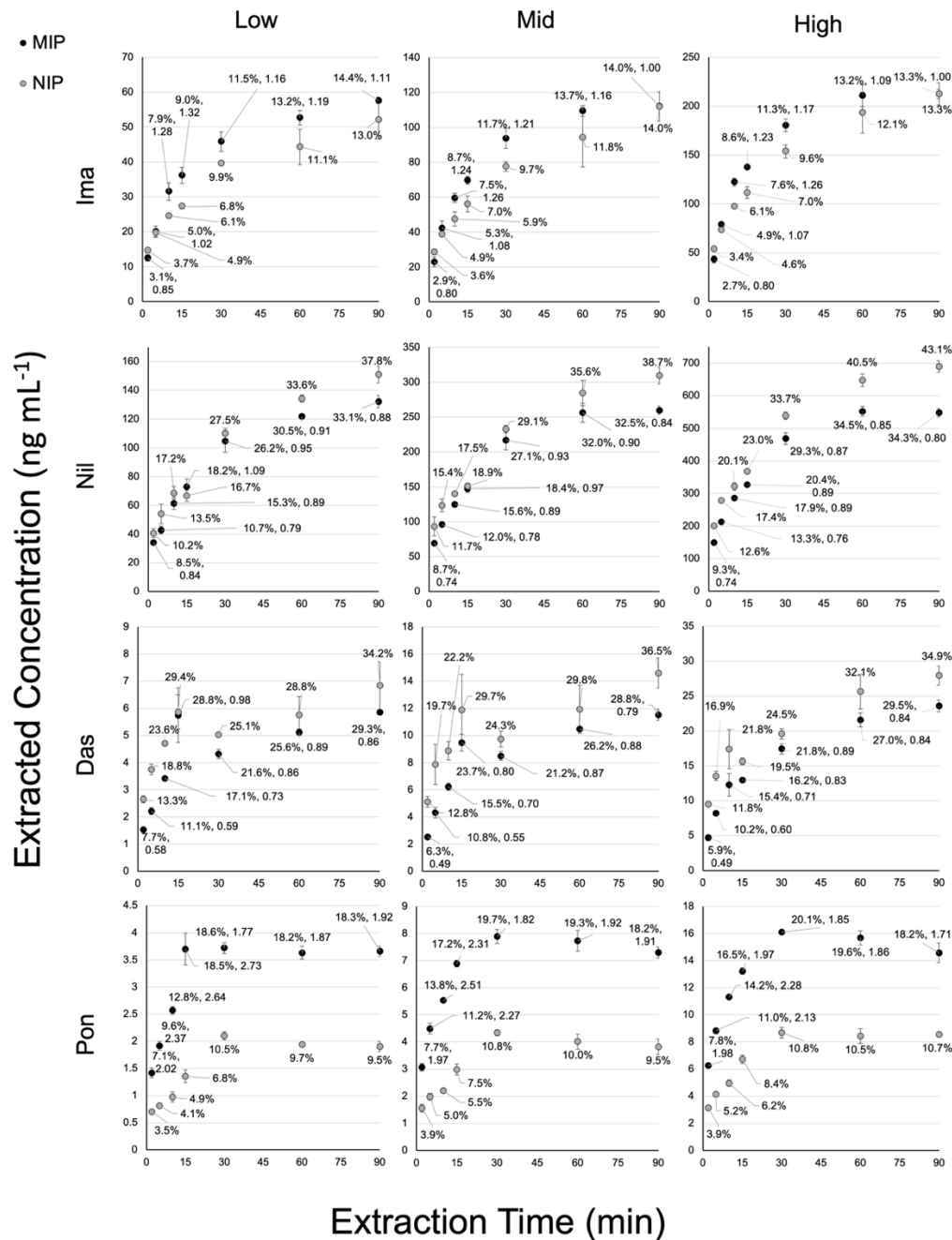


Figure 3.19. TKI Extraction time profiles. MIP data labels are percent recovery and IF, and NIP data labels are percent recovery. Low, mid, and high represent analyte QC concentrations which are 400, 800, and 1600 ng mL<sup>-1</sup> for Ima and Nil, and 20, 40, and 80 ng mL<sup>-1</sup> for Das and Pon. Error bars are SD (n=3).

From the prepared extraction time profiles, an extraction time of 30 min was selected to balance recovery and imprinting, while maintaining method throughput and practicality. It was important to minimize the method time while maximizing sensitivity and reliability of the data. Most of the percent change of recovery occurs in the first 30 min, and only incremental improvements in recoveries are gained over the 30-90 min interval. In addition, with longer extraction times, specificity of the MIPs goes down, affecting the ratio of desired analytes to interfering substances.

#### 3.3.15 Extraction Calibration Curves

Using the 30 min extractions established in section 3.3.4, we constructed extraction calibration curves of the TKIs to ensure the relationship between concentration and signal response is linear. In the first study, we carried out mixed extraction of the four TKIs at several concentration intervals to compare both MIP and NIP films (Figure 3.20). We see linearity across all concentrations for all the analytes with  $R^2$  values greater than 0.99. The blue range on the graphs represent the therapeutic plasma concentration ranges expected for each drug. All drug extraction calibration curves are linear both within and outside of normal clinical ranges.

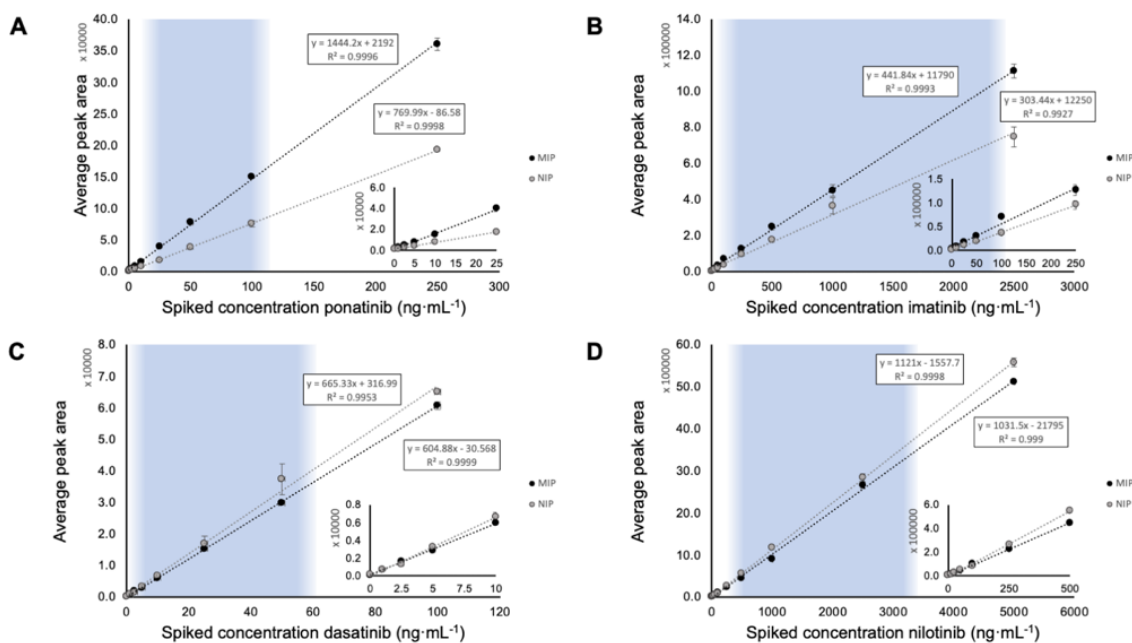


Figure 3.20. Extraction calibration curves comparing MIP and NIP extractions with mixed TKIs at several concentration intervals. A: ponatinib; B: imatinib; C: dasatinib; D: nilotinib. The enclosed, superimposed graphs represent the low concentration range to demonstrate linearity across the entire range. Error bars are SD ( $n=3$ ). Blue background indicates therapeutic range expected in plasma.

To determine if TKIs were competing on the films for binding sites, or if the films were becoming saturated considering the high drug load we were subjecting them to, we carried out an experiment to compare extraction calibration curves of both mixed and individual TKIs (Figure 3.21). We observed no significant difference between mixed and individual extractions, thus meaning this developed device could be used for any combination of the TKIs presented without effect on the results.

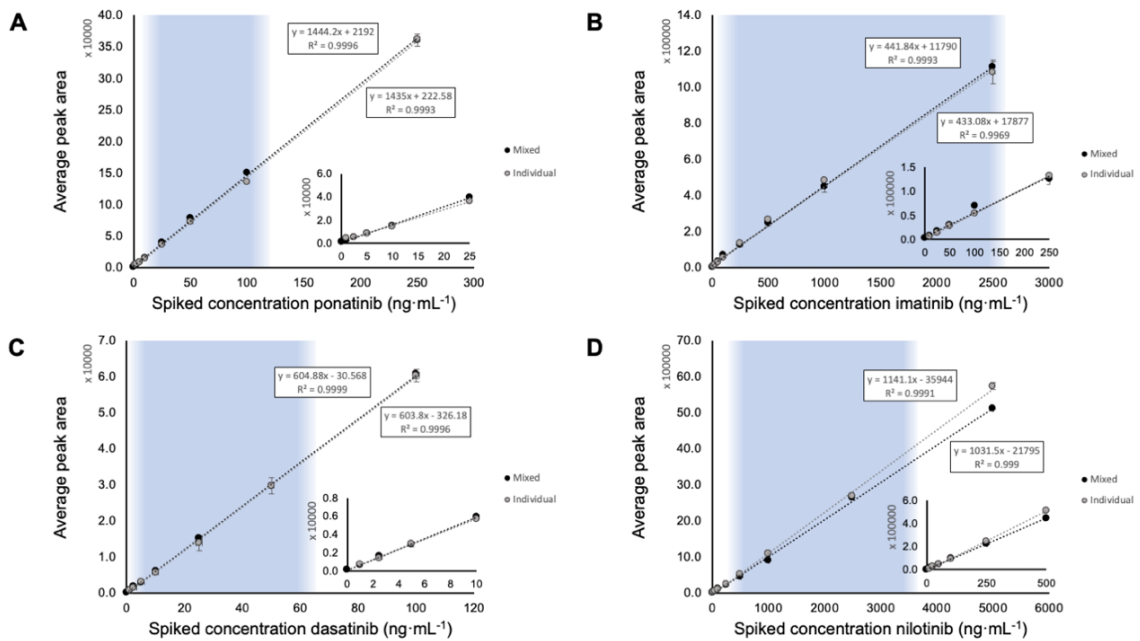


Figure 3.21. Extraction calibration curves comparing mixed and individual extractions of TKIs at several concentration intervals. A: Pon; B: Ima; C: Das; D: Nil. The enclosed, superimposed graphs represent the low concentration range to demonstrate linearity across the entire range. Error bars are SD (n=3). Blue background indicates therapeutic range expected in plasma.

### 3.3.16 Biological Validation: Endogenous Interferences

The effect of endogenous interference on the response of the method was studied using the endogenous interferents kit INT-01 from Sun Diagnostics (Figure 3.22). This kit contains the following human concentrated interferents: conjugated and unconjugated bilirubin, protein, hemolysate, and triglyceride-rich lipoproteins (TRL). These five interferents represent the most observed interference in the clinical diagnostic laboratory and represent various pathologies of plasma. To fully understand the reductions in

response related to the addition of interferents, an initial screen was conducted testing the highest concentration of interferent and unspiked plasma as a control. The highest concentration of each interferent is at an extremely high pathological range, indicative of serious ill-health, and are not expected in the average patient taking a TKI treatment, but rather used to stress the method. Interferents that caused a significant change in percent recovery, protein, hemolysate, and TRL, were then further investigated at various concentrations. Establishing acceptable levels of interferents is essential to clinical applications to ensure reliability of results. Current LC-MS methods have not reported the effects of endogenous interferents on method reliability.



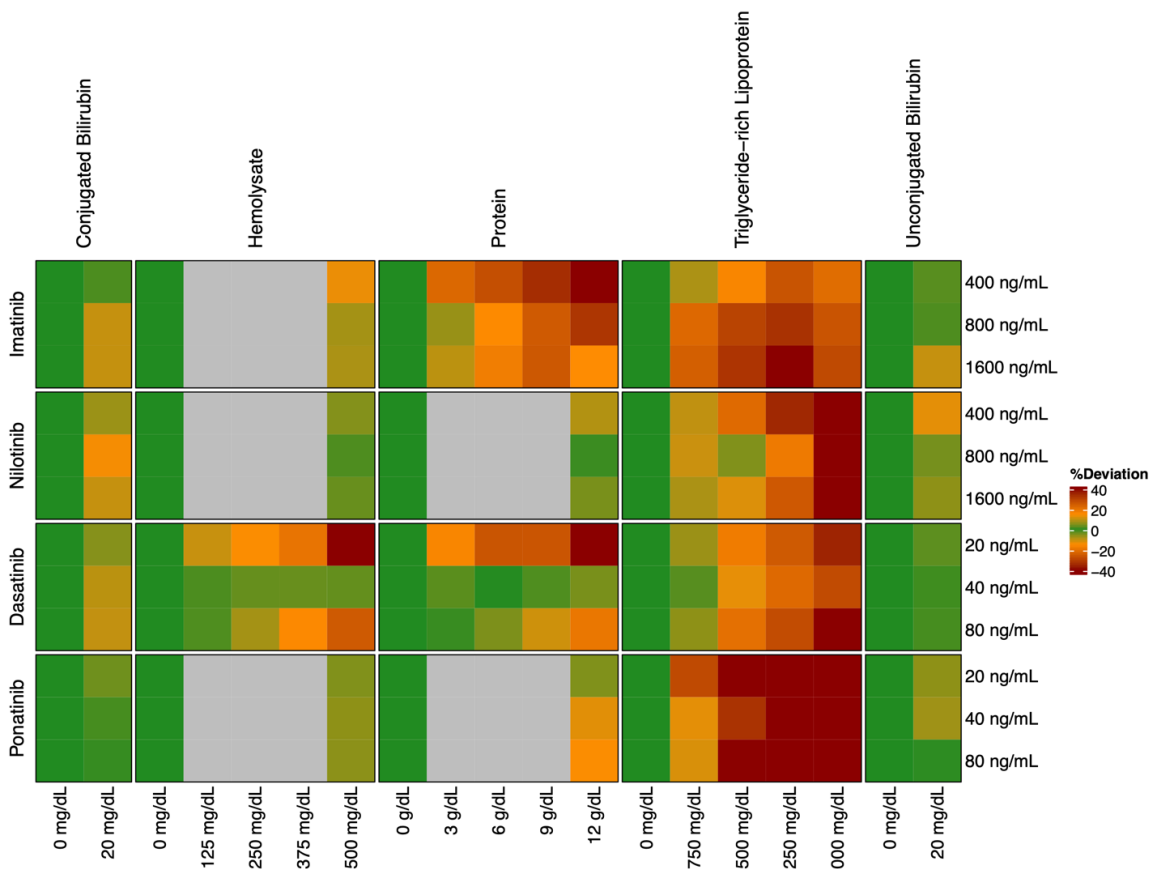


Figure 3.22. Heatmap illustrating percent deviation of recovery of TKIs from human plasma, at three therapeutically relevant levels, with spiked interferents at various concentrations. Percent deviation represents deviation from the recovery of TKIs from non-pathological pooled human plasma. Grey squares represent levels and concentrations that were not tested.

No significant differences (difference due to interferent <15%) were observed between bilirubins (both conjugated and unconjugated) and recovery of any of the drugs at all levels. The final spiked concentration of bilirubins in this experiment was

20 mg dL<sup>-1</sup> representing severe pathological conditions such as hyperbilirubinemia caused by several genetic, metabolic and physiological factors [154].

Protein (a mixture of human serum albumin and  $\gamma$ -globulins) was studied at 12 g dL<sup>-1</sup> (Figure 3.22), a concentration that is abnormal and would represent viral infection, some cancers, and severe dehydration, among other pathologies [145].

No significant effect in recovery was observed after increasing plasma protein for Nil and Pon, whereas Ima and Das suffered significant reductions. Specifically, Das at 20 ng mL<sup>-1</sup> was significantly affected by any added protein over about 2 g dL<sup>-1</sup>. At 40 ng mL<sup>-1</sup> Das, the reduction in response was non-significant. At 80 ng mL<sup>-1</sup> Das, there is only a significant reduction at an extreme 12 g dL<sup>-1</sup> added protein. Ima displayed similar results to Das at the lowest concentration tested, 400 ng mL<sup>-1</sup>, where response was significantly affected by any added protein over about 2 g dL<sup>-1</sup>. At both Ima 800 and 1600 ng mL<sup>-1</sup>, protein supplementation to a maximum of about 4 g dL<sup>-1</sup> is tolerated, but any higher significantly reduced the response for Ima.

Hemolysate, a product of hemolysis of red blood cells, was studied at 500 mg dL<sup>-1</sup> (Figure 3.22), an abnormal concentration that represents improperly collected, processed, or stored blood samples. No significant effect on recovery of Ima, Nil, and Pon was observed. Das showed reduced recovery, requiring further investigation through addition of hemolysate from 0-500 mg dL<sup>-1</sup> in 125 mg dL<sup>-1</sup> increments at three concentration levels of Das. At the low concentration of Das (20 ng mL<sup>-1</sup>) only hemolysate less than 250 mg dL<sup>-1</sup> was tolerated, although 125 mg dL<sup>-1</sup> is likely a more conservative cut-off. At the mid concentration of Das (40 ng mL<sup>-1</sup>), all concentrations of hemolysate seem to be

tolerated. At a high concentration of Das ( $80 \text{ ng mL}^{-1}$ ), hemolysate levels between 250 and  $375 \text{ mg dL}^{-1}$  are moderately tolerated.

Triglyceride-rich lipoproteins were studied at  $3 \text{ g dL}^{-1}$  (Figure 3.22), an abnormal concentration representative of an extremely fatty diet immediately prior to blood collection and/or metabolic disorders [37]. A significant decrease in recovery for all four TKIs was observed. This is unsurprising as the compounds all have  $\text{pK}_a$  values greater than 1.8, thus nonspecific interaction with insoluble lipid is expected where the target analytes will partition into lipidic phases. The effect of adding TRL was further studied at three concentration levels for all four TKIs. Though the addition of about  $1000 \text{ mg dL}^{-1}$  TRL did not affect recovery of Das and Nil (Figure 3.22), most TRL concentrations caused undesired and unacceptable reduction in analyte response. Across drug concentrations, we observed a consistent reduction in response proportional to the amount of TRL in the sample. Although this result initially seems negative, the Adult Reference Intervals for TRL in plasma are: normal ( $<150 \text{ mg dL}^{-1}$ ), high ( $150\text{-}199 \text{ mg dL}^{-1}$ ), hypertriglyceridemic ( $200\text{-}499 \text{ mg dL}^{-1}$ ), and very high ( $>499 \text{ mg dL}^{-1}$ ) [145,155]. All levels of TRL tested in this experiment are in the very high range and are unlikely to be encountered routinely. Focusing on the results of TRL  $750 \text{ mg dL}^{-1}$ , all TKI conditions have less than 15% deviation except Ima  $800 \text{ ng mL}^{-1}$  and  $1600 \text{ ng mL}^{-1}$ , and Pon  $20 \text{ ng mL}^{-1}$ .

There were no negative chromatographic effects observed in the samples, even in the most severely affected samples such as the high level of TRL, suggesting that matrix interferences affect the extraction behaviour of the devices. We hypothesize that our

devices assisted in removing endogenous interferents from the sample to be injected into the LC-MS. This is supported by the visual appearance of the washed films after extraction, the desorption solutions prior to injection, as compared to the plasma with highest interferent levels (Figure 3.23).

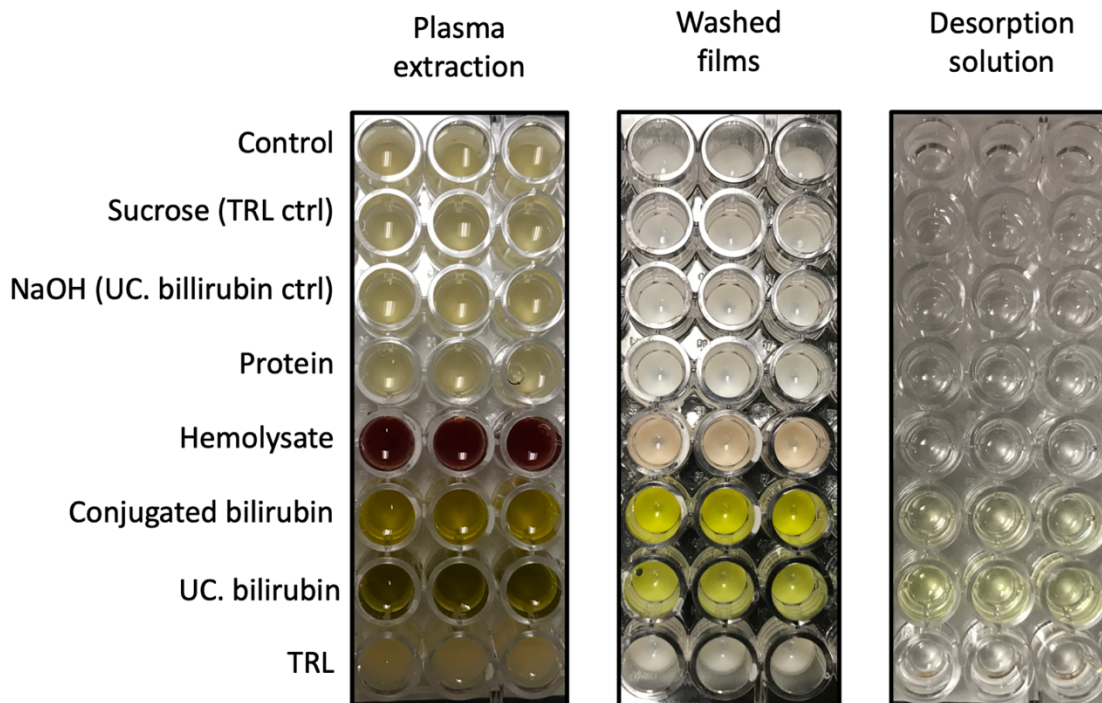


Figure 3.23. Photographs comparing extraction of plasma containing endogenous interferents, washed TF-MIPs, and the resulting desorption solutions. Treatment of endogenous interferents was at highest tested levels.

Establishing the effects of endogenous interferents is important to clinical decision making in therapeutic drug monitoring. To the best of our knowledge an endogenous interferents study this comprehensive has not been done for TKIs, likely because this is

not a current requirement for US based studies as in Clinical Association of Pathologists guidance documents AGC 24130 and GEN 42030.

### 3.3.17 Method Validation

### 3.3.18 Analytical Performance of Thin Film MIPs For Determination of TKIs in Plasma

The quantitative transition was used to quantify each TKI. External calibration curves were prepared using a mixed standard to determine the instrumental linear range for each compound (Figure 3.24). A linear relationship was obtained for Das (0.1-100 ng mL<sup>-1</sup>), Nil (1-1000 ng mL<sup>-1</sup>), and Pon (0.1-100 ng mL<sup>-1</sup>), while a quadratic fit was required for Ima (1-2500 ng mL<sup>-1</sup>).

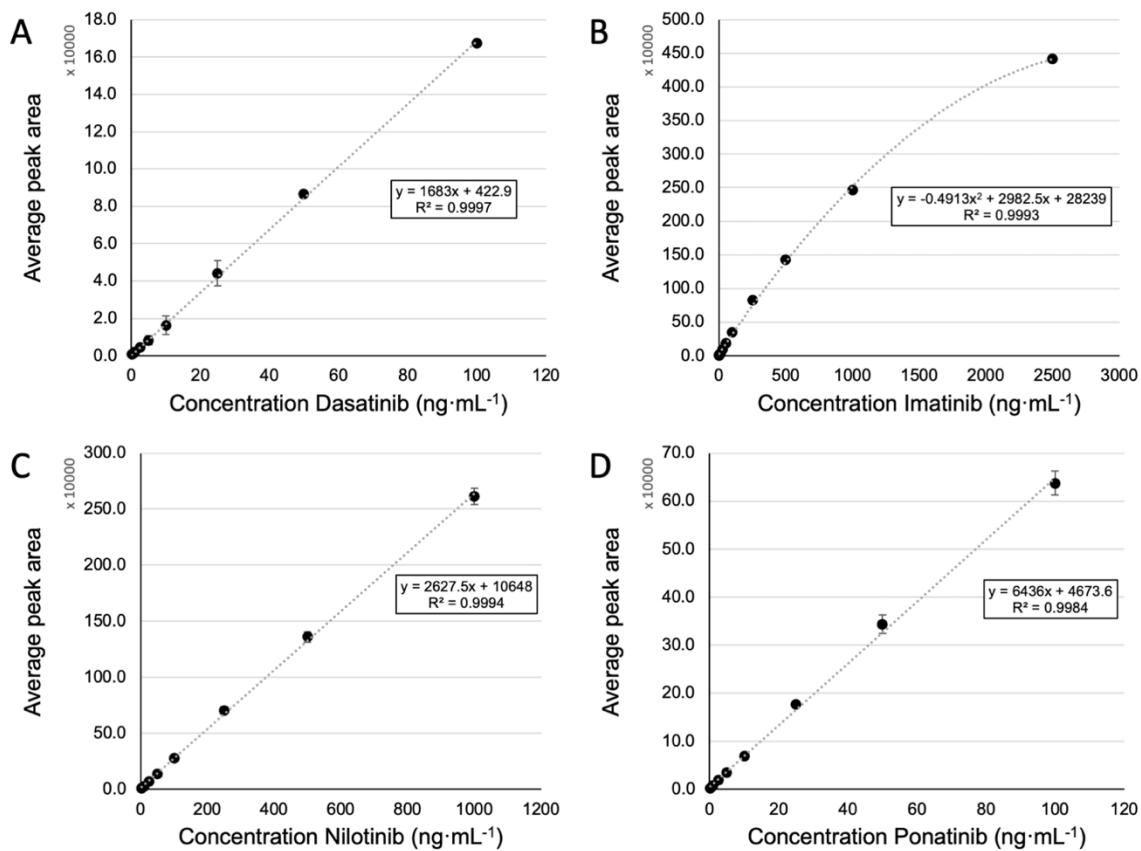


Figure 3.24. External calibration curves of TKIs. A) Das; B) Ima; C) Nil; D) Pon. Error bars are SD of three sets of calibration curves (n=9).

### 3.3.19 Figures of Merit of Analytical Method

The figures of merit for the method can be found in Table 3.5. All values are within acceptable range. The method linear ranges are well within the therapeutic amounts of TKIs observed in patients and are consistent with other reports of LC-MS/MS methods [139]. The limits of detection of this method are at the low clinically relevant range and thus this method would be suitable for application in clinical use and therapeutic drug monitoring.

Table 3.5: Analytical figures of merit for thin film MIP devices for the analysis of TKIs in human plasma. \* indicates quadratic calibration

	<b>Das</b>	<b>Ima</b>	<b>Nil</b>	<b>Pon</b>
<b>Instrumental linear range (ng mL<sup>-1</sup>)</b>	0.1-100 ng mL <sup>-1</sup>	1-2500 ng mL <sup>-1</sup> *	1-1000 ng mL <sup>-1</sup>	0.1-100 ng mL <sup>-1</sup>
<b>Percent recovery (%) at mid-therapeutic concentration</b>	24%	12%	29%	20%
<b>Method linear range (ng mL<sup>-1</sup>)</b>	1-400 ng mL <sup>-1</sup>	8-20,800 ng mL <sup>-1</sup>	3.5-3500 ng mL <sup>-1</sup>	0.5-500 ng mL <sup>-1</sup>
<b>Instrumental limit of detection (LOD)</b>	0.3 ng mL <sup>-1</sup>	0.7 ng mL <sup>-1</sup>	0.3 ng mL <sup>-1</sup>	0.1 ng mL <sup>-1</sup>
<b>Method limit of detection (LOD)</b>	1.25 ng mL <sup>-1</sup>	5.8 ng mL <sup>-1</sup>	1.0 ng mL <sup>-1</sup>	0.5 ng mL <sup>-1</sup>
<b>Instrumental lower limit of quantification (LLOQ)</b>	1.0 ng mL <sup>-1</sup>	2.0 ng mL <sup>-1</sup>	1.0 ng mL <sup>-1</sup>	0.3 ng mL <sup>-1</sup>
<b>Method lower limit of quantification (LLOQ)</b>	4.2 ng mL <sup>-1</sup>	16.7 ng mL <sup>-1</sup>	3.5 ng mL <sup>-1</sup>	1.5 ng mL <sup>-1</sup>

### 3.4 Conclusion

A successful method for measurement of Das, Ima, Nil and Pon from human plasma using TF-MIP extraction followed by UPLC-MS/MS is reported here. The films demonstrate a high level of reproducibility and robustness toward the analytes, being assisted by molecular imprinting. Molecular imprinting of the polymer significantly increased the extraction rate for Pon (IF 1.82) and Ima (IF 1.21), while a slight reduction in imprinting was observed for Das (IF 0.87) and Nil (IF 0.93). Percent recoveries ranged from 12-29%, consistent with other reported SPE and LLE methods for these analytes [139]. The method was optimized using pooled blank human plasma. Only 600  $\mu\text{L}$  of plasma is required for triplicate measurement ( $3 \times 200 \mu\text{L}$ ) of any combination of the four TKIs, which is beneficial if the method is to be used for TDM as a minimal amount of blood would need to be drawn at each collection for the monitoring schedule. Analysis of an extraction time profile showed 30 min provides sufficient recovery to meet detection limits required for the therapeutic clinical range. These extraction devices can be made quickly and reliably, they are cost-effective single-use devices in a 96-well format allowing for high throughput and easy integration of automation into the process. A total of 335 formulas were tested and all extraction parameters were thoroughly optimized to yield an inter-device and batch-to-batch variability less than 5%, demonstrating the reliability of production of these devices for single use. The full method, including sample preparation and UPLC-MS/MS analysis, can be completed in 13 min per sample (triplicate extraction and measurement), if an entire 96 well plate is to be analyzed.



The method detection limits meet low clinical ranges, and the linear range of the method encloses the therapeutic range of each drug. The intra- and inter-day variability is suitable for consistent multi-day use with RSDs below 15% in all cases. The films performed well in plasma, a complex biological matrix, even when plasma was supplemented with endogenous interferences such as protein, bilirubin, and hemolysate. To our knowledge, this is the most comprehensive investigation of the effect of endogenous interferences on TKI analysis methods. An excess of TRL was not well tolerated at extreme levels ( $>750 \text{ mg dL}^{-1}$ ), however was tolerated at a clinically high reference interval for both Das and Nil. Extraction calibration curves comparing mixed and individual drugs spiked in plasma showed no significant differences, demonstrating the flexibility of these devices for measuring one or more of the TKIs from the same sample, using the same method thereby simplifying the workflow for laboratory staff. Although four representative TKIs were used for this study, they represent all three generations of TKIs, thus we expect that these devices could be used successfully for the majority of currently prescribed TKIs.

## **4 Purification of functional gene transfer agents (GTAs) using two-step preparative monolithic chromatography**

### 4.1 Introduction

Gene transfer agents (GTAs) are tailed phage-like particles that facilitate gene transfer between cells, first observed in 1974 in the alphaproteobacterium *Rhodobacter capsulatus* [156–158]. Though GTAs are similar to phages in terms of morphology, a major difference is that GTAs do not actively propagate their own genome [159]. The GTA produced by *R. capsulatus* (RcGTA) packages DNA fragments approximately 4 kb in length [157,160] and is biased against packaging its own genome [161]. The approximately 15-kb RcGTA gene cluster is believed to have evolved from a prophage, which had integrated into the bacterial genome at some distant point in evolution [162] and its expression is now regulated by bacterial cellular pathways [163]. One hypothesis is that GTAs are beneficial by mediating horizontal gene transfer that may increase the involved cells' fitness [161,164,165].

The induction of RcGTA gene expression is a bistable stochastic process, limiting the production of RcGTA to a subset of the population [166,167], and is stimulated by nutrient depletion. Phage-derived holins and endolysins cause lysis of RcGTA-producing cells to release the particles [166], a process which is initiated through quorum sensing when the culture is nearing or at stationary phase and that is also affected by phosphate concentration [168–172]. Similarly, the ability of *R. capsulatus* cells to act as RcGTA

recipients is highest at stationary phase, which can also be induced by nutrient depletion [168,173,174].

Traditional purification strategies for GTAs are like those used for phages, usually involving polyethylene glycol (PEG)/NaCl precipitation followed by gradient ultracentrifugation for several hours [157,160,164,175] or the use of immobilized metal affinity chromatography (IMAC) to purify His-tagged GTA particles [176]. The resulting GTA-containing fractions then need to be dialyzed to remove the reagents used, such as sucrose, rubidium, or imidazole. These purification strategies can lead to damage and inactivation of particles, are limited by scale, and are time consuming. Monolithic columns have been employed for phage purification at both laboratory and industrial scales [177,178]. These columns possess a number of positive chromatographic behaviours such as high capacity, reusability, and easy scalability. Convective interaction media® (CIM) are methacrylate-based monoliths which are functionalized post-polymerization and supplied in an array of chemistries for different phage purification strategies [4]. CIM columns have several practical advantages for phage purification. The columns utilize convective mass transport (CMT), which relies on the relatively large (1-2  $\mu\text{m}$ ) open pores in the monolith to allow samples to move rapidly through the column [5,18,19]. The open nature of monoliths minimizes shear or turbulent forces acting on the particles, thus limiting the amount of degradation and inactivation [19]. Due to the porosity of the CIM monoliths, the binding capacity is very high as compared to other similar chromatographic media. Low backpressure due to the large pores allows these

columns to be used at preparative and industrial scales with no loss of chromatographic performance and they are practically unaffected by increasing flow rates [1,20].

In this work, we present the first report of an ultracentrifuge-free bulk preparation of purified GTA particles that are intact and capable of DNA transfer to recipient cells. We employ a two-step process where the particles are first captured and concentrated using an OH-functionalized CIM monolith, then the GTA-rich fraction of particles is polished using a strong anion exchange (SAX) monolith. The use of the SAX phase allows a buffer exchange to reduce the concentration of phosphate and exchange the elution buffer for the GTAs to be suitable for use in subsequent gene transfer to cells. This method allows for rapid purification of the particles from culture to final elution in less than 2 h on a preparative scale and is an important advancement in purifying GTAs for further study, in addition to being a broadly useful method for purifying small phages.

## 4.2 Materials and Methods

### 4.2.1 Strains and Growth Conditions

Cultures were grown under anaerobic, phototrophic conditions at 35 °C in complex Yeast Peptone Salts (YPS) medium [179], defined *Rhodobacter Capsulatus* V (RCV) medium [171,180], or variations of these media until remaining at stationary phase for several hours, as measured by culture turbidity. The *R. capsulatus* strains used in experiments are provided in Table 4.1. A growth curve was conducted on a closed system (25 mL) consisting of a Hungate tube (20 mL) in a water bath (35 °C) under tungsten illumination, a peristaltic pump, transfer tubing to flow cell (2 mL), and a quartz flow cell

(3 mL) with a pathlength of 10 mm. The spectrophotometer (UV-1600 PC, VWR, Ontario, Canada) monitored 600 nm at 60 s intervals. Lysis of cells indicating the release of RcGTA was tracked by measuring the absorbance of culture supernatant and fractions from purification from 700–900 nm, monitoring for peaks at 802 and 855 nm that correspond to released light-harvesting (LH2) complexes[166,181].

Table 4.1. List of *R. capsulatus* strains used in this study.

Strain	Relevant Properties	Reference
SB1003	Genome-sequenced strain, rifampicin resistant	Strnad <i>et al.</i> , 2010; Yen and Marrs 1976
SBpGΔ280	Knockout of <i>rcc00280</i> in SB1003 background, GTA overproducing strain	Ding <i>et al.</i> , 2019
DE442	GTA overproducing strain, rifampicin resistant	Yen <i>et al.</i> , 1979; Fogg <i>et al.</i> , 2012
DE442Δ <i>clpX</i>	Overproduces empty GTAs (no packaged DNA) without head spikes	Westbye <i>et al.</i> , 2018
B10	Wild type strain, rifampicin sensitive	Weaver <i>et al.</i> , 1975

#### 4.2.2 Chromatographic Purification of GTAs

Cultures (up to 250 mL) were pelleted by centrifugation at  $20,000 \times g$  for 30 minutes. The supernatant was filtered through a 0.22- $\mu\text{m}$  polyethersulfone (PES, Fisher Scientific, Ontario, Canada) membrane to remove any residual cells and large debris. Purifications were carried out on an HP 1050 HPLC system equipped with a

quaternary pump, 50 mL Superloop® (Cytiva, British Columbia, Canada) and 1050 preparative UV detector. Columns were obtained from Sartorius BIA Separations (Ajdovscina, Slovenia). Chromatography was carried out according to Table 4.2.

Table 4.2. Chromatographic parameters and instrument settings for GTA purification.

<i>Parameter</i>	<i>Step 1 – particle capture</i>	<i>Step 2 – particle polishing</i>
<i>Column, bed volume, pore size</i>	CIMmultus OH, 1 mL, 2 µm	CIMmultus QA, 1 mL, 2 µm
<i>Mobile phase A</i>	20 mM Sodium phosphate buffer, pH 7	20 mM Sodium phosphate buffer, pH 7
<i>Mobile phase B</i>	1.5 M Sodium phosphate buffer, pH 7	500 mM Ammonium sulfate, pH 7
<i>Flow rate</i>	5 mL/min	5 mL/min (loading) 3 mL/min (wash and elution)
<i>Run time (including loading)</i>	20 minutes	21 minutes
<i>Gradient</i>	Load 10 minutes, wash 0% <sub>A</sub> to 14 minutes, then to 20% <sub>A</sub> at 15 mins, hold 1 minute then to 100% <sub>A</sub> at 19 mins	Load 10 minutes, wash 100% <sub>A</sub> to 14 minutes, then to 70% <sub>A</sub> at 20 mins
<i>Injection volume/dilution</i>	50 mL 1:1 diluted filtrate to a final conc of 1.5M phosphate	≤50 mL 1:5 diluted fractions from step 1 in ultrapure water
<i>Fraction volume (mL)</i>	4	3
<i>Detection wavelength</i>	280 nm (for protein)	
<i>GTA retention time window (min)</i>	16.5-18.0	14.5-15.5

#### 4.2.3 Nanoparticle Tracking Analysis

Fractions of crude or chromatographically purified GTA particles were serially diluted from 1:10 to 1:10,000 in 20 mM phosphate-buffered saline (pH 7.4). Particle analysis took place in a Malvern Panalytical Nanosight NS300 (Malvern, UK) equipped with a 488 nm excitation laser. The flow cell was maintained at 25 °C and particles were introduced with manual, intermittent pressure of a syringe. The flow cell was monitored visually for particle arrival, then flushed with 200 µL of the test solution before a first reading was obtained on static (not-flowing) solution. Slowly, the syringe was advanced 100 µL more, and a second reading obtained. This was repeated for the third reading. After the three readings, the instrument automatically detected and measured each particle in the video files, and a size distribution was generated for each run.

#### 4.2.4 Gene Transfer Bioassays

RcGTA-mediated gene transfer activity was measured as described, with quantification of the transfer of resistance to rifampicin[182]. HPLC-purified particles were assayed for gene transfer activity through incubation with the recipient strain *R. capsulatus* B10 (Rif<sup>R</sup>) followed by plating on RCV supplemented with rifampicin at 65 µg mL<sup>-1</sup>. Dilutions of purified GTA from 10<sup>0</sup> to 10<sup>-2</sup> were assayed and plated in duplicate.

#### 4.2.5 GTA DNA Extraction

DNA was extracted from purified GTAs after both chromatographic steps. The final elution from the QA purification was concentrated in an Amicon Ultra-15 ultrafiltration device with a nominal weight cut-off (MWCO) of 30 kDa. This concentrate

(50  $\mu$ L) was treated with Proteinase K at 56 °C for 1 hour. Following incubation, DNA was purified using the MinElute Reaction Cleanup Kit (Qiagen, Ontario, Canada). DNA was eluted in 10  $\mu$ L of elution buffer after a 2-minute incubation. DNA was quantified using a Qubit 2.0 fluorometer with the DNA High Sensitivity Kit (ThermoFisher Scientific, Ontario, Canada).

#### 4.2.6 Next-Generation Sequencing

DE442 GTA DNA was subjected to next-generation sequencing using Oxford Nanopore technology. DNA repair and end preparation were completed in quarter reactions using reagents from the NEBNext library prep kit for Nanopore (NEB, Ontario, Canada) in addition to the Oxford Nanopore Ligation Sequencing Library Prep Kit (LSK-109, Oxford Nanopore, UK). In brief, 70 ng GTA DNA (1  $\mu$ L) was combined with control DNA, FFPE repair buffer and enzyme, UltraII End Prep buffer and enzyme mix, and water. The reaction was incubated at 20 °C for 5 minutes followed by 65 °C for 5 minutes. The reaction mixture was cleaned up using AmPure XP beads (Beckman Coulter, Indiana, USA) at 1:1 and eluted in 16  $\mu$ L water. DNA yield was quantified with a Qubit fluorometer.

Adapter ligation was achieved using quarter reactions of the Oxford Nanopore Library Prep Kit LSK-109. In brief, 15  $\mu$ L eluted DNA from the previous step was incubated with ligation buffer (6.25  $\mu$ L), adapter mix (1.25  $\mu$ L) and T4 DNA Ligase (200,000 u mL<sup>-1</sup>; 2.5  $\mu$ L, NEB). After incubation for 10 minutes at room temperature, the reaction mixture was cleaned up using AmPure beads at 0.4:1, and the final library was eluted in 7  $\mu$ L Elution Buffer and quantified with a Qubit fluorometer.



The Flongle flow cell (FLG-001, Oxford Nanopore), used in a MINion Mk1c sequencer was flushed with 100  $\mu$ L flush solution (117  $\mu$ L Flush Buffer and 3  $\mu$ L Flush Tether) before being loaded with the library solution. The library solution was mixed immediately before loading. The loading solution consisted of 6  $\mu$ L of final library, 10  $\mu$ L of Loading Beads II and 15  $\mu$ L of Sequencing Buffer II.

#### 4.2.7 SDS-PAGE and Western Blotting

SDS-PAGE and Western blotting were used to detect the RcGTA major capsid protein (approximately 30 kDa) as previously reported [183].

### 4.3 Results

Due to the high biological variability of GTA production between strains and growth conditions, we first sought to compare GTA release by several strains. Strains were grown to stationary phase under photoheterotrophic anaerobic conditions in RCV medium and supernatants were evaluated for GTA abundance through western blot (Figure 4.1A). Three strains produced significant and comparable amounts of GTA: DE442, DE442 $\Delta$ *fliC*, and SBpG $\Delta$ 280. Low, but detectable, amounts of GTA were present in SB1003. Preliminary chromatographic purifications demonstrated that flagella were not detrimental to the purity of isolated GTAs, thus a *fliC* knockout was not required. All further work was conducted using DE442.

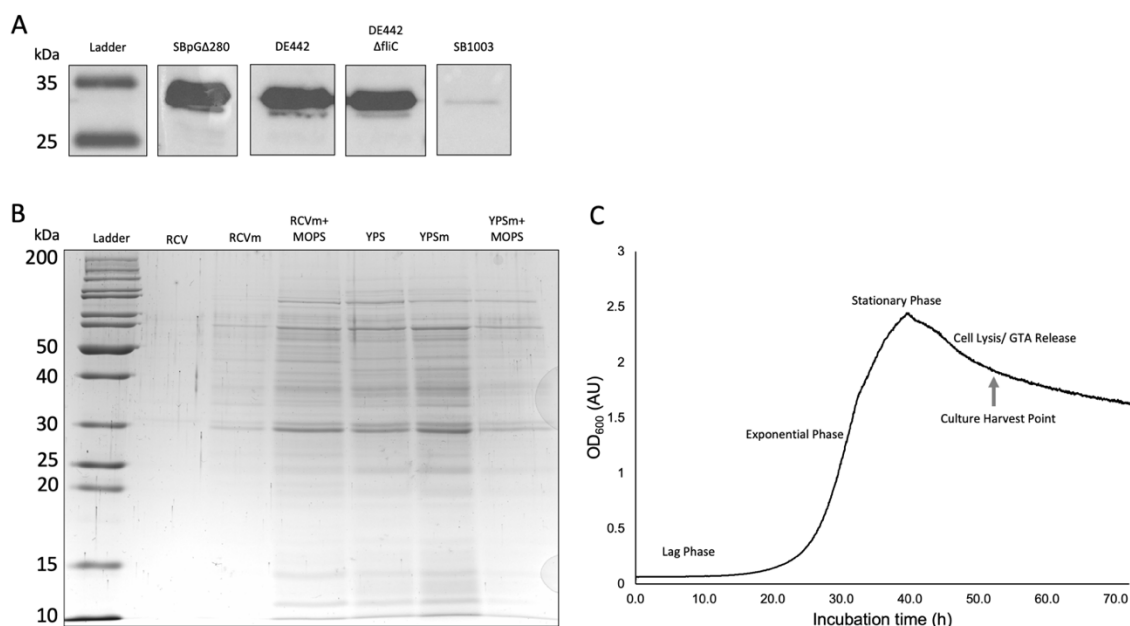


Figure 4.1. A) Western blot measuring RcGTA major capsid protein (approximately 30 kDa). Supernatants of photoheterotrophic anaerobic cultures in RCV were harvested at stationary phase to compare GTA release. B) SDS-PAGE (12%) comparing GTA release by DE442 in various culture media. Media were compared by the intensity of the RcGTA major capsid protein band at approximately 30 kDa. C) Growth curve of DE442 grown under photoheterotrophic anaerobic conditions in RCVm+MOPS at 35 °C.

The selection of culture media has previously been shown to affect GTA production, with increased phosphate concentration found to inhibit GTA release[171]. RCVm is a medium with reduced phosphate and YPSm has reduced magnesium and calcium. The addition of 3-(N-morpholino)propanesulfonic acid (MOPS) buffer makes up for the lack of buffering capacity in these modified media and results in a more stable pH during cell lysis[171]. DE442 was grown in six media to stationary phase and

supernatants were assayed for GTA release by SDS-PAGE (Figure 4.1B). Cultures grown in RCVm+MOPS and YPSm showed the most GTA protein in the supernatant, however the benefits of defined media, both for the growth of the organism and for chromatographic purification, led to our selection of RCVm+MOPS for further work.

A representative, high-resolution growth curve was constructed (Figure 4.1C) to determine optimal culture harvest time. An optimal harvest time was after the onset of stationary phase and lysis, but before significant degradation of GTA particles could occur, which was determined to be between 48 and 52 hours after inoculation.

The first chromatographic purification was completed by diluting culture filtrate with potassium phosphate to a final concentration of 1.5 M. This high salt environment promotes GTA interaction with the surface of the CIMmultus OH monolith. Culture media components and polar contaminants were unretained. GTA particles were then eluted using a descending gradient with a brief hold to improve chromatographic resolution between GTA and an earlier eluting contaminant peak, which is suspected to be membrane vesicles containing photosynthetic complexes (chromatophores) (Figure 4.2A). Fractions were collected from the purification and assayed for the GTA major capsid protein by SDS-PAGE (Figure 4.2B). It was observed that Fraction 4 contained the highest amount of GTA based on intensity of the capsid protein band at approximately 30 kDa. No GTA remained on the column as indicated by the regeneration wash (NaOH wash lane) and a significant pre-concentration of GTA was obtained as indicated by comparison of the intensities of the GTA band in the starting material (SM) and Fraction 4.

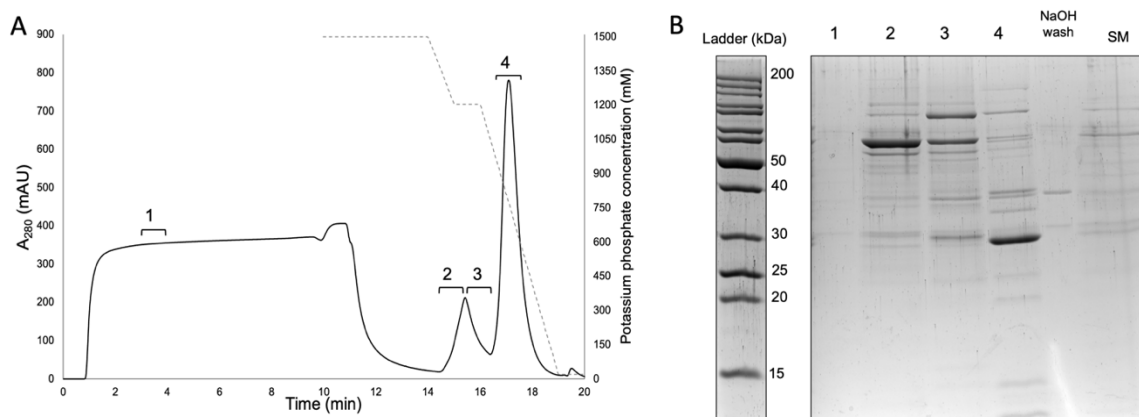


Figure 4.2. CIMmultus OH purification of DE442 GTA from culture filtrate. A) Purification chromatogram monitoring 280 nm (primary y-axis). Number labels indicate position of collected fractions. Dashed line indicates decreasing potassium phosphate gradient (secondary y-axis). B) SDS-PAGE (12%) of collected fractions (number labels 1-4 in A), a fraction collected from the regeneration wash (NaOH wash) and filtrate starting material (SM).

The fractions obtained were observed to be slightly green in colour, indicating the presence of photosynthetic pigments, likely contained within chromatophores. To quantify this contaminant, visible light absorbance spectra were collected from 700-900 nm (Figure 4.3A). Wavelengths of particular interest are 802 and 855 nm, which correspond to the LH2 photosynthetic pigments[166,181]. Absorbance by Fraction 4 was greatly reduced compared to the starting material. Interestingly, the column flowthrough (Fraction 1) showed a reduction in absorbance compared to starting material, while Fraction 2 showed the highest absorbance of the samples tested. This indicated that the

chromatophores bind to the column and were in the contaminating peak preceding the GTA particles.

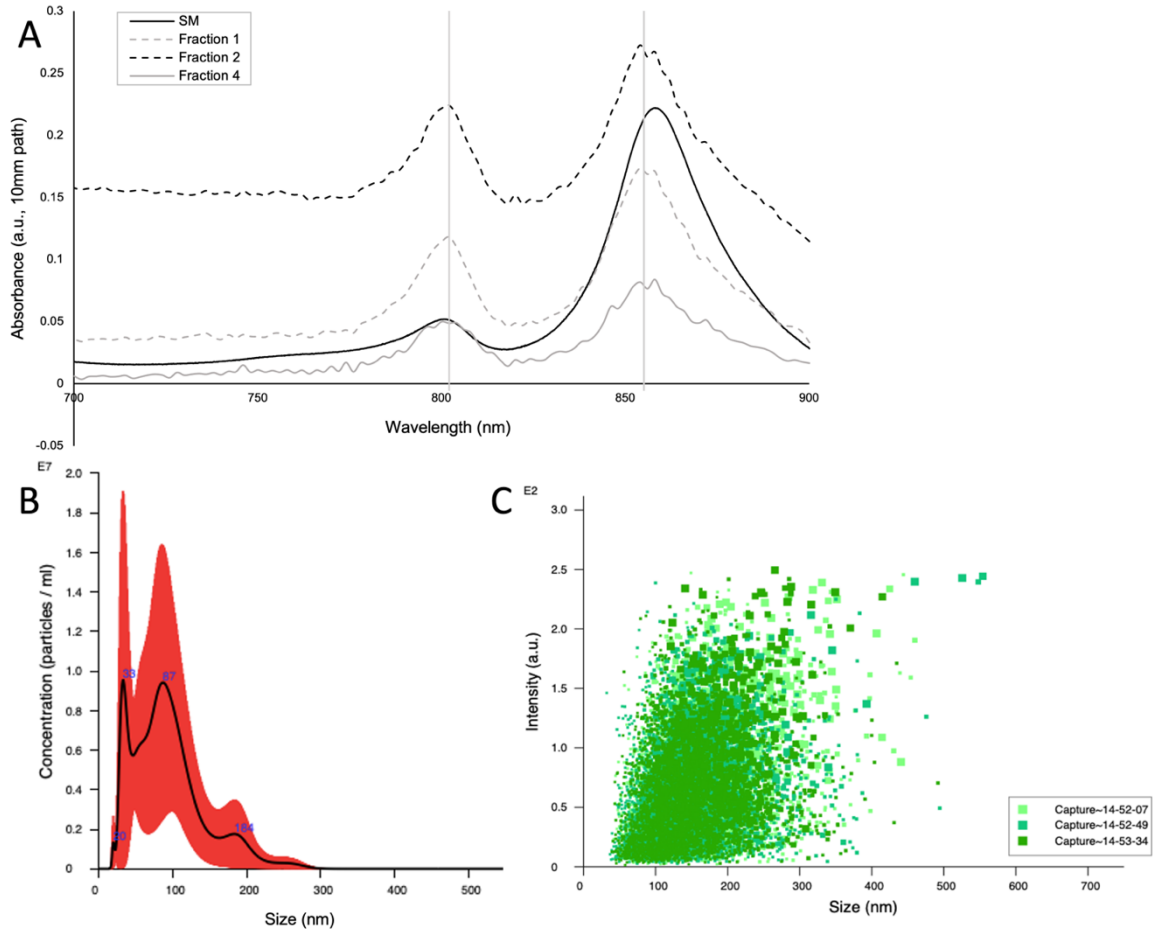


Figure 4.3. CIMmultus OH purification of DE442 GTA from culture filtrate. A) Visible light spectra of filtrate starting material (SM) and fractions collected in Figure 2A. Vertical lines at 802 nm and 855 nm indicate LH2 absorption peaks, indicative of presence of chromatophores. B) Comparison of the concentration and size of measured particles in Fraction 4 through nanoparticle tracking analysis, n=3. C) Particle size distribution scatter of Fraction 4 through nanoparticle tracking analysis, n=3 as indicated in legend.

To further investigate the purity of Fraction 4, nanoparticle tracking analysis was carried out (Figure 4.3B and C). GTA capsids have a diameter of 35 nm [164] and chromatophores vary in size but are generally larger than GTAs, with the majority of chromatophores between 40-160 nm [184]. The relative portion of GTA-sized particles in Fraction 4 was higher than that of the contaminating peaks, however a large range of particle sizes was observed.

Though many contaminants had been removed, a second purification step was completed using a CIMmultus QA monolith (Figure 4.4). Fraction 4 was diluted 1:5 in distilled water to reduce the ionic strength of the loading solution. In this purification, GTAs interact with the column stationary phase through their net surface charge and are eluted through disruption of interaction by increasing ionic strength (Figure 4.4A). Ammonium sulfate was used as the elution salt to allow biocompatibility with subsequent gene transfer activity of the particles. GTAs eluted as a sharp peak with a retention time of 14.5-15.5 min. Contaminating material eluted as small peaks before and after GTAs, however almost no absorbance was detected in the flowthrough during loading (0-10 min). The purified GTA was assayed by SDS-PAGE (Figure 4.4B). The RcGTA major capsid protein is visible at approximately 30 kDa, as well as GTA-related bands comparable to previous SDS-PAGE and subsequent mass spectrometric analysis [164]. All bands present in the lane can be putatively attributed to the GTA structure such as the megatron (138 kDa), portal (43 kDa), tail fibre (38 kDa), distal tail (23 kDa), and adaptor (21 kDa) proteins [164].

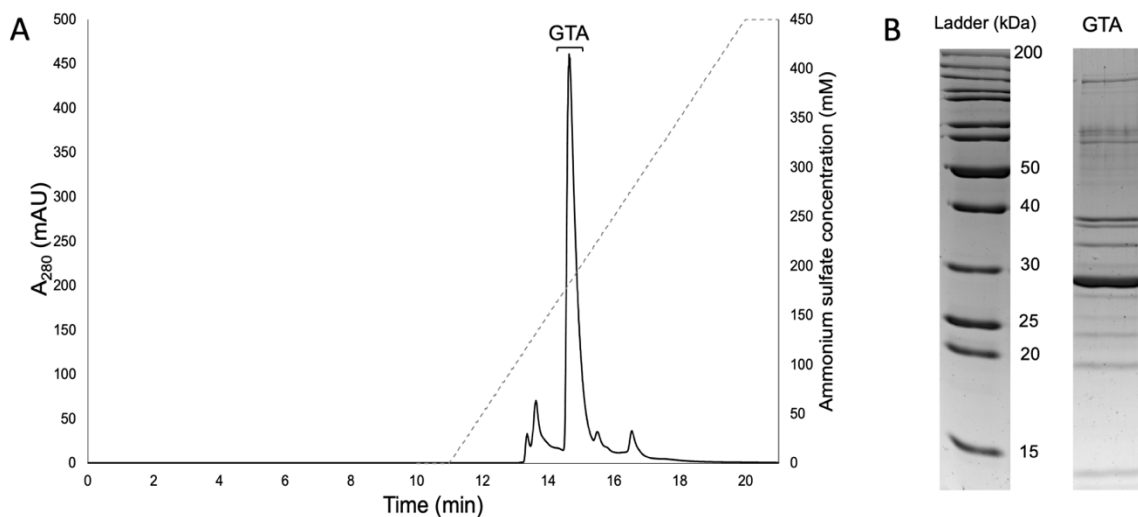


Figure 4.4. CIMmultus QA purification of DE442 GTA from OH purification fraction 4.

A) Purification chromatogram monitoring 280 nm (primary y-axis). The GTA fraction was collected as indicated. The dashed line indicates increasing ammonium sulfate gradient (secondary y-axis). B) SDS-PAGE (12%) of the collected GTA.

A visible light spectrum of purified GTA (QA GTA) from this step was compared to the starting material (Culture Filtrate) and fraction 4 (OH purified) from the first purification step (Figure 4.5A). Absorbance at 802 and 855 nm was negligible in the final purified GTA, a significant reduction compared to the end material from the previous purification step. Nanoparticle tracking analysis was carried out on the purified GTA (Figure 4.5B and C). In the particle size distribution plot, a large single peak is observed at 35 nm diameter with negligible concentrations of other particle sizes. This is supported by the particle size scatter plot, showing a concentrated distribution of particles at the desired size of 35 nm. Some contaminating particles were detected but significantly fewer than after the previous purification stage (Figure 4.3C). In contrast to the first purification

that yielded particles up to 550 nm (Figure 4.3C), particle size was limited to less than 175 nm.



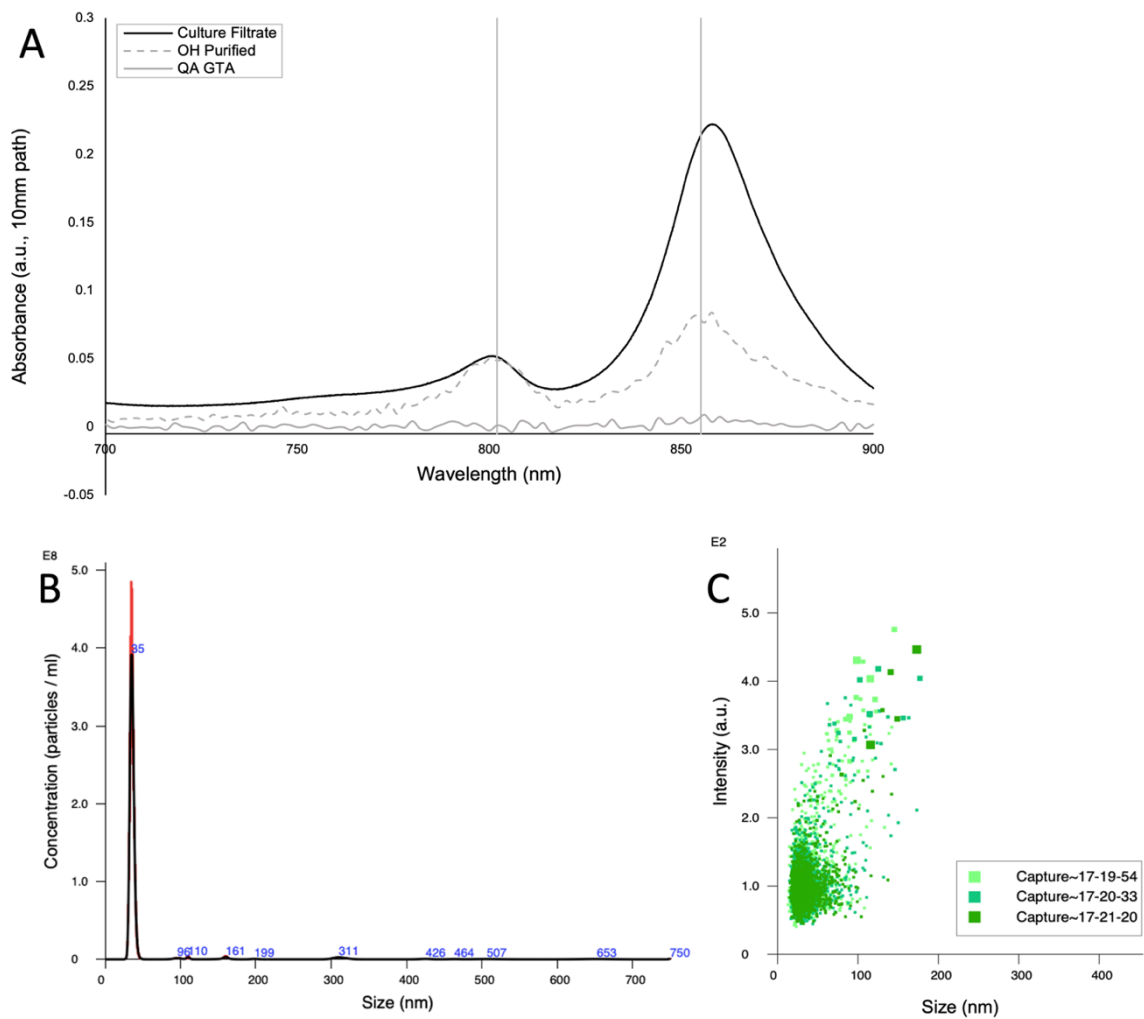


Figure 4.5. CIMmultus QA purification of DE442 GTA from OH purification fraction 4. A) Visible light spectra of filtrate starting material (SM), OH purification fraction 4 (OH purified), and the collected GTA peak from QA purification (QA GTA). Vertical lines at 802 nm and 855 nm indicate LH2 absorption peaks, indicative of presence of chromatophores. B) Comparing the concentration and size of measured particles in collected GTAs through nanoparticle tracking analysis, n=3. C) Particle size distribution scatter of collected GTAs through nanoparticle tracking analysis, n=3 as indicated in legend.

Obtaining functional particles was the ultimate goal of this study. To determine if the purified GTAs still exhibited gene transfer activity, a bioassay was conducted to quantify transfer of rifampicin resistance to the rifampicin-sensitive recipient strain, *R. capsulatus* B10 (Table 4.3). Rifampicin-resistant colonies were obtained following incubation of the purified GTAs with the rifampicin-sensitive strain (Table 4.3). The number of resistant colonies decreased with dilution and therefore minimal inhibitory effects of the final elution mixture were observed. The dilutions were achieved through addition of G-buffer, a well-established solution known to support gene transfer [174,182]. This validates that the purified GTAs were functional and that the elution chemistry of the second purification step is compatible with subsequent GTA activity.

Table 3. Gene transfer bioassay using purified GTA.

Dilution	Average colony count <sup>a</sup>
Negative control	0
Undiluted	135
10 <sup>-1</sup>	35
10 <sup>-2</sup>	25

<sup>a</sup> Averages were calculated from duplicate assays.

DNA was isolated from purified GTAs and evaluated for purity and size (Figure 4.6). Agarose gel electrophoresis was conducted to compare the GTAs isolated from both DE442 and DE442 $\Delta$ *clpx* that does not package DNA (Figure 4.5A). As expected, there was no DNA observed from DE442 $\Delta$ *clpx*, and a large amount of approximately 4-kb DNA was extracted from the DE442 GTAs. A library was prepared using DNA

extracted from DE442 GTA and loaded onto a Flongle flow cell (Figure 4.5B). The read distribution histogram shows a sharp peak with a base-called length of approximately 4 kb, corresponding to the expected full-length DNA isolated from RcGTAs, with obtained 4 kb sequences aligning with the *R. capsulatus* SB1003 reference sequence (NCBI accession number [CP001312.1](https://www.ncbi.nlm.nih.gov/nuccore/CP001312.1)). Reads observed at less than 4 kb in Figure 7 are likely due to fragmentation of the DNA during extraction and library preparation. Similarly, the small peak between 7-8 kb is an artifact of ligation-based library preparation where a small proportion of the DNA dimerizes, yielding chimeras.

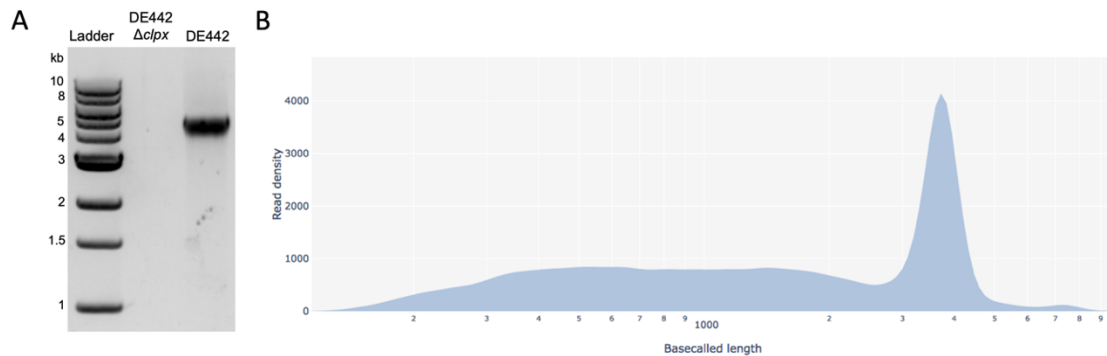


Figure 4.6. Analysis of DNA extracted from purified DE442 GTAs. A) Agarose gel (1%) of DNA extracted from purified GTAs from two strains of *R. capsulatus*. The DE442 DNA band is at approximately 4 kb and the negative control DE442 $\Delta$ *cIpx* lacks a DNA band. B) Oxford Nanopore MinION read distribution histogram of DE442 GTA DNA, comparing base-called length and read density.

#### 4.4 Discussion

Isolation of GTAs from *R. capsulatus* under photoheterotrophic anaerobic growth conditions is challenging using density gradient centrifugation methods because of the co-purification of chromatophores, flagella, and cell debris. Although IMAC using His-tagged particles has been previously reported as a method to purify GTAs, the purification is expensive and poorly scalable, and in the paper cited here, the resultant particles do not appear to have been tested for functionality[176]. One-step IMAC using nickel- nitrilotriacetic acid (Ni-NTA) agarose also has associated challenges such as non-specific binding of undesired proteins to the column and the use of high imidazole concentrations that can interfere with stability of particles[185].

The method developed here is valuable, robust, and yielded pure GTAs from bacterial cultures on a milligram scale with minimal contaminants in less than two hours. The use of two monolithic phases, with different chemistries, removes many interfering contaminants and allows a higher level of purity to be achieved. This process is not only useful for the purification of GTAs but can also be applied for difficult phage purifications with only slight modifications to the ionic strength gradients. In addition to culture-based investigations, it seems possible the process could be modified for isolation of trace level GTAs from environmental samples for GTA discovery. As demonstrated here, the isolated GTA DNA can be used in next generation sequencing applications, and therefore mixtures of GTAs contained in environmental samples could be co-purified and analyzed.

The two-step chromatographic approach delivers particles in a solution that is compatible with use for subsequent experiments. The process is gentle enough to yield GTA particles that are intact and able to transfer DNA to recipient cells, confirmed by gene transfer events that appear to have a linear relationship with the dilution of purified particles with negligible inhibitory effects from the elution mixture. Particles obtained from this process will allow for further study of the mechanism of function of GTAs in *R. capsulatus* and should be applicable to all species that produce GTAs, including those that have yet to be discovered. The method also has broader applicability for other small phages, particularly in applications such as therapeutics where a highly purified phage preparation is desired.

#### 4.5 Acknowledgements

We thank Sartorius BIA Separations for the generous gift of the columns. Additionally we thank both Marko Narobe and Thomas Koseltec for their guidance and discussion about using the CIMmultus line of monolithic columns. We also thank Roshni Kollipara for her comments on the manuscript. This project was supported by funding from the Natural Sciences and Engineering Research Council of Canada to ASL (RGPIN-2017-04636 and RGPIN-2022-03791).

## 5 Direct Coupling of Extraction Devices to MS

### 5.1 Introduction

#### 5.1.1 Coated Blade Spray Mass Spectrometry

Coated blade spray mass spectrometry (CBS-MS) is an emerging area of focus in clinical chemistry due to several technical and performance benefits the approach offers, namely speed and ease of analyses in time sensitive situations with simplified equipment and processes as compared to LC-MS/MS workflows. In contrast to assays which use chromatographic front ends, the approach in CBS-MS is to couple extraction devices directly to a detection instrument (normally a MS), eliminating many sample preparation and separation steps. The general scheme of CBS-MS workflows are highly similar [56,60,186,187] (Figure 5.1); samples (normally a biofluid) are either spotted onto a polymeric sorbent, or the extraction device is immersed into the biofluid. Following extraction, a rinsing step reduces background interferences. Finally, the device is placed in front of an MS inlet, where a desorption solvent is applied. A high voltage (HV) is applied either to the sorbent itself, in the case of conductive materials [187,188], or the solid support (commonly a stainless-steel blade) [57,61] to initiate ionization of analytes. With the inlet of the MS at ground relative to the potential applied to the blade, a Taylor cone is generated forming a spray of charged droplets at the tip of the device. As the total volume of desorption/ionization solvent is at the  $\mu\text{L}$  scale, desolvation process occurs readily at the inlet of the MS allowing for efficient ion generation. Direct coupling allows for introduction of the a high proportion of extracted mass (depending on the efficiency of

the desorption process) into the MS in a short burst of ions in a relatively small volume (compared to LC-MS), thus lowering detection limits [60].

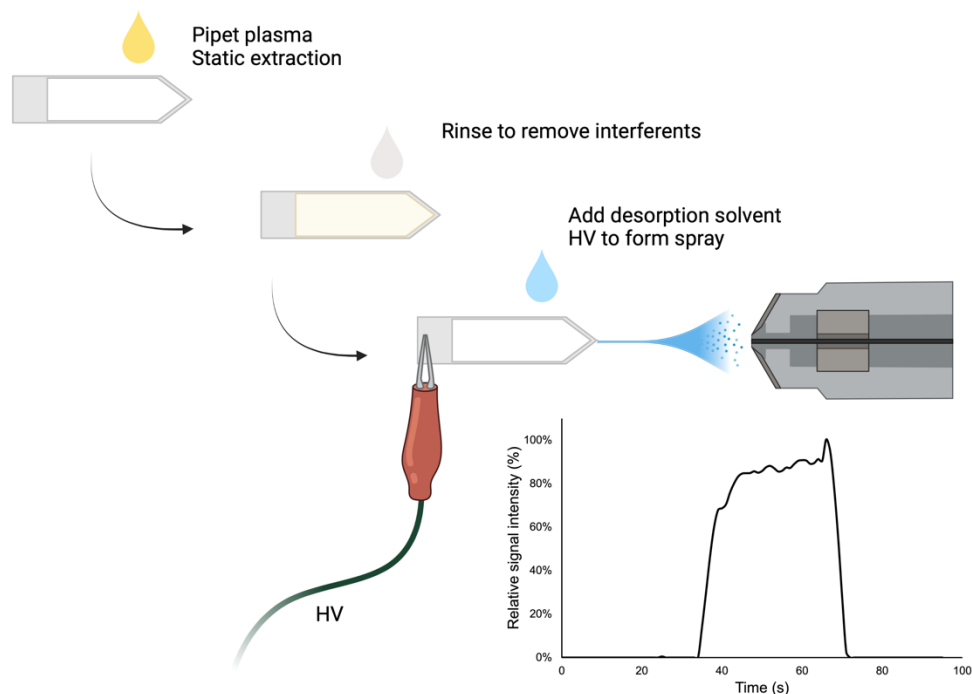


Figure 5.1. Scheme for CBS-MS experiments using plasma. Created using Biorender.com.

CBS-MS has several advantages over traditional analyses using chromatographic separation including reduced cost of analysis, lower solvent consumption, time and consumable savings and culminate in higher throughput. The trade-off of these benefits can be less accurate quantitation, matrix interference and increased inter-patient and -device variability, as outlined in this chapter. The application of CBS-MS in a clinical setting is limited by several factors, namely the sensitivity and accuracy required for the test, the implications of erroneous test results and assay-specific interactions between

interferents and analytes. There are many applications where CBS-MS technologies would be highly suited, including screening (presence/absence) tests that require the use of MS, including drugs of abuse, performance-enhancing drugs, and toxicology screens. Some therapeutic drugs, when clinically justified for therapeutic drug monitoring, are also suited to CBS-MS workflows where rapid results are required, with minimal sample draw from the patient. The cases where CBS-MS would not be suitable as an alternate to LC-MS based assays would include trace quantification of drugs, hormones and metabolites, cases where interferents significantly affect quantitation and situations where an error in quantification could lead to catastrophic clinical outcomes and/or detriment to the patient's treatment regime.

The assays for which CBS-MS can be used need to be carefully evaluated for clinical risks and benefits in combination with experimentation that investigates if the responses are robust under varying conditions and if performance criteria for the test can be met. Traditional analyses generally require more complex instrumentation such as tandem MS that may only be present in larger testing centres that are normally associated with instrument backlog, potentially resulting in a delayed analysis. These questions need to be answered not only by the analytical chemist, but by a multidisciplinary healthcare team, who can better weigh the trade-offs between the figures of merit of the proposed assay and how it could affect the patient's treatment.

#### 5.1.2 Handheld Mass Spectrometry

Along with the development of CBS-MS extraction devices, handheld and miniature mass spectrometers are gaining popularity[189–191]. In the context of clinical



application and CBS-MS, the benefits of handheld MS includes decentralized, portable, inexpensive, and simple methods for measurement of compounds. The use of handheld MS may allow for bedside testing in critical care and emergency situations, which can also be implemented in remote and/or small communities to provide timely access to a broader range of tests. To fit these applications, miniaturized MS systems will need simplified interfaces along with software to allow non-experts in MS to conduct tests and obtain high quality data.

In the past decade, a number of handheld MS devices have become commercially available [189,190], some of which are summarized in Table 5.1. Each developed device has some distinguishing features; however they all face similar challenges, including attaining and maintaining vacuum, sample introduction pressure spikes and limitations in dynamic range due to small physical size of mass analyzers[189,190].

Table 5.1. Selected portable trap-based MS instruments and their respective properties.

System Name	MX908	Mini 12	cheMSense 600	MMS 1000
Reference	[191,192]	[189,193]	[194]	[195]
Developer	908 Devices	Purdue University	Griffin Analytical technologies, Inc.	1 <sup>st</sup> Detect
Weight (kg)	4	15	25	8
Power (w)	NR*	100	<1200	70
Mass Analyzer	Microscale ion trap	Rectilinear ion trap	Cylindrical ion trap	Microscale ion trap
MS/MS?	Yes	Yes	Yes	Yes
Sample Introduction/ Ionization	API, TD, Vapor, CD	API, PS, ES	MIMS, vapor and gas, EI	MIMS, EI
Mass Range (m/z)	55-470	50-900	40-425	45-400

\* At least 3h continuous use using two, hot-swappable rechargeable batteries.

Abbreviations: TD: thermal desorption; PS: paper spray; EI: electron impact; MIMS: membrane introduction mass spectrometry; CD: corona discharge; ES: electrospray; API: atmospheric pressure inlet

One particularly successful innovation in miniature MS is the handheld M908 and its successor, the MX908 designed by 908 Devices[192]. These devices were manufactured with law enforcement, military, and homeland security applications in mind, and feature onboard software for measurement of chemical warfare agents, explosives, drugs, and industrial chemicals (including those used in clandestine drug manufacturing labs). The M908 and MX908 are handheld MS systems that rely on a

microscale trap for mass analysis. The original model, M908, was designed with a glow discharge ionization source, while the MX908 utilizes a corona discharge ionization source. In-source collision-induced dissociation (CID) is used to increase fragmentation through controlled acceleration of the analyte ions through the source-trap aperture. The creation of secondary fragments allows for an enhanced spectral complexity that helps offset the low resolution of the MS for compound identification. The benefit of the MX908 over other portable MS instruments is the emphasis on compound detection algorithms that aid in accurate identification (Figure 5.2).

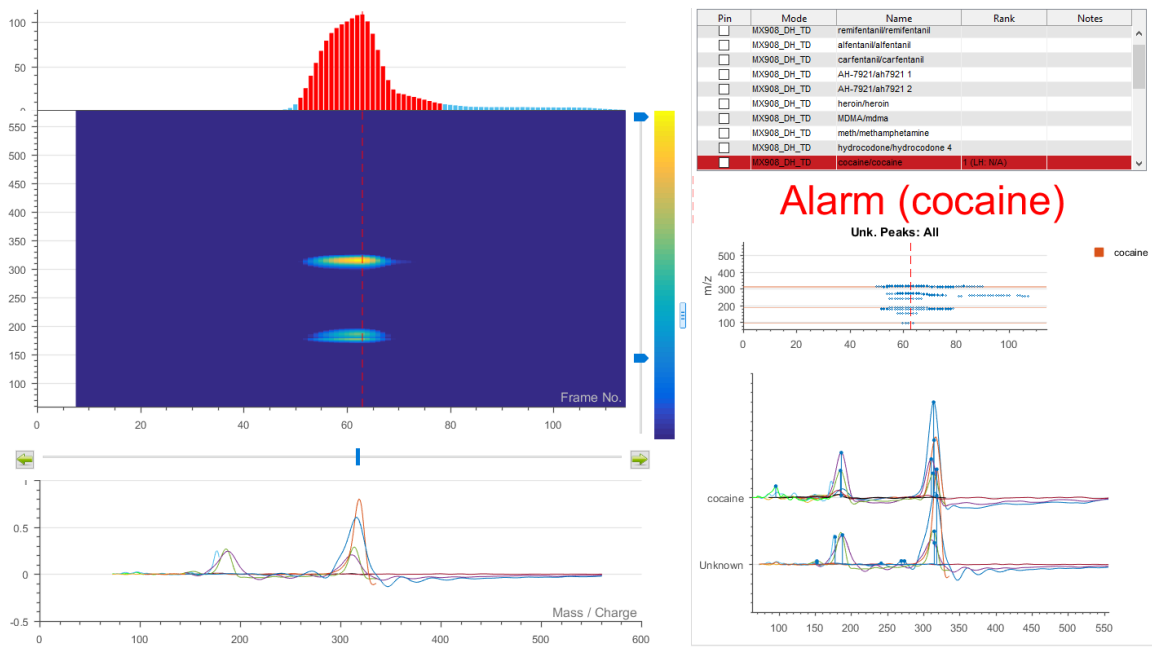


Figure 5.2. MX908 software interface with built in drug detection algorithms showing the spectral matching, heatmap of signal and relative scan intensity in thermal desorption mode.

As can be observed from Figure 5.2, the spectra obtained have wide peak widths, which hinders accurate mass determination. Multiple fragments and their relative signal intensities are used to confirm the identity of the analyte, such as in the example presented for cocaine where the molecular ion is present at  $m/z$  303 and a prominent fragment ion at  $m/z$  182. The spectra are matched against a reference library, with consideration for peak patterning and relative intensities, which functions similar to conventional EI libraries, such as those published by NIST. These intelligent software algorithms are able to identify several structural variants through spectral differentiation. Exemplifying this point is the ability for the MX908 to differentiate over 2000 analogues of fentanyl [196], a potent and highly lethal synthetic opioid that has become increasingly present in the illicit drug markets[197]. Variants of fentanyl such as carfentanyl, which is 100 times more potent than fentanyl can cause death at  $\mu\text{g}$  scale doses [198]. In this chapter, direct coupling of monolithic thin film microextraction devices to both benchtop and handheld mass spectrometers are presented. A custom coated-blade spray source was developed for the Xevo TQ-S where data is presented for measurement of mycophenolic acid, cocaine, MDMA, methamphetamine, methadone and methadone- $\text{d}_3$  in human biological fluids. A second custom source was designed and used to semi-quantitatively measure mycophenolic acid on the MX908 handheld MS. Finally, a MIP mesh designed to extract OPPs from water was used with the thermal desorption accessory of the MX908 to measure malathion and chlorpyrifos in water.

## 5.2 Materials and Methods

### 5.2.1 General

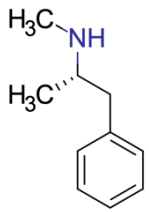
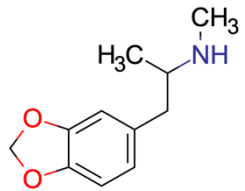
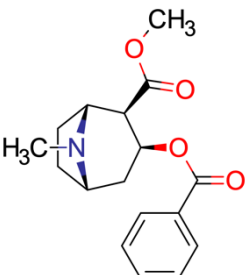
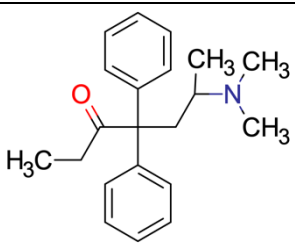
Solvents and reagents used for desorption and standard preparation (MeOH, ACN, water, and formic acid) were of Optima LC-MS grade and purchased from Fisher Scientific (ON, Canada). All reagents used for preparing extraction devices were obtained from Fisher Scientific (ON, Canada). Ultrapure water ( $18.2 \text{ M}\Omega \text{ cm}^{-1}$ ) was prepared in-house using a Milli-Q water purification system (ON, Canada). Stainless-steel substrates for preparation of extraction devices were purchased from McMaster Carr (GA, US) and cut using a WAZER waterjet cutter (NY, USA). Synthetic human urine pooled human urine and pooled human plasma ( $2\times$  charcoal stripped) were purchased from BioIVT (CT, USA). Biological specimens were frozen at  $-20 \text{ }^\circ\text{C}$  and thawed at  $4 \text{ }^\circ\text{C}$  for one hour prior to use.

## 5.3 Analytical Targets and Device Preparation

### 5.3.1 Drugs of Abuse

Standard solutions of cocaine in acetonitrile ( $1.0 \text{ mg mL}^{-1}$ ), methamphetamine, 3,4-methylenedioxymethamphetamine (MDMA) methadone and methadone- $\text{d}_3$  in methanol ( $1.0 \text{ mg mL}^{-1}$ ), were purchased from Cerilliant (TX, USA). A mixed standard solution of drugs ( $100 \text{ mg L}^{-1}$ ) was prepared from purchased standards in methanol. The structures and relevant properties of these compounds are listed in Table 5.2. Thin film devices were prepared as previously reported[199].

Table 5.2. Structures and physical properties of selected drugs of abuse

Compound	MW (g/mol)	Structure	pKa	logP
Methamphetamine	149.2		9.87	2.07
MDMA	193.2		10.38	1.68
Cocaine	303.3		8.6	2.3
Methadone	309.4		9.2	3.93

### 5.3.2 Mycophenolic acid

Materials, methods, and procedures for MPA can be found in Chapter 2.

### 5.3.3 Organophosphorus pesticides

Malathion and chlorpyrifos were purchased from Sigma Aldrich (Oakville, ON, Canada). The structures and relevant properties of these compounds are listed in Table 5.5. Synthesis of pseudo template 2- $\{[diethoxy(sulfanylidene)-\lambda\text{-phosphanyl}]amino\}$ acetic acid was performed according to procedure described by Wang et al. [200] with modifications. Glycine (3 mmol, 2.253 g) was dissolved with stirring in 30 mL 2.5 M NaOH in a 50 mL round bottom flask for 30 min under nitrogen. *O,O'*-diethyl chlorothiophosphate (3 mmol, 4.65 mL) was then added dropwise over a 10 min period. The solution was stirred for 6 h at room temperature. The unreacted components were removed by washing the reaction mixture with diethyl ether ( $2 \times 25$  mL). The pH was adjusted to 2.0 using 1 M HCl and the product was extracted into diethyl ether ( $3 \times 50$  mL). The diethyl ether extracts were pooled and dried using anhydrous magnesium sulfate. Following solvent removal using a rotary evaporator, the product was obtained as a white solid in a good yield (5.888 g, 86%). The product was characterized by high resolution ESI-MS. For the protonated molecule  $[C_6H_{13}NO_4PSH]^+$  the  $m/z$  was 227.03742, which is in excellent agreement with the calculated value of 227.03812 ( $\delta = -3.05$  ppm). MIP mesh devices were prepared as previously reported [110].

## 5.4 Instrumentation and Operating Conditions

### 5.4.1 Benchtop MS

A Xevo TQ-S equipped with a custom-built Z- axis nano electrospray ionization (nESI) source was used for quantitation and used in positive mode MRM. Ionization was obtained by setting blade voltage at +3.0 kV, ESI source temperature at 20 °C, and desolvation temperature at 500 °C. A nitrogen generator (Peak Scientific, Scotland, UK) was used to supply cone gas at 150 L h<sup>-1</sup>. Details on MRM transitions, cone voltage, and collision energy for drugs of abuse and an internal standard for are included in Table 5.3. The conditions for measurement of MPA are identical to those presented in Chapter 2.

Table 5.3. MRM transitions, cone voltage, and collision energy of selected drugs of abuse on Waters Xevo TQ-S.

Drug	Precursor ion (m/z)	Cone voltage (V)	Product ion 1 (m/z)	Collision energy (eV)	Product ion 2 (m/z)	Collision energy (eV)
Methamphetamine	150.2	50	91.1	15	119.1	27
MDMA	194.1	30	105	30	163	10
Cocaine	304.2	30	105	40	182.1	25
Methadone	310.2	30	105	25	265.1	19
Methadone-d <sub>3</sub>	313.2	30	105	25	268.3	13

### 5.4.2 Handheld MS

A handheld, corona-discharge, high-pressure trap mass spectrometer (MX 908, on loan from 908 devices, Boston, MA) was held at 1.2 Torr for all experiments. The trap



aperture voltage was maintained at 25 V with the appropriate polarity for the ionization mode. For analysis of MIPs targeting mycophenolic acid, a custom source configuration was designed in-house consisting of a stainless-steel ion source housing, lined with a PTFE insert for electrical isolation (908 Devices, MA, USA). The blade was attached to a micromanipulator (Narishige, Tokyo, Japan) and positioned in-line with the inlet slit. HV was applied from an external variable power supply (U33010, American 3B Scientific, GA, USA) with a potential range of 0-5000 V and a current limit of 2 mA. The MX908 spectrometer and the HV power supply shared a common ground to complete the circuit. For analysis of fabric mesh extraction devices, the thermal desorption swab source attachment was used with a heating cycle as follows: ambient temperature over 0-15 s, rapid ramp to 250 °C held over 15-35 s, rapid cooling and held at ambient during 35-45 s. The thermal desorption sampling pump (drawing air through the fabric) was operated at a 50 % power (corresponding to 6 V) from 0-42 s. The corona discharge source was operated at either +4.4 kV or -3.9 kV for positive and negative ionization, respectively.

## 5.5 Results and Discussion

### 5.5.1 Xevo TQ-S Custom Source Interface

A custom source interface for the Xevo TQ-S was fabricated by Technical Services at Memorial University of Newfoundland. A functional prototype of a nano electrospray source was created (Figure 5.3). In this prototype, a computer mouse (Figure 5.3D) was used to activate data collection processes on the MS just before the addition of desorption solvent to the blade. This system was necessary as the normal method to

trigger data acquisition using Waters software could not be activated remotely, or in a timely fashion. A second crucial component added were gas plugs on the source interface (Figure 5.3D). The use of gas plugs allows a required source line pressure to be reached. Without the use of gas plugs the system went into failure mode due to a perceived gas leak.

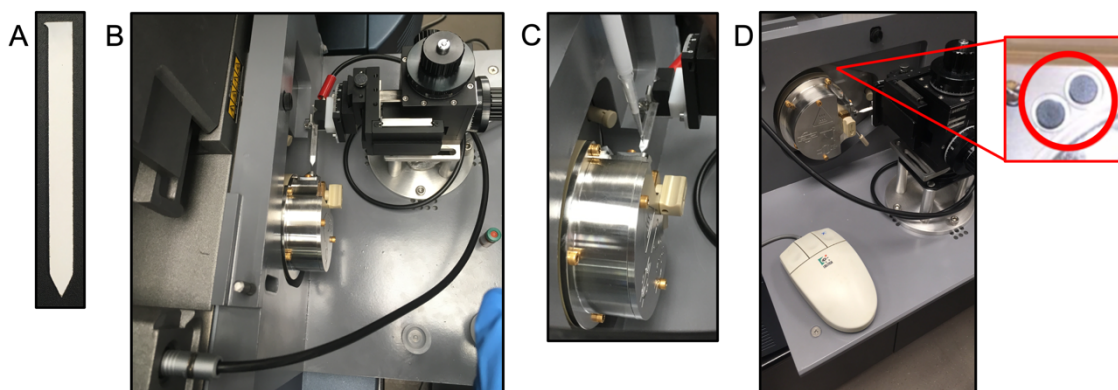


Figure 5.3. Direct coupling of coated blades to Xevo TQ-S. A: An example of a coated blade used in this configuration. B: Overhead view of the micromanipulator and HV connections on the Z-axis source. C: Using a pipette to deliver desorption solvent for sample introduction. D: Gas plugs (indicated in red). Computer mouse (on source stage) programmed through the MS (contact closure) to initiate data collection.

The instrument software is operated as if the Waters commercial nano-electrospray source is installed, except the source electrical harness is wired to deliver HV to the micromanipulator grippers which hold the coated blades. The coated blades are mounted so that the tip is 1-2 mm from the cone aperture; the distance was optimized by moving the blade forward incrementally just until arcing is observed, then backward

about 0.5 mm. Preliminary experiments indicated that this distance gives the highest signal. Once data collection is initiated, 10-20 seconds of data is recorded prior to the addition of a small volume of desorption solvent (1-10  $\mu\text{L}$ ). The signal commences as the solvent sprays from the tip. The movement of solvent front in the sorbent from the deposition position to the tip is observable (similar as seen in thin layer chromatography), with no further signal observed once all of the solvent has been spray from the device. The data is analyzed as a single 'peak' where the entire spike in signal is integrated (Figure 5.4).

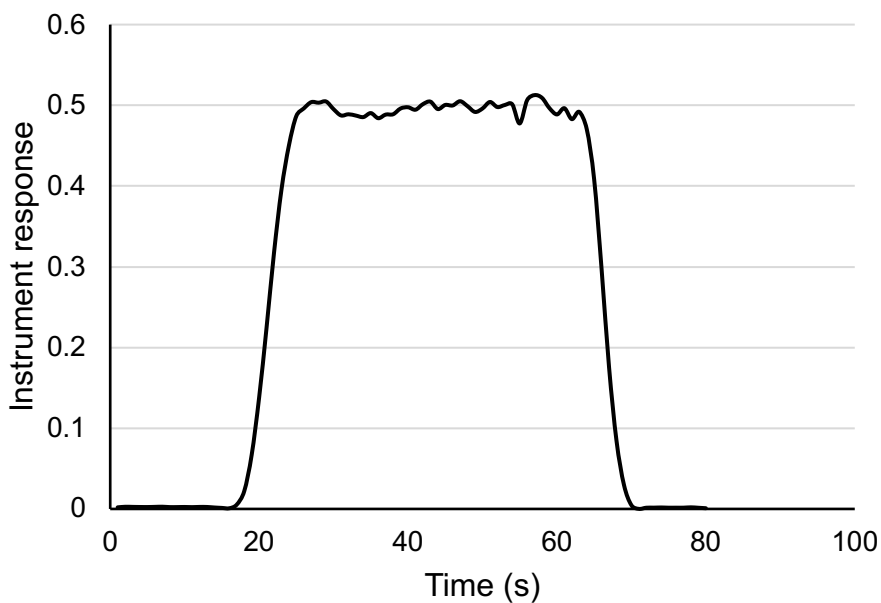


Figure 5.4. Representative trace of mycophenolic acid captured from coated blade spray from MIP device where 5  $\mu\text{L}$  was used as desorption volume.

A calibration curve for MPA standards using CBS-MS (Figure 5.5) showed great linearity and reproducibility from 0.5 to 10 mg L<sup>-1</sup>. Error between sprays was minimal as illustrated from the error bars (0.2-12.7% RSD), which are not visible on the scale of the calibration presented.

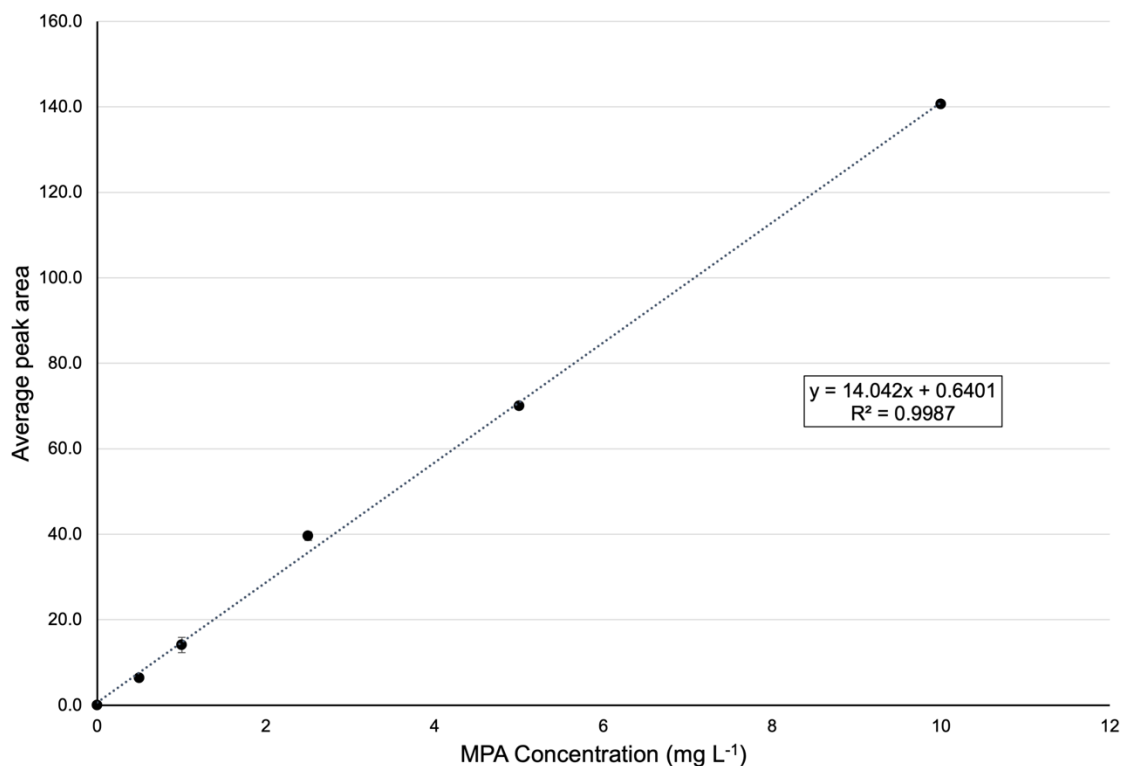


Figure 5.5. Calibration curve constructed from coated blade spray of mycophenolic acid standards. Error bars are  $\pm$ SD (n=3) and are too small to be observed on this scale.

### 5.5.2 Drugs of Abuse in Biological Matrices by Coated Blade Spray on Xevo TQ-S

Mixed standards of the selected drugs of abuse were used to generate calibration curves (Figure 5.6). A satisfactory linearity and repeatability were obtained from

0.1-100 ng mL<sup>-1</sup> with the exception of cocaine, saturating the detector channels at 50 ng mL<sup>-1</sup>. The low range calibrations (from 0.1 to 2.5 ng mL<sup>-1</sup>) also showed satisfactory linearity, and a very close slope to the full calibration ranges. This indicates that the devices are suitable for measurement across the entire presented ranges. The figures of merit for the developed method were calculated and presented in Table 5.4.

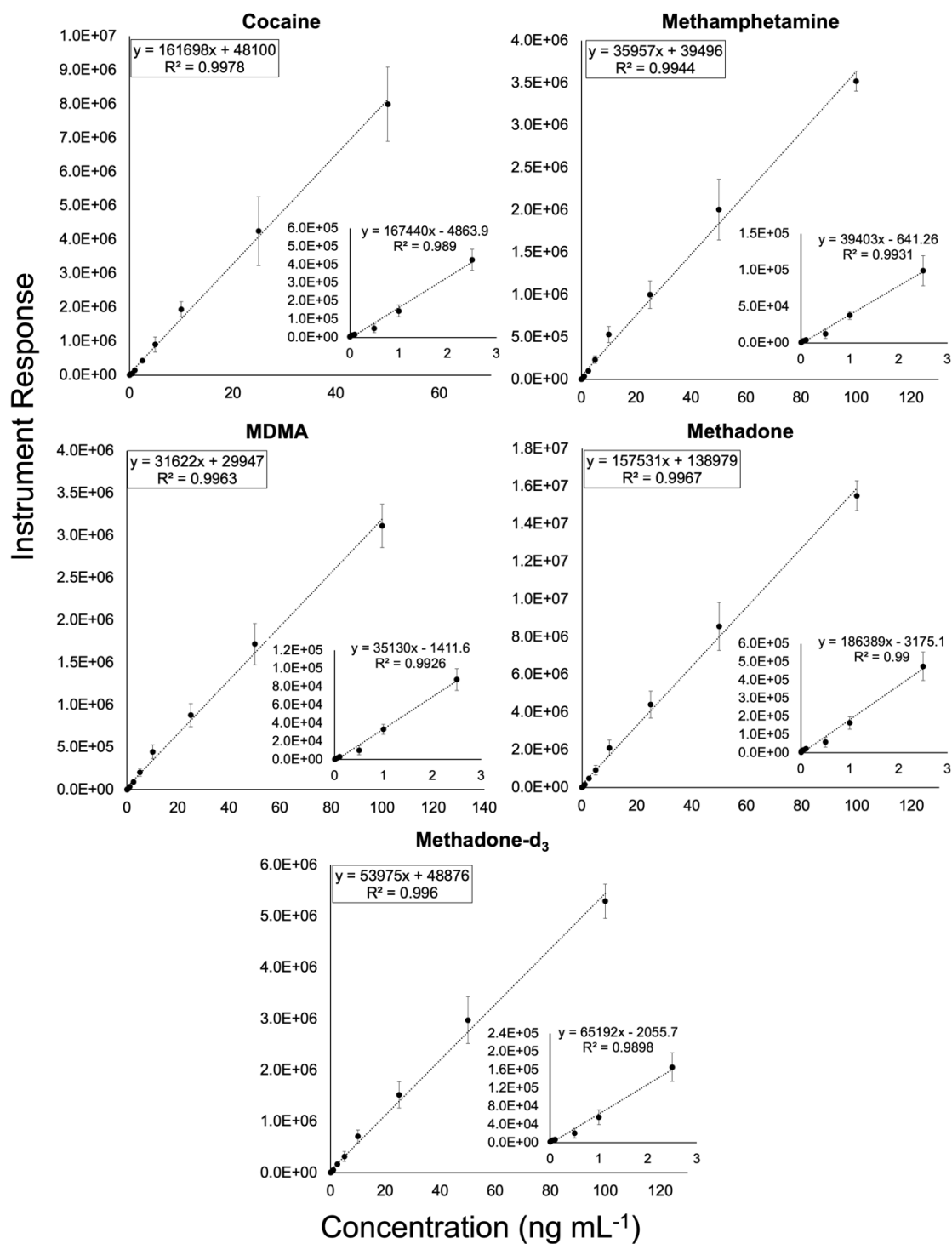


Figure 5.6. Calibration curves constructed by coated blade spray of mixed drugs of abuse standards using Xevo TQ-S. Error bars are  $\pm$ SD (n=3).

Table 5.4. Figures of merit including linear range, LOD, LOQ for analysis of drugs of abuse using coated blade spray on Xevo TQ-S

Compound	Linear range (ng mL <sup>-1</sup> )	LOD (ng mL <sup>-1</sup> )	LOQ (ng mL <sup>-1</sup> )	slope	R <sup>2</sup>
Cocaine	0.1-50	0.09	0.24	161698	0.9978
Methamphetamine	0.1-100	0.09	0.26	35957	0.9944
MDMA	0.1-100	0.06	0.11	31622	0.9963
Methadone	0.1-100	0.09	0.25	157531	0.9967
Methadone-d <sub>3</sub>	0.1-100	0.09	0.24	53975	0.9960

Using pooled patient plasma, urine, and a synthetic human urine, the effect of severe matrix on relative signal were examined (Figure 5.7). The experiment consisted of spiking the biofluid, dispensing 10 µL of the fluid on the coated blade and allowing it to air dry. This dried biological fluid represented the worst matrix interference possible with no washing and mass precipitation of biomolecules on the sorbent. Desorption solvent was applied to the films and analysis using the CBS-MS on the TQ-S was conducted.

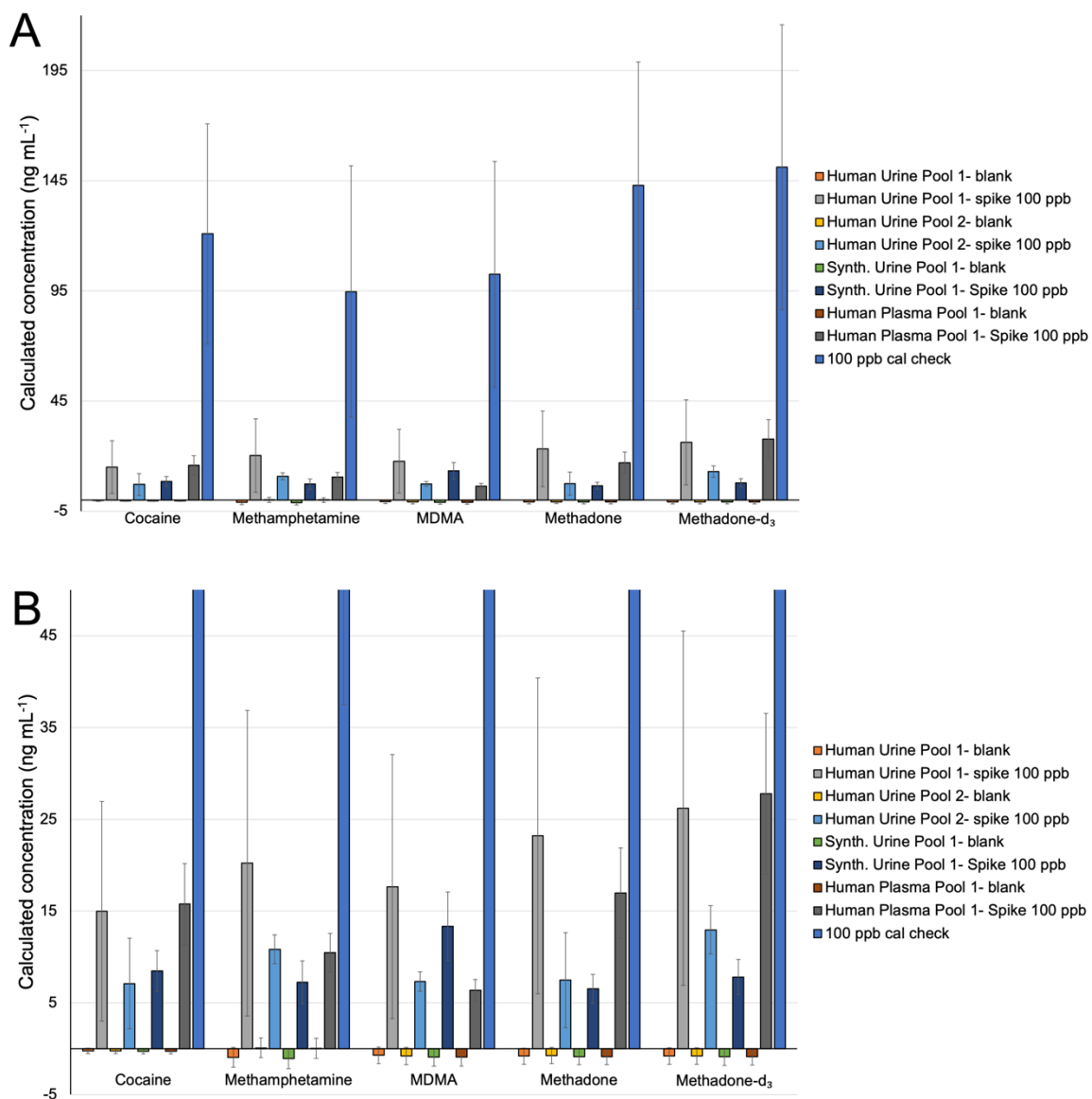


Figure 5.7. Evaluation of matrix effects in blank and DOA spiked biological fluids by coated blade spray MS. A) Full scale figure; B) Y-axis adjusted for better representation of matrix differences. Error bars are  $\pm$ SD (n=3).

The results using the extreme matrix loadings presented in Figure 5.7 show a significant decrease in response, yielding reductions in signal to approximately 20% of



the control response at 100 ng mL<sup>-1</sup>. As expected, based on biofluid complexity, signals from human urine were better than from plasma. Removal of the biofluid, followed by washing and drying the film prior to desorption were used for subsequent experiments as described in previous thesis chapters.

Inter-device variability was assessed through static extraction of DOA spiked human plasma followed by CBS-MS (Figure 5.8). Percent recovery, shown as data labels ranged from 34% for methamphetamine to 86% for methadone-d<sub>3</sub>, with an average recovery of 60% for all drugs tested. The inter-device variability was nearly independent of drug tested, ranging from 43-54% with an average variability of 49%. This result is quite high as compared to traditional analyses, though expected for this type of analysis. As the placement of a new extraction device cannot be perfectly repeated, it is suspected that most of the variability may be due to imperfect placement of the devices, rather than the monoliths themselves. This is further supported by considering the low variability observed with the same devices used in desorption and LC-based analyses. The variability observed in Figure 5.8 would not be detrimental to the method in a presence/absence type of test, such as that required for routine drug screening in a hospital setting.

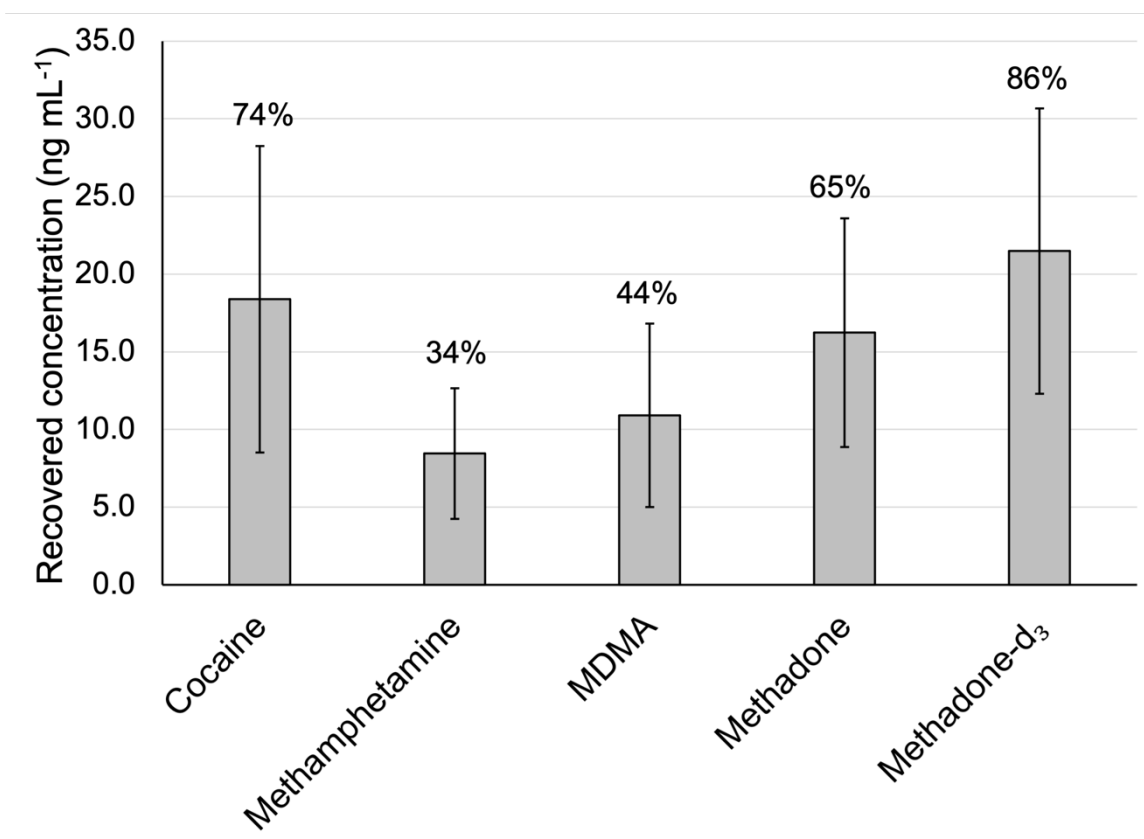


Figure 5.8. Evaluation of inter-device variability and percent recovery in 25 ng mL<sup>-1</sup> mixed DOA-spiked plasma with a 1-minute static extraction, followed by a wash with pH-unadjusted water and desorption by 10  $\mu$ L MeOH 0.1% FA by coated blade spray MS. Data labels are percent recovery. Error bars are  $\pm$ SD of three individual devices (n=3).

### 5.5.3 Coupling MIP Mesh to MX908

A MIP-coated mesh can be easily coupled to the MX908, since the instrument has been previously optimized for strips of fabric used for swabbing potential threats (Figure 5.9). MIP mesh was cut to match the exact dimensions of the commercial swabs and is cut from a sheet of polymerized material using a Cricut Maker® (Figure 5.9B).

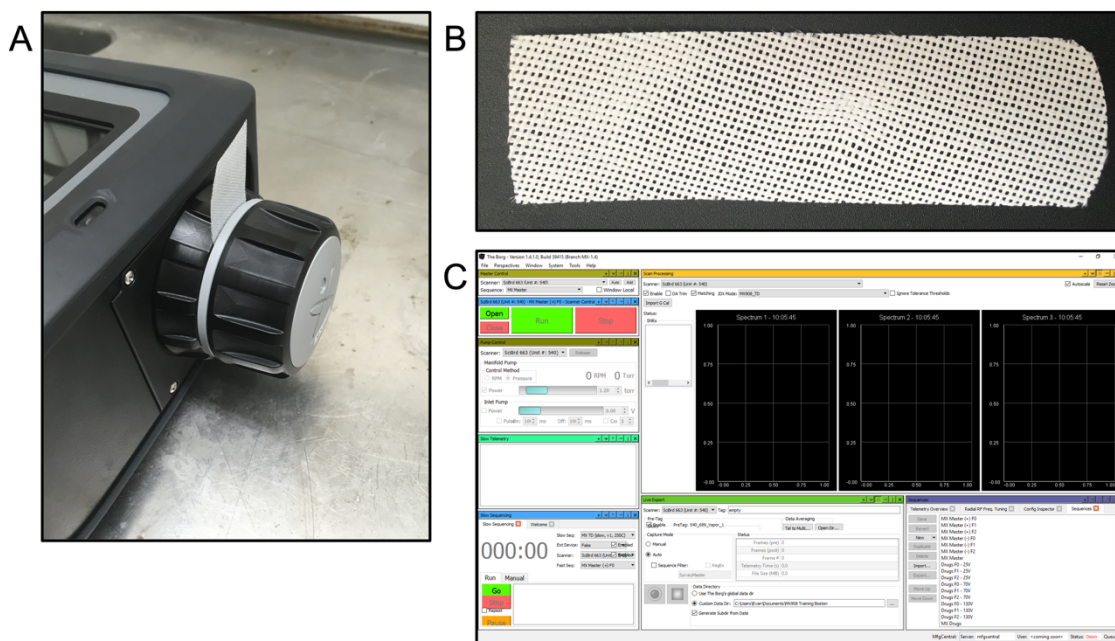


Figure 5.9. MIP mesh coupled to MX908. A: Thermal desorption module attached to corona-discharge source, with MIP mesh seated in analysis position. B: An example of a MIP mesh used with the MX908. C: A screen capture of the BORG software used for instrument control and data analysis.

For the specific MIP mesh used in this work for organophosphorus pesticides, the washing solvent was optimized for the lowest non-targeted signal (Figure 5.10).

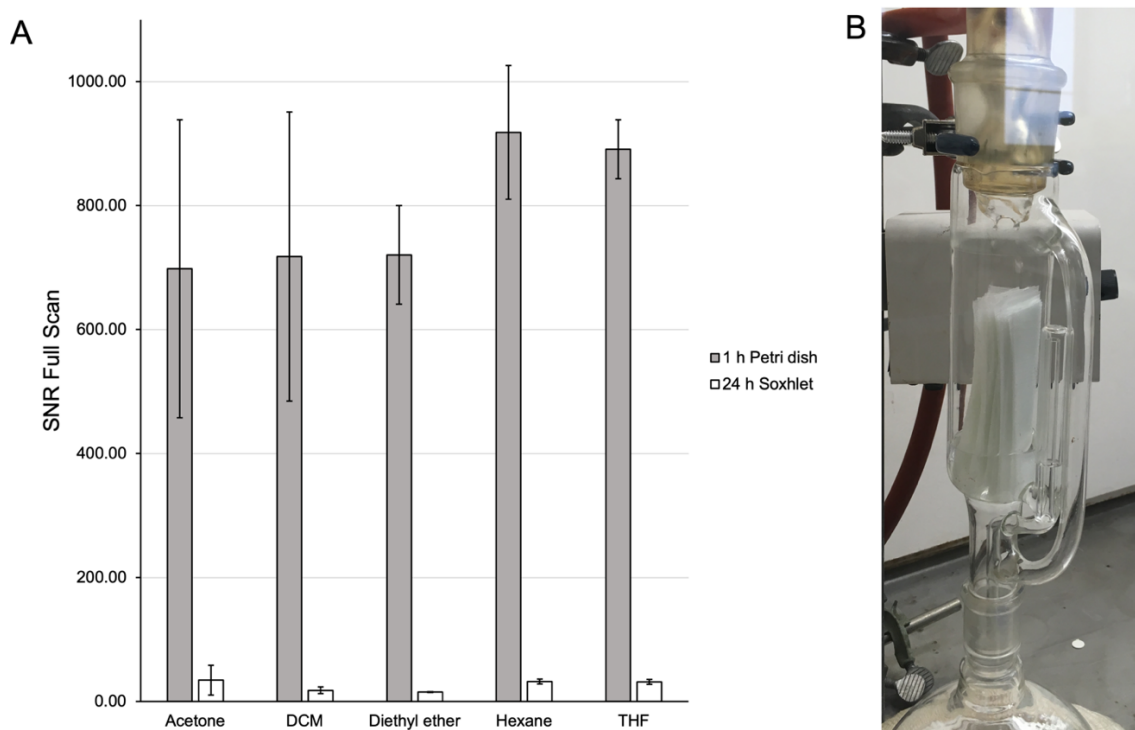


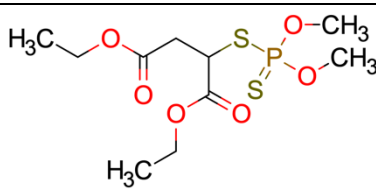
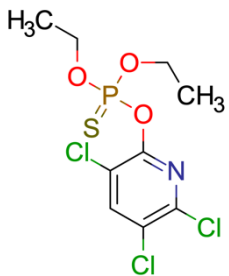
Figure 5.10. Solvent wash optimization. A: Comparing different wash solvents using a stirred desorption for 1 h in a Petri dish versus 24 h in a Soxhlet extractor. Error bars are  $\pm$ SD (n=3). SNR is signal to noise ratio of a full scan from m/z 55-470, comparing counts on the detector pre and post thermal ramp of source. B: Soxhlet extractor with MIP mesh devices in the chamber.

A simple wash step where solvent is agitated in a Petri dish was not suitable to reduce the signal-to-noise ratio to a suitable level for trace detection (Figure 5.10A). To overcome this, Soxhlet extraction was used to avail of an automated removal of unreacted polymer components over a long period of time (Figure 5.10B). The previous approach for blade devices uses several washes of solvent, which creates a large volume of solvent waste for a batch of devices. By using a Soxhlet extractor, less solvent is used to

minimize the environmental impact of the method and washing steps can be carried out overnight with appreciable reduction in background signal (Figure 5.10A). Once the template is removed through washing, the fabric strips are dried in a vacuum oven to remove trace solvent and residual volatiles and can be stored for use.

To examine the potential quantitative use of the MX908, which was used to this point as a presence/absence detection tool, a fabric mesh coated with a MIP designed for organophosphorus pesticides (OPPs) from water was used. Malathion and chlorpyrifos were selected as two representative OPPs for construction of calibration curves using the MX908 (Table 5.5).

Table 5.5. Structure and relevant physical properties of selected OPPs.

Compound	Chemical Structure	Mol. Wt.	logP	pKa	Boiling pt. (°C)
malathion		330.36	2.75	-	Decomposes
chlorpyrifos		350.59	4.96	4.55	375.9

The measurement method was optimized by running a series of standards extracted from water and thermally desorbed into the MX908 (Figure 5.11). Mass spectra collected from ionization in both positive (not shown) and negative mode (Figure 5.11B). The signal-abundant negative chemical ionization mass spectrum was studied to select the most prominent fragment(s) for quantitation. For malathion, a single fragment with a m/z of 157 was strong, with about ten percent the m/z 157 peak being the negative molecular ion at m/z 330. The calibration curve of malathion was linear from 100-1000 mg L<sup>-1</sup> (Figure 5.11A).

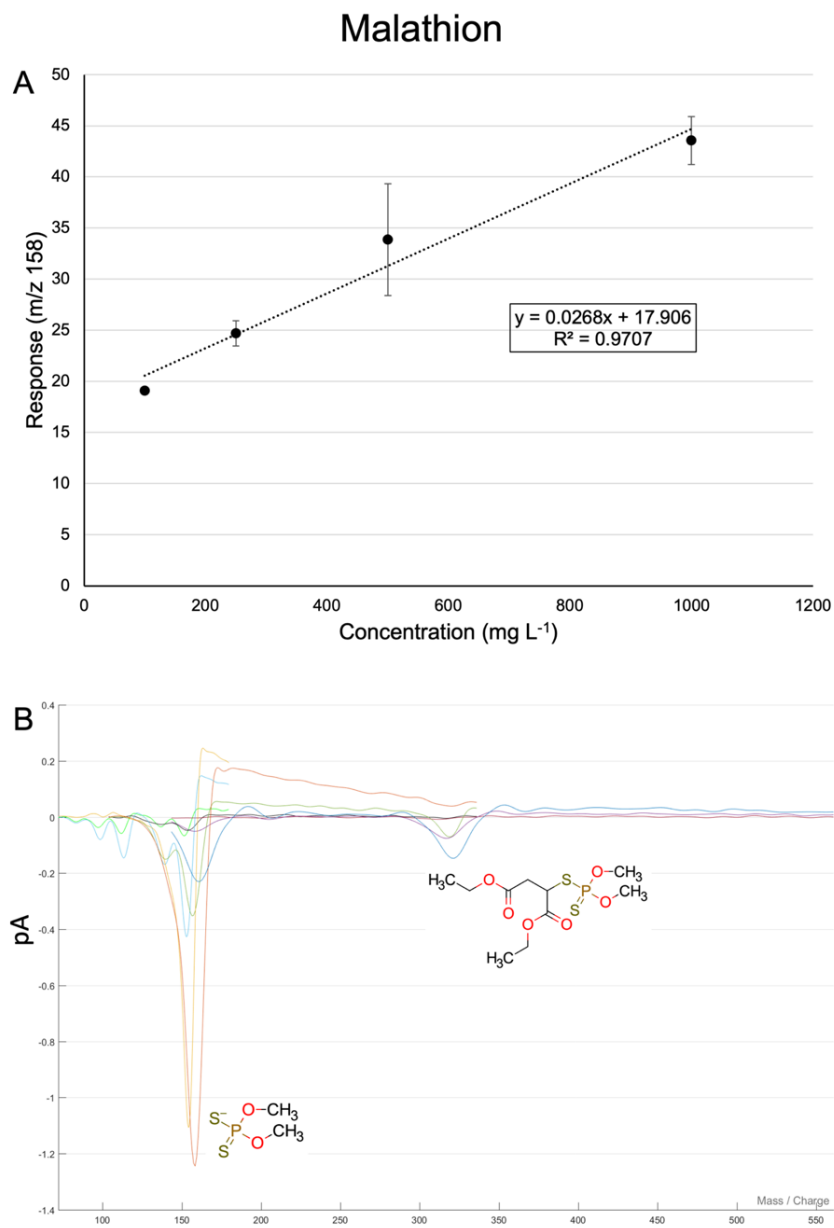


Figure 5.11. Malathion analysis using MIP OPP mesh. A: Calibration curve constructed through 30 min extraction of malathion spiked water, followed by drying and thermal desorption of the device into the MX908. Error bars are  $\pm$ SD ( $n=3$ ). B: Mass spectrum obtained from 1000 mg L<sup>-1</sup> extraction of malathion. Colored lines depict spectra collection from various f-stops, used to create the complete spectrum.

Negative chemical ionization of chlorpyrifos also yielded the most fruitful spectrum (Figure 5.12). From this spectrum, two prominent ions were selected for further study:  $m/z$  172 and 201. These two ions correspond to two expected fragments based on structure, and consistent with previous reports. The sum of both ions was used for quantitation in Figure 5.12. The presence of about 30% signal from the negative molecular ion is also noted.



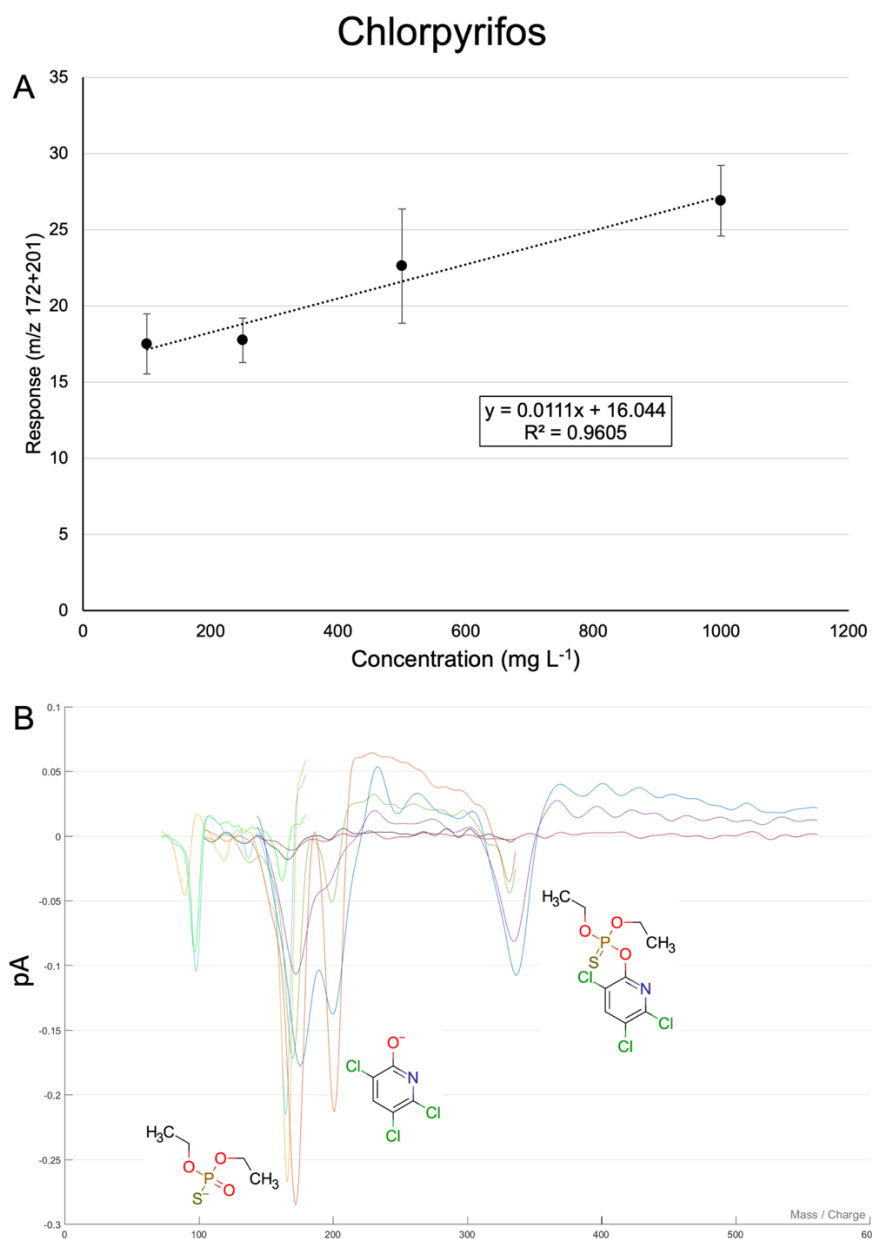


Figure 5.12. Chlorpyrifos analysis using MIP OPP mesh. A: Calibration curve constructed through 30 min extraction of chlorpyrifos spiked water, followed by drying and thermal desorption of the device into the MX908. Error bars are  $\pm$ SD (n=3). B: Mass spectrum obtained from 1000 mg L<sup>-1</sup> extraction of chlorpyrifos. Colored lines depict spectra collection from various f-stops, used to create the complete spectrum.

The use of a MIP mesh with the MX908 is an attractive and convenient way to sample in the field. The preliminary data presented here demonstrate the ability of the handheld instrument to obtain semi-quantitative data for OPPs extracted from water using MIPs. One key step in development of subsequent coated mesh devices to be used in conjunction with 908 Devices thermal desorption adapter is the reduction of background bleed from the films.

As the spectra obtained from the instrument have extremely wide bands (in the range of  $m/z$  30-70), it is crucial when obtaining data that a complete spectrum is analyzed, measuring ratios of multiple fragments, and estimating the molecular ion from the broad molecular ion peak. The main limitation in developing these methods are limitations in software. The software used for the data collection on the MX908 was developed only for presence/absence method development for internal company use and thus lacked a number of features to improve reliability of data.

#### 5.5.4 MX908 Custom Source Interface

The design of the nano electrospray source for the MX908 was conducted with experience with the TQ-S source and considering limitations of the handheld instrument. At first, the onboard HV source was used to power the coated blade; this power is normally used for the corona discharge (Figure 5.13). This approach was not satisfactory due to space limitations and interference from the HV wiring in close proximity to the MS.

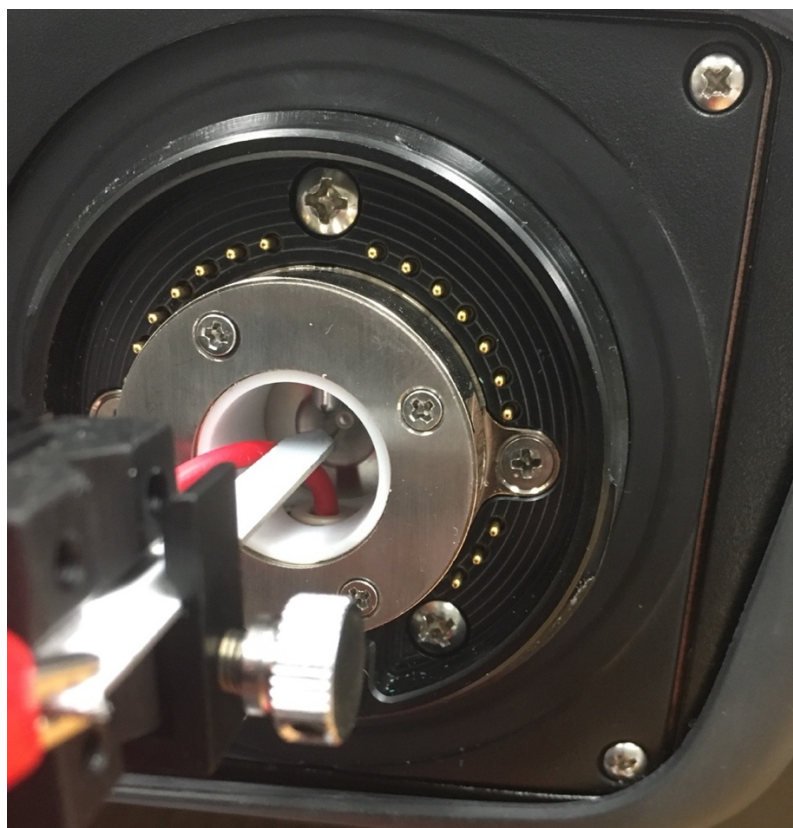


Figure 5.13. Attempted design of HV routing from corona discharge post in MX908. Note the PTFE lined source for electrical insulation.

An overview of the working prototype can be found in Figure 5.14. Instead of the onboard HV approach, which would have been convenient to maintain portability of the MS, external power supplies were used for the subsequent steps (Figure 5.14C). A micromanipulator positioned in front of the PTFE lined and electrically insulated source was used to hold the coated blades (Figure 5.14 A and B). Important to the operation of this setup is a wire that bridges the 12 V DC instrument power with the 5 kV HV power supply (Figure 5.14C). Finally, for user protection, a resistor (1 G $\Omega$ , 0.25 W) was placed in series with the blade to prevent excessive arcing and user electrocution (Figure 5.14D).

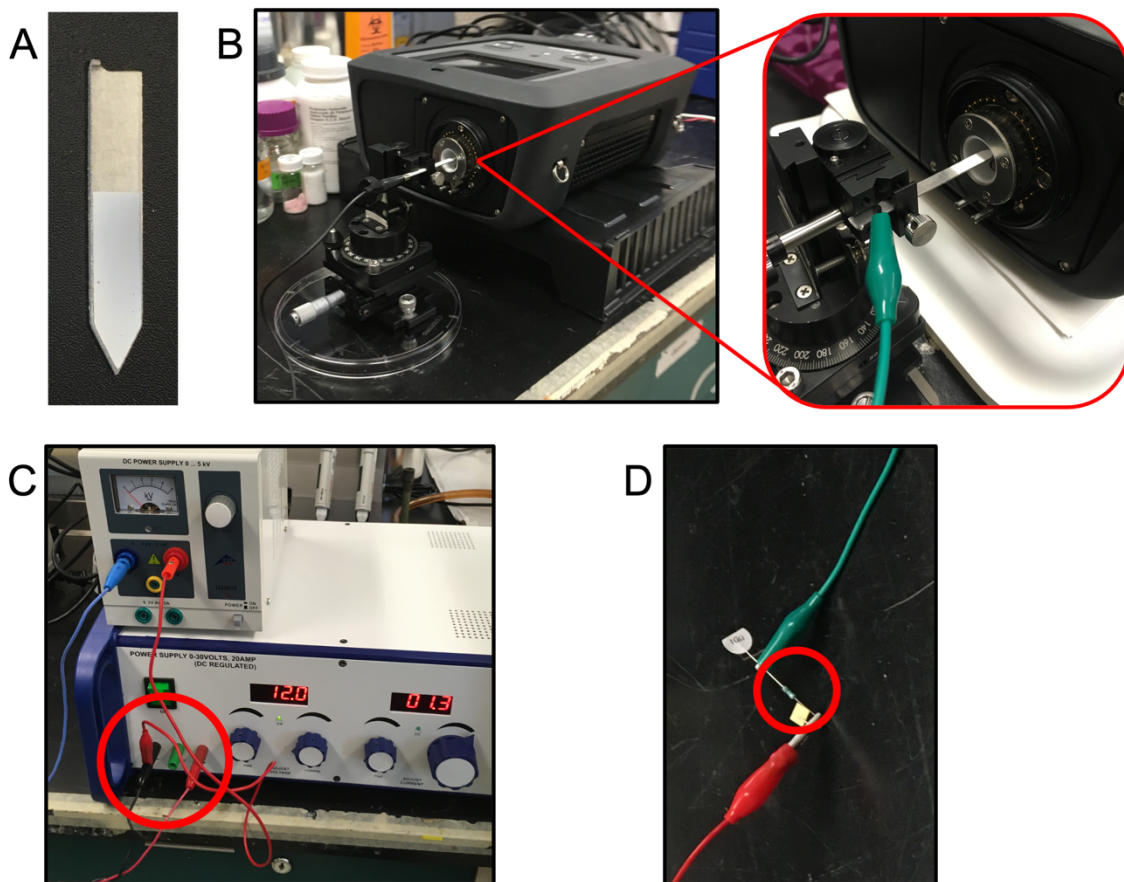


Figure 5.14. Custom nano-electrospray interface for coated blade spray using the MX908 handheld MS. A: TF-MIP for mycophenolic acid used in direct coupling. B: micromanipulator holding the coated blade within the PTFE coated ion source. Electrical potential is delivered via the alligator clip attached to the blade. C: Power supplies for running the system. On the bottom is the 12 V, 2 A DC power supply used to run the MS instrument. On the top is a 5 kV, 2 mA high-voltage power supply. The red circle indicates a crucial common connection between the power supplies to complete the circuit. D: 1 G $\Omega$  resistor (0.25 W), in-line with HV source to coated blade to prevent arcing.

The BORG software (908 Devices, Boston, MA, USA) was used for all data collection. Similar to the Xevo TQ-S setup for coated blade spray, background spectra were collected for several seconds, followed by addition of desorption solvent to the blade, at which point the nano-electrospray introduced ions to the MS. Following the return of the signal to the baseline, data collection was stopped. The entire signal rise was integrated across the time course of the spray. The software was operated in full scan mode and extracted ion chromatograms were generated for semi-quantitative work.

#### 5.5.5 Coated Blade TF-MIP Mycophenolic Acid Analysis on MX908

MIPs developed for extraction of mycophenolic acid presented in Chapter 2 were coupled to the MX908 using the custom CBS source. After extraction and rinsing the films were dried and attached to the micromanipulator positioned in front of the MX908. A spray was obtained through pipetting 5  $\mu$ L of desorption solvent onto the blades a few seconds following the commencement of data collection (to obtain baseline). A spray with a duration of 30-45 seconds was observed, where the entire rise in baseline was integrated for quantitation.

Spectra were collected of mycophenolic acid in negative ionization mode under both low and high collision energy (Figure 5.15). In Figure 5.15 A, where 25 V radial RF collision energy is employed, the most prominent peak observed is the  $[M-H]^-$  of mycophenolic acid. Some additional less intense peaks are present, however due to the high relative noise and broad peak width, interpretation of the obtained spectra using the MX908 alone was difficult. The results shown Figure 5.15B correspond to experiments

where the ion trap was subjected to a 25 V-130 V ramp in radial RF collision energy, which provided a strong fragment at approximately  $m/z$  230. An additional fragment with a mass of approximately  $m/z$  100 is also present in both spectra. The fragment at approximately  $m/z$  230 is somewhat unexpected, as the most commonly reported quantitative, and thus stable, MRM transitions for MPA yield product ion mass of  $m/z$  207. It was unclear if the fragment we were observing could be this commonly used fragment in previous quantitative work, or if it was something else unidentified, but it may likely be the expected  $m/z$  207 fragment and reading as  $m/z$  230 due to the broad peaks observed in MX908 spectra. Literature on fragmentation patterns of mycophenolic acid under different conditions is lacking and this hindered the efforts to identify this fragment easily using the MX908.

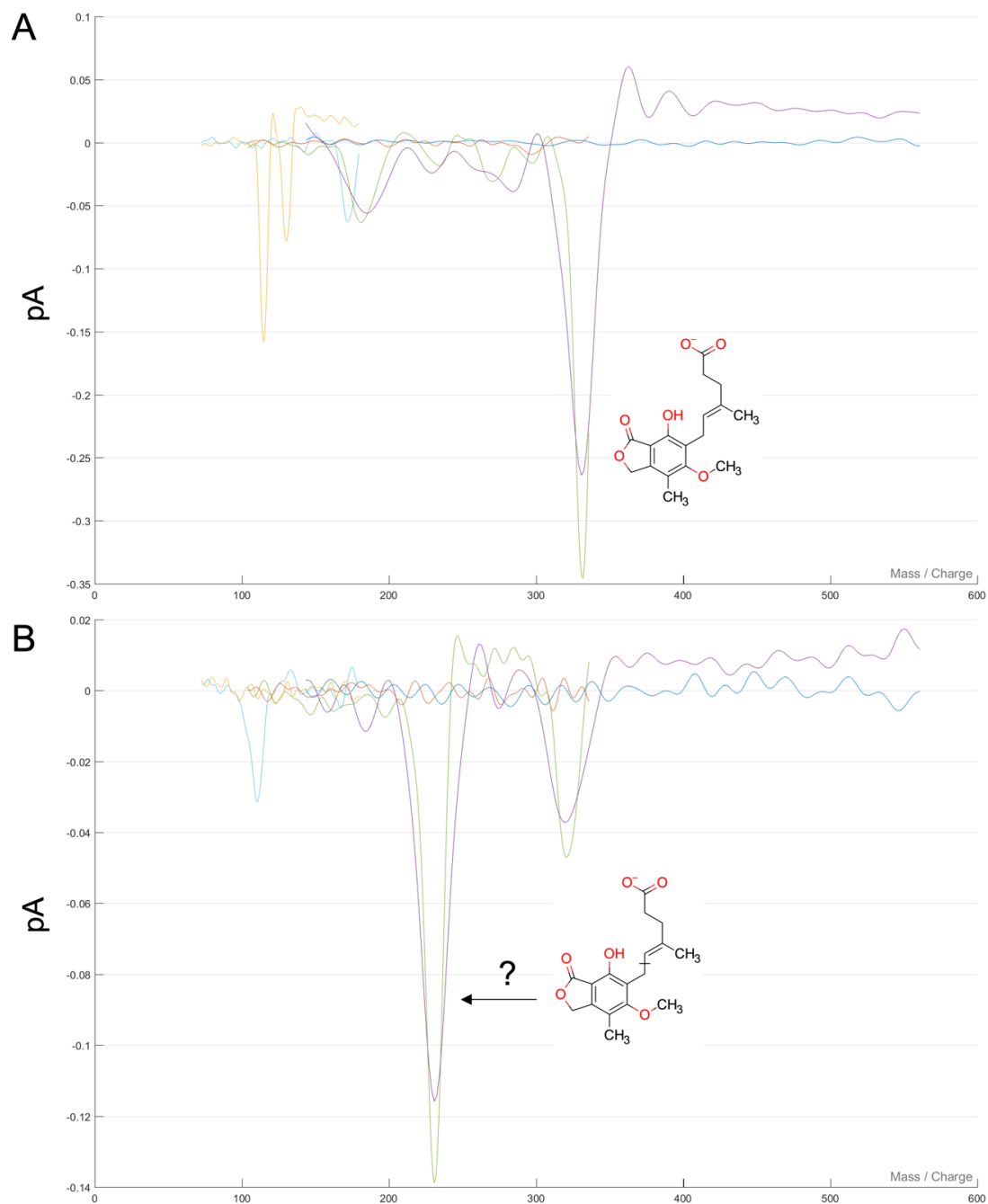


Figure 5.15. MX908 Spectra of mycophenolic acid. A: ESI (-) spectrum with no collision energy ramp, maintained at 25 V. B: ESI (-) spectrum with collision energy ramping (radial RF ramping) from 25 V to 130 V showing fragmentation products at approximately m/z 100 and 230.

To try and answer the question of what the fragment at  $m/z$  230 is, the Xevo TQ-S was employed as it is more reliable in terms of mass accuracy and has the capability of more controlled CID fragmentation experiments. Spectra were collected under varying collision energies, but masses between  $m/z$  200 and 270 were not observed (Figure 5.16). As this resulting mass was unable to be repeated on the Xevo TQ-S, it was unclear what this fragment was. If the  $m/z$  230 fragment were detected on the TQ-S, then product ion scans from the  $m/z$  230 peak could have been conducted to aid in structural elucidation.

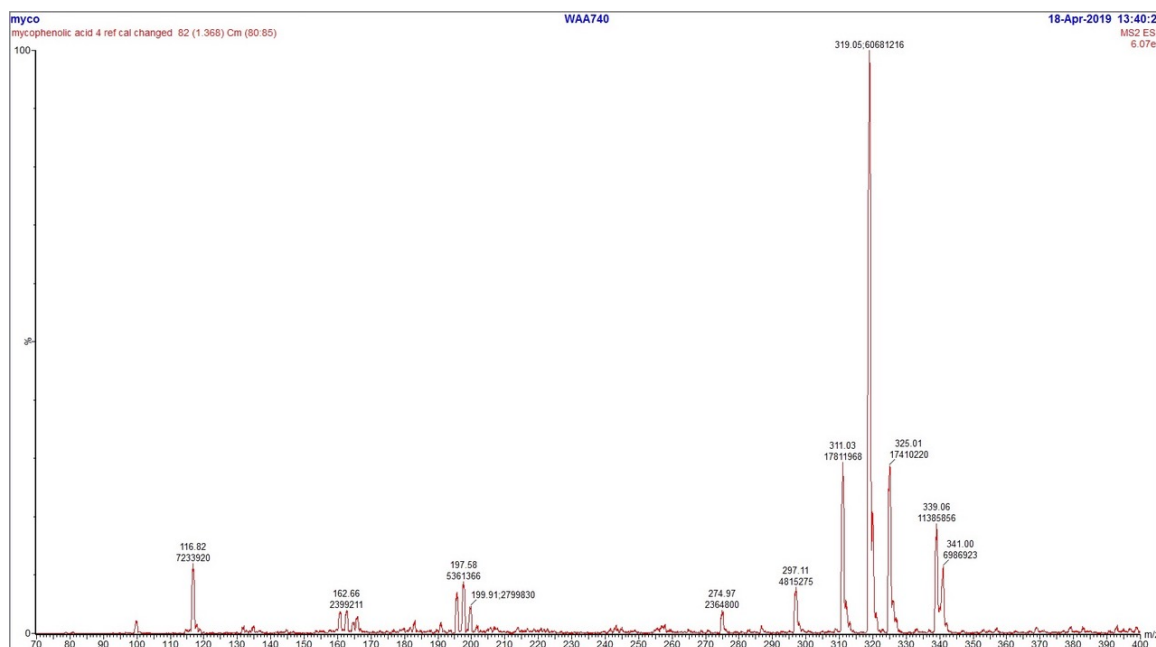


Figure 5.16. ESI (-) spectrum of mycophenolic acid at  $5 \text{ mg L}^{-1}$  on Xevo TQ-S. The molecular ion,  $[M]^-$ , is the most prominent peak at  $m/z$  319.

There are two potential scenarios that may yield the  $m/z$  230 product but lack clear evidence from the presented data to have high confidence in these proposals. The first would be the neutral loss of two  $\text{CO}_2$  molecules from MPA, which would yield at



monoisotopic peak  $[\text{MPA-H-2CO}_2]^-$  at  $m/z$  231.1187, and similar mechanisms have been reported in the literature for the loss of  $\text{CO}_2$  from comparable functionalities (the acyl carboxylic acid and the lactone of the phthalide) [201–203]. The second, is a series of spectra publicly archived on MassBank (accession# MSBNK-AAFC-AC000676-AC000680) and collected based on a series of collision energy experiments using frontend chromatography coupled to a Thermo Scientific Q-Exactive Orbitrap MS with the following instrument settings: MS2 spectral scans; Collision Energy: 10-55; Resolution: 17500;  $[\text{M-H}]^-$  (Figure 5.17). The experiments were carried out using a pure MPA standard by Agriculture and Agri-food Canada in London, ON and is the only lab which has reported fragments around  $m/z$  230 for MPA. The two fragments that are candidates for the observed peak are  $m/z$  231.0643 yielding molecular formula  $[\text{C}_{13}\text{H}_{11}\text{O}_4]^-$  and a mass error of -8.53 ppm. The second fragment identified is  $m/z$  233.0803 yielding molecular formula  $[\text{C}_{13}\text{H}_{13}\text{O}_4]^-$  and a mass error of -6.97 ppm. As can be observed from Figure 5.17, the negative molecular ion decreases in abundance with increasing collision energy, becoming nearly undetectable by a CE of 55. Inversely, at low collision energies the peaks at  $m/z$  231 and 233 are nearly undetectable and increase with CE. In addition to the peaks of interest around  $m/z$  230, peaks that are also present in the MX908 CID ramp spectrum (Figure 5.15B) such as  $m/z$  107, 135 and 287 are also found in higher CE spectra in Figure 5.17.

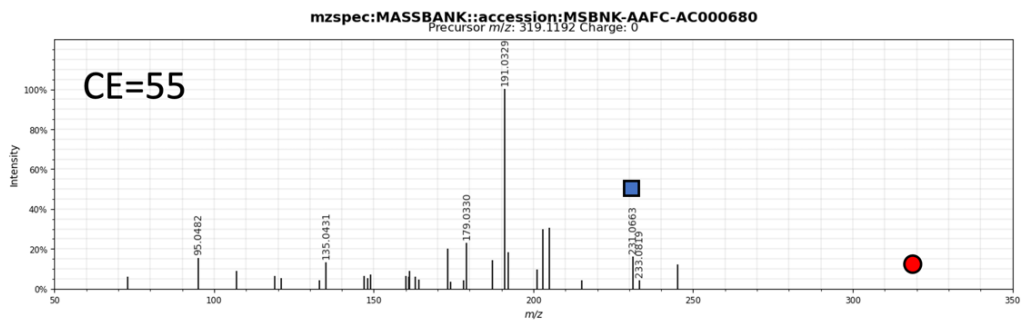
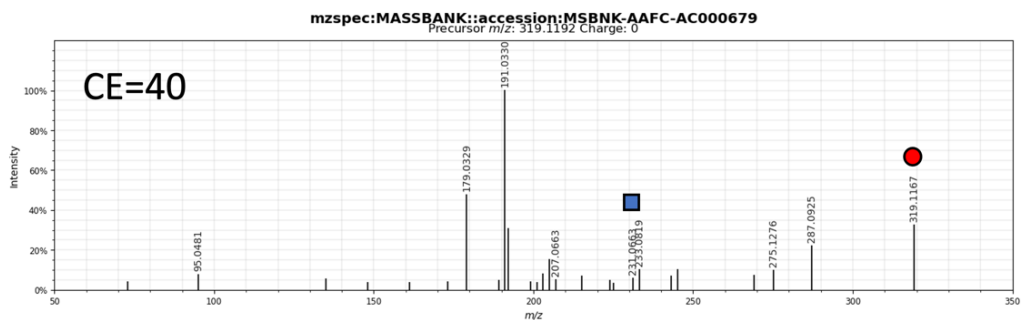
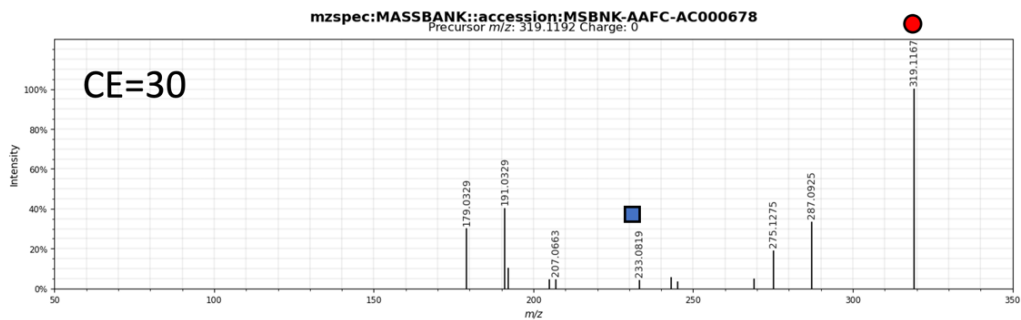
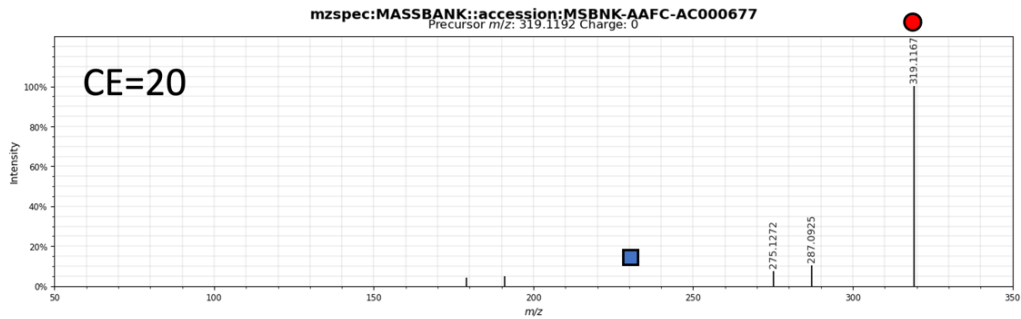
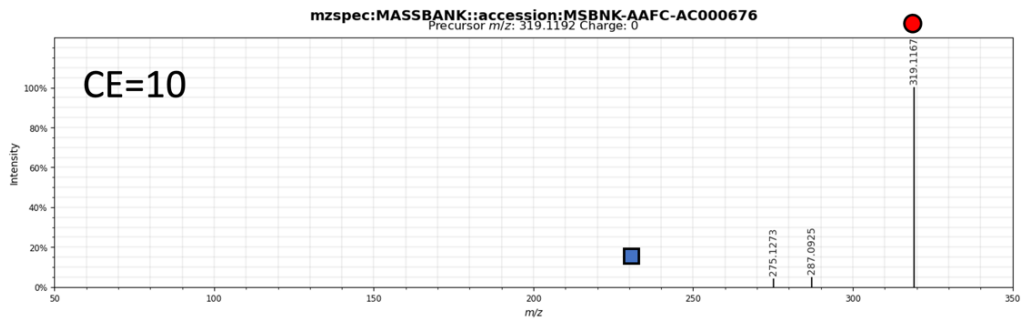


Figure 5.17. Collision energy experiments of MPA on Q-Exactive Orbitrap MS produced by AAFC and publicly archived on MassBank with accession numbers MSBNK-AAFC-AC000676-AC000680. The red circle indicates the negative molecular ion peak of MPA at  $m/z$  319 and the blue square indicates the two peaks observed at  $m/z$  231 and 233.

The evidence of both of these plausible cases supports the idea that the peak observed at  $m/z$  230 is a fragmentation product of MPA, particularly since this peak was more prominent when in-source CID was used on the MX908, which corresponds with the presence of the two  $m/z$  230 products observed on the orbitrap, in addition to other peaks corresponding between the MX908 and orbitrap spectra. When viewing the experiments conducted on the orbitrap, the  $m/z$  230 products are not prominently observed in the spectra until a relatively high CE was used. CE is not directly comparable between instrument manufacturers and is based on the physics and type of collision cell in the instrument. The Xevo TQ-S has a controlled linear CID in Q2 where presence of argon and application of RF are the driving forces for fragmentation. On the Q-Exactive, higher-energy C-trap dissociation (HCD) is the CID method [204], and allows for more rich spectra to be obtained, particularly because ions can be activated multiply thereby allowing for multiple fragmentation products. Therefore, it is probable that an insufficient amount of CE and that the different type of CID used on the Xevo TQ-S resulted in no detectable fragmentation of MPA at  $m/z$  230. The mechanism of in-source CID in the MX908 more closely resembles the orbitrap as it is a high-pressure MS and collisions with gases are more probable as pressure increases.

Considering the several steps undertaken to identify the fragments with the resources available not yielding direct evidence and supporting evidence from other high mass-accuracy studies suggesting the large peak observed at  $m/z$  230 was indeed a product of MPA fragmentation, a crude calibration curve was constructed over 0.25-10  $\text{mg L}^{-1}$  (Figure 5.18). The signals in bins  $m/z$  228-230 and  $m/z$  319-320, which

corresponded to the most intense detector response for the molecular ion and the unidentified fragment were compared. It was determined that the sum of the m/z 230 fragment and the m/z 319 molecular ion provided the most reliable signal, and that the independent signal of each fragment alone was not as linear as the sum (Figure 5.18). This result, although not definitive, supports the hypothesis that the m/z 230 fragment is a product of MPA fragmentation.

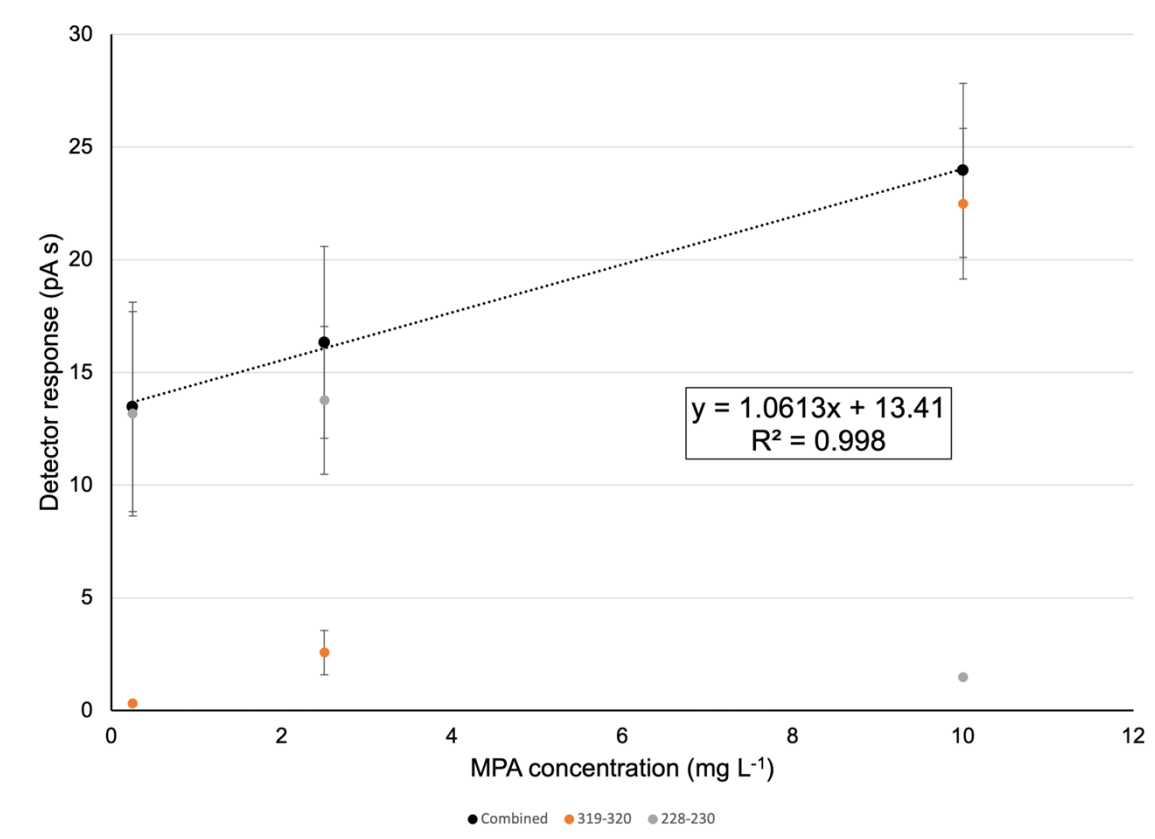


Figure 5.18. Calibration curve constructed from coated blade spray of mycophenolic acid standards. The response is the sum of mass response of m/z 228-230 and m/z 319-320. Error bars are  $\pm$ SD (n=3). Legend at the bottom of the graph corresponds to m/z bins for each set of data points.

## 5.6 Conclusions

In this chapter, several interfaces for direct sample introduction from monoliths to MS were demonstrated. Specifically, the benchtop Waters Xevo TQ-S was used in conjunction with a custom ambient coated blade spray source that operates in a nano electrospray type configuration. This configuration allowed coupling monolithic thin films cast on stainless steel substrates with a point, allowing for direct electrospray into the MS. Preliminary data was presented using the MIPs targeting MPA (presented in Chapter 2) in the form of a calibration data from CBS-MS.

Data was presented showing the applicability of a thin film monolith (non-imprinted) with CBS-MS for the analysis of drugs of abuse in several biological fluids. Calibration data in the range of 0.1-100 ng mL<sup>-1</sup> was presented with great linearity, even at low concentrations below 1 ng mL<sup>-1</sup>. Spiked biological fluids were assessed for matrix effects through CBS-MS where fluids, including plasma and urine reduced the recovery to about 20% of the response of standards. Finally, three independent devices were used to determine inter-device variability which was about 50%. This high value is most likely due to the prototype-like nature of the source and blade holder, where accurate positioning is difficult when the holder is moved to change the coupled device.

A mesh MIP designed for extraction of OPPs from water was used with the thermal desorption attachment of the MX908 handheld MS to create a semi-quantitative method for measurement of OPPs in water. Spectra from the instrument were presented which allowed for extracted ion chromatograms to be used to quantitate compounds of interest. The design would allow for simple and fast measure of OPPs in the field without

the need for typical analytical laboratory equipment, and analysis takes about 1 minute per swab.

A custom source for the MX 908 was developed which allows coupling of stainless-steel based monoliths with the handheld MS. This configuration allowed for preliminary data collection using the mycophenolic acid MIP developed in Chapter 2. The main drawbacks of the presented interface are shared with the Xevo TQ-S source and are related to the precise requirements for blade positioning and the imprecisions in the blade manufacturing. Additional to this drawback are several limitations in software interpretation of the data. Ideally, a similar software would be developed that allows for easy instrument control, settings, and ability to perform specific MS experiments and data handling processes.

Overall this chapter has presented a number of brief examples of how monolithic extraction devices can be coupled to both handheld and benchtop MS systems in a number of formats including polymer coated mesh and monolithic coated stainless-steel blades. The data in this chapter took a significant effort to obtain given the physical and software constraints of the respective systems. This work presents the first report of coupling a coated blade to a handheld MS for coated blade spray MS. The first report of a coupling of a MIP mesh to a handheld MS has also been presented in this work. Both of the achievements are significant steps toward reaching the ultimate goal of making these devices more accessible to a broader group of scientists (and even non-scientists) that can be used in many creative ways to improve the world.

It is anticipated that innovations based on these results could lead to onsite sampling and analysis of water pollutants using monolith coated mesh with thermal desorption into the MX908. Another innovation that is close to fruition is bedside therapeutic drug monitoring. The achievements in this chapter presented with mycophenolic acid as a representative drug for therapeutic drug monitoring allow for future work where a drop of blood taken from a simple finger prick can be spotted on a monolith and sprayed into a handheld MS at the bedside for instantaneous drug quantitation.

## 5.7 Acknowledgements

The coated blade spray stage for the Xevo TQ-S was designed by Dr. Hamed Piri-Moghadam. The handheld MS (MX908) was graciously loaned by 908 Devices for this project. I thank the entire team at 908 Devices, and particularly Dr. Kerin Gregory, for their guidance and assistance in developing novel application and interfaces with the MX908. I thank Drs. Justin B. Renaud and Mark W. Sumarah from Agriculture and Agri-Food Canada, London, Ontario, for publicly archiving the MPA orbitrap experiments.



## 6 Summary and Conclusions

Over the past three decades, monoliths have become prominent in bioanalytical chemistry. Monoliths are a particularly powerful tool for separations involving biomolecules or in the presence of biological matrices. The design and formulation of monolithic phases is highly tunable to the desired application. Additional selectivity can even be introduced to these polymers through the introduction of molecular imprinting. The methacrylate-co-ethylene glycol dimethacrylate polymers are of particular use, due to their high biocompatibility, robust nature, ease of preparation and high capacities, along with the ability to customize the functionality. An exemplary commercialization of these polymers is from Sartorius BIA Separations in which they utilize glycidyl methacrylate as a monomer, which leaves intact epoxides after polymerization. These epoxides can be used to functionalize the surfaces of the polymers after casting and are capable of hosting a multitude of functionalization choices, including intact biomolecules to perform bio-affinity chromatography. The results of this thesis support the notions that these methacrylate monoliths are powerful and flexible tools for an array of analytical applications in the presence of biological matrices.

In Chapter 2, a TF-MIP for the extraction of MPA from human plasma was developed. 4-VP as the functional monomer acted as a base capable of interacting with the acidic template mycophenolate mofetil. The ratio of porogenic solvents in the binary system was optimized to maximize both analytical performance and mechanical stability of the films cast on stainless-steel substrates. The method developed showed a good throughput rate and required manual handling of each film for the processing steps. The

MIP yielded higher recovery of MPA relative to the corresponding NIP. The method allows for the determination of MPA in 45 min including analysis time and can easily be scaled for high throughput to allow for a single technician to process more than 96 samples per h. The method gave an LOD of  $0.3 \text{ ng mL}^{-1}$  and was linear from 1-250  $\text{ng mL}^{-1}$ . Patient plasma samples were initially tested but the drug concentration was quite high. To correct for this, the plasma (35  $\mu\text{L}$ ) was diluted using charcoal-stripped pooled-plasma to a final extraction volume of 700  $\mu\text{L}$  which allowed measurement within the method linear range. Intra- and inter-day variability were 13.8% and 4.3% (at  $15 \text{ ng mL}^{-1}$ ) and 13.5% and 11.0% (at  $85 \text{ ng mL}^{-1}$ ), respectively ( $n = 3$ ); inter-device variability was 9.6% ( $n=10$ ). The low inter-device variability makes these devices suitable for single use in a clinical setting, and the fast and robust method is suitable for TDM.

In Chapter 3, a TF-MIP for the analysis of TKIs in human plasma was developed using a 96-well microplate format. A DOE system was initially used to optimize the formulation of the polymer, however there were several qualitative factors that could not be assessed by the computer, or easily converted to a numerical value, which lead to physically unstable formulations. A final film formula was developed through an iterative process, chronologically optimizing each parameter, then re-optimizing at the start once each round gave a desirable result. The less commonly used functional monomer, N-MEMA was used as it gave superior performance; it is more water compatible than other monomers like MAA and 4-VP and has a free hydroxyl group that can interact with analytes. The developed method and allows for rapid, reliable, and concurrent extraction

of TKIs with quantitation using LC-MS/MS. The extraction, washing, and desorption steps are simplified using a multichannel pipette and neutral, unadjusted water for washing, with minimal manual handling and ability for fully automated integration. These devices have an inter-device and batch-to-batch variability of about 5%, meaning results between batches of devices and individual devices are highly comparable. The linear ranges of all four TKIs are well below and above the therapeutic ranges, with limits of detection and quantification far below the lowest clinically significant result. The results and ease of the protocol indicate these devices would be suitable for clinical applications or therapeutic drug monitoring of Das, Ima, Nil, and Pon, either individually or in any combination. Based on these results using four representative TKIs with varying chemistries for this study, it is expected that the whole family of TKIs could be extracted using these devices.

The developed MIPs were stress tested under a number of atypical physiological conditions and the performance of the devices under these conditions was evaluated. One unique aspect of the presented work is the amount of biological validation presented, which outlines which interferences are tolerated in the test, and their respective effect on the analytical result. This type of biological information is valuable in determining the robustness and reliability of an analytical method in the clinic, particularly when patients undergoing such treatments would be considered unwell, and thus atypical blood physiology could be expected. Outlining the biological limits of the method and the reliability when stress tested is useful for future work where a larger clinical based study could fully explore the potential of the developed devices for routine clinical use.

Along with the particular application-specific MIP, new 96-well format devices were prepared and utilized, which represent significant time, cost and handling savings as compared to blade formats such as those presented in Chapter 2. The 96-well format is able to be directly introduced to typical high-throughput processes, allowing the handling of 96 individual samples to be processed as one unit, saving time and manual manipulation steps. The 96-well format could be carried through from the preparation of the films all the way through to the instrumental analysis. Allowing for this type of automation, where manual handling is minimized, is also greatly beneficial in regulated laboratory environments where sample mix-ups could potentially lead to catastrophic results for patients. Along with the benefits of sample processing, is also the benefit of a platform for side-by-side, high throughput comparison of several formula compositions and ratios in the plate format. This benefit allowed for many more formula compositions to be screened than in Chapter 2 where individual devices were individually cast and manipulated.

In Chapter 4, a two-step chromatographic approach for the isolation of GTA particles from *Rhodobacter capsulatus* culture was developed. Two monolithic columns were used with different chemistries for crude isolation followed by polishing. This was achieved by first isolating the particles from culture filtrate through dilution of the filtrate to 1.5 M potassium phosphate buffer. This high ionic strength solution was then loaded into a hydroxyl functionalized methacrylate monolith with 2  $\mu\text{m}$  open pores and separated from the media components and other lysis products through hydrophobic interaction chromatography. After loading up to 100 mL of solution onto the 1 mL column at a rapid

flow rate of 5 mL min<sup>-1</sup>, the monolith could be washed, followed by a descending potassium phosphate gradient which eluted the GTA particles. We also observed a major interferent, photosynthetic vesicles or chromatophores, which abundantly co-eluted with the GTA particles requiring a second purification step. The second step was achieved by diluting the eluted fractions from the OH column with 9 volumes of distilled water and loading onto a 1 mL quaternary ammonium functionalized monolith under low ionic strength. The GTAs were eluted through an increasing gradient of ammonium sulfate which allowed for on-column buffer exchange required to maintain GTA activity in the final product since the potassium phosphate buffer was not conducive to biological activity of the isolated particles. Nearly pure GTAs were obtained at the end of the workflow. This work demonstrates the power of bulk polymerized monoliths for preparative scale purifications. The noticeable benefits are the ability to run the columns at high flow rates 5-10 mL min<sup>-1</sup> without backpressures exceeding ~8 bar. It was demonstrated that the isolated GTA particles maintained their ability to transfer genetic material, meaning that the particles remained intact and did not experience major shear or turbulent forces that would deform or break apart the component proteins. These columns have proven useful for many industrial-scale purifications and columns with bed volumes as high as 8 L are commercially available in several chemistries, allowing for the efficient isolation of up to 200 g pure macromolecules such as plasmid DNA, mRNA, proteins, phages and viruses as well as vesicles [4]. The developed process in this chapter represents a broadly applicable approach that is suitable for not only GTAs but also other small phages that are of particular interest for phage-based therapies. As the monoliths

possess atypical chromatographic properties, scaling up processes to industrial scale is more straightforward and can be directly translated from lab to industrial scale with minimal re-optimization.

In Chapter 5, custom coated blade spray sources, developed for both the benchtop Xevo TQ-S and the handheld MX908 are used to demonstrate how CBS-MS can be used to expedite analysis time and provide results in locations that may not otherwise have labs equipped with benchtop MS instrumentation. The therapeutic drug MPA was analyzed by CBS-MS on both the MX908 and Xevo TQ-S using the TF-MIP developed in Chapter 2. Selected drugs of abuse were also analyzed by CBS-MS using the Xevo TQ-S, with an emphasis on evaluating how rinsing the devices reduce matrix interference and allow for a reliable signal to be measured. Finally, a MIP mesh previously developed in the group was used with the thermal desorption adapter of the MX908 to demonstrate how semi-quantitative measurement of OPPs could be achieved in the field. The developed sources and extraction devices presented in this chapter represent early examples of the future direction of the field. Remote and on-site monitoring of biologics, drugs and contaminants has been of interest for several decades and has seen great developments with the introduction of several portable MS analyzers, GC-MS systems, and other handheld detectors. This work represents the beginning of the next generation of such devices and interfaces where more complex questions can be asked and answered using such equipment. For example, drug quantitation from a finger prick of a patient in a remote community using CBS into a handheld MS should be able to become a reality this decade. Particular milestones achieved were CBS-MS of MPA using the MX908,

employing a MIP coated fabric mesh for rapid water OPP analysis and drugs of abuse screening from plasma and urine using CBS-MS on the Xevo TQ-S.

In this work, both custom and commercial monoliths were employed in various formats for analyte extraction and purification from complex biological matrices. Through the development of two thin film MIP devices for clinical application, two formats (both stainless steel blade and 96 well plate) were successfully employed. Reproducible and easily useable devices were created each with their own benefits. The coated blades benefit from being recyclable and can be used for CBS-MS while the 96-well plate format allowed for rapid throughput work in both screening of formulas, conditions as well as actual sample processing. The 96-well format can also be fully integrated into high throughput lab infrastructure with minimal modification, providing a rapid and simple way to improve bioanalytical methods. In addition, commercial bulk monoliths for the isolation of a GTAs were used to develop a two-step approach to yield clean particles. The developed process is broadly applicable to other phages and virus like particles and is easily scalable to be a useful tool in biomanufacturing.

In this work, both small molecule and macromolecular purification workflows have been developed. Both approaches are vastly different and traditional chromatographic theory could not easily be applied to macromolecular separations. Monoliths are a unique tool that overcome many pitfalls experienced by traditional particle based chromatographic approaches and theory.

Biological matrices pose significant challenges to analytical workflows. The complex matrices of mammalian or bacterial samples studied in this thesis contain many

biomolecules including proteins, nucleic acids, lipids, and saccharides which routinely interfere with commonly employed methods. All four of the presented projects focused on removing these biomatrices to obtain a method or device that can perform independent of varying conditions and pathologies. Of particular merit was the biological validation work of the TKI TF-MIP. The devices performed very well when challenged with bilirubin, triglyceride-rich lipoproteins, severe hemolysis in addition to elevated plasma protein levels. The devices performed well under most conditions at elevated levels, and performance only began to deteriorate under extreme conditions at the maximum physiological limits.

In conclusion, a broad suite of work is presented that employed monoliths for extraction of analytes from complex biological matrices. A greater understanding of the validation required for clinical based testing and developed two unique solutions for therapeutic drug monitoring was gained. The first development consisted of a stainless-steel coated blade, which was employed in both a typical LC-MS based workflow in addition to being directly coupled to both benchtop and handheld mass spectrometers. The second development was a high-throughput TF-MIP 96-well plate for the quick and simple processing of many patient samples. The development of the 96-well format also allowed for rapid formula and extraction screening and method development. The scale, ease and ability to fully integrate into existing 96-well infrastructure is of great benefit. This method would be suitable for large clinical centres where hundreds of samples can be processed per hour. The fourth chapter reported assessment of commercial monolithic columns to isolate virus-like particles from bacterial culture. This process is analogous to



common processes in biopharmaceutical manufacturing where the benefits of bulk monoliths are already being exploited. Unlike traditional chromatographic sorbents, these monoliths tolerate very high flow rates at minimal pressures with high binding capacity for biomolecules. The developed two-step approach using an initial capture step driven by a mechanism similar to hydrophobic interaction chromatography, followed by a polishing step using a QA functionalized monolith as a SAX phase allowed for the gentle isolation of functional particles that were of high purity and still functional. This process is broadly applicable to many small phages and virus-like-particles and the developments contribute to advancing bioprocessing, particularly of GTA. Monoliths are, and will continue to be, highly useful materials for chromatographic separation and extraction of molecules of biological importance.

## **7 Challenges, Limitations and Future Work**

In Chapters 2 and 3, extraction devices and corresponding analytical methods for measurement of therapeutic drugs that are candidates for TDM were presented. The main drawback in both of these studies was the limitation of patient samples. Specifically in the case of MPA which is a drug given to prevent rejection of a transplanted organ, organ transplantation is not conducted in the province of Newfoundland & Labrador and therefore it would be nearly impossible to organize a study obtaining blood samples from local patients. Additionally, due to the small population of Newfoundland & Labrador relative to other provinces in Canada, the number of patients in the province undergoing treatments that require TDM is extremely small. Similarly for TKIs, these drug regimens do not currently benefit from TDM in this province, therefore obtaining blood samples from ill patients for this research study would have to undergo rigorous and time-consuming ethics approval and would likely be determined to be unethical as it may not provide a direct benefit to the current patients. An opportunity for future work would be a collaboration with a larger research hospital where research on TDM methods is being conducted. Often in these clinical research settings, biobanks are established where previously collected blood and tissue are held with all scientifically relevant patient information. The availability of fresh patient samples and a larger population of patients would have allowed for additional studies of interpatient analytical variability and studying varying levels of both endogenous and exogenous interferents in patients with co-morbidities in both projects. Opportunities involving a large dataset that could consider other factors not considered in this study like exogenous interferents, effects of

race, gender or age, co-morbidities or other confounding treatments could be studied. A large dataset with a high number of well documented patients could support outlining the benefits and limitations of both methods in the clinic. As exemplified by the CBS-MS work in Chapter 5, both of these TDM methods could be adapted to handheld MS applications where access to a rapid and simple analytical tool for patients in remote or small centers could be possible.

In Chapter 4, a novel process for isolation of GTAs from bacterial culture of *Rhodobacter capsulatus* was presented. One unique challenge with *Rhodobacter* and all photoheterotrophic bacterial species is the presence of chromatophores, or photosynthetic vesicles. These versatile bacteria are often exploited for their energy efficiency for heterologous production of a variety of small molecules, however these chromatophores often complicate purification processes. This method significantly reduced this chromatophore load and will be a useful tool to exploit many photoheterotrophic bacteria for useful heterologous biochemical transformations. This method is directly supporting concurrent project work where GTAs from different species of bacteria are being isolated and their DNA extracted for sequencing, to be used as a comparative tool to look at GTA packaging across species. Although this method was developed for pure cultures, another unique opportunity is present to isolate of GTAs from environmental samples such as ocean or lake water. By translating the presented methods for a 1 mL bed volume to a 0.1 mL bed volume, which would be used to minimize the elution volume from the expected low abundance of GTA, water can be processed on a liter-scale in a relatively short time and the GTA eluted just a few hundred  $\mu\text{L}$ , which would be used for next-

generation sequencing to identify which species, and if any novel GTA-producing species, are present. Aside from the sequencing aspects of isolating highly purified GTAs, there are also a number of functional and biochemical assays involving GTAs that would benefit from a reliably pure and high concentration sample of GTAs. The developed method will allow for more detailed study of mechanism of GTAs in an environment with a very low amount of interferences, providing a higher quality of data than previously possible using single column or ultracentrifuge density-gradient based approaches. The approach is also broadly applicable to many small phages where this work could be a foundation for both research and production scale purifications.

In Chapter 5, preliminary data is presented on several examples of how both polymer-coated mesh and monolith-coated stainless-steel blade can be used directly with mass spectrometers. This chapter presented diverse data from OPPs, which are pesticides and environmental contaminants, to drugs of abuse and therapeutic drugs. The benefits and ease of directly coupling extraction devices to MS are huge and will likely gain popularity for a number of assays in the coming years. As the work in this chapter was preliminary, there is much to expand on. The main physical drawback of the work was the mounting apparatus for the coated blades on both the Xevo TQ-S and the MX908. The precision requirement for the blade manufacture and the holder positioning was a major limiting factor in obtaining consistent and repeatable signal across extraction devices. Although the signal could generally be normalized with an internal standard, the bulk signal variation was several orders of magnitude, thus it was easy for results to fall out of the linear range. Further design and engineering by instrument manufacturers on

both the interface mechanisms as well as some sort of cartridge for the coated blades would be welcome. The approach of a cartridge has been used successfully for a number of years on PS sources, so this could be easily achievable with industry interest. There is also a PS source with integrated washing and desorption system, which would enhance throughput and data reliability should it be able to be converted to the CBS-MS system.

In addition to the manual setup and variability in positioning the coated blades, the software to operate the handheld trap MS was highly specialized for detecting the presence/absence of neat drugs of abuse, chemical warfare agents and industrial chemical hazards meaning it was difficult to obtain specific and quantitative analytical data and responses that were flexible to the presented targets. The software was programming-heavy with multiple MATLAB scripts needing to be written for each type of analysis and experimental condition. The communication between the instrument and computer were sometimes unreliable, yielding a corrupt data file for a given run. Crucial fail stops were also not built into the software, meaning if erroneous commands or buttons were executed on MATLAB, the system may enter an unsafe condition. Examples of this are the uncontrolled ability to turn off the vacuum even with the trap HV/RF on and the source on. This loss of vacuum can cause arcing in the trap and ruin the instrument in milliseconds. Additionally, there was no temperature timeout on the thermal desorption heater so, in theory, one could leave it at 300°C and walk away which could lead to damage to the plastic enclosure. The lack of these fail stops at present lead to safety issues that need to be addressed by creation of more flexible instrument programming user interfaces such as those used by the large instrument manufacturers. Should these

technological and engineering barriers be overcome, direct coupling of extraction devices to handheld mass spectrometers is quite an elegant approach to provide crucial information to healthcare providers, environmental researchers, and chemists in a timely manner, with minimal instrument or technological resources, making them employable in the field, at the bedside, or on a production floor.

## References

- [1] Iberer G, Hahn R, Jungbauer A. Monoliths as stationary phases for separating biopolymers--fourth generation chromatography sorbents. *LC-GC* 1999;17:998–1005.
- [2] Kubín M, Špaček P, Chromeček R. Gel permeation chromatography on porous poly(ethylene glycol methacrylate). *Collect Czechoslov Chem Commun* 1967;32:3881–7. <https://doi.org/10.1135/cccc19673881>.
- [3] Ross W, Jefferson R. *J Chromatogr Sci* 1970;8:386–9.
- [4] Belenkii BG. Monolithic stationary phases: yesterday, today, and tomorrow. *Russ J Bioorganic Chem* 2006;32:323–32. <https://doi.org/10.1134/S1068162006040029>.
- [5] Tennikova TB, Svec F, Belenkii BG. High-performance membrane chromatography. A novel method of protein separation. *J Liq Chromatogr* 1990;13:63–70. <https://doi.org/10.1080/01483919008051787>.
- [6] Josic D, Buchacher A, Jungbauer A. Monoliths as stationary phases for separation of proteins and polynucleotides and enzymatic conversion. *J Chromatogr B Biomed Sci App* 2001;752:191–205. [https://doi.org/10.1016/S0378-4347\(00\)00499-0](https://doi.org/10.1016/S0378-4347(00)00499-0).
- [7] Hjertén S, Liao J-L, Nakazato K, Wang Y, Zamaratskaia G, Zhang H-X. Gels mimicking antibodies in their selective recognition of proteins. *Chromatographia* 1997;44:227–34. <https://doi.org/10.1007/BF02466386>.
- [8] Arvidsson P, Plieva FM, Savina IN, Lozinsky VI, Fexby S, Bülow L, et al. Chromatography of microbial cells using continuous supermacroporous affinity and ion-exchange columns. *J Chromatogr A* 2002;977:27–38. [https://doi.org/10.1016/S0021-9673\(02\)01114-7](https://doi.org/10.1016/S0021-9673(02)01114-7).
- [9] Tanaka N, Kobayashi H, Ishizuka N, Minakuchi H, Nakanishi K, Hosoya K, et al. Monolithic silica columns for high-efficiency chromatographic separations. *J Chromatogr A* 2002;965:35–49. [https://doi.org/10.1016/S0021-9673\(01\)01582-5](https://doi.org/10.1016/S0021-9673(01)01582-5).
- [10] Minakuchi H, Nakanishi K, Soga N, Ishizuka N, Tanaka N. Octadecylsilylated Porous Silica Rods as Separation Media for Reversed-Phase Liquid Chromatography. *Anal Chem* 1996;68:3498–501. <https://doi.org/10.1021/ac960281m>.
- [11] Nakanishi K, Soga N. Phase Separation in Gelling Silica-Organic Polymer Solution: Systems Containing Poly(sodium styrenesulfonate). *J Am Ceram Soc* 1991;74:2518–30. <https://doi.org/10.1111/j.1151-2916.1991.tb06794.x>.
- [12] Tanaka N, Kobayashi H, Nakanishi K, Minakuchi H, Ishizuka N. Peer Reviewed: Monolithic LC Columns. *Anal Chem* 2001;73:420 A-429 A. <https://doi.org/10.1021/ac012495w>.
- [13] Olcer YA, Tascon M, Eroglu AE, Boyacı E. Thin film microextraction: Towards faster and more sensitive microextraction. *TrAC Trends Anal Chem* 2019;113:93–101. <https://doi.org/10.1016/j.trac.2019.01.022>.
- [14] Ertürk G, Mattiasson B. Molecular Imprinting Techniques Used for the Preparation of Biosensors. *Sensors* 2017;17:288. <https://doi.org/10.3390/s17020288>.

- [15] Ansari S, Karimi M. Novel developments and trends of analytical methods for drug analysis in biological and environmental samples by molecularly imprinted polymers. *TrAC Trends Anal Chem* 2017;89:146–62. <https://doi.org/10.1016/j.trac.2017.02.002>.
- [16] Cegłowski M, Smoluch M, Reszke E, Silberring J, Schroeder G. Molecularly imprinted polymers as selective adsorbents for ambient plasma mass spectrometry. *Anal Bioanal Chem* 2017;409:3393–405. <https://doi.org/10.1007/s00216-017-0281-2>.
- [17] Chen L, Xu S, Li J. Recent advances in molecular imprinting technology: current status, challenges and highlighted applications. *Chem Soc Rev* 2011;40:2922. <https://doi.org/10.1039/c0cs00084a>.
- [18] Zöchling A, Hahn R, Ahrer K, Urthaler J, Jungbauer A. Mass transfer characteristics of plasmids in monoliths. *J Sep Sci* 2004;27:819–27. <https://doi.org/10.1002/jssc.200401777>.
- [19] Podgornik A, Strancar A. Convective Interaction Media® (CIM)- Short layer monolithic chromatographic stationary phases. In: M.R. El-Gewely, editor. *Biotechnol. Annu. Rev.*, vol. 11, Amsterdam; Netherlands: Elsevier; 2005, p. 153–90. [https://doi.org/10.1016/S1387-2656\(05\)11005-9](https://doi.org/10.1016/S1387-2656(05)11005-9).
- [20] Mihelič I, Koloini T, Podgornik A, Štrancar A. Dynamic capacity studies of CIM (Convective Interaction Media)® monolithic columns. *J High Resolut Chromatogr* 2000;23:39–43. [https://doi.org/10.1002/\(SICI\)1521-4168\(20000101\)23:1<39::AID-JHRC39>3.0.CO;2-F](https://doi.org/10.1002/(SICI)1521-4168(20000101)23:1<39::AID-JHRC39>3.0.CO;2-F).
- [21] van Deemter JJ, Zuiderweg FJ, Klinkenberg A. Longitudinal diffusion and resistance to mass transfer as causes of nonideality in chromatography. *Chem Eng Sci* 1956;5:271–89. [https://doi.org/10.1016/0009-2509\(56\)80003-1](https://doi.org/10.1016/0009-2509(56)80003-1).
- [22] Hahn R, Panzer M, Hansen E, Møllerup J, Jungbauer A. Mass transfer properties of monoliths. *Sep Sci Technol* 2002;37:1545–65. <https://doi.org/10.1081/SS-120002736>.
- [23] Hahn R, Jungbauer A. Peak Broadening in Protein Chromatography with Monoliths at Very Fast Separations. *Anal Chem* 2000;72:4853–8. <https://doi.org/10.1021/ac000688y>.
- [24] Svec F, Frechet JMJ. Kinetic Control of Pore Formation in Macroporous Polymers. Formation of “Molded” Porous Materials with High Flow Characteristics for Separations or Catalysis. *Chem Mater* 1995;7:707–15. <https://doi.org/10.1021/cm00052a016>.
- [25] Merhar M, Podgornik A, Barut M, Žigon M, Štrancar A. Methacrylate monoliths prepared from various hydrophobic and hydrophilic monomers - Structural and chromatographic characteristics. *J Sep Sci* 2003;26:322–30. <https://doi.org/10.1002/jssc.200390038>.
- [26] Okay O. Macroporous copolymer networks. *Prog Polym Sci* 2000;25:711–79. [https://doi.org/10.1016/S0079-6700\(00\)00015-0](https://doi.org/10.1016/S0079-6700(00)00015-0).
- [27] Strancar A, Podgornik A, Barut M, Necina R. Short Monolithic Columns as Stationary Phases for Biochromatography. In: Freitag R, editor. *Mod. Adv.*



- Chromatogr., vol. 76, Berlin, Heidelberg: Springer Berlin Heidelberg; 2002, p. 49–85. [https://doi.org/10.1007/3-540-45345-8\\_2](https://doi.org/10.1007/3-540-45345-8_2).
- [28] Svec F, Fréchet JMJ. Molded Rigid Monolithic Porous Polymers: An Inexpensive, Efficient, and Versatile Alternative to Beads for the Design of Materials for Numerous Applications. *Ind Eng Chem Res* 1999;38:34–48. <https://doi.org/10.1021/ie970598s>.
- [29] Tanaka N, Motokawa M, Kobayashi H, Hosoya K, Ikegami T. Monolithic Silica Columns for Capillary Liquid Chromatography. *J. Chromatogr. Libr.*, vol. 67, Elsevier; 2003, p. 173–96. [https://doi.org/10.1016/S0301-4770\(03\)80024-6](https://doi.org/10.1016/S0301-4770(03)80024-6).
- [30] Endres HN, Johnson JAC, Ross CA, Welp JK, Etzel MR. Evaluation of an ion-exchange membrane for the purification of plasmid DNA. *Biotechnol Appl Biochem* 2003;37:259. <https://doi.org/10.1042/BA20030025>.
- [31] Oellerich M, Armstrong VW. The Role of Therapeutic Drug Monitoring in Individualizing Immunosuppressive Drug Therapy: Recent Developments. *Ther Drug Monit* 2006;28:7. <https://doi.org/10.1097/FTD.0b013e31802c5cf5>.
- [32] Steimer W. Performance and Specificity of Monoclonal Immunoassays for Cyclosporine Monitoring: How Specific Is Specific? *Clin Chem* 1999;45:371–81. <https://doi.org/10.1093/clinchem/45.3.371>.
- [33] Jannetto PJ. Chapter 8 - Therapeutic drug monitoring using mass spectrometry. *Mass Spectrom. Clin. Lab.* 1st ed., Elsevier; 2016.
- [34] Tesfaye H. The importance of Therapeutic Drug Monitoring (TDM) for parenteral busulfan dosing in conditioning regimen for Hematopoietic Stem Cell Transplantation (HSCT) in children. *Ann Transplant* 2014;19:214–24. <https://doi.org/10.12659/AOT.889933>.
- [35] Decosterd LA, Widmer N, André P, Aouri M, Buclin T. The emerging role of multiplex tandem mass spectrometry analysis for therapeutic drug monitoring and personalized medicine. *TrAC Trends Anal Chem* 2016;84:5–13. <https://doi.org/10.1016/j.trac.2016.03.019>.
- [36] Jourdil JF, Bartoli M, Stanke-Labesque F. Lack of specificity for the analysis of raltegravir using online sample clean-up liquid chromatography–electrospray tandem mass spectrometry. *J Chromatogr B* 2009;877:3734–8. <https://doi.org/10.1016/j.jchromb.2009.08.031>.
- [37] Langille E, Lemieux V, Garant D, Bergeron P. Development of small blood volume assays for the measurement of oxidative stress markers in mammals. *PLOS ONE* 2018;13:e0209802. <https://doi.org/10.1371/journal.pone.0209802>.
- [38] Fayet A, Béguin A, Zanolari B, Cruchon S, Guignard N, Telenti A, et al. A LC–tandem MS assay for the simultaneous measurement of new antiretroviral agents: Raltegravir, maraviroc, darunavir, and etravirine. *J Chromatogr B* 2009;877:1057–69. <https://doi.org/10.1016/j.jchromb.2009.02.057>.
- [39] Bowen RAR, Remaley AT. Interferences from blood collection tube components on clinical chemistry assays. *Biochem Medica* 2014:31–44. <https://doi.org/10.11613/BM.2014.006>.

- [40] Koch TR, Platoff G. Suitability of Collection Tubes with Separator Gels for Therapeutic Drug Monitoring: *Ther Drug Monit* 1990;12:277–80. <https://doi.org/10.1097/00007691-199005000-00011>.
- [41] Karppi J, Åkerman KK, Parviainen M. Suitability of Collection Tubes with Separator Gels for Collecting and Storing Blood Samples for Therapeutic Drug Monitoring (TDM). *Clin Chem Lab Med* 2000;38. <https://doi.org/10.1515/CCLM.2000.045>.
- [42] Wang W, Liu J, Han Y, Huang W, Wang Q. The most convenient and general approach for plasma sample clean-up: multifunction adsorption and supported liquid extraction. *Bioanalysis* 2012;4:223–5. <https://doi.org/10.4155/bio.11.332>.
- [43] Herbrink M, de Vries N, Rosing H, Huitema ADR, Nuijen B, Schellens JHM, et al. Development and validation of a liquid chromatography-tandem mass spectrometry analytical method for the therapeutic drug monitoring of eight novel anticancer drugs. *Biomed Chromatogr* 2018;32:e4147. <https://doi.org/10.1002/bmc.4147>.
- [44] Patel M, Kothari C. Critical review of statins: A bio-analytical perspective for therapeutic drug monitoring. *TrAC Trends Anal Chem* 2017;86:206–21. <https://doi.org/10.1016/j.trac.2016.10.011>.
- [45] McShane AJ, Bunch DR, Wang S. Therapeutic drug monitoring of immunosuppressants by liquid chromatography–mass spectrometry. *Clin Chim Acta* 2016;454:1–5. <https://doi.org/10.1016/j.cca.2015.12.027>.
- [46] Abdel-Rehim M, Hassan Z, Blomberg L, Hassan M. On-Line Derivatization Utilizing Solid-Phase Microextraction (SPME) for Determination of Busulphan in Plasma Using Gas Chromatography–Mass Spectrometry (GC-MS): *Ther Drug Monit* 2003;25:400–6. <https://doi.org/10.1097/00007691-200306000-00024>.
- [47] Looby NT. Solid phase microextraction coupled to mass spectrometry via microfluidic interface for rapid therapeutic drug monitoring. *The Analyst* 2013;141:100–10. <https://doi.org/10.1039/C5AN01382H>.
- [48] Roszkowska A, Miękus N, Bączek T. Application of solid-phase microextraction in current biomedical research. *J Sep Sci* 2019;42:285–302. <https://doi.org/10.1002/jssc.201800785>.
- [49] Shahhoseini F, Langille EA, Azizi A, Bottaro CS. Thin film molecularly imprinted polymer (TF-MIP), a selective and single-use extraction device for high-throughput analysis of biological samples. *The Analyst* 2021;146:3157–68. <https://doi.org/10.1039/D0AN02228D>.
- [50] Shahhoseini F, Azizi A, Bottaro CS. Single-use porous polymer thin-film device: A reliable sampler for analysis of drugs in small volumes of biofluids. *Anal Chim Acta* 2022;1203:339651. <https://doi.org/10.1016/j.aca.2022.339651>.
- [51] Capiou S, Veenhof H, Koster RA, Bergqvist Y, Boettcher M, Halmingh O, et al. Official International Association for Therapeutic Drug Monitoring and Clinical Toxicology Guideline: Development and Validation of Dried Blood Spot–Based Methods for Therapeutic Drug Monitoring. *Ther Drug Monit* 2019;41:22. <https://doi.org/10.1097/FTD.0000000000000643>.

- [52] Conti M, Matulli Cavedagna T, Ramazzotti E, Mancini R, Calza L, Rinaldi M, et al. Multiplexed therapeutic drug monitoring (TDM) of antiviral drugs by LC–MS/MS. *Clin Mass Spectrom* 2018;7:6–17. <https://doi.org/10.1016/j.clinms.2017.12.002>.
- [53] Pouliopoulos A, Tsakelidou E, Krokos A, Gika HG, Theodoridis G, Raikos N. Quantification of 15 Psychotropic Drugs in Serum and Postmortem Blood Samples after a Modified Mini-QuEChERS by UHPLC–MS-MS. *J Anal Toxicol* 2018;42:337–45. <https://doi.org/10.1093/jat/bky006>.
- [54] Avataneo V, D’Avolio A, Cusato J, Cantù M, De Nicolò A. LC-MS application for therapeutic drug monitoring in alternative matrices. *J Pharm Biomed Anal* 2019;166:40–51. <https://doi.org/10.1016/j.jpba.2018.12.040>.
- [55] Gómez-Ríos GA, Tascon M, Reyes-Garcés N, Boyacı E, Poole J, Pawliszyn J. Quantitative analysis of biofluid spots by coated blade spray mass spectrometry, a new approach to rapid screening. *Sci Rep* 2017;7. <https://doi.org/10.1038/s41598-017-16494-z>.
- [56] Tascon M, Gómez-Ríos GA, Reyes-Garcés N, Poole J, Boyacı E, Pawliszyn J. High-Throughput Screening and Quantitation of Target Compounds in Biofluids by Coated Blade Spray-Mass Spectrometry. *Anal Chem* 2017;89:8421–8. <https://doi.org/10.1021/acs.analchem.7b01877>.
- [57] Gómez-Ríos GA, Tascon M, Reyes-Garcés N, Boyacı E, Poole JJ, Pawliszyn J. Rapid determination of immunosuppressive drug concentrations in whole blood by coated blade spray-tandem mass spectrometry (CBS-MS/MS). *Anal Chim Acta* 2018;999:69–75. <https://doi.org/10.1016/j.aca.2017.10.016>.
- [58] Chiang S, Zhang W, Ouyang Z. Paper spray ionization mass spectrometry: recent advances and clinical applications. *Expert Rev Proteomics* 2018;15:781–9. <https://doi.org/10.1080/14789450.2018.1525295>.
- [59] Takyi-Williams J, Dong X, Gong H, Wang Y, Jian W, Liu C-F, et al. Application of paper spray–MS in PK studies using sunitinib and benzethonium as model compounds. *Bioanalysis* 2015;7:413–23. <https://doi.org/10.4155/bio.14.288>.
- [60] Gómez-Ríos GA, Pawliszyn J. Development of Coated Blade Spray Ionization Mass Spectrometry for the Quantitation of Target Analytes Present in Complex Matrices. *Angew Chem Int Ed* 2014;53:14503–7. <https://doi.org/10.1002/anie.201407057>.
- [61] Tascon M, Gómez-Ríos GA, Reyes-Garcés N, Poole J, Boyacı E, Pawliszyn J. Ultra-fast quantitation of voriconazole in human plasma by coated blade spray mass spectrometry. *J Pharm Biomed Anal* 2017;144:106–11. <https://doi.org/10.1016/j.jpba.2017.03.009>.
- [62] Gross JH. Direct analysis in real time—a critical review on DART-MS. *Anal Bioanal Chem* 2014;406:63–80. <https://doi.org/10.1007/s00216-013-7316-0>.
- [63] Rossi A, Castrati L, Colombo P, Flammini L, Barocelli E, Bettini R, et al. Development and validation of a DESI-HRMS/MS method for the fast profiling of esomeprazole and its metabolites in rat plasma: a pharmacokinetic study: DESI-HRMS/MS method for the fast profiling of esomeprazole and its metabolite pharmacokinetics in rat plasma. *Drug Test Anal* 2016;8:208–13. <https://doi.org/10.1002/dta.1805>.

- [64] Maurer HH. Mass Spectrometry for Research and Application in Therapeutic Drug Monitoring or Clinical and Forensic Toxicology: *Ther Drug Monit* 2018;40:389–93. <https://doi.org/10.1097/FTD.0000000000000525>.
- [65] Abu-Rabie P, Spooner N. Direct Quantitative Bioanalysis of Drugs in Dried Blood Spot Samples Using a Thin-Layer Chromatography Mass Spectrometer Interface. *Anal Chem* 2009;81:10275–84. <https://doi.org/10.1021/ac901985e>.
- [66] Abu-Rabie P, Denniff P, Spooner N, Chowdhry BZ, Pullen FS. Investigation of Different Approaches to Incorporating Internal Standard in DBS Quantitative Bioanalytical Workflows and Their Effect on Nullifying Hematocrit-Based Assay Bias. *Anal Chem* 2015;87:4996–5003. <https://doi.org/10.1021/acs.analchem.5b00908>.
- [67] Staudinger H, Fritschi J. Über Isopren und Kautschuk. 5. Mitteilung. Über die Hydrierung des Kautschuks und über seine Konstitution. *Helv Chim Acta* 1922;5:785–806. <https://doi.org/10.1002/hlca.19220050517>.
- [68] Gold V, editor. *The IUPAC Compendium of Chemical Terminology: The Gold Book*. 4th ed. Research Triangle Park, NC: International Union of Pure and Applied Chemistry (IUPAC); 2019. <https://doi.org/10.1351/goldbook>.
- [69] Minkin VI. Glossary of terms used in theoretical organic chemistry. *Pure Appl Chem* 1999;71:1919–81. <https://doi.org/10.1351/pac199971101919>.
- [70] Rosa SS. mRNA vaccines manufacturing: Challenges and bottlenecks 2021:11.
- [71] Abbas SA. Separation and Purification of a Monoclonal Antibody for use in Patients Suffering from Wet Macular Degeneration. Honours. University of Nevada, 2015.
- [72] Poddar S, Sharmeen S, Hage DS. Affinity monolith chromatography: A review of general principles and recent developments. *ELECTROPHORESIS* 2021;42:2577–98. <https://doi.org/10.1002/elps.202100163>.
- [73] Porath J, Flodin P. Gel Filtration: A Method for Desalting and Group Separation. *Nature* 1959;183:1657–9. <https://doi.org/10.1038/1831657a0>.
- [74] Peterson EA, Sober HA. Chromatography of Proteins. I. Cellulose Ion-exchange Adsorbents. *J Am Chem Soc* 1956;78:751–5. <https://doi.org/10.1021/ja01585a016>.
- [75] Chang SH, Gooding KM, Regnier FE. Use of oxiranes in the preparation of bonded phase supports. *J Chromatogr A* 1976;120:321–33. [https://doi.org/10.1016/S0021-9673\(76\)80009-X](https://doi.org/10.1016/S0021-9673(76)80009-X).
- [76] Kato Y, Nakamura K, Hashimoto T. Characterization of tsk-gel deae-toyopearl 650 ion exchanger. *J Chromatogr A* 1982;245:193–211. [https://doi.org/10.1016/S0021-9673\(00\)88589-1](https://doi.org/10.1016/S0021-9673(00)88589-1).
- [77] Rodrigues AE. Permeable packings and perfusion chromatography in protein separation. *J Chromatogr B Biomed Sci App* 1997;699:47–61. [https://doi.org/10.1016/S0378-4347\(97\)00197-7](https://doi.org/10.1016/S0378-4347(97)00197-7).
- [78] Afeyan NB, Gordon NF, Mazsaroff I, Varady L, Fulton SP, Yang YB, et al. Flow-through particles for the high-performance liquid chromatographic separation of biomolecules: perfusion chromatography. *J Chromatogr A* 1990;519:1–29. [https://doi.org/10.1016/0021-9673\(90\)85132-F](https://doi.org/10.1016/0021-9673(90)85132-F).

- [79] Horvath J, Boschetti E, Guerrier L, Cooke N. High-performance protein separations with novel strong ion exchangers. *J Chromatogr A* 1994;679:11–22. [https://doi.org/10.1016/0021-9673\(94\)80307-2](https://doi.org/10.1016/0021-9673(94)80307-2).
- [80] Rodrigues AE, Lopes JC, Lu ZP, Loureiro JM, Dias MM. Importance of intraparticle convection in the performance of chromatographic processes. *J Chromatogr A* 1992;590:93–100. [https://doi.org/10.1016/0021-9673\(92\)87009-W](https://doi.org/10.1016/0021-9673(92)87009-W).
- [81] Roper DK, Lightfoot EN. Estimating plate heights in stacked-membrane chromatography by flow reversal. *J Chromatogr A* 1995;702:69–80. [https://doi.org/10.1016/0021-9673\(94\)01068-P](https://doi.org/10.1016/0021-9673(94)01068-P).
- [82] Shiosaki A, Goto M, Hirose T. Frontal analysis of protein adsorption on a membrane adsorber. *J Chromatogr A* 1994;679:1–9. [https://doi.org/10.1016/0021-9673\(94\)80306-4](https://doi.org/10.1016/0021-9673(94)80306-4).
- [83] Zhang D, Chow DS-L. Clinical Pharmacokinetics of Mycophenolic Acid in Hematopoietic Stem Cell Transplantation Recipients. *Eur J Drug Metab Pharmacokinet* 2017;42:183–9. <https://doi.org/10.1007/s13318-016-0378-6>.
- [84] Gray Derek WR. Mycophenolate mofetil for transplantation: new drug, old problems? *The Lancet* 1995;346:390. [https://doi.org/10.1016/S0140-6736\(95\)92775-1](https://doi.org/10.1016/S0140-6736(95)92775-1).
- [85] Ransom JT. Mechanism of Action of Mycophenolate Mofetil. *Ther Drug Monit* 1995;17:681–4. <https://doi.org/10.1097/00007691-199512000-00023>.
- [86] Kiang TKL, Ensom MHH. Population Pharmacokinetics of Mycophenolic Acid: An Update. *Clin Pharmacokinet* 2018;57:547–58. <https://doi.org/10.1007/s40262-017-0593-6>.
- [87] Staatz CE, Tett SE. Pharmacology and toxicology of mycophenolate in organ transplant recipients: an update. *Arch Toxicol* 2014;88:1351–89. <https://doi.org/10.1007/s00204-014-1247-1>.
- [88] Bullingham R, Monroe S, Nicholls A, Hale M. Pharmacokinetics and Bioavailability of Mycophenolate Mofetil in Healthy Subjects after Single-Dose Oral and Intravenous Administration. *J Clin Pharmacol* 1996;36:315–24. <https://doi.org/10.1002/j.1552-4604.1996.tb04207.x>.
- [89] Sollinger HW, Deierhoi MH, Belzer FO, Diethelm AG, Kauffman RS. RS-61443—A PHASE I CLINICAL TRIAL AND PILOT RESCUE STUDY 1: Transplantation 1992;53:428–32. <https://doi.org/10.1097/00007890-199202010-00031>.
- [90] Hale MD, Nicholls AJ, Bullingham RES, Hené R, Hoitsma A, Squifflet J-P, et al. The pharmacokinetic-pharmacodynamic relationship for mycophenolate mofetil in renal transplantation\*. *Clin Pharmacol Ther* 1998;64:672–83. [https://doi.org/10.1016/S0009-9236\(98\)90058-3](https://doi.org/10.1016/S0009-9236(98)90058-3).
- [91] Jeong H, Kaplan B. Therapeutic Monitoring of Mycophenolate Mofetil. *Clin J Am Soc Nephrol* 2007;2:184–91. <https://doi.org/10.2215/CJN.02860806>.
- [92] Filler G, Buffo I. Safety considerations with mycophenolate sodium. *Expert Opin Drug Saf* 2007;6:445–9. <https://doi.org/10.1517/14740338.6.4.445>.
- [93] Filler G, Ferrand A. Do we need to worry about mycophenolate overdose? *Expert Opin Drug Saf* 2014;13:521–4. <https://doi.org/10.1517/14740338.2014.905540>.

- [94] Kuypers DRJ, Meur YL, Cantarovich M, Tredger MJ, Tett SE, Cattaneo D, et al. Consensus Report on Therapeutic Drug Monitoring of Mycophenolic Acid in Solid Organ Transplantation. *Clin J Am Soc Nephrol* 2010;5:341–58. <https://doi.org/10.2215/CJN.07111009>.
- [95] Aucella F, Lauriola V, Vecchione G, Tiscia GL, Grandone E. Liquid chromatography–tandem mass spectrometry method as the golden standard for therapeutic drug monitoring in renal transplant. *J Pharm Biomed Anal* 2013;86:123–6. <https://doi.org/10.1016/j.jpba.2013.08.001>.
- [96] Brandhorst G, Streit F, Goetze S, Oellerich M, Armstrong VW. Quantification by Liquid Chromatography Tandem Mass Spectrometry of Mycophenolic Acid and Its Phenol and Acyl Glucuronide Metabolites. *Clin Chem* 2006;52:1962–4. <https://doi.org/10.1373/clinchem.2006.074336>.
- [97] Rong Y, Kiang TKL. Development and validation of a sensitive liquid-chromatography tandem mass spectrometry assay for mycophenolic acid and metabolites in HepaRG cell culture: Characterization of metabolism interactions between *p*-cresol and mycophenolic acid. *Biomed Chromatogr* 2019:e4549. <https://doi.org/10.1002/bmc.4549>.
- [98] Willis C, Taylor PJ, Salm P, Tett SE, Pillans PI. Quantification of free mycophenolic acid by high-performance liquid chromatography–atmospheric pressure chemical ionisation tandem mass spectrometry. *J Chromatogr B Biomed Sci App* 2000;748:151–6. [https://doi.org/10.1016/S0378-4347\(00\)00273-5](https://doi.org/10.1016/S0378-4347(00)00273-5).
- [99] Atcheson B, Taylor PJ, Pillans PI, Tett SE. Measurement of free drug and clinical end-point by high-performance liquid chromatography–mass spectrometry. *Anal Chim Acta* 2003;492:157–69. [https://doi.org/10.1016/S0003-2670\(03\)00359-3](https://doi.org/10.1016/S0003-2670(03)00359-3).
- [100] Daurel-Receveur M, Titier K, Picard S, Ducint D, Moore N, Molimard M. Fully Automated Analytical Method for Mycophenolic Acid Quantification in Human Plasma Using On-line Solid Phase Extraction and High Performance Liquid Chromatography With Diode Array Detection: *Ther Drug Monit* 2006;28:505–11. <https://doi.org/10.1097/00007691-200608000-00004>.
- [101] Farhadi K, Hatami M, Matin AA. Microextraction techniques in therapeutic drug monitoring: Microextraction techniques in therapeutic drug monitoring. *Biomed Chromatogr* 2012:n/a-n/a. <https://doi.org/10.1002/bmc.2774>.
- [102] Zambonin C, Aresta A, Palmisano F. Determination of the immunosuppressant mycophenolic acid in human serum by solid-phase microextraction coupled to liquid chromatography. *J Chromatogr B* 2004;806:89–93. <https://doi.org/10.1016/j.jchromb.2004.03.039>.
- [103] Azizi A, Shahhoseini F, Modir-Rousta A, Bottaro CS. High throughput direct analysis of water using solvothermal headspace desorption with porous thin films. *Anal Chim Acta* 2019;1087:51–61. <https://doi.org/10.1016/j.aca.2019.08.022>.
- [104] Shahhoseini F, Azizi A, Egli SN, Bottaro CS. Single-use porous thin film extraction with gas chromatography atmospheric pressure chemical ionization tandem mass spectrometry for high-throughput analysis of 16 PAHs. *Talanta* 2020;207:120320. <https://doi.org/10.1016/j.talanta.2019.120320>.

- [105] Abu-Alsoud GF, Bottaro CS. Porous thin-film molecularly imprinted polymer device for simultaneous determination of phenol, alkylphenol and chlorophenol compounds in water. *Talanta* 2021;223:121727. <https://doi.org/10.1016/j.talanta.2020.121727>.
- [106] Egli SN, Butler ED, Bottaro CS. Selective extraction of light polycyclic aromatic hydrocarbons in environmental water samples with pseudo-template thin-film molecularly imprinted polymers. *Anal Methods* 2015;7:2028–35. <https://doi.org/10.1039/C4AY02849J>.
- [107] Hijazi HY, Bottaro CS. Molecularly imprinted polymer thin-film as a micro-extraction adsorbent for selective determination of trace concentrations of polycyclic aromatic sulfur heterocycles in seawater. *J Chromatogr A* 2020;1617:460824. <https://doi.org/10.1016/j.chroma.2019.460824>.
- [108] Shahhoseini F, Langille E, Azizi A, Bottaro C. Thin film molecularly imprinted polymer (TF-MIP), a selective and single-use extraction device for high throughput analysis of biological samples. *Analyst* n.d.
- [109] Streit F, Shipkova M, Armstrong VW, Oellerich M. Validation of a Rapid and Sensitive Liquid Chromatography–Tandem Mass Spectrometry Method for Free and Total Mycophenolic Acid. *Clin Chem* 2004;50:152–9. <https://doi.org/10.1373/clinchem.2003.024323>.
- [110] Azizi A, Shahhoseini F, Langille EA, Akhoondi R, Bottaro CS. Micro-gel thin film molecularly imprinted polymer coating for extraction of organophosphorus pesticides from water and beverage samples. *Anal Chim Acta* 2021;1187:339135. <https://doi.org/10.1016/j.aca.2021.339135>.
- [111] Lipsky JJ. Mycophenolate mofetil. *The Lancet* 1996;348:1357–9. [https://doi.org/10.1016/S0140-6736\(96\)10310-X](https://doi.org/10.1016/S0140-6736(96)10310-X).
- [112] Wilems TS, Lu X, Kurosu YE, Khan Z, Lim HJ, Smith Callahan LA. Effects of free radical initiators on polyethylene glycol dimethacrylate hydrogel properties and biocompatibility: ORIGINAL ARTICLE. *J Biomed Mater Res A* 2017;105:3059–68. <https://doi.org/10.1002/jbm.a.36160>.
- [113] Li H, Mager DE, Sandmaier BM, Storer BE, Boeckh MJ, Bemer MJ, et al. Pharmacokinetic and Pharmacodynamic Analysis of Inosine Monophosphate Dehydrogenase Activity in Hematopoietic Cell Transplantation Recipients Treated with Mycophenolate Mofetil. *Biol Blood Marrow Transplant* 2014;20:1121–9. <https://doi.org/10.1016/j.bbmt.2014.03.032>.
- [114] Chace DH, Clinical and Laboratory Standards Institute, International Federation of Clinical Chemistry and Laboratory Medicine. *Mass spectrometry in the clinical laboratory: general principles and guidance : approved guideline*. Wayne, Pa.: Clinical and Laboratory Standards Institute : International Federation of Clinical Chemistry and Laboratory Medicine; 2007.
- [115] Yaish P, Gazit A, Gilon C, Levitzki A. Blocking of EGF-dependent cell proliferation by EGF receptor kinase inhibitors. *Science* 1988;242:933–5. <https://doi.org/10.1126/science.3263702>.

- [116] Merienne C, Rousset M, Ducint D, Castaing N, Titier K, Molimard M, et al. High throughput routine determination of 17 tyrosine kinase inhibitors by LC–MS/MS. *J Pharm Biomed Anal* 2018;150:112–20. <https://doi.org/10.1016/j.jpba.2017.11.060>.
- [117] Gambacorti-Passerini C, le Coutre P, Mologni L, Fanelli M, Bertazzoli C, Marchesi E, et al. Inhibition of the ABL Kinase Activity Blocks the Proliferation of BCR/ABL+Leukemic Cells and Induces Apoptosis. *Blood Cells Mol Dis* 1997;23:380–94. <https://doi.org/10.1006/bcmd.1997.0155>.
- [118] Druker BJ, Tamura S, Buchdunger E, Ohno S, Segal GM, Fanning S, et al. Effects of a selective inhibitor of the Abl tyrosine kinase on the growth of Bcr–Abl positive cells. *Nat Med* 1996;2:561–6. <https://doi.org/10.1038/nm0596-561>.
- [119] Anafi M, Gazit A, Zehavi A, Ben-Neriah Y, Levitzki A. Tyrphostin-induced inhibition of p210bcr-abl tyrosine kinase activity induces K562 to differentiate. *Blood* 1993;82:3524–9. <https://doi.org/10.1182/blood.V82.12.3524.3524>.
- [120] Gambacorti-Passerini C. Part I: Milestones in personalised medicine—imatinib. *Lancet Oncol* 2008;9:600. [https://doi.org/10.1016/S1470-2045\(08\)70152-9](https://doi.org/10.1016/S1470-2045(08)70152-9).
- [121] Hochhaus A, Druker B, Sawyers C, Guilhot F, Schiffer CA, Cortes J, et al. Favorable long-term follow-up results over 6 years for response, survival, and safety with imatinib mesylate therapy in chronic-phase chronic myeloid leukemia after failure of interferon- $\alpha$  treatment 2008;111:6.
- [122] Gambacorti-Passerini C, Antolini L, Mahon F-X, Guilhot F, Deininger M, Fava C, et al. Multicenter Independent Assessment of Outcomes in Chronic Myeloid Leukemia Patients Treated With Imatinib. *JNCI J Natl Cancer Inst* 2011;103:553–61. <https://doi.org/10.1093/jnci/djr060>.
- [123] Hoemberger M, Pitsawong W, Kern D. Cumulative mechanism of several major imatinib-resistant mutations in Abl kinase. *Proc Natl Acad Sci* 2020;117:19221–7. <https://doi.org/10.1073/pnas.1919221117>.
- [124] Manley PW, Stiefl N, Cowan-Jacob SW, Kaufman S, Mestan J, Wartmann M, et al. Structural resemblances and comparisons of the relative pharmacological properties of imatinib and nilotinib. *Bioorg Med Chem* 2010;18:6977–86. <https://doi.org/10.1016/j.bmc.2010.08.026>.
- [125] Jabbour E. Nilotinib for the treatment of chronic myeloid leukemia: An evidence-based review. *Core Evid* 2009;207. <https://doi.org/10.2147/CE.S6003>.
- [126] Huang W-S, Metcalf CA, Sundaramoorthi R, Wang Y, Zou D, Thomas RM, et al. Discovery of 3-[2-(Imidazo[1,2-*b*]pyridazin-3-yl)ethynyl]-4-methyl-*N*-{4-[(4-methylpiperazin-1-yl)methyl]-3-(trifluoromethyl)phenyl}benzamide (AP24534), a Potent, Orally Active Pan-Inhibitor of Breakpoint Cluster Region-Abelson (BCR-ABL) Kinase Including the T315I Gatekeeper Mutant. *J Med Chem* 2010;53:4701–19. <https://doi.org/10.1021/jm100395q>.
- [127] O’Hare T, Shakespeare WC, Zhu X, Eide CA, Rivera VM, Wang F, et al. AP24534, a Pan-BCR-ABL Inhibitor for Chronic Myeloid Leukemia, Potently Inhibits the T315I Mutant and Overcomes Mutation-Based Resistance. *Cancer Cell* 2009;16:401–12. <https://doi.org/10.1016/j.ccr.2009.09.028>.
- [128] Das J, Chen P, Norris D, Padmanabha R, Lin J, Moquin RV, et al. 2-Aminothiazole as a Novel Kinase Inhibitor Template. *Structure–Activity Relationship Studies*



- toward the Discovery of *N*-(2-Chloro-6-methylphenyl)-2-[[6-[4-(2-hydroxyethyl)-1-piperazinyl]-2-methyl-4-pyrimidinyl]amino]-1,3-thiazole-5-carboxamide (Dasatinib, BMS-354825) as a Potent *pan*-Src Kinase Inhibitor. *J Med Chem* 2006;49:6819–32. <https://doi.org/10.1021/jm060727j>.
- [129] Braun TP, Eide CA, Druker BJ. Response and Resistance to BCR-ABL1-Targeted Therapies. *Cancer Cell* 2020;37:530–42. <https://doi.org/10.1016/j.ccell.2020.03.006>.
- [130] Josephs DH, Fisher DS, Spicer J, Flanagan RJ. Clinical Pharmacokinetics of Tyrosine Kinase Inhibitors: Implications for Therapeutic Drug Monitoring. *Ther Drug Monit* 2013;35:26.
- [131] van Erp NP, Gelderblom H, Guchelaar H-J. Clinical pharmacokinetics of tyrosine kinase inhibitors. *Cancer Treat Rev* 2009;35:692–706. <https://doi.org/10.1016/j.ctrv.2009.08.004>.
- [132] Gao B, Yeap S, Clements A, Balakrishnar B, Wong M, Gurney H. Evidence for Therapeutic Drug Monitoring of Targeted Anticancer Therapies. *J Clin Oncol* 2012;30:4017–25. <https://doi.org/10.1200/JCO.2012.43.5362>.
- [133] Picard S, Titier K, Etienne G, Teilhet E, Ducint D, Bernard M-A, et al. Trough imatinib plasma levels are associated with both cytogenetic and molecular responses to standard-dose imatinib in chronic myeloid leukemia. *Blood* 2007;109:3496–9. <https://doi.org/10.1182/blood-2006-07-036012>.
- [134] Wang X, Hochhaus A, Kantarjian HM, Agrawal S, Roy A, Pfister M, et al. Dasatinib pharmacokinetics and exposure-response (E-R): Relationship to safety and efficacy in patients (pts) with chronic myeloid leukemia (CML). *J Clin Oncol* 2008;26:3590–3590. [https://doi.org/10.1200/jco.2008.26.15\\_suppl.3590](https://doi.org/10.1200/jco.2008.26.15_suppl.3590).
- [135] Larson RA, Yin OQP, Hochhaus A, Saglio G, Clark RE, Nakamae H, et al. Population pharmacokinetic and exposure-response analysis of nilotinib in patients with newly diagnosed Ph<sup>+</sup> chronic myeloid leukemia in chronic phase. *Eur J Clin Pharmacol* 2012;68:723–33. <https://doi.org/10.1007/s00228-011-1200-7>.
- [136] Narasimhan NI, Dorer DJ, Niland K, Haluska F, Sonnichsen D. Effects of food on the pharmacokinetics of ponatinib in healthy subjects 2013:5.
- [137] Ajimura TO, Borges KB, Ferreira AF, de Castro FA, de Gaitani CM. Capillary electrophoresis method for plasmatic determination of imatinib mesylate in chronic myeloid leukemia patients. *ELECTROPHORESIS* 2011;32:1885–92. <https://doi.org/10.1002/elps.201000642>.
- [138] Saita T, Shin M, Fujito H. Development of a Specific and Sensitive Enzyme-Linked Immunosorbent Assay for the Quantification of Imatinib. *Biol Pharm Bull* 2013;36:1964–8. <https://doi.org/10.1248/bpb.b13-00597>.
- [139] Miura M, Takahashi N. Routine therapeutic drug monitoring of tyrosine kinase inhibitors by HPLC–UV or LC–MS/MS methods. *Drug Metab Pharmacokinet* 2016;31:12–20. <https://doi.org/10.1016/j.dmpk.2015.09.002>.
- [140] Zeng J, Cai H lin, Jiang Z ping, Wang Q, Zhu Y, Xu P, et al. A validated UPLC–MS/MS method for simultaneous determination of imatinib, dasatinib and nilotinib in human plasma. *J Pharm Anal* 2017;7:374–80. <https://doi.org/10.1016/j.jpha.2017.07.009>.

- [141] Koller D, Vaitsekhovich V, Mba C, Steegmann JL, Zubiaur P, Abad-Santos F, et al. Effective quantification of 11 tyrosine kinase inhibitors and caffeine in human plasma by validated LC-MS/MS method with potent phospholipids clean-up procedure. Application to therapeutic drug monitoring. *Talanta* 2020;208:120450. <https://doi.org/10.1016/j.talanta.2019.120450>.
- [142] Herviou P, Thivat E, Richard D, Roche L, Dohou J, Pouget M, et al. Therapeutic drug monitoring and tyrosine kinase inhibitors. *Oncol Lett* 2016;12:1223–32. <https://doi.org/10.3892/ol.2016.4780>.
- [143] Barker SL, LaRocca PJ. Method of production and control of a commercial tissue culture surface. *J Tissue Cult Methods* 1994;16:151–3. <https://doi.org/10.1007/BF01540642>.
- [144] Zeiger AS, Hinton B, Van Vliet KJ. Why the dish makes a difference: Quantitative comparison of polystyrene culture surfaces. *Acta Biomater* 2013;9:7354–61. <https://doi.org/10.1016/j.actbio.2013.02.035>.
- [145] Rifai N, Horvath AR, Wittwer CT, Tietz NW, editors. *Tietz textbook of clinical chemistry and molecular diagnostics*. Sixth edition. St. Louis, Missouri: Elsevier; 2018.
- [146] Shaw DJ. *Introduction to colloid and surface chemistry*. 4th ed. Oxford ; Boston: Butterworth-Heinemann; 1992.
- [147] Lloyd LL. Rigid macroporous copolymers as stationary phases in high-performance liquid chromatography. *J Chromatogr A* 1991;544:201–17. [https://doi.org/10.1016/S0021-9673\(01\)83986-8](https://doi.org/10.1016/S0021-9673(01)83986-8).
- [148] Sellergren B, Shea KJ. Influence of polymer morphology on the ability of imprinted network polymers to resolve enantiomers. *J Chromatogr A* 1993;635:31–49. [https://doi.org/10.1016/0021-9673\(93\)83112-6](https://doi.org/10.1016/0021-9673(93)83112-6).
- [149] Hubert Ph, Chiap P, Crommen J, Boulanger B, Chapuzet E, Mercier N, et al. The SFSTP guide on the validation of chromatographic methods for drug bioanalysis: from the Washington Conference to the laboratory. *Anal Chim Acta* 1999;391:135–48. [https://doi.org/10.1016/S0003-2670\(99\)00106-3](https://doi.org/10.1016/S0003-2670(99)00106-3).
- [150] European Medicines Agency. *Guideline on bioanalytical method validation* 2011.
- [151] Tiwari G, Tiwari R. Bioanalytical method validation: An updated review. *Pharm Methods* 2010;1:25. <https://doi.org/10.4103/2229-4708.72226>.
- [152] U.S. Department of Health and Human Services, Food and Drug Administration, Center for Drug Evaluation and Research, Center for Veterinary Medicine. *Bioanalytical Method Validation: Guidance for Industry* 2018:44.
- [153] Xia B, Heimbach T, He H, Lin T. Nilotinib preclinical pharmacokinetics and practical application toward clinical projections of oral absorption and systemic availability: NILOTINIB PRECLINICAL PHARMACOKINETICS. *Biopharm Drug Dispos* 2012;33:536–49. <https://doi.org/10.1002/bdd.1821>.
- [154] Fargo MV, Activity BM. *Evaluation of Jaundice in Adults* 2017;95:5.
- [155] Burtis CA, Ashwood ER, Bruns DE, Tietz NW. *Tietz textbook of clinical chemistry and molecular diagnostics*. 5th ed. St. Louis, Mo.: Saunders; 2013.
- [156] Marrs B. Genetic recombination in *Rhodopseudomonas capsulata*. *Proc Natl Acad Sci* 1974;71:971–3. <https://doi.org/10.1073/pnas.71.3.971>.

- [157] Yen HC, Hu NT, Marrs BL. Characterization of the gene transfer agent made by an overproducer mutant of *Rhodopseudomonas capsulata*. *J Mol Biol* 1979;131:157–68. [https://doi.org/10.1016/0022-2836\(79\)90071-8](https://doi.org/10.1016/0022-2836(79)90071-8).
- [158] Lang AS, Westbye AB, Beatty JT. The distribution, evolution, and roles of gene transfer agents in prokaryotic genetic exchange. *Annu Rev Virol* 2017;4:87–104. <https://doi.org/10.1146/annurev-virology-101416-041624>.
- [159] Lang AS, Zhaxybayeva O, Beatty JT. Gene transfer agents: phage-like elements of genetic exchange. *Nat Rev Microbiol* 2012;10:472–82. <https://doi.org/10.1038/nrmicro2802>.
- [160] Solioz M, Marrs B. The gene transfer agent of *Rhodopseudomonas capsulata* purification and characterization of its nucleic acid. *Arch Biochem Biophys* 1977;181:300–7. [https://doi.org/10.1016/0003-9861\(77\)90508-2](https://doi.org/10.1016/0003-9861(77)90508-2).
- [161] Hynes AP, Mercer RG, Watton DE, Buckley CB, Lang AS. DNA packaging bias and differential expression of gene transfer agent genes within a population during production and release of the *Rhodobacter capsulatus* gene transfer agent, RcGTA: Gene transfer agent gene expression and DNA packaging. *Mol Microbiol* 2012;85:314–25. <https://doi.org/10.1111/j.1365-2958.2012.08113.x>.
- [162] Lang AS, Beatty JT. Genetic analysis of a bacterial genetic exchange element: The gene transfer agent of *Rhodobacter capsulatus*. *Proc Natl Acad Sci* 2000;97:859–64. <https://doi.org/10.1073/pnas.97.2.859>.
- [163] Fogg PCM. Identification and characterization of a direct activator of a gene transfer agent. *Nat Commun* 2019;10:595. <https://doi.org/10.1038/s41467-019-08526-1>.
- [164] Bárdy P, Füzik T, Hrebík D, Pantůček R, Thomas Beatty J, Plevka P. Structure and mechanism of DNA delivery of a gene transfer agent. *Nat Commun* 2020;11. <https://doi.org/10.1038/s41467-020-16669-9>.
- [165] Redfield RJ, Soucy SM. Evolution of bacterial gene transfer agents. *Front Microbiol* 2018;9:2527. <https://doi.org/10.3389/fmicb.2018.02527>.
- [166] Fogg PCM, Westbye AB, Beatty JT. One for all or all for one: heterogeneous expression and host cell lysis are key to gene transfer agent activity in *Rhodobacter capsulatus*. *PLoS ONE* 2012;7:e43772. <https://doi.org/10.1371/journal.pone.0043772>.
- [167] Ding H, Grüll MP, Mulligan ME, Lang AS, Beatty JT. Induction of *Rhodobacter capsulatus* gene transfer agent gene expression is a bistable stochastic process repressed by an extracellular calcium-binding RTX protein homologue. *J Bacteriol* 2019;201. <https://doi.org/10.1128/JB.00430-19>.
- [168] Brimacombe CA, Stevens A, Jun D, Mercer R, Lang AS, Beatty JT. Quorum-sensing regulation of a capsular polysaccharide receptor for the *Rhodobacter capsulatus* gene transfer agent (RcGTA): *R. capsulatus* gene transfer agent receptor. *Mol Microbiol* 2013;87:802–17. <https://doi.org/10.1111/mmi.12132>.
- [169] Westbye AB, Beatty JT, Lang AS. Guaranteeing a captive audience: coordinated regulation of gene transfer agent (GTA) production and recipient capability by cellular regulators. *Curr Opin Microbiol* 2017;38:122–9. <https://doi.org/10.1016/j.mib.2017.05.003>.

- [170] Westbye AB, O'Neill Z, Schellenberg-Beaver T, Beatty JT. The *Rhodobacter capsulatus* gene transfer agent is induced by nutrient depletion and the RNAP omega subunit. *Microbiology* 2017;163:1355–63. <https://doi.org/10.1099/mic.0.000519>.
- [171] Westbye AB, Leung MM, Florizone SM, Taylor TA, Johnson JA, Fogg PC, et al. Phosphate concentration and the putative sensor kinase protein CckA modulate cell lysis and release of the *Rhodobacter capsulatus* gene transfer agent. *J Bacteriol* 2013;195:5025–40. <https://doi.org/10.1128/JB.00669-13>.
- [172] Leung MM, Brimacombe CA, Spiegelman GB, Beatty JT. The GtaR protein negatively regulates transcription of the gtaRI operon and modulates gene transfer agent (RcGTA) expression in *Rhodobacter capsulatus*: quorum-sensing in *Rhodobacter capsulatus*. *Mol Microbiol* 2012;83:759–74. <https://doi.org/10.1111/j.1365-2958.2011.07963.x>.
- [173] Seitz P, Blokesch M. Cues and regulatory pathways involved in natural competence and transformation in pathogenic and environmental Gram-negative bacteria. *FEMS Microbiol Rev* 2013;37:336–63. <https://doi.org/10.1111/j.1574-6976.2012.00353.x>.
- [174] Solioz M, Yen HC, Marris B. Release and uptake of gene transfer agent by *Rhodopseudomonas capsulata*. *J Bacteriol* 1975;123:651–7. <https://doi.org/10.1128/jb.123.2.651-657.1975>.
- [175] Tomasch J, Wang H, Hall ATK, Patzelt D, Preusse M, Petersen J, et al. Packaging of *Dinoroseobacter shibae* DNA into gene transfer agent particles is not random. *Genome Biol Evol* 2018;10:359–69. <https://doi.org/10.1093/gbe/evy005>.
- [176] Westbye AB, Kuchinski K, Yip CK, Beatty JT. The gene transfer agent RcGTA contains head spikes needed for binding to the *Rhodobacter capsulatus* polysaccharide cell capsule. *J Mol Biol* 2016;428:477–91. <https://doi.org/10.1016/j.jmb.2015.12.010>.
- [177] Rajamanickam V, Herwig C, Spadiut O. Monoliths in bioprocess technology. *Chromatography* 2015;2:195–212. <https://doi.org/10.3390/chromatography2020195>.
- [178] Bourdin G, Schmitt B, Marvin Guy L, Germond J-E, Zuber S, Michot L, et al. Amplification and purification of T4-like *Escherichia coli* phages for phage therapy: from laboratory to pilot scale. *Appl Environ Microbiol* 2014;80:1469–76. <https://doi.org/10.1128/AEM.03357-13>.
- [179] Weaver PF, Wall JD, Gest H. Characterization of *Rhodopseudomonas capsulata*. *Arch Microbiol* 1975;105:207–16. <https://doi.org/10.1007/BF00447139>.
- [180] Beatty JT, Gest H. Biosynthetic and bioenergetic functions of citric acid cycle reactions in *Rhodopseudomonas capsulata*. *J Bacteriol* 1981;148:584–93. <https://doi.org/10.1128/jb.148.2.584-593.1981>.
- [181] Feick R, Van Grondelle R, Rijgersberg CP, Drews G. Fluorescence emission by wild-type- and mutant-strains of *Rhodopseudomonas capsulata*. *Biochim Biophys Acta BBA - Bioenerg* 1980;593:241–53. [https://doi.org/10.1016/0005-2728\(80\)90062-6](https://doi.org/10.1016/0005-2728(80)90062-6).

- [182] Hynes A, Lang A. *Rhodobacter capsulatus* gene transfer agent (RcGTA) activity bioassays. *BIO-Protoc* 2013;3. <https://doi.org/10.21769/BioProtoc.317>.
- [183] Fu Y, MacLeod D, Rivkin R, Chen F, Buchan A, Lang A. High diversity of *Rhodobacterales* in the subarctic North Atlantic Ocean and gene transfer agent protein expression in isolated strains. *Aquat Microb Ecol* 2010;59:283–93. <https://doi.org/10.3354/ame01398>.
- [184] Gubellini F, Francia F, Turina P, Lévy D, Venturoli G, Melandri BA. Heterogeneity of photosynthetic membranes from *Rhodobacter capsulatus*: Size dispersion and ATP synthase distribution. *Biochim Biophys Acta BBA - Bioenerg* 2007;1767:1340–52. <https://doi.org/10.1016/j.bbabi.2007.08.007>.
- [185] Bornhorst JA, Falke JJ. Purification of proteins using polyhistidine affinity tags. *Methods Enzymol.*, vol. 326, Elsevier; 2000, p. 245–54. [https://doi.org/10.1016/S0076-6879\(00\)26058-8](https://doi.org/10.1016/S0076-6879(00)26058-8).
- [186] Piri-Moghadam H, Ahmadi F, Gómez-Ríos GA, Boyacı E, Reyes-Garcés N, Aghakhani A, et al. Fast Quantitation of Target Analytes in Small Volumes of Complex Samples by Matrix-Compatible Solid-Phase Microextraction Devices. *Angew Chem Int Ed* 2016;55:7510–4. <https://doi.org/10.1002/anie.201601476>.
- [187] Wei S-C, Fan S, Lien C-W, Unnikrishnan B, Wang Y-S, Chu H-W, et al. Graphene oxide membrane as an efficient extraction and ionization substrate for spray-mass spectrometric analysis of malachite green and its metabolite in fish samples. *Anal Chim Acta* 2018;1003:42–8. <https://doi.org/10.1016/j.aca.2017.11.076>.
- [188] Song X, Chen H, Zare RN. Conductive Polymer Spray Ionization Mass Spectrometry for Biofluid Analysis. *Anal Chem* 2018;90:12878–85. <https://doi.org/10.1021/acs.analchem.8b03460>.
- [189] Snyder DT, Pulliam CJ, Ouyang Z, Cooks RG. Miniature and Fieldable Mass Spectrometers: Recent Advances. *Anal Chem* 2016;88:2–29. <https://doi.org/10.1021/acs.analchem.5b03070>.
- [190] Ouyang Z, Cooks RG. Miniature Mass Spectrometers. *Annu Rev Anal Chem* 2009;2:187–214. <https://doi.org/10.1146/annurev-anchem-060908-155229>.
- [191] Blakeman KH, Miller SE. Development of High-Pressure Mass Spectrometry for Handheld and Benchtop Analyzers. In: Crocombe R, Leary P, Kammrath B, editors. *Portable Spectrosc. Spectrom.* 1st ed., Wiley; 2021, p. 391–413. <https://doi.org/10.1002/9781119636489.ch16>.
- [192] 908devices. MX908 Spec Sheet n.d.
- [193] Li L, Chen T-C, Ren Y, Hendricks PI, Cooks RG, Ouyang Z. Mini 12, Miniature Mass Spectrometer for Clinical and Other Applications—Introduction and Characterization. *Anal Chem* 2014;86:2909–16. <https://doi.org/10.1021/ac403766c>.
- [194] Griffin Analytical. cheMSense 600 spec sheet n.d.
- [195] 1st Detect. 1st Detect MMS-1000 Spec Sheet n.d.
- [196] 908devices. MX908 Application Brief on Fentanyl 2019.
- [197] Jiang X, Guy Jr. GP, Dunphy C, Pickens CM, Jones CM. Characteristics of adults reporting illicitly manufactured fentanyl or heroin use or prescription opioid misuse

- in the United States, 2019. *Drug Alcohol Depend* 2021;229:109160.  
<https://doi.org/10.1016/j.drugalcdep.2021.109160>.
- [198] Zawilska JB, Kuczyńska K, Kosmal W, Markiewicz K, Adamowicz P. Carfentanil – from an animal anesthetic to a deadly illicit drug. *Forensic Sci Int* 2021;320:110715. <https://doi.org/10.1016/j.forsciint.2021.110715>.
- [199] Azizi A, Shahhoseini F, Bottaro CS. Biological matrix compatible porous thin film for quick extraction of drugs of abuse from urine prior to liquid chromatography-mass spectrometry analysis. *Talanta* 2022;241:123264.  
<https://doi.org/10.1016/j.talanta.2022.123264>.
- [200] Wang Y-L, Gao Y-L, Wang P-P, Shang H, Pan S-Y, Li X-J. Sol-gel molecularly imprinted polymer for selective solid phase microextraction of organophosphorous pesticides. *Talanta* 2013;115:920–7. <https://doi.org/10.1016/j.talanta.2013.06.056>.
- [201] Yao C, Wang J, Chan P, Feng Y-L. A novel non-targeted screening method for urinary exposure biomarker discovery of phthalates using liquid chromatography-mass spectrometry. *Anal Methods* 2018;10:959–67.  
<https://doi.org/10.1039/C7AY02941A>.
- [202] Holčápek M, Volná K, Vaněrková D. Effects of functional groups on the fragmentation of dyes in electrospray and atmospheric pressure chemical ionization mass spectra. *Dyes Pigments* 2007;75:156–65.  
<https://doi.org/10.1016/j.dyepig.2006.05.040>.
- [203] Levsen K, Schiebel H-M, Terlouw JK, Jobst KJ, Elend M, Preiß A, et al. Even-electron ions: a systematic study of the neutral species lost in the dissociation of quasi-molecular ions. *J Mass Spectrom* 2007;42:1024–44.  
<https://doi.org/10.1002/jms.1234>.
- [204] Olsen JV, Macek B, Lange O, Makarov A, Horning S, Mann M. Higher-energy C-trap dissociation for peptide modification analysis. *Nat Methods* 2007;4:709–12.  
<https://doi.org/10.1038/nmeth1060>.
- [205] Roughley SD, Jordan AM. The Medicinal Chemist's Toolbox: An Analysis of Reactions Used in the Pursuit of Drug Candidates. *J Med Chem* 2011;54:3451–79.  
<https://doi.org/10.1021/jm200187y>.
- [206] Bogdan AR, Charaschanya M, Dombrowski AW, Wang Y, Djuric SW. High-Temperature Boc Deprotection in Flow and Its Application in Multistep Reaction Sequences. *Org Lett* 2016;18:1732–5. <https://doi.org/10.1021/acs.orglett.6b00378>.
- [207] Britton J, Raston CL. Multi-step continuous-flow synthesis. *Chem Soc Rev* 2017;46:1250–71. <https://doi.org/10.1039/C6CS00830E>.
- [208] Li B, Li R, Dorff P, McWilliams JC, Guinn RM, Guinness SM, et al. Deprotection of *N*-Boc Groups under Continuous-Flow High-Temperature Conditions. *J Org Chem* 2019. <https://doi.org/10.1021/acs.joc.8b02909>.
- [209] Ley SV, Baxendale IR, Bream RN, Jackson PS, Leach AG, Longbottom DA, et al. Multi-step organic synthesis using solid-supported reagents and scavengers: a new paradigm in chemical library generation. *J Chem Soc Perkin 1* 2000:3815–4195.  
<https://doi.org/10.1039/b006588i>.

- [210] Wang Y, Miller RL, Sauer DR, Djuric SW. Rapid and Efficient Synthesis of 1,2,4-Oxadiazoles Utilizing Polymer-Supported Reagents under Microwave Heating. *Org Lett* 2005;7:925–8. <https://doi.org/10.1021/ol050007r>.
- [211] Shaikh NS, Gajare AS, Deshpande VH, Bedekar AV. A mild procedure for the clay catalyzed selective removal of the tert-butoxycarbonyl protecting group from aromatic amines. *Tetrahedron Lett* 2000;41:385–7. [https://doi.org/10.1016/S0040-4039\(99\)02028-6](https://doi.org/10.1016/S0040-4039(99)02028-6).
- [212] Nigama SC, Mann A, Taddei M, Wermutha C-G. Selective Removal of the Tert-Butoxycarbonyl Group from Secondary Amines: ZnBr<sub>2</sub> as the Deprotecting Reagent. *Synth Commun* 1989;19:3139–42. <https://doi.org/10.1080/00397918908052712>.
- [213] Wu Y, Limburg DC, Wilkinson DE, Vaal MJ, Hamilton GS. A mild deprotection procedure for tert-butyl esters and tert-butyl ethers using ZnBr<sub>2</sub> in methylene chloride. *Tetrahedron Lett* 2000;41:2847–9. [https://doi.org/10.1016/S0040-4039\(00\)00300-2](https://doi.org/10.1016/S0040-4039(00)00300-2).
- [214] Tahir R, Banert K, Solhy A, Sebti S. Zinc bromide supported on hydroxyapatite as a new and efficient solid catalyst for Michael addition of indoles to electron-deficient olefins. *J Mol Catal Chem* 2006;246:39–42. <https://doi.org/10.1016/j.molcata.2005.10.012>.
- [215] Cengiz B, Gokce Y, Yildiz N, Aktas Z, Calimli A. Synthesis and characterization of hydroxyapatite nanoparticles. *Colloids Surf Physicochem Eng Asp* 2008;322:29–33. <https://doi.org/10.1016/j.colsurfa.2008.02.011>.
- [216] Chandrasekar A, Sagadevan S, Dakshnamoorthy A. Synthesis and characterization of nano-hydroxyapatite (n-HAP) using the wet chemical technique. *Int J Phys Sci n.d.*:8.
- [217] Wan H, Blomberg LG. Optimized Chiral Separation of 20 Amino Acids Derivatized with 9-Fluorenylmethyl Chloroformate Using Cyclodextrins as Chiral Selectors in Capillary Electrophoresis. *J Chromatogr Sci* 1996;34:540–6. <https://doi.org/10.1093/chromsci/34.12.540>.

## Appendix 1: Other Scientific Contributions

**Langille, E.;** Bottaro, C. S.; Drouin, A. A Novel Use of Catalytic Zinc-Hydroxyapatite Columns for the Selective Deprotection of N-Tert-Butyloxycarbonyl (BOC) Protecting Group Using Flow Chemistry. *J Flow Chem* **2020**, *10* (2), 377–387.

<https://doi.org/10.1007/s41981-019-00052-x>.

In this published article, I developed a solid-supported catalyst for use in flow chemistry-based BOC deprotection. The full-length manuscript (as accepted) can be found in Appendix 2. I designed and carried out all syntheses, characterization, and experiments. I wrote the manuscript, with subsequent editorial input from A. Drouin.

**Langille, E.;** Lemieux, V.; Garant, D.; Bergeron, P. Development of Small Blood Volume Assays for the Measurement of Oxidative Stress Markers in Mammals. *PLOS ONE* **2018**, *13* (12), e0209802. <https://doi.org/10.1371/journal.pone.0209802>.

In this published article, I developed a number of analytical methods for quantifying oxidative stress in small mammals using ultra-low volumes of plasma. I designed and carried out all experiments. I wrote the manuscript, with subsequent editorial input from V. Lemieux and P. Bergeron.



**Langille, E.** Optimized Oxidative Stress Protocols for Low-Microliter Volumes of Mammalian Plasma. *BIO-PROTOCOL* **2019**, 9 (9).

<https://doi.org/10.21769/BioProtoc.3221>.

In this published methods article, I present protocols of my published analytical methods for quantifying oxidative stress in small mammals using ultra-low volumes of plasma. I designed and carried out all experiments. I wrote the manuscript, with subsequent editorial input from P. Bergeron.

Pallegar, P.; Canuti, M.; **Langille, E.**; Peña-Castillo, L.; Lang, A. S. A Two-Component System Acquired by Horizontal Gene Transfer Modulates Gene Transfer and Motility via Cyclic Dimeric GMP. *Journal of Molecular Biology* **2020**, 432 (17), 4840–4855.

<https://doi.org/10.1016/j.jmb.2020.07.001>.

In this published article, I contributed HPLC quantification of the bacterial secondary messenger: cyclic-diguanylate (c-di-GMP). I adapted a previously reported analytical method for suitability with the samples analyzed and carried out all HPLC experiments and data analysis. I wrote the methods portions of the manuscript pertaining to the HPLC analysis and provided critical analysis of the results pertaining to the HPLC quantification to the first and last authors.

Pallegar, P.; Peña-Castillo, L.; **Langille, E.**; Gomelsky, M.; Lang, A. S. Cyclic Di-GMP-Mediated Regulation of Gene Transfer and Motility in *Rhodobacter Capsulatus*. *J Bacteriol* **2020**, *202* (2). <https://doi.org/10.1128/JB.00554-19>.

In this published article, I contributed HPLC quantification of the bacterial secondary messenger: cyclic-diguanylate (c-di-GMP). I adapted a previously reported analytical method for suitability with the samples analyzed and carried out all HPLC experiments and data analysis. I wrote the methods portions of the manuscript pertaining to the HPLC analysis and provided critical analysis of the results pertaining to the HPLC quantification to the first and last authors.

Shahhoseini, F.; **Langille, E. A.**; Azizi, A.; Bottaro, C. S. Thin Film Molecularly Imprinted Polymer (TF-MIP), a Selective and Single-Use Extraction Device for High-Throughput Analysis of Biological Samples. *Analyst* **2021**, *146* (10), 3157–3168. <https://doi.org/10.1039/D0AN02228D>.

In this published article, I contributed synthesis of a pseudo-TCA template. I aided the first author in experimental work and contributed experiential knowledge about working with biological matrices.

Azizi, A.; Shahhoseini, F.; **Langille, E. A.**; Akhoondi, R.; Bottaro, C. S. Micro-Gel Thin Film Molecularly Imprinted Polymer Coating for Extraction of Organophosphorus Pesticides from Water and Beverage Samples. *Analytica Chimica Acta* **2021**, *1187*, 339135. <https://doi.org/10.1016/j.aca.2021.339135>.

In this published article, I contributed synthesis of a pseudo-OPP template. I aided the first author in experimental work and significantly contributed to the development of the MIP mesh format, including spraying, curing, and cutting method development. I also assisted the first author by carrying out GC-MS work using the MIP mesh, in addition to assisting with laboratory experiments using the mesh.

Aliasghar, G.; Shahhoseini, F.; Bottaro, C.; **Langille, E.** Porous Sorptive Solid Phase Microextraction Devices and Preparation Thereof. 24519-P61029US00, March 4, 2021.

In this patent application, I contributed equally with all co-authors to develop porous extraction devices for a wide variety of analytes and applications, as exemplified by this thesis work. We present a number of innovative advances including spraying the polymer component solutions onto sheets or mesh, cutting extraction devices from sheets of fabric, metal or other materials using a number of tools including waterjet cutting and craft cutters.

## **Appendix 2: A novel use of catalytic zinc-hydroxyapatite columns for the selective deprotection of *N*-tert-butyloxycarbonyl (BOC) protecting group using flow chemistry**

### **Introduction**

In a recent review about the reactions used in the pharmaceutical industry, Roughley and Jordan reported that most popular protecting group for the amine functional group is the tert-butoxycarbonyl (BOC) [205]. Thus, there is a demand for faster, greener, easily scalable and cleaner flow processes to remove the BOC protecting group. The main approach using flow chemistry to date for BOC deprotection is high temperature reactions between 220-300°C using a plug flow reactor (PFR) system [206–208]. We present an improved method of BOC deprotection utilizing a zinc-hydroxyapatite (Zn-HAP) catalytic column in a custom built PFR system.

Solid supported catalysis in flow has been previously employed for several classes of reactions, but has not yet been reported for BOC deprotection [209,210]. The solid supported deprotection of BOC has been reported using a kaolinic clay material however no discussion over mechanism has been reported [211]. It is well known that zinc bromide has been used as a catalyst for the mild deprotection of BOC [212,213]. We first employed these conditions for a substrate that was not tolerating traditional TFA deprotection. The yield was still unsatisfactory, and we proposed that if we could find a way to solid support the zinc and conduct the reaction at elevated pressure and

temperature, then we may increase the yield, especially for sensitive substrates. During a literature review, an article from Tahir et al. described the use of a solid supported zinc catalyst on hydroxyapatite [214].

In this article, Tahir and coworkers used Zn-HAP as a catalyst to perform a Michael addition in a flask [214]. We have used the same preparation protocol for Zn-HAP as Tahir but have packed the solid supported zinc catalyst into a stainless-steel column. Using a GC oven, an HPLC pump, and backpressure regulator, we built a custom PFR system with maximum operating conditions of 4500 PSI and 350°C (Figure A2.1). This low-cost alternative to commercial flow chemistry systems allows for a more economical way to use such technology.

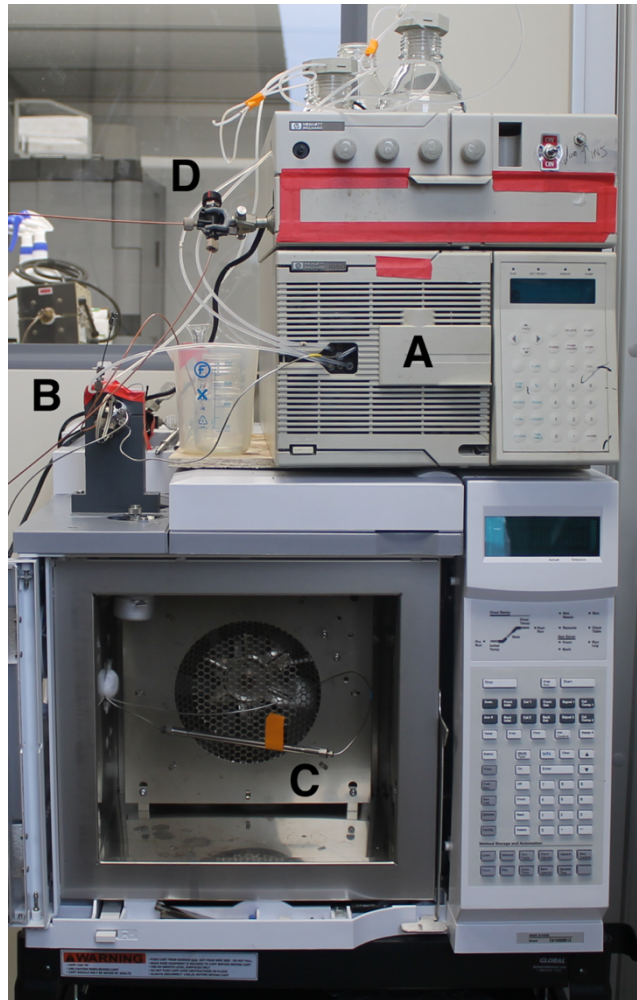


Figure A2.1. Photograph of custom-built plug flow reactor (PFR) system. A: solvent pump, B: automated injector, C: packed Zn-HAP column, D: backpressure regulator.

In contrast to current work at Pfizer and AbbVie, we employ milder conditions under Zn-HAP catalysis of 150°C with a 30-minute residence time. Because of the lower oven temperature, safety concerns when using acetonitrile are reduced and thus it can be used in this work. This avoids any solubility issues reported by other groups, as well as

allows for better scalability due to the commonality of acetonitrile in comparison to other, more exotic reported solvents [208].

## Results and Discussion

A successful method of using a catalytic solid supported zinc column has been demonstrated for the selective deprotection of the BOC protecting group. Nineteen compounds with varying functional groups were tested and demonstrated the wide applicability of this catalytic column for BOC deprotection (Table A2.2). Firstly, we can see that our methodology works for both aromatic amines (entry 1, 4, 15 and 17) and for aliphatic amines (entry 2, 3, 5, 6, 7, 8, 9, 10, 11, 12, 13, 14, 16, 18 and 19). Esters are compatible with the reaction conditions (entry 1, 4, 5, 9, 10, 14, 16, 17, 18 and 19). In every example, no products resulting from the degradation of the esters were observed. Out of the 19 compounds tested, 10 compounds had a yield greater than 90%. The FMOC and BOC protecting groups are widely used in peptide synthesis, thus it was of great importance to develop conditions that would successfully remove the BOC protecting group while leaving the FMOC unreacted [205]. The stability of the fluorenylmethoxycarbonyl (FMOC) protecting group was assessed (entry 4, 5, 17 and 19) and it was demonstrated that FMOC was well tolerated under the variety of conditions; all four entries were recovered with a yield  $\geq 95\%$ . The N-carbobenzyloxy (CBz) protecting group was assessed (entry 14) and demonstrated a high stability under the selected reaction conditions, with a yield of 93%. The tert-butyl dimethyl silyl (TBDMS) ether was assessed (entry 12) and was also stable under the tested conditions.

Since the BOC protecting group is used in peptide chemistry, we wanted to confirm that amines and amides were compatible with the reaction conditions. It was tested with a free amine (entry 6) and an amide (entry 7), both of which gave the desired products after the reaction. We also assessed the suitability of BOC protected dipeptides under the selected reaction conditions (entries 13 and 16). Yields over 75% were obtained for both dipeptides.

Three other functional groups were tested with success, free alcohols (entries 2 and 8), ketone (entries 3 and 15) and nitro (entries 10 and 11). The only incompatible functional group that we tested is the carboxylic acid on entry 11. This may be explained by the basic nature of hydroxyapatite. Free carboxylic acid compounds such as *N*-protected amino acids, may precipitate from the solvent and remain on the column. As a result, no desired product nor starting material were recovered. This is not the case for all carboxylic acids, as entries 13, 16, 17 and 19 were recovered in high yield. This would lead us to postulate that it was this specific example which was not well tolerated in this study.

Compound **1a** was used as a model compound in order to study the effect of residence time and temperature on the reaction. A number of experiments were carried out to optimize temperature, residence time and pressure to determine the optimal conditions for our system. It was determined that 30 mins and 150 °C at 3000 PSI is the optimal condition for BOC deprotection. At temperatures over 200 °C cleavage of the methyl ester was observed for **1**. 200 °C was chosen for the kinetic study as model compound **1** was the first compound investigated and was very tolerant to heating (Figure



A2.2). With smaller follow-up experiments on other examples that are less thermally stable, we determined that 150 °C is still converting efficiently while not destroying the majority of tested substrates.

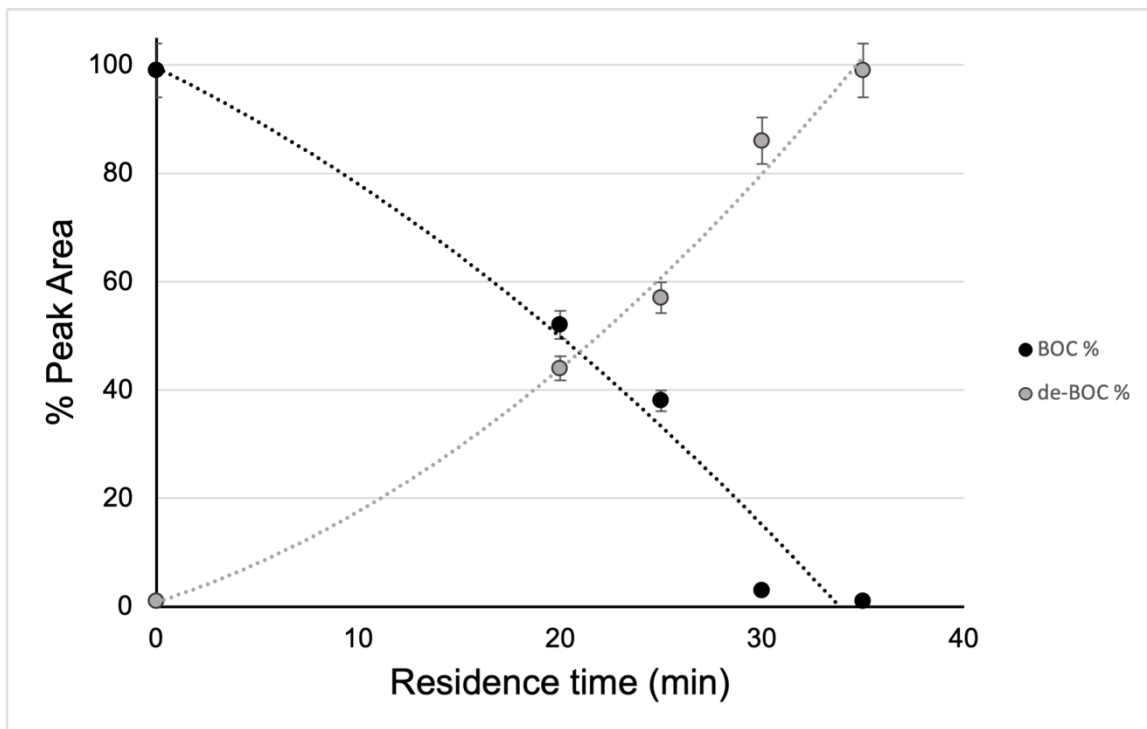


Figure A2.2. Kinetic study of compound 1 at 200 °C in the PFR.

To compare the efficiency of the flow system versus a flask reaction, compound 1 was also subjected to deprotection under various conditions in a flask (Table A2.1).

Table A2.1. Deprotection of compound 1a in a flask

Entry	Solvent	Reagent	Treatment and time	Yield
F1	Acetonitrile	TFA (1%)	Reflux, 45 mins	15%
F2	Dichloromethane	TFA (1%)	Reflux, 45 mins	8%
F3	Acetonitrile	TFA (1%)	Reflux, 24 hours	30%
F4	Dichloromethane	TFA (1%)	Reflux, 24 hours	37%
F5	Dichloromethane	Zinc Bromide (cat.)	Reflux, 48 hours	25%
F6	Dichloromethane	HAP (no Zn)	Reflux, 48 hours	0%*
F7	Acetonitrile	Empty column	Flow, 30 mins, 150°C	2%†

\* This reaction was carried out to see if the HAP alone could catalyze the reaction. We did not see any conversion with HAP as the catalyst.

† This reaction was carried out to determine the amount of conversion due to thermal decomposition.

The results of Table A2.1 support the need for a more efficient method for the cleavage of the BOC protecting group. The flask reactions were not as clean when compared to a flow reaction. Typically, more than 3 peaks with an area of more than 5% were observed in the reaction products. The cleavage of the methyl ester was detected in several of the flask reactions and, in contrast, was only detected during prolonged heating of the compound at 200 °C in the PFR. The result of the zinc bromide flask reaction (entry F5) demonstrates that zinc bromide alone cannot convert these substrates in a

timely manner. In addition, HAP with no zinc did not yield any conversion (entry F6). This example demonstrates that the conversion is due to the zinc in the HAP rather than the HAP having a catalytic behaviour for this conversion. Compound **1a** was also passed through an empty column to determine the amount of conversion due to thermal decomposition (entry F7). About 2% of compound **1a** was converted to **1b** under the standard conditions.

Table A2.2. Deprotection of N-Boc protected amines using the Zn-HAP column  
*Structures and yields for the conversion of 19 N-Boc protected amines in flow in ACN at 150 °C for 30 minutes.*

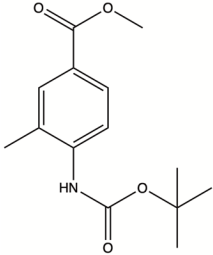
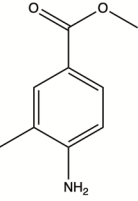
Entry	Starting Material (BOC protected)	Desired product (BOC deprotected)	Yield of desired product by HPLC*
1	 Compound 1a	 Compound 1b	93%

Table A2.2. Deprotection of N-Boc protected amines (continued)

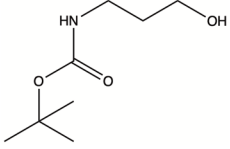
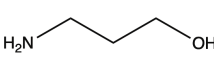
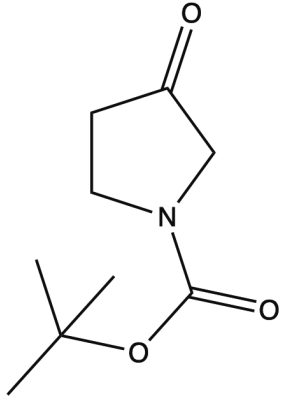
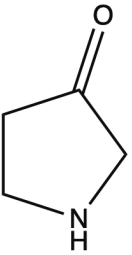
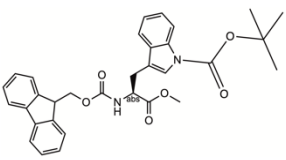
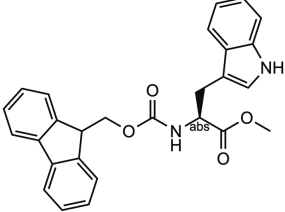
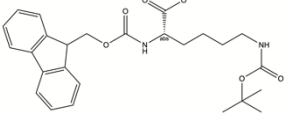
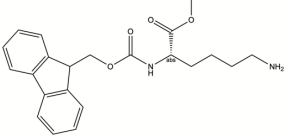
2	 <p>Compound 2a</p>	 <p>Compound 2b</p>	97%
3	 <p>Compound 3a</p>	 <p>Compound 3b</p>	95%
4	 <p>Compound 4a</p>	 <p>Compound 4b</p>	98%
5	 <p>Compound 5a</p>	 <p>Compound 5b</p>	95%

Table A2.2. Deprotection of N-Boc protected amines (continued)

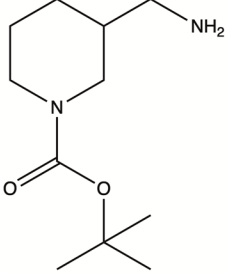
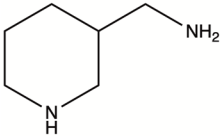
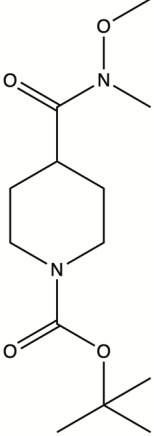
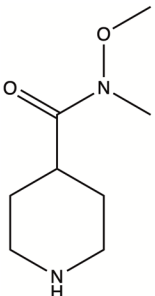
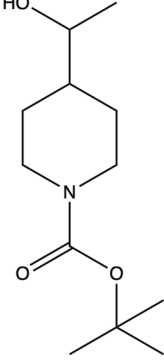
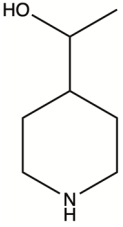
6	 <p>Compound 6a</p>	 <p>Compound 6b</p>	98%
7	 <p>Compound 7a</p>	 <p>Compound 7b</p>	70%
8	 <p>Compound 8a</p>	 <p>Compound 8b</p>	74%

Table A2.2. Deprotection of N-Boc protected amines (continued)

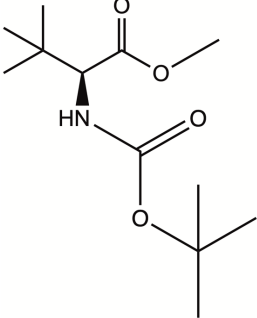
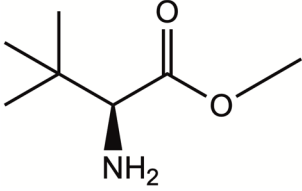
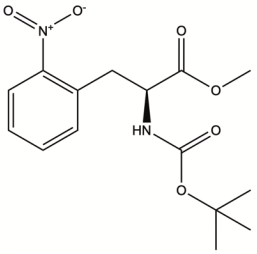
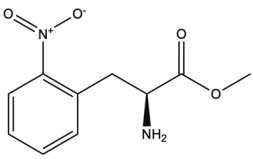
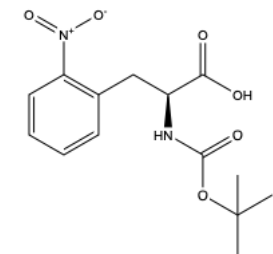
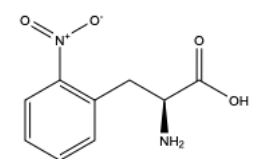
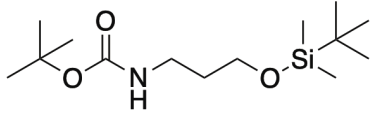
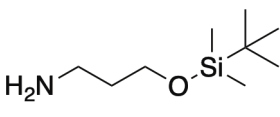
<p>9</p>	 <p>Compound 9a</p>	 <p>Compound 9b</p>	<p>82%</p>
<p>10</p>	 <p>Compound 10a</p>	 <p>Compound 10b</p>	<p>51%</p>
<p>11</p>	 <p>Compound 11a</p>	 <p>Compound 11b</p>	<p>0%</p>
<p>12</p>	 <p>Compound 12a</p>	 <p>Compound 12b</p>	<p>78%</p>

Table A2.2. Deprotection of N-Boc protected amines (continued)

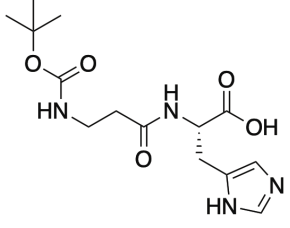
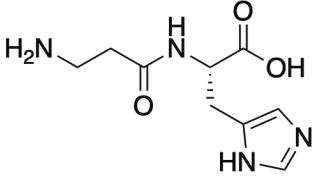
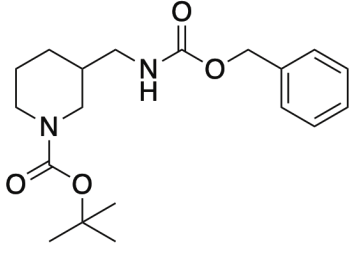
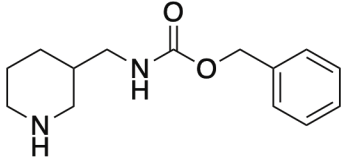
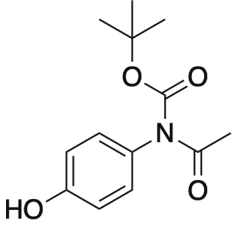
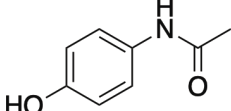
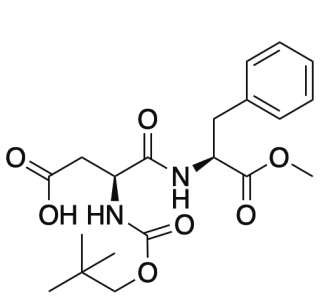
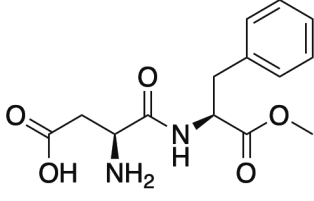
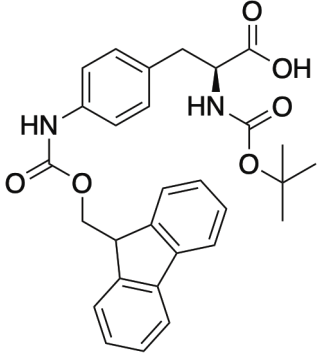
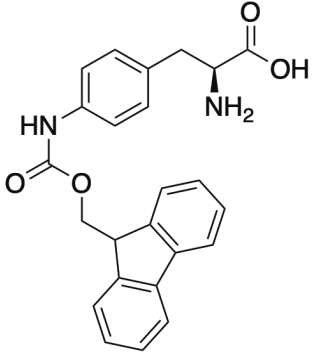
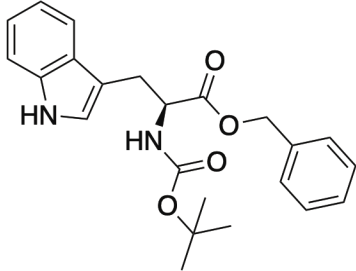
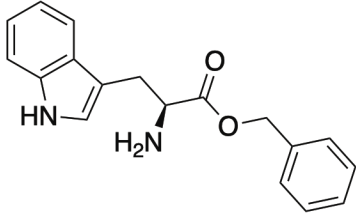
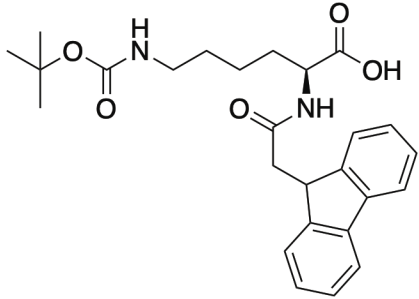
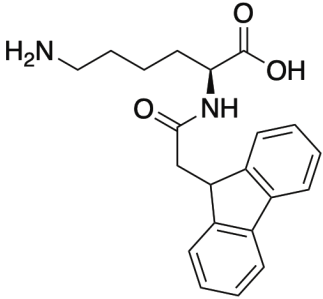
<p>13</p>	 <p>Compound 13a</p>	 <p>Compound 13b</p>	<p>75%</p>
<p>14</p>	 <p>Compound 14a</p>	 <p>Compound 14b</p>	<p>93%</p>
<p>15</p>	 <p>Compound 15a</p>	 <p>Compound 15b</p>	<p>87%</p>
<p>16</p>	 <p>Compound 16a</p>	 <p>Compound 16b</p>	<p>86%</p>

Table A2.2. Deprotection of N-Boc protected amines (continued)

17	 <p>Compound 17a</p>	 <p>Compound 17b</p>	95%
18	 <p>Compound 18a</p>	 <p>Compound 18b</p>	96%
19	 <p>Compound 19a</p>	 <p>Compound 19b</p>	95%†

\*Purity obtained is the percent area of the product compared to all other products present, including the unconverted starting material. Peak mass was confirmed using LC-MS/MS.

† Of the 95% yield, 100% of the detected product was enantiomerically pure (100% L) by chiral MEKC.



Overall these results demonstrate the benefit of using a catalyzed cleavage of the BOC protecting group in flow. Various functional groups are tolerated under the operating conditions of our PFR setup and the mild thermal conditions allow for a more selective deprotection of the BOC protecting group. The column and flow system are scalable and thus can be used in production processes. We have also demonstrated that no racemization is detected when testing enantiopure substrates.

## Experimental

### General Methods

All chemicals and reagents were purchased from Sigma-Aldrich (Oakville, ON, Canada) and were of reagent grade or higher and were used without further purification unless otherwise noted. HPLC solvents were purchased from VWR Int. (Mississauga, ON, Canada). Ultrapure water was made in-house using a Millipore Milli-Q water system (Resistivity  $\geq 18.2 \text{ M}\Omega \text{ cm}^{-1}$ ).

$^1\text{H}$  NMR spectra were recorded at 400 MHz and 500 MHz (Bruker Spectrospin 400 and Bruker AVANCE 500, respectively) in  $\text{CDCl}_3$  with  $\text{Me}_4\text{Si}$  as the internal standard. Analytical HPLC was carried out on an Agilent Technologies 1100 system equipped with a Hichrom Genesis AQ 4  $\mu\text{m}$   $\text{C}_{18}$   $150 \times 4.6\text{mm}$  column. Detection was a diode array detector monitoring both 214 and 254 nm. LC-MS was performed on a Waters Acquity H-Class UPLC system with a Waters Xevo TQ-S mass spectrometer under the same chromatographic conditions as the UV detection (Table A2.3), using an ESI source in positive ionization mode. The mass spectrometer was operated in selected reaction monitoring (SRM) mode. The internal software “IntelliStart” was used to

optimize the collision parameters and select stable transitions. Exact mass measurements were performed on an Agilent Technologies 6230 TOF MS coupled to an Agilent Technologies Infinity 1260 HPLC system using flow-injection analysis with both ESI and APPI sources.

Table A2.3. Chromatographic parameters for BOC compound separation

Analytical HPLC- Agilent 1100-VWD system	
Column	Hichrom Genesis AQ 4 $\mu$ m C <sub>18</sub> 100Å, 4.6 × 150 mm
Solvents	A: Acetonitrile B: 0.1% TFA in ddH <sub>2</sub> O
Flow Rate	1.00 mL min <sup>-1</sup>
Run Time	12 minutes
Gradient	25% <sub>A</sub> to 85% <sub>A</sub> in 10 mins, to 98% <sub>A</sub> in 12 mins
Injection Volume	10 $\mu$ L
Detection Wavelength	214 nm (for peptide bond and nonaromatic amino acids), 254 nm (for aromatic amino acids)

### Hydroxyapatite Solid Support Preparation

Hydroxyapatite was prepared according to Tahir et al. 2006 [214]. In brief, 250 mL of a solution of 7.92 g diammonium phosphate ((NH<sub>4</sub>)<sub>2</sub>PO<sub>4</sub>) and 70 mL conc. (14.8 M) ammonium hydroxide (NH<sub>4</sub>OH) were added dropwise, under nitrogen into a solution of

23.6 g calcium nitrate monohydrate ( $\text{CaNO}_3 \cdot \text{H}_2\text{O}$ ) in 150 mL distilled water with strong stirring using an overhead mixer. Once the entire volume was added, a heating mantle was placed under the solution and the addition funnel was replaced with a condenser. The solution was heated to reflux under a flow of nitrogen for four hours.

The obtained insoluble hydroxyapatite (HAP) was filtered from the solution using a medium porosity glass filter and the residue was washed three times with fresh portions of ice-cold distilled water. This residue was transferred to an evaporating dish and placed in an oven at 80 °C for 48 hours. The dried residue was then transferred to two 50 mL quartz crucibles and placed in a horizontal tube furnace. Nitrogen flowed through the tube for the entire calcination process. The furnace was then heated to 850 °C where the material was calcined for one hour. The furnace was cooled to RT under nitrogen, and the material was transferred to a glass desiccator.

### **Zinc-Hydroxyapatite**

10.0 g of the dried HAP was transferred to a 100 mL round bottom flask with a stir bar. A solution of 2.25 g  $\text{ZnBr}_2$  in 25 mL distilled water was added and the solution was stirred for 2 hours. The solution was filtered off and the residue rinsed with two 10 mL portions of distilled water. The residue was transferred to a new evaporating dish and dried at 105°C in an oven before packing the column. The material was subjected to both powder XRD and FT-IR spectroscopy to confirm the structure (see Figures S1 and S2 in the supplementary material). Both characterization techniques confirmed the structure using the spectral library for XRD and previous literature for FT-IR [215,216].

### **Zinc-Hydroxyapatite Column**

A 150 mm × 4.6 mm stainless steel HPLC column was dry packed with 1.0 g of the Zn-HAP solid-supported catalyst. The column was then placed in the reaction oven, where a flow of acetonitrile at 1.00 mL min<sup>-1</sup> rinsed the material and packed the column to a pressure of about 200 PSI. The heat was increased in the oven to 105 °C to drive out any excess water before executing reactions.

### **Example Deprotection Protocol**

The deprotection reactions were performed on scales ranging from 10 – 100 mg of the starting BOC protected amines. Here is a representative procedure of the deprotection: a 10 mg load of a BOC protected amino compound was dissolved in 100 μL acetonitrile and loaded in the sample loop (100 μL). The compound was injected and subsequently loaded onto the column at a flow rate of 1 mL min<sup>-1</sup>. 1 mL was measured at the output using a graduated cylinder to ensure loading of the compound on the column before the backpressure regulator was closed to restrict the flow to about 0.1 mL min<sup>-1</sup> for the duration of the reaction. This change in setting increased the pressure in the column to a final operating pressure of 3000 PSI. Fractions were collected at the output and subjected to quantitative and qualitative analysis using HPLC-UV and LC-MS.

### Chiral Separation by Micellar Electrokinetic Chromatography (MEKC)

A Hewlett Packard CE system was used for separation of enantiomers of Fmoc-Lys-OH (compound **19b**) using a modified method from Wan and Blomberg [217]. A 64.5 cm fused silica capillary with a 75  $\mu\text{m}$  internal diameter was employed. The effective length of the capillary to the diode array detector was 56 cm. The capillary was flushed with 1M NaOH for one hour, followed by a one-hour flush with background electrolyte (BGE). The BGE consisted of a phosphate buffer 50 mM pH 9.5, 50 mM SDS, 15% 2-propanol v/v and 12 mM  $\beta$ -cyclodextrin as the chiral selector. Before each run, the capillary was flushed for 5 minutes with 0.1 M NaOH in 10% methanol followed by 8 minutes of background electrolyte. Injection of samples in distilled water was carried out using a pressure of 50 mbar for 3 seconds followed by a plug of BGE at 50 mbar for 5 seconds to load the band onto the capillary. Separation was carried out at 25°C, 24 kV and 50  $\mu\text{A}$ . Detection was at 254 nm. The D enantiomer migrated first, reaching the detector at 25.6 mins while the L enantiomer migrated at 25.8 mins. To confirm the identification of the desired product, a reaction with enantiopure **19a** (99% L) was conducted and the product was measured with CE. A single peak was detected. To confirm the identity of this peak, the L enantiomer standard of the expected product was spiked into the analysis solution. An increase in peak area was observed, confirming that this was the L isomer. The D enantiomer was spiked into the same reaction solution leading to two peaks being identified. This confirmed that the L enantiomer was the major product maintained during the reaction (no D was detected in the original solution).

## Preparation of the precursors

### *methyl 4-[(tert-butyloxycarbonyl)amino]-3-methylbenzoate 1a*

3.00 g methyl 4-amino-3-methylbenzoate (1 eq, 0.018 mol) was added to a 250 mL round bottom flask with a stir bar and 15 mL THF. 5.04 g (3.0 eq) NaHCO<sub>3</sub> was then added and the solution was cooled in an ice bath for ten minutes. 4.75 g (1.2 eq, 0.022 mol) di-tert-butyl dicarbonate (BOC<sub>2</sub>O) were then added. The reaction mixture was stirred overnight then was extracted twice with 100 mL portions of diethyl ether and then the aqueous phase was acidified to a pH of 4-5 with half-saturated citric acid solution. The resulting acidified phase was extracted twice with 100 mL portions of DCM. The combined organic phases were washed once with brine, dried over anhydrous magnesium sulfate, filtered and concentrated under reduced pressure yielding **1a**, as an off-white solid (4.56 g /95%). High- and low-resolution MS and NMR were used to verify the exact mass and structure of the prepared product. <sup>1</sup>H NMR spectrum, (400MHz, CDCl<sub>3</sub>):  $\delta$ , ppm (J, Hz): 7.8 (2H), 6.7 (1H), 3.9 (3H), 2.2 (3H) 1.6 (9H). MS (ESI) m/z calculated for [C<sub>14</sub>H<sub>19</sub>NO<sub>4</sub>]<sup>+</sup>: 265.13141[M+H]<sup>+</sup>; found: 265.13134;  $\delta = -0.26$  ppm

### *N $\alpha$ -Fmoc-N(in)-Boc-L-tryptophan methyl ester 4a*

526 mg (1.0 mmol) of Fmoc-BOC-Trp-OH was dissolved in 4 mL a 1:1 mixture of methanol and dichloromethane. TMS-diazomethane (1.25 mmol, 2 M in Hexane, 0.63 mL) was added dropwise until a faint yellow color persisted in the solution. The solution was left to stir for 30 minutes at room temperature before being quenched with

100  $\mu$ L of glacial acetic acid. The solvent was evaporated under reduced pressure and the residue was partitioned between ethyl acetate and water. The aqueous phase was extracted three times with ethyl acetate and the combined organic phases were dried with anhydrous magnesium sulfate, filtered and concentrated under reduced pressure.

High- and low-resolution MS and NMR were used to verify the exact mass and structure of the prepared product.  $^1\text{H}$  NMR spectrum (500 MHz, Chloroform- $d$ )  $\delta$  8.12 (d,  $J = 7.1$  Hz, 1H), 7.76 (d,  $J = 7.5$  Hz, 2H), 7.58 – 7.48 (m, 3H), 7.44 – 7.36 (m, 3H), 7.36 – 7.19 (m, 4H), 5.42 – 5.37 (m, 1H), 4.76 (q,  $J = 6.7, 6.3$  Hz, 1H), 4.43 – 4.32 (m, 2H), 4.21 (t,  $J = 7.3$  Hz, 1H), 3.71 (s, 3H), 3.49 (s, 1H), 3.27 (t,  $J = 5.7$  Hz, 2H), 1.65 (s, 9H). MS (ESI)  $m/z$  calculated for  $[\text{C}_{32}\text{H}_{32}\text{N}_2\text{O}_6]^+$ : 540.22604  $[\text{M}+\text{H}]^+$ ; found: 540.2273 ;  $\delta = 2.34$  ppm

#### *Fmoc-L-tryptophan methyl ester 4b*

426 mg (1.0 mmol) Fmoc-Trp-OH was dissolved in 4 mL of a 1:1 mixture of methanol and dichloromethane. TMS-diazomethane (1.25 mmol, 2 M in Hexane, 0.63 mL) was added dropwise until a faint yellow color persisted in the solution. The solution was left to stir for 30 minutes at room temperature before being quenched with 100  $\mu$ L of glacial acetic acid. The solvent was evaporated under reduced pressure and the residue was partitioned between ethyl acetate and water. The aqueous phase was extracted three times with ethyl acetate and the combined organic phases were dried with anhydrous magnesium sulfate, filtered and concentrated under reduced pressure. High- and low-resolution MS and NMR were used to verify the exact mass and structure of the prepared

product.  $^1\text{H}$  NMR spectrum, (500 MHz, Chloroform-*d*)  $\delta$  8.07 (s, 1H), 7.76 (d,  $J = 7.6$  Hz, 2H), 7.55 (dd,  $J = 11.1, 7.8$  Hz, 3H), 7.43 – 7.33 (m, 3H), 7.33 – 7.27 (m, 2H), 7.20 (t,  $J = 7.4$  Hz, 1H), 7.16 – 7.09 (m, 1H), 6.94 (d,  $J = 2.2$  Hz, 1H), 5.35 (d,  $J = 8.4$  Hz, 1H), 4.74 (dt,  $J = 8.4, 5.4$  Hz, 1H), 4.42 (dd,  $J = 10.4, 7.3$  Hz, 1H), 4.36 (dd,  $J = 10.7, 6.9$  Hz, 1H), 4.20 (t,  $J = 7.1$  Hz, 1H), 3.69 (s, 3H), 3.33 (d,  $J = 5.4$  Hz, 2H). MS (APPI)  $m/z$  calculated for  $[\text{C}_{27}\text{H}_{24}\text{N}_2\text{O}_4]^+$ : 440.17361  $[\text{M}+\text{H}]^+$ ; found: 440.17444 ;  $\delta = 1.9$  ppm

*N $\alpha$ -Fmoc-N $\epsilon$ -Boc-L-lysine methyl ester 5a*

468.54 mg (1.0 mmol) of Fmoc-BOC-Lys-OH was dissolved in 4 mL a 1:1 mixture of methanol and dichloromethane. TMS-diazomethane (1.25 mmol, 2 M in Hexane, 0.63 mL) was added dropwise until a faint yellow color persisted in the solution. The solution was left to stir for 30 minutes at room temperature before being quenched with 100  $\mu\text{L}$  of glacial acetic acid. The solvent was evaporated under reduced pressure and the residue was partitioned between ethyl acetate and water. The aqueous phase was extracted three times with ethyl acetate and the combined organic phases were dried with anhydrous magnesium sulfate, filtered and evaporated under reduced pressure. High- and low-resolution MS and NMR were used to verify the exact mass and structure of the prepared product.  $^1\text{H}$  NMR (500 MHz, Chloroform-*d*)  $\delta$  7.74 (d,  $J = 7.5$  Hz, 2H), 7.58 (dd,  $J = 7.7, 3.7$  Hz, 2H), 7.37 (t,  $J = 7.5$  Hz, 2H), 7.29 (tt,  $J = 7.4, 1.4$  Hz, 2H), 5.37 (d,  $J = 8.2$  Hz, 1H), 4.54 (s, 1H), 4.48 (s, 0H), 4.37 (ddd,  $J = 18.4, 9.1, 4.3$  Hz, 3H), 4.20 (t,  $J = 7.0$  Hz, 1H), 3.72 (s, 3H), 3.09 (q,  $J = 7.0, 6.6$  Hz, 2H), 1.83 (ddt,  $J = 15.2, 10.5, 5.4$  Hz,



1H), 1.48 (t,  $J = 7.1$  Hz, 2H), 1.41 (s, 9H), 1.37 – 1.29 (m, 2H). MS (ESI)  $m/z$  calculated for  $[C_{27}H_{34}N_2O_6]^+$ :  $[M+Na]^+$ ; 505.23091 found: 505.22997;  $\delta = -1.94$  ppm

*Fmoc-L-lysine methyl ester 5b*

404.89 mg (1.0 mmol) of Fmoc-Lys-OH was dissolved in 4 mL of a 1:1 mixture of methanol and dichloromethane. TMS-diazomethane (1.25 mmol, 2 M in Hexane, 0.63 mL) was added dropwise until a faint yellow color persisted in the solution. The solution was left to stir for 30 minutes at room temperature before being quenched with 100  $\mu$ L of glacial acetic acid. The solvent was evaporated under reduced pressure and the residue was partitioned between ethyl acetate and water. The aqueous phase was extracted three times with ethyl acetate and the combined organic phases were dried with anhydrous magnesium sulfate, filtered and evaporated under reduced pressure. High- and low-resolution MS and NMR were used to verify the exact mass and structure of the prepared product.  $^1H$  NMR spectrum, (400MHz,  $CDCl_3$ ):  $\delta$ , ppm (J, Hz): 7.8 (2H), 6.7 (1H), 3.9 (3H), 2.2 (3H) 1.6 (9H). MS (ESI)  $m/z$  calculated for  $[C_{22}H_{26}N_2O_4]^+$ : 382.18926  $[M+H]^+$ ; found: 382.19043 ;  $\delta = 3.07$  ppm

*BOC-L-tert-leucine methyl ester 8a*

1.0 g (5.5 mmol) of *L-tert-leucine methyl ester hydrochloride* was added to a 250 mL round bottom flask with a stir bar and 100 mL of a 1:1 mixture of THF and  $H_2O$ . 2.52 g (3.0 eq) of  $NaHCO_3$  was then added, and the solution was cooled in an ice bath for ten minutes. 1.44 g di-*tert*-butyl dicarbonate ( $BOC_2O$ , 1.2 eq) was then added. The

reaction mixture was extracted twice with 100 mL portions of diethyl ether and then the aqueous layer was acidified to a pH of 4-5 with half-saturated citric acid solution. The resulting acidified phase was extracted twice with 100mL portions of DCM. The combined organic phases were washed once with brine, dried over anhydrous magnesium sulfate and the solvent was evaporated under reduced pressure yielding **8**, as an off-white solid (1.0 g / 74%) High- and low-resolution MS and NMR were used to verify the exact mass and structure of the prepared product. (<sup>1</sup>H NMR spectrum, (400MHz, CDCl<sub>3</sub>):  $\delta$ , ppm (J, Hz): 5.05 (1H), 3.8 (1H), 1.5 (9H) MS (ESI) m/z calculated for [C<sub>12</sub>H<sub>23</sub>NO<sub>4</sub>]<sup>+</sup>:245.16271 [M+H]<sup>+</sup>; found: 245.16383 ;  $\delta$  = 4.58 ppm

*(2S)-2-{[(tert-butoxy)carbonyl]amino}-3-(2-nitrophenyl)propanoic acid* **10b**

2.1 g 2-Nitrophenylalanine (1 eq, 10 mmol) was added to a 250 mL round bottom flask with a stir bar and 100 mL of a 1:1 mixture of THF and H<sub>2</sub>O was added. 2.52 g (3.0 eq) of NaHCO<sub>3</sub> was then added, and the solution was cooled in an ice bath for ten minutes. 2.62 g di-tert-butyl dicarbonate (BOC<sub>2</sub>O, 1.2 eq) was then added. The reaction mixture was extracted twice with 100 mL portions of diethyl ether and then acidified to a pH of 4-5 with half-saturated citric acid solution. The resulting acidified phase was extracted twice with 100 mL portions of DCM. The combined organic phase was washed once with brine, dried over anhydrous magnesium sulfate and the solvent was evaporated under reduced pressure yielding **10b**, as a yellow oil (3.05 g /98 %) High- and low-resolution MS and NMR were used to verify the exact mass and structure of the prepared product. <sup>1</sup>H NMR spectrum, (400MHz, CDCl<sub>3</sub>):  $\delta$ , ppm (J, Hz): 8.2 (2H), 7.4 (2H), 3.8 (1H), 1.6 (3H) and 1.3 (9H)

*Methyl (2S)-2-[[tert-butoxy]carbonyl]amino}-3-(2-nitrophenyl)propanoate **10a***

310 mg (1.0 mmol) (2S)-2-[[tert-butoxy]carbonyl]amino}-3-(2-nitrophenyl)propanoic acid **10b** was added to a 10 mL RBF equipped with a stir bar followed by 5 mL DMF and 318 mg Na<sub>2</sub>CO<sub>3</sub> (3 eq, 3.0 mmol). After stirring at room temperature for 30 mins, 187  $\mu$ L of MeI (3 eq, 3.0 mmol) was added and the mixture was stirred at room temperature overnight. The solvent was evaporated under reduced pressure at 35°Celsius and then the residue was partitioned between 50 mL ethyl acetate and 50 mL water. The aqueous phase was extracted thrice with ethyl acetate and the combined organic phases were washed with water (50 mL) followed by three 50 mL washes of 5% Na<sub>2</sub>S<sub>2</sub>O<sub>3</sub> solution. Finally, the organic phase was washed with brine and dried over anhydrous magnesium sulfate. The solvent was evaporated under reduced pressure yielding **10a** as an off-white dry powder (300 mg, 93%). High- and low-resolution MS and NMR were used to verify the exact mass and structure of the prepared product. <sup>1</sup>H NMR spectrum (500 MHz, Chloroform-*d*)  $\delta$  8.19 – 8.13 (m, 2H), 7.34 – 7.29 (m, 2H), 5.05 (d, *J* = 8.0 Hz, 1H), 4.64 (d, *J* = 7.2 Hz, 1H), 3.74 (s, 3H), 3.27 (dd, *J* = 13.7, 5.6 Hz, 1H), 3.12 (dd, *J* = 14.1, 6.4 Hz, 1H), 1.41 (s, 9H). MS (ESI) *m/z* calculated for [C<sub>15</sub>H<sub>20</sub>N<sub>2</sub>O<sub>6</sub>]<sup>+</sup>:324.13214 [M+H]<sup>+</sup>; found: 324.1321 ;  $\delta$  = -0.12 ppm

*tert-butyl N-{3-[(tert-butyldimethylsilyl)oxy]propyl}carbamate **12a***

2.00 g (11.0 mmol) N-Boc-3-amino-1-propanol was added to a 100 mL round bottom flask equipped with a stir bar followed by 5 mL DCM, 2.25 g imidazole (3 eq) and 5.58g iodine (2eq). Then, 12.5 mL (1.1 eq) of tert-butyldimethylsilyl chloride (TBDMSCl)

was added dropwise over 30 minutes. After stirring at room temperature for 6 hours, the solvent was evaporated under reduced pressure at 35°C and then the residue was partitioned between 50 mL ethyl acetate and 50 mL water. The aqueous phase was extracted thrice with ethyl acetate and the combined organic phases were washed with water (50 mL). Finally, the organic phase was washed with brine and dried over anhydrous magnesium sulfate. The solvent was evaporated under reduced pressure yielding **12a** as a pale-yellow oil (3.0 g, 94%). High- and low-resolution MS were used to verify the exact mass and structure of the prepared product. MS (ESI) m/z calculated for [C<sub>14</sub>H<sub>31</sub>NO<sub>3</sub>Si]<sup>+</sup>: 289.20732 [M+H]<sup>+</sup>; found: 289.20749 ;  $\delta = 0.6$  ppm

*(2S)-2-(3-{[(tert-butoxy)carbonyl]amino}propanamido)-3-(1H-imidazol-5-yl)propanoic acid 13a*

2.00 g  $\beta$  –alanyl-L-histidine (1 eq, 8.8 mmol) was added to a 100 mL round bottom flask with a stir bar and 40 mL ACN. 1.00 g (1.0 eq, 8 mmol) DMAP was then added. 2.88 g (1.6 eq, 13 mmol) di-tert-butyl dicarbonate (BOC<sub>2</sub>O) were then added. The reaction mixture was stirred overnight then was evaporated to dryness under reduced pressure. The residue was partitioned between ethyl acetate and water. The aqueous phase was extracted three times with ethyl acetate. The combined organic phases were washed once with brine, dried over anhydrous magnesium sulfate, filtered and concentrated under reduced pressure yielding **13a**, as an off-white solid (1.31 g /46 %). High- and low-resolution MS were used to verify the exact mass of the prepared product. MS (ESI) m/z calculated for [C<sub>14</sub>H<sub>22</sub>N<sub>4</sub>O<sub>5</sub>]<sup>+</sup>: 326.15902 [M+H]<sup>+</sup>; found: 326.15916 ;  $\delta = 0.43$  ppm

*tert-butyl 3-([(benzyloxy)carbonyl]amino)methyl)piperidine-1-carboxylate* **14a**

A mass of 431 mg (2 mmol) *tert-butyl 3-(aminomethyl)piperidine-1-carboxylate* **6a** was dissolved in 20 mL THF and 9 mL 2M NaOH in a 50 mL round bottom flask. Benzyl chloroformate (0.416 g, 1.2 eq) was then added dropwise. The reaction mixture was stirred overnight under nitrogen. The crude mixture was then dried under reduced pressure and the residue was partitioned between water and ethyl acetate. The aqueous phase was extracted three times with ethyl acetate. The combined organic phases were washed once with brine, dried over anhydrous magnesium sulfate, filtered and concentrated under reduced pressure yielding **14a**, as a clear oil (0.7 g / 100%). High- and low-resolution MS were used to verify the exact mass of the prepared product. MS (ESI)  $m/z$  calculated for  $[C_{19}H_{28}N_2O_4]^+$ : 348.20491  $[M+H]^+$ ; found: 348.20329 ;  $\delta = 4.66$  ppm

*(3S)-3-([(tert-butoxy)carbonyl]amino)-3-([(2S)-1-methoxy-1-oxo-3-phenylpropan-2yl]carbamoyl)propanoic acid* **16a**

3.00 g aspartame (1 eq, 10 mmol) was added to a 100 mL round bottom flask with a stir bar and 50 mL ACN. 1.25 g (1.0 eq, 10 mmol) DMAP was then added. 3.27 g (1.5 eq, 15 mmol) di-*tert-butyl* dicarbonate ( $BOC_2O$ ) were then added. The reaction mixture was stirred overnight then was evaporated to dryness under reduced pressure. The residue was partitioned between ethyl acetate and water. The aqueous phase was extracted three times with ethyl acetate. The combined organic phases were washed once with brine, dried over anhydrous magnesium sulfate, filtered and concentrated under reduced pressure yielding **16a**, as an off-white solid (1.17 g / 30 %). Low-resolution MS was used to verify the mass.

MS (ESI) m/z calculated for [C<sub>19</sub>H<sub>26</sub>N<sub>2</sub>O<sub>7</sub>]<sup>+</sup>: 394.42 [M+H]<sup>+</sup>; found: 394.42.